

 <p>ROMA TRE UNIVERSITÀ DEGLI STUDI</p>	<p>DOTTORATO IN SCIENZE DELLA TERRA (SDT)</p>
	<p>CURRICULUM <i>‘Geodinamica e Vulcanologia / o Risorse naturali, Territorio e Ambiente’</i></p>

CYCLE XXX

Ph.D. Student Claudio BAFFIONI

Academic year 2016/2017..... Year of study Third

Project Title

**Numerical exploration for medium - low enthalpy fluids in
Roman Geothermal Province**

TUTOR: Prof. Guido Giordano

CONTENTS

Abstract	5
Chapter 1 – Overview on climate change and on the mitigation policy strategies	7
OBSERVED CHANGES AND THEIR CAUSES.....	8
<i>OBSERVED CHANGES IN THE CLIMATE SYSTEM</i>	8
<i>CAUSES OF CLIMATE CHANGE</i>	10
CLIMATE CHANGE MITIGATION AND GHG EMISSION REDUCTION.....	11
<i>REFERENCES</i>	12
Chapter 2 – Overview of the State of the Art in geothermal energy use.....	13
GEOHERMAL RESOURCES: A CLASSIFICATION	14
CONVENTIONAL HYDROTHERMAL GEOHERMAL RESOURCE	14
HOT DRY ROCK, HDR OR ENHANCED GEOHERMAL SYSTEMS, EGS.....	15
DEEP HYDROTHERMAL	17
GEOHERMAL IN SUSTAINABLE ENERGY STRATEGY.....	17
VISION FOR DEPLOYMENT AND CO2 ABATEMENT.....	18
GEOHERMAL ENERGY IN ITALY.....	19
THE ITALIAN GEOHERMAL POTENTIAL.....	19
GEOHERMAL ENERGY WITHIN THE NATIONAL ENERGY FRAMEWORK.....	19
REFERENCES.....	22
Chapter 3 – Overview of the different kinds of numerical geothermal models existing in literature	24
Local modelling.....	25
General remarks.....	25
Conceptual model and data collection.....	25
Model design — structure and boundary conditions.....	25
Numerical integration of physical background in the equation systems.....	28
Limitations and criticalities of numerical simulation of geothermal reservoirs.....	29
Calibration	29
A brief review of Italian case studies referred to experimentally investigated geothermal fields.....	30

Larderello geothermal field, 2010 model.....	30
Larderello geothermal field, 2008 model.....	30
The Campi Flegrei magmatic system.....	31
The Campi Flegrei hydrothermal system.....	32
Continental and Basin Modelling for the Enhanced Geothermal Systems exploration.....	33
Continental Modelling.....	35
Basin Modelling.....	36
References.....	39
Chapter 4 – Presentation of the main characteristics of HEAT3D numerical code.....	42
The KWare HEAT3D geophysical heat flow simulator.....	43
Analytical Approach.....	44
Method for Numerical Solution of Conductive Heat Flow.....	45
Method for Solution of Convective Heat Flow.....	47
Method for Solution of Heat Sources/Sinks.....	47
Using HEAT3D.....	48
Options for the simulations.....	48
Building up a mesh.....	49
References.....	50
Chapter 5 – Building of the conceptual model for the Roman Geothermal Province used in this work.....	51
Geological setting.....	52
Potential of the geothermal resource in Latium.....	53
Heat source.....	54
Stratigraphy, structure and permeability.....	57
Recharging and vertical permeability.....	59
The conceptual model.....	61
References.....	66
Chapter 6 – Description of how the conceptual model is implemented in HEAT3D: mesh, rocks physical parameters, thermal gradients and time steps.....	68
THE BASE CONFIGURATION.....	69

COMPUTATIONAL MODEL, SELECTION OF THE CELL-SIZE, SELECTION OF THE HORIZONTAL AND VERTICAL EXTENT 69

INITIAL ROCK TEMPERATURES 70

SURFACE TEMPERATURE 70

VALUES OF PHYSICAL PARAMETERS IN BASE SIMULATIONS 70

THERMAL GRADIENT..... 71

SIMULATIONS IMPLEMENTED 74

TIME STEP 75

OPTIONS FOR THE SIMULATIONS 75

INTRUSION/ADVECTION..... 75

P-T DEPENDENCIES 75

HEAT CONSERVATION 76

ANNEX 1 PHYSICAL PARAMETERS FOR DIFFERENT ROCKS 77

REFERENCES..... 79

Chapter 7 – Presentation of the parametric study of the main variables (density, specific heat, thermal conductivity) in the basement, and in the magma source (temperature, depth of the top and geometry).. 80

Parametric variation in crystalline basement..... 83

Parametric variation in temperature and geometry for the magma chamber 84

Outputs analysis for the parametric variations in the crystalline basement 85

 Variation of thermal conductivity k 85

 Variation of specific heat c_p 86

 Variation of density 88

Outputs analysis for parametric variation in temperature and geometry for the magma chamber..... 89

 Variation of the magma chamber temperature T 89

 Variation of magma chamber top level..... 91

 Variation of magma chamber length..... 92

Summary..... 93

 ANNEX 1 Meshes implemented for the variation in geometry of the magma chamber 94

References..... 96

Chapter 8 - Presentation and analysis of the main outputs obtained with the model configuration selected after the parametric study 97

Output Analysis	98
Conductive Temperature field in the Computational Domain.....	98
Conductive-Convective Temperature field in the Mesh Domain.....	105
Chapter 9 - Calibration of the model respect to existing thermal data	113
HISTORY OF MAGMA CHAMBER BUILDS UP THE THERMAL GRADIENT?	114
MODEL CALIBRATION	116
MODEL CALIBRATION IN COLLI ALBANI AREA	116
MODEL CALIBRATION IN MONTI SABATINI AREA.....	118
COMPARING NUMERICAL MODEL OUTPUT WITH WELLS DATA IN MONTI SABATINI AREA	124
<i>WELLS WITH STABILIZED TEMPERATURE DATA</i>	125
<i>WELLS WITH WITH EXTRAPOLATED TEMPERATURE DATA</i>	127
CONCLUSIONS	130
REFERENCES.....	131
Chapter 10 – Forward modeling of the geothermal system across Roma Capital City.....	132
An HEAT3D model for the Province of Rome	133
Outputs from the purely conductive model.....	135
Outputs from the conductive-convective model	136
Conclusion	140
References.....	141
Summary and conclusion	142

Abstract

This work explores the potential of numerical modeling for the study of magmatic heat source of the Roman Geothermal Province.

The used numerical code models the thermal state within a heterogeneous material with heat sources. We assume the existence of a heat source at depth, transferring the heat to other layers by conduction/convection and evaluate its characteristics. The final results is the evolution in time of the thermal field, without explicitly describing the fluid flow.

The Roman Geothermal Province (RGP) is one of the largest geothermal areas in Europe, related to the presence of Quaternary volcanic complexes (known in the literature as the Roman Magmatic Province; Giordano et al., 2014), where significant studies had been carried out in between the 1970s and 1990s by the national electric company ENEL. These extensive geological, geochemical and geophysical studies allowed to define with a good degree of confidence the existence of a regional geothermal reservoir made of Meso-Cenozoic carbonatic successions characterized by secondary permeability, at depths comprised between 1 and 2 km from the surface and total thickness of a few kms, which accommodates both the Tertiary orogenic tectonics and the Pliocene-Quaternary extensional tectonics. The regional reservoir is covered by syn-orogenic and post-orogenic pelitic successions that allow the instauration and persistence up-today of accessible high enthalpy geothermal resources in correspondence of the main Quaternary calderas (250°-350°C at 2-3 km depth), and of medium to low enthalpy resources away from them, driven by lateral advection of fluids. Most of the direct thermometric data acquired in the past from deep and shallow geothermal boreholes have been only qualitatively propagated in the 3D rock volume, and generated maps of the temperature at -1000m, -2000m, and -3000m in the region, that are presently the official documentation available and public through the Italian Ministry of Economic Development (unmig.mise.gov.it). These maps are reasonably constrained in areas where data are dense and well distributed that correspond to the target areas for high enthalpy, but become totally unreliable where geothermal drill-holes are not present at all, such is the case, for example, of the Municipality of Roma Capital City, which hosts more than 2.5 million people who may represent a very interesting market for investments dedicated to the use of low to medium enthalpy resources, matching the need for reduction of CO₂ emissions and use of renewable energy resources. Nevertheless, there are no studies that have attempted to model the first order features of the Roman Geothermal Province.

The modeling of geothermal fields usually follows two different approaches: inverse and forward. Inverse models need a large quantity of input data that, though, are not available for the scale of the RGP, but in specific areas. We herein therefore choose to use a forward approach, that is based on building of a robust conceptual model, grounded on the available geological, volcanological, geophysical and geochemical data. While the geometry and nature of the rocks forming the cap-rock and the geothermal reservoir system are rather well constrained allowing to model those with a good degree of confidence, the most critical part of the forward approach relates to the uncertainties related to the geometry, depth, longevity and thermal history of the magma heat sources and their surrounding basement rocks. This thesis therefore approaches the uncertainties with a parametric study aimed at identifying the extent and contribution to errors that may derive from such uncertainties. Afterwards a more deterministic approach is used to evaluate how, when and where the thermal evolution of the magma source reaches the conditions that are encountered in the RGP, from which considerations are made on the actual propagation of thermal conditions to distal domains of the geothermal province such as the case of Roma Capital City.

The numerical code used in this thesis is the open source HEAT3D (Wohletz, 1999). The code models the thermal state by finite difference solution of energy and momentum conservation equations. These equations express heat transfer by conduction and convection with nonlinearities arising from variations of thermal conductivity within a heterogeneous material and heat sources/sinks.

This thesis is organized in 10 chapters as it follows:

Chapter 1 – Overview on climate change and on the mitigation policy strategies.

Chapter 2 – Overview of the State of the Art in geothermal energy use.

Chapter 3 – Overview of the different kinds of numerical geothermal models existing in literature.

Chapter 4 – Presentation of the main characteristics of HEAT3D numerical code.

Chapter 5 – Building of the conceptual model for the Roman Geothermal Province used in this work.

Chapter 6 – Description of how the conceptual model is implemented in HEAT3D: mesh, rocks physical parameters, thermal gradients and time steps.

Chapter 7 – Presentation of the parametric study of the main variables (density, specific heat, thermal conductivity) in the basement, and in the magma source (temperature, depth of the top and geometry).

Chapter 8 - Presentation and analysis of the main outputs obtained with the model configuration selected after the parametric study

Chapter 9 - Calibration of the model respect to existing thermal data

Chapter 10 – Forward modeling of the geothermal system across Roma Capital City.

Chapter 1 - Overview on climate change and on the mitigation policy strategies

In this chapter climate change observed changes and causes are discussed.

Then adaptation and mitigation strategies are introduced, focusing on the role played by the reduction of fossil fuels consumption, increasing the Energy Efficiency and the Renewable Energy use.

Commitments at international and European Union level are introduced. National commitments for EU Countries follow from the European commitment.

OBSERVED CHANGES AND THEIR CAUSES

Human influence on the climate system is clear, and recent anthropogenic emissions of greenhouse gases are the highest in history. Recent climate changes have had widespread impacts on human and natural systems (Pachauri et al., 2014).

OBSERVED CHANGES IN THE CLIMATE SYSTEM

Each of the last three decades has been successively warmer at the Earth's surface than any preceding decade since 1850. The period from 1983 to 2012 was likely the warmest 30-year period of the last 1400 years in the Northern Hemisphere, where such assessment is possible (medium confidence¹). The globally averaged combined land and ocean surface temperature data as calculated by a linear trend show a warming of 0.85 [0.65 to 1.06] °C² over the period 1880 to 2012, when multiple independently produced datasets exist (Fig. 1a).

Over the period 1901 to 2010, global mean sea level rose by 0.19 [0.17 to 0.21] m (Fig. 1b). The rate of sea level rise since the mid-19th century has been larger than the mean rate during the previous two millennia (high confidence).

Anthropogenic greenhouse gas (GHG) emissions since the pre-industrial era have driven large increases in the atmospheric concentrations of carbon dioxide (CO₂), methane (CH₄) and nitrous oxide (N₂O) (Fig. 1c). Between 1750 and 2011, cumulative anthropogenic CO₂ emissions to the atmosphere were 2040 ± 310 GtCO₂. About 40% of these emissions have remained in the atmosphere (880 ± 35 GtCO₂); the rest was removed from the atmosphere and stored on land (in plants and soils) and in the ocean. The ocean has absorbed about 30% of the emitted anthropogenic CO₂, causing ocean acidification.

About half of the anthropogenic CO₂ emissions between 1750 and 2011 have occurred in the last 40 years (high confidence) (Fig. 1d). (Pachauri et al., 2014)

1 For the "level of confidence" definition expressed using five qualifiers: "very low," "low," "medium," "high," and "very high." see Mastrandrea et al., 2010.

2 Ranges in square brackets or following '±' are expected to have a 90% likelihood of including the value that is being estimated, unless otherwise stated.

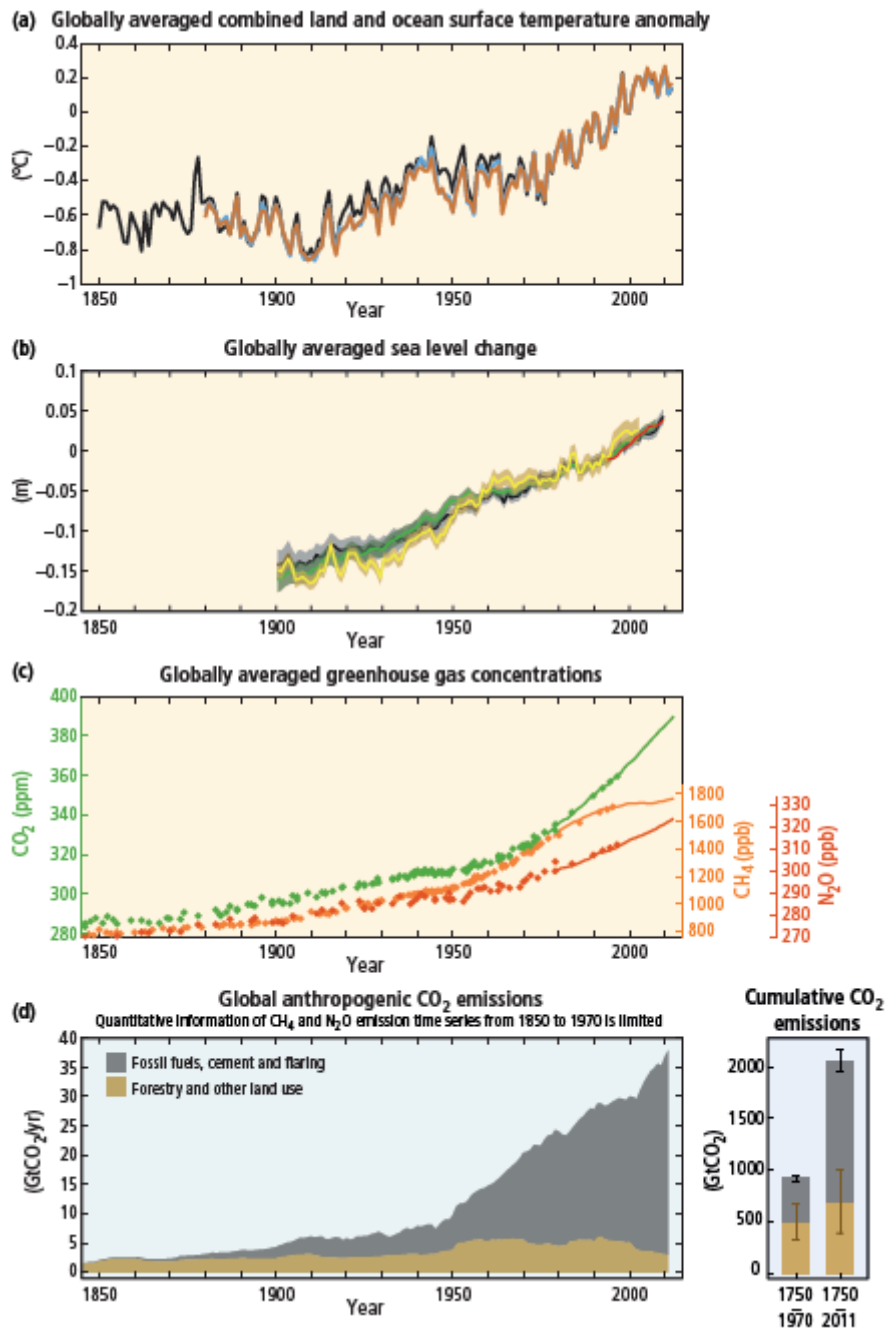


Fig. 1 Observations and other indicators of a changing global climate system. (Pachauri et al., 2014)

Observations:

(a) Annually and globally averaged combined land and ocean surface temperature anomalies relative to the average over the period 1986 to 2005. Colours indicate different data sets.

(b) Annually and globally averaged sea level change relative to the average over the period 1986 to 2005 in the longest-running dataset. Colours indicate different data sets. All datasets are aligned to have the same value in 1993, the first year of satellite altimetry data (red). Where assessed, uncertainties are indicated by coloured shading.

(c) Atmospheric concentrations of the greenhouse gases carbon dioxide (CO₂, green), methane (CH₄, orange) and nitrous oxide (N₂O, red) determined from ice core data (dots) and from direct atmospheric measurements (lines).

Indicators:

(d) Global anthropogenic CO₂ emissions from forestry and other land use as well as from burning of fossil fuel, cement production and flaring. Cumulative emissions of CO₂ from these sources and their uncertainties are shown as bars and whiskers, respectively, on the right hand side.

CAUSES OF CLIMATE CHANGE

Changes in solar irradiance and volcanic aerosols cause natural radiative forcing (Fig. 2). The radiative forcing from stratospheric volcanic aerosols can have a large cooling effect on the climate system for some years after major volcanic eruptions. Changes in total solar irradiance are calculated to have contributed only around 2% of the total radiative forcing in 2011, relative to 1750.

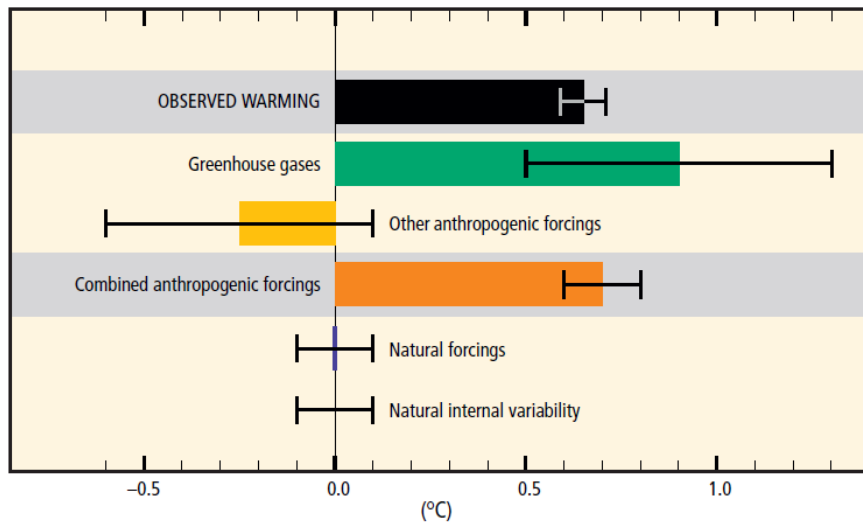


Fig. 2 Contributions to observed surface temperature change over the period 1951–2010 (Pachauri et al., 2014). Assessed likely ranges (whiskers) and their mid-points (bars) for warming trends over the 1951–2010 period from well-mixed greenhouse gases, other anthropogenic forcings (including the cooling effect of aerosols and the effect of land use change), combined anthropogenic forcings, natural forcings and natural internal climate variability (which is the element of climate variability that arises spontaneously within the climate system even in the absence of forcings). The observed surface temperature change is shown in black, with the 5 to 95% uncertainty range due to observational uncertainty.

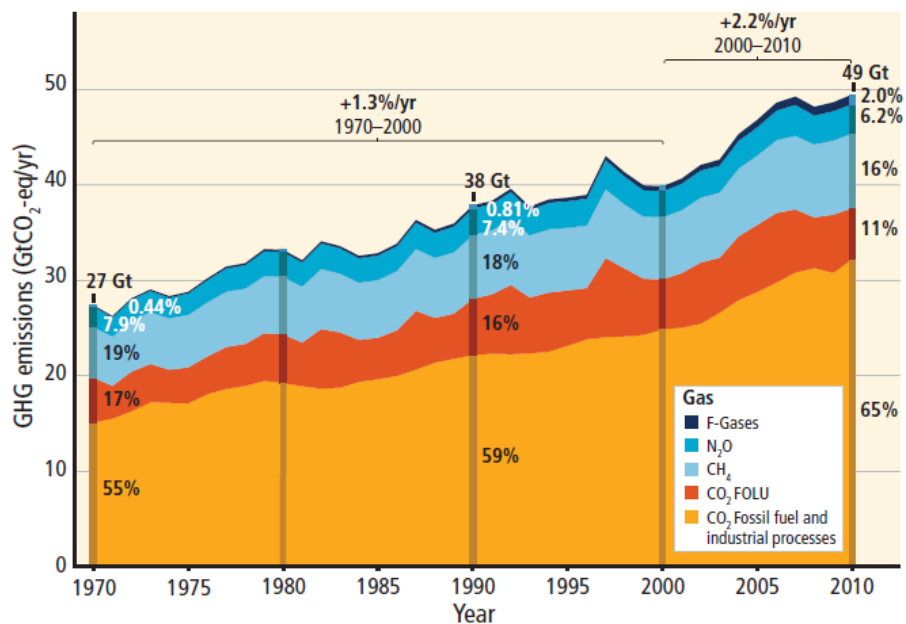


Fig. 3 Contributions to observed surface temperature change over the period 1951–2010. (Pachauri et al., 2014). Total annual anthropogenic greenhouse gas (GHG) emissions (gigatonne of CO₂-equivalent per year, GtCO₂-eq/yr) for the period 1970 to 2010 by gases: CO₂ from fossil fuel combustion and industrial processes; CO₂ from Forestry and Other Land Use (FOLU); methane (CH₄); nitrous oxide (N₂O); fluorinated gases covered under the Kyoto Protocol (F-gases).

Emissions of CO₂ from fossil fuel combustion and industrial processes contributed about 78% of the total GHG emissions increase from 1970 to 2010, with a similar percentage contribution for the increase during the period 2000 to 2010 (high confidence) (Fig. 3).

CLIMATE CHANGE MITIGATION AND GHG EMISSION REDUCTION

Adaptation³ and mitigation⁴ are complementary strategies for reducing and managing the risks of climate change. Substantial emissions reductions over the next few decades can reduce climate risks in the 21st century and beyond, increase prospects for effective adaptation, reduce the costs and challenges of mitigation in the longer term and contribute to climate-resilient pathways for sustainable development.

The United Nations Framework Convention on Climate Change (UNFCCC) entered into force on 21 March 1994. The 197 countries that have ratified the Convention are called Parties to the Convention. Preventing “dangerous” human interference with the climate system is the ultimate aim of the UNFCCC.

(UNFCCC, 2014)

The twenty-first edition of the annual United Nations conference on climate change (Conference of the Parties, COP21) was held in Paris in December 2015. The Paris Agreement is an important step forward in international climate change negotiations. Its main merits include a legally binding 2 °C target, the introduction of a five-yearly review process from 2018 onwards with a first global stocktake scheduled for 2023 and an agreement on international climate financing. In the run-up to COP21, most countries submitted climate action pledges labelled ‘Nationally Determined Contributions’ (NDCs). (Secretariat UNFCCC, 2015).

The announced withdrawal of the United States from the Paris Agreement could have an effect on possible withdrawals of other Countries (like Syria announced).

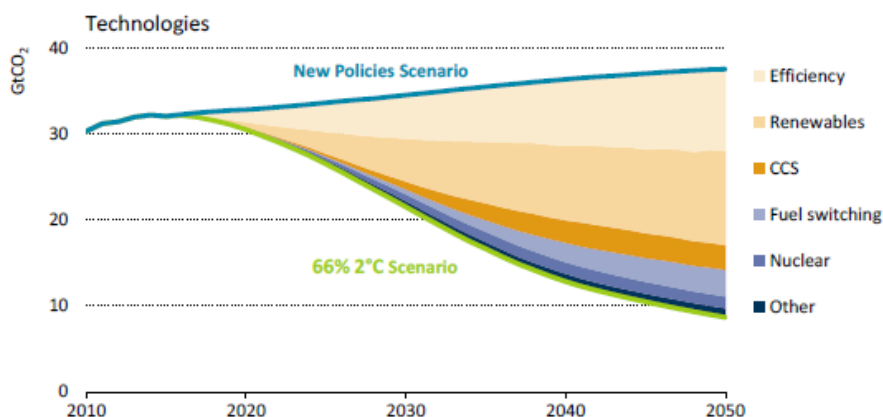


Fig. 4 Global emissions abatement by technology in the 66% 2°C Scenario relative to the New Policies Scenario. (OECD/IEA and IRENA, 2017)

There are multiple mitigation pathways that are likely to limit warming to below 2°C relative to pre-industrial levels.

Here we introduce two main scenarios: the New Policies Scenario and the 66% 2°C Scenario.

The New Policies Scenario reflects the implications for the energy sector of the climate pledges (NDCs).

The 66% 2°C Scenario describes a trajectory for energy-related emissions consistent with a 66% probability of limiting the long-term rise in global temperatures to less than 2 degrees Celsius (°C).

Accelerated deployment of renewable energy and energy efficiency measures are the key elements of the energy transition. By 2050, renewables and energy efficiency would meet the vast majority of emission reduction needs (90%), with some 10% achieved by fossil fuel switching and CCS (Fig. 4). (OECD/IEA and IRENA, 2017)

3 The process of adjustment to actual or expected climate and its effects. In human systems, adaptation seeks to moderate or avoid harm or exploit beneficial opportunities. In some natural systems, human intervention may facilitate adjustment to expected climate and its effects (.

4 A human intervention to reduce the sources or enhance the sinks of greenhouse gases (GHGs).

REFERENCES

- Edenhofer, O., Pichs-Madruga, R., Sokona, Y., Seyboth, K., Matschoss, P., Kadner, S., ... & von Stechow, C. (2011). IPCC special report on renewable energy sources and climate change mitigation. *Prepared By Working Group III of the Intergovernmental Panel on Climate Change*, Cambridge University Press, Cambridge, UK.
- European Commission, 2017 <https://ec.europa.eu/energy/en/topics/energy-strategy-and-energy-union/2030-energy-strategy>
- European Commission, 2017a <https://ec.europa.eu/energy/en/topics/energy-strategy-and-energy-union/2050-energy-strategy>
- Field, C. B. (Ed.). (2012). *Managing the risks of extreme events and disasters to advance climate change adaptation: special report of the intergovernmental panel on climate change*. Cambridge University Press.
- Mach, K., & Mastrandrea, M. (2014). *Climate change 2014: impacts, adaptation, and vulnerability* (Vol. 1). C. B. Field, & V. R. Barros (Eds.). Cambridge and New York: Cambridge University Press.
- Mastrandrea, M. D., Field, C. B., Stocker, T. F., Edenhofer, O., Ebi, K. L., Frame, D. J., ... & Plattner, G. K. (2010). Guidance note for lead authors of the IPCC fifth assessment report on consistent treatment of uncertainties.
- Nakicenovic, N., Alcamo, J., Grubler, A., Riahi, K., Roehrl, R. A., Rogner, H. H., & Victor, N. (2000). *Special Report on Emissions Scenarios (SRES), A Special Report of Working Group III of the Intergovernmental Panel on Climate Change*. Cambridge University Press.
- OECD/IEA and IRENA (2017). Perspectives for the energy transition – investment needs for a low-carbon energy system
- Secretariat, U. N. F. C. C. C. (2015). Synthesis Report on the Aggregate Effect of the Intended Nationally Determined Contributions. In *Bonn, Germany: United Nations Framework Convention on Climate Change*.
- Seneviratne, S. I., Nicholls, N., Easterling, D., Goodess, C. M., Kanae, S., Kossin, J., ... & Reichstein, M. (2012, April). Changes in climate extremes and their impacts on the natural physical environment: An overview of the IPCC SREX report. In *EGU General Assembly Conference Abstracts* (Vol. 14, p. 12566).
- Pachauri, R. K., Allen, M. R., Barros, V. R., Broome, J., Cramer, W., Christ, R., ... & Dubash, N. K. (2014). *Climate change 2014: synthesis report. Contribution of Working Groups I, II and III to the fifth assessment report of the Intergovernmental Panel on Climate Change* (p. 151). IPCC.
- Vandyck, T., Keramidas, K., Saveyn, B., Kitous, A., & Vrontisi, Z. (2016). A global stocktake of the Paris pledges: implications for energy systems and economy. *Global Environmental Change*, 41, 46-63.
- UNFCCC, 2014 http://unfccc.int/essential_background/convention/items/6036.php

Chapter 2 – Overview of the State of the Art in geothermal energy use

GEOTHERMAL RESOURCES: A CLASSIFICATION

Geothermal energy is considered a strategic resource in many countries, even if its use appears to be often marginal in the national energy systems. Its continuous operating mode distinguishes geothermal energy from the other renewable sources, intermittent or stochastic.

It is possible to consider three different kinds of geothermal resource (Di Pippo, 2012).

CONVENTIONAL HYDROTHERMAL GEOTHERMAL RESOURCE

There appear to be five features that are essential to making a hydrothermal (i.e., hot water) geothermal resource commercially viable. They are:

- A large heat source
- A permeable reservoir
- A supply of water
- An overlying layer of impervious rock
- A reliable recharge mechanism.

A highly schematic depiction of such a system is shown in Fig. 1.

The intent of a geothermal development project is to locate such systems and produce them by means of strategically drilled wells. As might be presumed, most (but not all) hydrothermal systems give away their general location through surface thermal manifestations such as the ones described above.

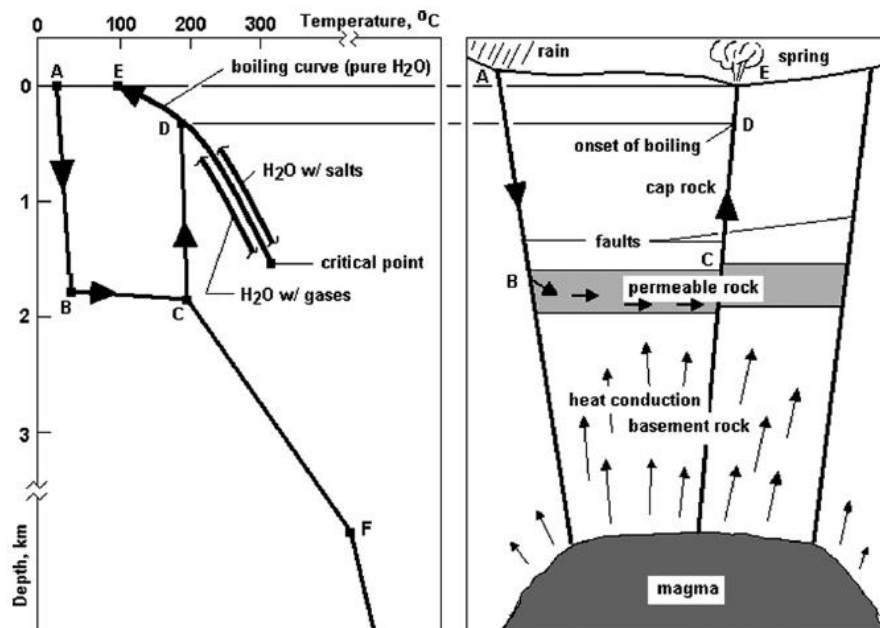


Fig. 1 Schematic model of a hydrothermal geothermal system (White, 1973).

If any one of the five features listed as needed for a viable hydrothermal resource is lacking, the field generally will not be worth exploiting.

For example,

- a) without a large heat source geofluid temperatures will be relatively low, i.e., the thermal energy of the system will be insufficient to support exploitation long enough to make it economic.
- b) without sufficient permeability in the formation, the fluid will not be able to move readily through it, i.e., it will not be able to remove much of the stored thermal energy in the rock. Furthermore, low permeability will cause poor well flow or, even worse, may prevent any production from the reservoir.
- c) without fluid in the system there is no heat transfer medium and the thermal energy of the formation will remain in the reservoir.

d) without an impermeable cap rock, the geofluids will easily escape to the surface appearing as numerous thermal manifestations and the pressure in the formation will quickly dissipate. And lastly, without a reliable and ample recharge to the reservoir, the geofluid will eventually become depleted when it supplies a power plant.

With the exception of requirements a) and d), deficiencies in the others have been addressed through research and field practice. Insufficient permeability can sometimes be remedied by artificial means such as hydraulic fracturing (called “hydrofracking”) in which high-pressure liquid is injected from the surface through wells to open fractures by means of stress cracking. However, unless the newly created widened fractures are held open with “proppants” they will re-close when the injection ceases. If little water is present in the formation or recharge is meager, all unused geofluid from the plant can be reinjected. Furthermore, external fluids can be brought to the site by some means and injected into the formation.

HOT DRY ROCK, HDR OR ENHANCED GEOTHERMAL SYSTEMS, EGS

There are many geothermal prospects that have high temperature but are lacking fluid in the formation or the permeability is too low to support commercial development (see point c) in paragraph before).

These systems can be “enhanced” by engineering the reservoirs through hydraulic fracturing. The Enhanced Geothermal System (EGS) concept (Gérard et al., 2006) consists essentially of drilling at least two boreholes (a “doublet”) into deep fractured rock, extracting hot fluid from a production well and injecting the cooled fluid back into the fractured reservoir through an injection well. To this end, both boreholes have been stimulated to connect the two wells to the natural surrounding geothermal reservoir by artificially enhancing the permeability of the natural network of fractures in their vicinity (Fig. 2).

This may imply some direct connections between the wells through natural fractures. The EGS, in theory, will provide abundant environmentally friendly quantities of heat or electricity in the future.

Success of hydraulic stimulation is dependent on the thermo-mechanical properties of the crust. Critically stressed regions, marked by active deformation, require little excess pressure for stimulation and are therefore favoured. In addition such regions are marked by pre-existing faults and fractures, forming preferential pathways for stimulated flow. To analyze these aspects, specific numerical models at continental and basin scale are implemented (see below).

The binary cycle technology with Organic Rankine Cycle (ORC)⁵ appears to be the most efficient and convenient solution for such a kind of resource. Binary power plants are now objects of wide attention by energy markets, although their diffusion is still made difficult by a lacking technology standardization and due to the quite high specific costs (Franco & Villani, 2009; Franco, 2011). The great variability of the resource characteristics worldwide is one of the possible reasons. The proper matching between the reservoir capability and the plants parameters (power size, extraction/reinjection rate) is a critical key point.

5 The Organic Rankine Cycle (ORC) is named for its use of an organic, high molecular mass fluid with a liquid-vapor phase change, or boiling point, occurring at a lower temperature than the water-steam phase change. The fluid allows Rankine cycle heat recovery from lower temperature sources. The low-temperature heat is converted into useful work, that can itself be converted into electricity. The Rankine cycle is an idealized thermodynamic cycle of a heat engine that converts heat into mechanical work while undergoing phase change. The heat is supplied externally to a closed loop.

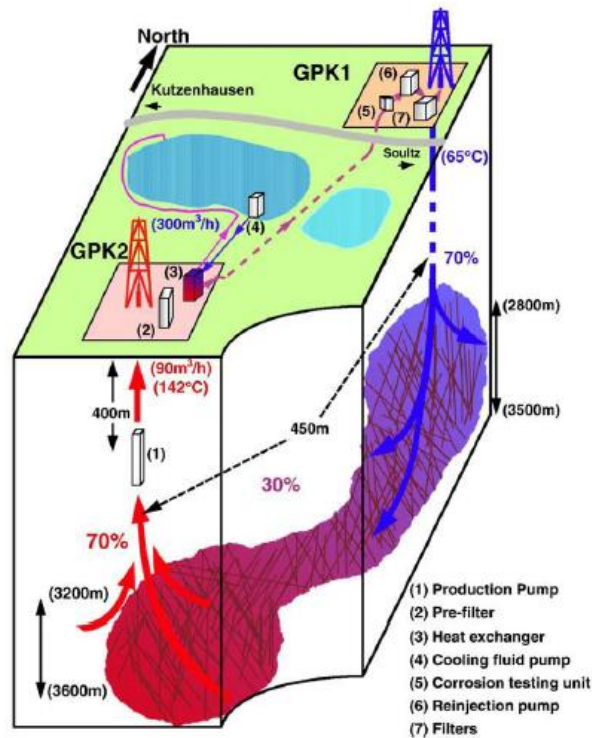


Fig. 2 Schematic block diagram of the 1997 Enhanced geothermal System (EGS) circulation test performed at Soultz (Upper Rhine Graben, eastern France) when heat was extracted at a rate of 10MWth. GPK1 and GPK2 are the injection and production well, respectively. The pumps used to circulate the fluids consumed less than 250 kW of electricity (Gérard et al., 2006).

In power plants using dry steam (high enthalpy) geothermal resources, pressure and temperature reduction can be compensated by an increase of the mass flow rate. In case of binary plants, a variation of the resource properties (T , p) could also lead to a fast end of life of the plant (Rybach & Mongillo, 2006). The first and most important activity to design a geothermal energy plant is an accurate investigation of the geothermal potential assessment, as well as the prediction of reservoir response at given industrial exploitation configurations. For these reasons, a multidisciplinary approach to the problem of exploitation of geothermal fields (in particular at medium-low temperature) is necessary. Thermal engineering, geochemistry, geophysics, and reservoir engineering are the fields involved in this technique. To analyze these aspects, specific numerical models at local scale are implemented (see below).

At the same time, critically stressed regions are often also marked by high density of natural earthquakes. In the deep heat mining projects in Soultz (France) and Basel (Switzerland), it has been observed that 'felt' microseismic events occur after shut-in of the hydraulic stimulation (Charl ty et al., 2007; H ring et al., 2008). In Basel after shutting in the well for about 5 h, a seismic event of M_L 3.4 occurred during preparations for bleeding off the well to hydrostatic conditions. Over the following 56 days, three aftershocks of $M_L > 3$ were recorded. At present the project is suspended but not abandoned pending an independent risk analysis and identification of acceptable ways of reservoir enhancement (H ring et al., 2008). Favourable conditions of tectonic stress are required to allow hydraulic stimulation of the naturally fractured rock mass with limited injection pressure.

There are many practical problems in developing a HDR system. It is difficult to control very deep, directional, geothermal wells. Drilling techniques in the oil industry now permit wells to be turned 90° while being drilled, allowing the well to drain several vertical pockets of petroleum. However, oil wells tend to be shallower than the ones envisioned for HDR, the temperatures encountered are far lower, and the rocks are not as hard as those found in geothermal regions. Furthermore, the HDR wells must be precisely aimed to hit the deep target in order to form a closed fluid circuit. Lastly, if some of the engineered fractures are not connected to the production well, injected fluid may be lost to the formation. This would require

continuous makeup water to maintain the power plant in operation. Some of these difficulties appear to have been at least partially solved in the on-going research.

DEEP HYDROTHERMAL

Deep hydrothermal resources, that has only recently been accessed and developed, are those that lie at depths of 2,500 to 4,000 m and deeper. They may lie in areas marked by normal geothermal temperature gradients, and as such may yield fluids at only low to moderate temperatures. For example in a place where the gradient is say 30 °C/km, fluids found at 4,000 m might range from 120-140 °C.

Deep drilling in Europe and Australia as a part of HDR (EGS) efforts has discovered that reservoirs of fluid exist at these depths and that the formations possess some permeability. In fact, deep sedimentary layers can be exploited even without hydrofracturing the formation. These wells produce geofluids that can be used in energy conversion systems specifically designed for lower temperature fluids. The waste discharge fluid from the power plant may often be further utilized for direct heating of buildings and homes before being reinjected. The cost of such deep wells is significantly higher than the usual shallower geothermal wells, but with sufficient financial incentives offered by governments, private developers are able to successfully exploit what were previously thought to be uneconomic geothermal resources.

GEOHERMAL IN SUSTAINABLE ENERGY STRATEGY

Rationale for geothermal energy

Geothermal technologies use renewable energy resources to generate electricity and/or heating and cooling while producing very low levels of greenhouse-gas (GHG) emissions.

Sustainable use of geothermal energy implies that the heat removed from the resource is replaced on a similar time scale. Production of geothermal fluid and/or heat from a reservoir/resource decreases its fluid/heat content, but also increases the natural recharge rate into created pressure and temperature sinks (i.e. dynamic recovery). For each geothermal system, and for each mode of production, there exists a certain level of maximum energy production, below which it will be possible to maintain constant energy production from the system for 100 to 300 years (Axelsson, 2016).

Geothermal energy has an important role to play in realizing targets in energy security, economic development and mitigating climate change (Beerepoot, 2011).

Electricity generation usually requires geothermal resources temperatures of over 100 °C. For heating, geothermal resources spanning a wider range of temperatures can be used in applications such as space and district heating, spa and swimming pool heating, greenhouse and soil heating, aquaculture pond heating, industrial process heating and snow melting. Space cooling can also be supplied through geothermal heat, through the use of heat-driven adsorption chillers as an alternative to electrically driven compression chillers.

Global technical potential for geothermal electricity has been estimated at 45 EJ/yr - 12,500 TWh_e, i.e. about 62% of 2008 global electricity generation while resources suitable for direct use are at 1,040 EJ/yr - 289,000 TWh_t; worldwide final energy use for heat in 2008 was 159.8 EJ/ - 44,392 TWh_t (Krewitt et al. 2009). The estimated technical potential for geothermal electricity and geothermal heat excludes advanced geothermal technologies

Geothermal technology development has focused so far on extracting naturally heated steam or hot water from natural hydrothermal reservoirs. However, geothermal energy has the potential to make a more significant contribution on a global scale through the development of the advanced technologies, especially the exploiting of hot rock resources using enhanced geothermal systems (EGS) techniques. Geothermal energy is projected to provide 1,400 TWh annually for global electricity consumption in 2050. Geothermal heat use is projected to supply 5.8 EJ/yr in 2050 (Beerepoot, 2011; Taylor, 2010).

Geothermal energy today

Although the use of geothermal hot springs has been known since ancient times, active geothermal exploration for industrial purposes started at the beginning of the 19th century with the use of geothermal fluids (boric acid) in Larderello (Italy). At the end of the 19th century, the first geothermal district heating system began operating in Boise (United States), with Iceland following in the 1920s. At the start of the 20th century, again in Larderello, the first successful attempt to produce electricity from geothermal heat was achieved. Since then, installed geothermal electricity has steadily increased. In 2009, global geothermal power capacity was 10.7 GW_e and generated approximately 67.2 TWh_e/yr of electricity, at an average efficiency rate of 6.3 GWh/MW_e (Bertani, 2010).

VISION FOR DEPLOYMENT AND CO₂ ABATEMENT

Geothermal deployment to 2050 and CO₂ abatement in electricity production

The ETP 2010 BLUE Map Hi-REN scenario assumes that renewable energy sources will provide 75% of global electricity production in 2050 and foresees geothermal electricity producing 1,400 TWh annually by 2050. This will amount to around 3.5% of global electricity production by that time on the basis of a projected 37,500 TWh/yr in 2050. Conventional high-temperature resources as well as deep aquifers with low- and medium-temperature resources are expected to play an important role in geothermal development (Taylor, 2010).

This roadmap's vision for geothermal electricity foresees 200 GW_e of installed capacity by 2050, including 100 GW_e hydrothermal electricity capacity and 100 GW_e from EGS (Figure 6). EGS is expected to mostly use binary power generation technology. In addition to the 10 EGS plants currently under development, at least 50 more with an average capacity of 10 MW_e will be needed over the next 10 years to achieve the deployment levels envisaged in this roadmap. EGS plant capacities are expected to increase: while the pilot plant in Soultz-sous-Forêts is producing power from a 1.5 MW_e capacity, plants under development aim for capacities from 3 MW_e to 10 MW_e in the next decade. In course of time, plants are expected to increase capacities to 50 MW_e and eventually more than 200 MW_e by stacking modules in series and parallel (Taylor, 2010).

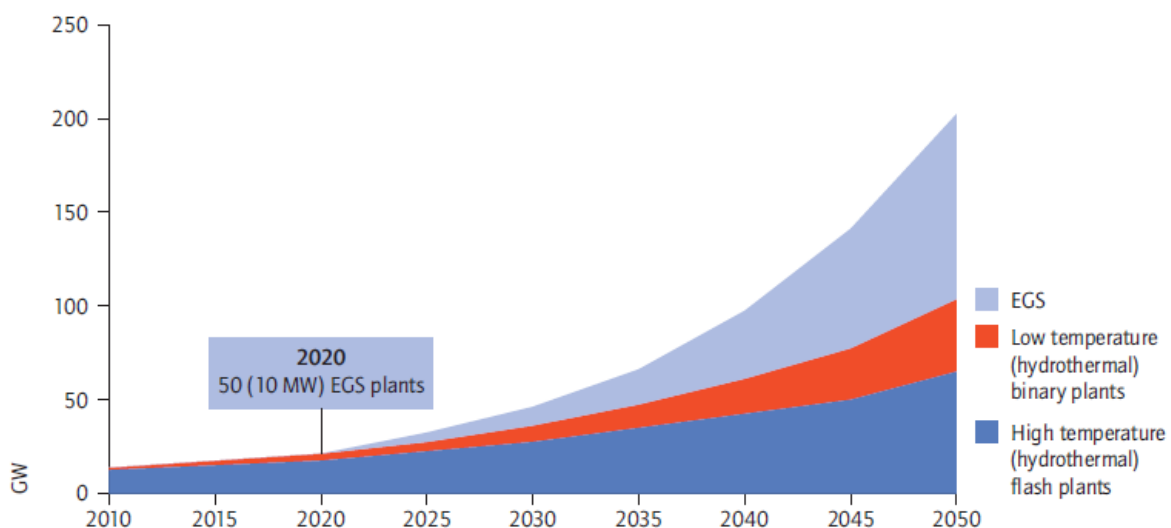


Fig. 3 Growth of geothermal power capacities by technology (GW) (Taylor, 2010).

The 1,400 TWh of geothermal electricity generated by 2050 is expected to avoid around 760 MtCO₂/yr worldwide according to the ETP 2010 (Taylor, 2010). The reductions have been estimated by assuming that the additional geothermal generation replaces the average fossil generation mix. All new geothermal plants are assumed to be CO₂-free (Taylor, 2010).

Geothermal heat use

Geothermal heat use may be most relevant in colder countries, but in warmer climates geothermal heat can be made useful in agricultural and industrial applications, and for space cooling using heat in excess of 60 °C as the driving energy for sorption chillers.

Recent rapid increases in the numbers of geothermal heat-only plants and in geothermal CHP binary plants in northern Europe confirm that interest in the direct use of geothermal heat is growing. Several East European countries face the need to renovate ageing district heating systems, while realising that they are located above or close to deep geothermal aquifers such as the Pannonian Basin. Even tropical countries such as the Philippines and Indonesia are starting to become aware of the potential benefits of geothermal heat for agricultural applications.

Projections for geothermal heat use are related to the development of advanced technologies, which will benefit from the combined use of heat and power as this can increase economic viability of more expensive technology.

In 2050 the roadmap's vision foresees the global sum of annual direct use amounts to 5.8 EJ (about 1,600 TWh thermal energy). This scenario assumes that hot rock technology becomes commercially viable soon after 2030. Under this assumed condition, the utilisation of heat from deep rock formations should theoretically become possible wherever rock temperatures and the properties of the underground allow the economic sale of energy. The largest potential for geothermal heat can be found in regions with high heat demand: Europe, China and North America.

GEOHERMAL ENERGY IN ITALY

THE ITALIAN GEOTHERMAL POTENTIAL

Italian geothermal resources potentially harnessable within 5 km depth are in the range of 21 EJ. Two thirds of them have temperatures below 150 °C. Regardless of temperature, the Italian geothermal potential down to 5 km depth accounts for 3.5% of the whole European one (Buonasorte & Cataldi, 2008).

Resources at temperatures suitable for electricity generation ($T > 80-90^{\circ}\text{C}$), at costs currently competitive with those of other energy sources, exist only in areas with strong heat flow anomalies: the Tuscany-Latium-Campania pre-Apennine belt, the two main Italian islands, and some volcanic islands of the Tyrrhenian Sea, all located in western and south-western Italy.

Conversely, medium- and low-temperature resources ($T < 80-90^{\circ}\text{C}$) suitable for direct uses are found not only in the above areas of high heat flow, but in many other zones. Additionally, thanks to the use of heat pumps, even resources at lower temperature ($T < 30^{\circ}\text{C}$) and at small depth could be exploited almost everywhere in Italy.

The above infers that, within accessible depths, Italy is endowed with geothermal resources of any kind and temperature in many large areas, especially for direct uses. Hence, it has a huge geothermal potential, which could be tapped much more intensively than hitherto (Buonasorte et al., 2011).

GEOHERMAL ENERGY WITHIN THE NATIONAL ENERGY FRAMEWORK

Political framework

The existing Renewable Energy Directive, adopted by codecision on 23 April 2009 (Directive 2009/28/EC, repealing Directives 2001/77/EC and 2003/30/EC), established that a mandatory 20% share of EU energy consumption must come from renewable energy sources by 2020. The directive specifies national renewable energy targets for each country, taking into account its starting point and overall potential for renewables.

Italy's Renewable Energy Action Plan was adopted in 2010 and its overall target is to achieve 17% of final energy consumption from renewable sources by 2020. The development of RES is among the priorities of

Italy's energy policy alongside the promotion of energy efficiency. The objectives of such a policy are: energy supply security, lower energy costs for consumers, promotion of innovative new technologies, environmental protection (including lower GHG emissions) and therefore, ultimately, sustainable development. In the medium to long term, Italy aims to redress the balance of its energy mix, which remains overly dependent on imported fossil fuels (Fig. 4) (IEA, 2016).

	2005	2010	2015	2020
RES heating and cooling	2.8%	6.53%	10.09%	17.09%
RES electricity	16.29%	18.71%	22.39%	26.39%
RES transport	0.87%	3.5%	6.63%	10.17%
Overall share of RES	4.92%	8.05%	11.24%	17%

Fig. 4 National 2020 target and estimated trajectory of energy from renewable sources (Italy's National Renewable Energy Action Plan in line with Directive 2009/28/EC) (IEA, 2016).

Energy production and supply

Italy produced 35.5 Mtoe of energy in 2015. Energy production has been on an upward trend since 2001, and has increased by 17.7% from 2005 to 2015. Before 2001, production was mildly volatile albeit declining from a 1997 local peak of 30.4 Mtoe (Figure 8) (IEA, 2016).

Renewable energy development is the main driver of recent production growth. Renewable energy represented 68.4% of total energy production in 2015, up from 61.9% in 2010 and 46.4% in 2005. In 2015, biofuels and waste accounted for 32.2%, followed by geothermal (15.4%), hydro (10.6%), solar (6.6%) and wind (3.6%).

Italy's total primary energy supply (TPES)⁶ was 150.7 Mtoe in 2015. It has declined by 19.1% over the past ten years, down from 186.4 Mtoe in 2005 (Figure 9). TPES has declined despite the increase in energy production, owing to falling domestic demand.

Fossil fuels accounted for 79.1% of TPES in 2015, broken down in natural gas (36.7%), oil (34.2%) and coal (8.2%). Over the past decade, the fossil fuels share has shrunk from 89.8% of TPES, as renewable energy has gained a larger share of the total energy mix. Energy from oil was 35.7% lower in 2015 than in 2005, while natural gas and coal were 21.7% and 24.6% below, respectively.

Renewables represented 18.2% of TPES in 2015, up from 7.9% ten years earlier. Biofuels and waste contributed 9.7% to TPES in 2015, followed by geothermal (3.6%), hydro (2.5%), solar (1.6%) and wind (0.8%). Energy from geothermal was 14.1% higher in 2015 than in 2005, exhibiting the slowest growth among renewable energy sources (IEA, 2016).

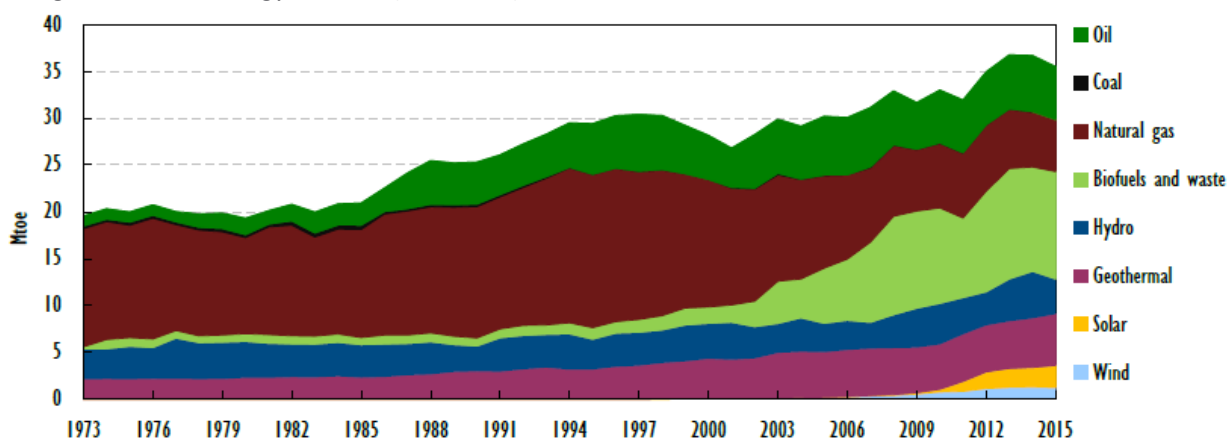


Fig. 5 Energy production in Italy by source, 1973-2015 (IEA, 2016)

⁶ TPES is made up of production + imports - exports - international marine bunkers - international aviation bunkers ± stock changes. This equals the total supply of energy that is consumed domestically, either in transformation (for example, refining)

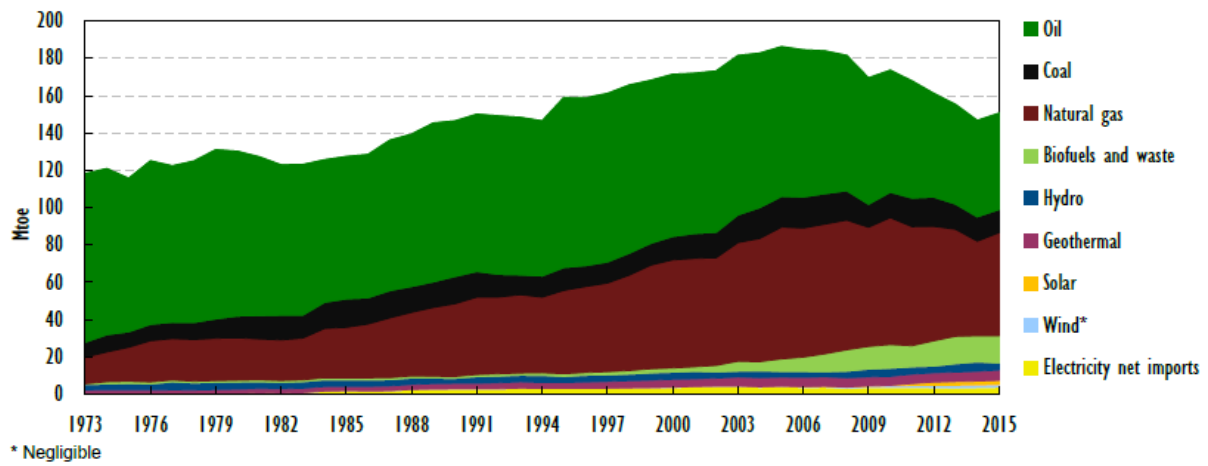


Fig. 6 Total Primary Energy Supply in Italy, 1973-2015 (IEA, 2016)

REFERENCES

- Axelsson, G. (2016). Sustainable management of geothermal resources. 001436794.
- Beerepoot, M. (2011). Technology roadmap: Geothermal heat and power. *Renewable Energy Division, International Energy Agency, OECD/IEA, Paris ed.*
- Bertani, R. (2012). Geothermal power generation in the world 2005–2010 update report. *Geothermics*, 41, 1-29.
- Buonasorte G.-Cataldi R., 2008: Il calore di Madre Terra. La Geotermia nel mondo: Generalità e Sviluppo nel 2007. Anno del Pianeta Terra - Mostra itinerante su "La Geologia e l'Ambiente in Sicilia"; Tav. n. 30
- Buonasorte, G., Cataldi, R., Franci, T., Grassi, W., Manzella, A., Meccheri, M., & Passaleva, G. (2011). Previsioni di crescita della geotermia in Italia fino al 2030-Per un Nuovo Manifesto della Geotermia Italiana. *Pacini Edit., Pisa, Italy.*
- Charley, J., Cuenot, N., Dorbath, L., Dorbath, C., Haessler, H., & Frogneux, M. (2007). Large earthquakes during hydraulic stimulations at the geothermal site of Soultz-sous-Forêts. *International Journal of Rock Mechanics and Mining Sciences*, 44(8), 1091-1105.
- DiPippo, R. (2012). *Geothermal power plants: principles, applications, case studies and environmental impact.* Butterworth-Heinemann.
- European Parliament, 2017
http://www.europarl.europa.eu/atyourservice/en/displayFtu.html?ftuid=FTU_5.7.4.html
- Franco, A., & Villani, M. (2009). Optimal design of binary cycle power plants for water-dominated, medium-temperature geothermal fields. *Geothermics*, 38(4), 379-391.
- Franco, A. (2011). Power production from a moderate temperature geothermal resource with regenerative Organic Rankine Cycles. *Energy for Sustainable Development*, 15(4), 411-419.
- Gérard, A., Genter, A., Kohl, T., Lutz, P., Rose, P., & Rummel, F. (2006). The deep EGS (enhanced geothermal system) project at Soultz-sous-Forêts (Alsace, France).
- Häring, M. O., Schanz, U., Ladner, F., & Dyer, B. C. (2008). Characterisation of the Basel 1 enhanced geothermal system. *Geothermics*, 37(5), 469-495.
- Taylor, P. (2010). Energy technology perspectives 2010–scenarios and strategies to 2050. *International Energy Agency, Paris, 74.*
- IEA, O. (2015). Energy and climate change, world energy outlook special report.
- IEA, Energy Policies of IEA Countries – Italy, 2016, OECD/IEA, Paris.
- Krewitt, W., Nienhaus, K., Kleßmann, C., Capone, C., Stricker, E., Graus, W., ... & Samadi, S. (2012). Role and potential of renewable energy and energy efficiency for global energy supply.
- Lund, J. W., Freeston, D. H., & Boyd, T. L. (2011). Direct utilization of geothermal energy 2010 worldwide review. *Geothermics*, 40(3), 159-180.
- Rybach, L., & Mongillo, M. (2006). Geothermal sustainability-a review with identified research needs. *GRC Transactions*, 30, 1083-1090.

Stefansson, V. (2005, April). World geothermal assessment. In *Proceedings of the world geothermal congress* (pp. 24-29).

White, D. E. (1973). Characteristics of geothermal resources. *EOS, Trans., Am. Geophys. Union*, 54(4).

Chapter 3 - Overview of the different kinds of numerical geothermal models existing in literature

Local modelling

General remarks

With the advent of digital computers, the numerical solution of complex non-linear partial differential equations became possible in the late 1960s. However, the application of these techniques to modeling the behavior of geothermal reservoirs lagged behind their application in groundwater, and oil and gas reservoir modeling.

This is not surprising, as the coupling between mass and energy transport in a geothermal reservoir adds considerable complexity. Coupled heat and mass transfer in the highly heterogeneous environment of a geothermal reservoir is a very complex physical process. Often phase changes are involved and often the flow is complicated by the presence of additional chemical species such as gases or dissolved salts (O'Sullivan et al, 2001).

The numerical simulation of a geothermal reservoir is a well known field in the literature. First of all, for the kind of geothermal field: from medium enthalpy water- dominant field to dry-steam dominant field. The differences between the models deal with simulation domains (size and features), scenarios simulated (unperturbed or exploitation) and software used.

To implement activities with a numerical geothermal model, some steps must to be implemented. The elements here introduced are general, with some specific elements for EGS modelling.

Conceptual model and data collection

Before a computer model of a geothermal field can be set up, a conceptual model must be developed. A good understanding of the important aspects of the structure of the system and the most significant (physical and chemical) aspects in it is referred to as its "conceptual model". The conceptual model is usually represented by two or three sketches, showing a plan view and vertical sections of the geothermal system.

At local level, these sketches show the most important characteristics, such as surface manifestations, main geologic features, geophysical data, etc.

Setting up a conceptual model requires the synthesis of information from a multidisciplinary team composed of geologists, geophysicists, geochemists, reservoir engineers and project managers. Some of the raw data require expert interpretation before they can be used. In addition, the data sets tend to be incomplete and often the conceptual models proposed by the various contributing scientists and engineers are inconsistent or incorrect.

Thus, the "art" of computer modeling involves the synthesis of conflicting opinions, interpretation and extrapolation of data to set up a coherent and sensible conceptual model that can be developed into a computer model.

Model design — structure and boundary conditions

Recent models have a complex 3D. Most modelers have simply used a porous medium approach while a few have used double porosity models (Butler et al., 2000; Nakanishi and Iwai, 2000). Others have included explicit representation of a few dominant fractures and faults (Yamaguchi et al., 2000).

In some special cases the presence of small volume high-permeability fractures in a generally low-permeability matrix has an important effect on the reservoir behavior and the simple porous medium approach is not adequate.

The fracture network approach has been applied to studies of some hot dry rock (HDR) projects. HDR reservoirs are simpler to model in some respects because no convection occurs in the pre-exploitation state. On the other hand, the presence of fractures is important and even early HDR models have consisted of a large number of blocks, with very small blocks in and near the main fracture.

The use of large blocks in a geothermal model also makes the task of matching well-by-well performance difficult. Some modelers have overcome this difficulty by introducing embedded sub-grids around each well.

The most widely used simulators that have been used to implement these complex 3D models are STAR (Pritchett, 1995), TETRAD (Vinsome and Shook, 1993) and TOUGH2 (Pruess, 1990; Pruess et al., 1998).

A regular rectangular mesh structure is required by TETRAD and STAR, whereas TOUGH2 can handle general unstructured meshes. However, most geothermal models set up using TOUGH2 have some structure, such as layering.

The major codes all have the capability of handling multiphase, multi-component flows, and several models have included a reservoir fluid that is a mixture of water and carbon dioxide.

Specifically, TOUGH2 is a really used model in different fields (Todesco, 2009; Barelli et al., 2010; Romagnoli et al., 2010; Blanco-Martin et al., 2015).

Two important matters to be decided in setting up a model of a geothermal system are its size and the boundary conditions to be applied on the sides of the model.

Geothermal systems, apart from low-temperature systems, involve the large-scale convection of heat and mass, driven by the deep input of heat. The thermal boundary conditions (BC) usually represent the heat geothermal source entering the reservoir: heat flow from the bottom, fixed temperature values at bottom/top or intermediate layers and adiabatic/impermeable conditions. BCs usually also represent the natural manifestations, natural recharge, lateral or regional flows, wells withdrawal/ reinjection in the aquifers and hydraulic head both for the hydrological problem and for the heat transfer. The BC kinds are similar when considering fluid or heat transport (Fig. 4).

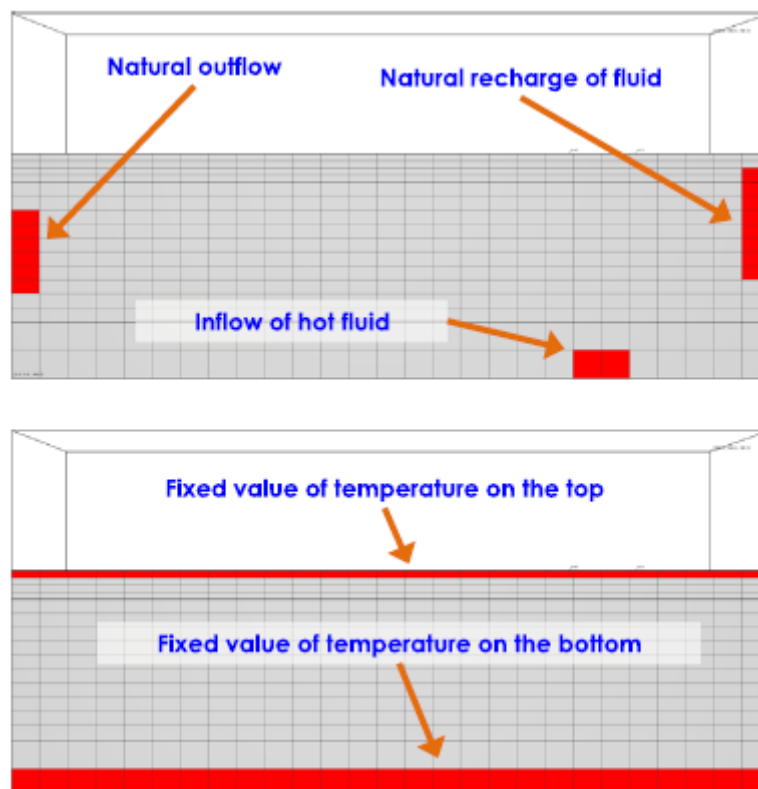


Fig. 4 Example of boundary conditions (both thermal and mass conditions) in a 3D numerical model grid (Franco & Vaccaro, 2014).

Mainly three types of BC are used:

- (1) First kind (or Dirichlet) condition — along a border or a boundary the hydraulic head or temperature are assigned.
- (2) Second kind (or Neumann) condition - along a border or a boundary the fluid or heat flux is assigned.
- (3) Third kind condition - transfer coefficients are used particularly for the hydraulic head.

Moreover, a single well or a singular point source can be assigned (implementing Dirac δ function).

In particularly dry reservoirs, conduction is the prevalent mechanism of heat transfer. In hydrothermal aquifers and traditional geothermal systems convection flow also contributes to the mass/heat transport phenomena. Thermophysical parameters database are also available in the most used codes. Anyway, as it is stated in this work, a characterization of the parameters should be site—dependent in order to obtain reliable and physically consistent results.

The initial conditions are usually the thermal gradient, pressure distribution in the domain and hydraulic head levels of rivers or reservoirs. To hold the results range near a specific value, constraints about max/min fluid rate, pressure or heat flow can be set.

Defining the boundary conditions and initial conditions is not a trivial task.

Fig. 5 summarizes the various steps described here: first the definition of geological elements and dimension of the reservoir, then spatial discretization and materials calibration, finally the definition of boundary conditions, initial conditions and definition of temporal domain.

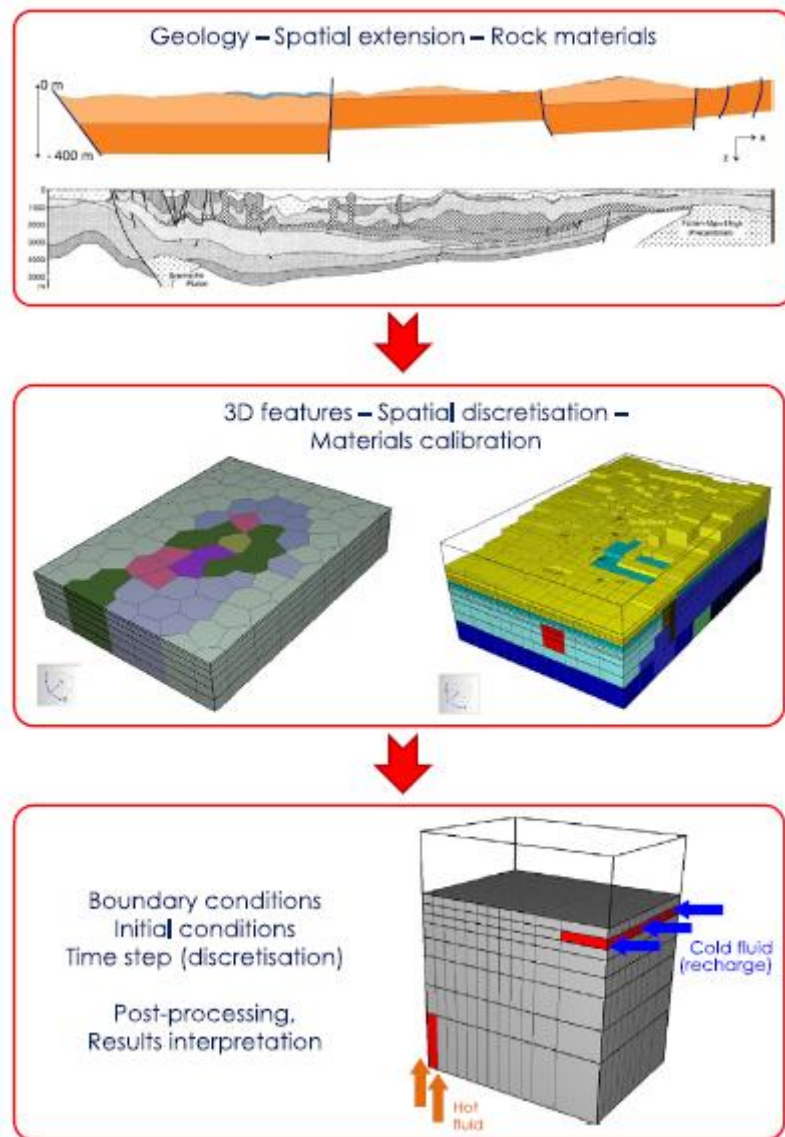


Fig. 5 Overall graphic view of the numerical simulation process (Franco & Vaccaro, 2014; Vogt et al., 2013).

Numerical integration of physical background in the equation systems

The integration of all the interdisciplinary inputs and procedures is the most challenging and crucial part of a modeling process. An important issue of this process deals with the quality of information and data flowing through the starting phase and the simulation itself. Numerical simulation must be treated and used as an iterative process, continuously changing and improving, as the information flow goes both ways (Ungemach et al, 2007).

There are different techniques for space discretization: finite difference, finite volume methods, as well as finite element methods. Different numerical integration techniques are implemented in codes and softwares.

Other softwares are used in literature and in industry. Many softwares have been developed and used by Research Institutes or Universities. In those softwares a lot of the most known resolution algorithms (from numerical analysis and calculus) are implemented.

The mesh refinement is a fundamental instrument that can be adopted to improve the analysis and optimize the computational tasks (concentrating for example the mesh number in the wells area or along the faults). Different techniques can be adopted for modeling of the faults, but the accuracy about the data in input (upflow / downflow, fluid rate, permeability, thermal anomaly) for these structures has to be very high to achieve reliable results.

All the most used softwares are multipurpose, involving the possibility of simulating different types of diffusion phenomena. Pre and post-processors are typically embedded in commercial softwares, so that graphical interface and elaboration of the data can be easily carried out.

Limitations and criticalities of numerical simulation of geothermal reservoirs

Notwithstanding its strategic importance, it is clear that numerical simulation of geothermal reservoirs has some important limitations:

- it strongly depends on the reliability and accuracy of the data;
- numerically stable models can be physically inconsistent.

The first limit can be also expressed by the principle “trash in– trash out”. It must be clear which is the physical–numerical problem to recourse numerical simulation for.

Moreover, the strong dependence of the results of the numerical analysis on the quality of the inputs and the difficulty that would be afforded in realizing the models must be subtitled: the data and the geo–thermo–physical parameters necessary are not always available or measurable.

One should evaluate if the numerical simulation is the more appropriate instrument to face a specific problem. Usually a problem can be simplified in a proper way to be solved according to calculus or numerical analysis without using dedicated softwares and complicated geometric domains. Reservoir model simulation has to be pursued only if it is the most suitable and appropriate way to elaborate a design strategy. “Lumped parameters” models can be very useful for some medium-low temperature fields, considering plain lithological layers. Sometimes, particularly for linear and simple problems, they can be satisfactory, in spite of more sophisticated elaborations.

One possible risk is to start “asking too much” or “asking too bad response” to the numerical models, making them “too much” or “too less powerful”. For example, starting from the same geological features of a field, a model can give different results depending on the resolution of the spatial distribution of the data.

Calibration

A general procedure for model calibration has developed (O’Sullivan, 1985; Bodvarsson et al., 1986; Pruess, 1990a). It consists of natural state modeling followed, if possible, by history matching. Most modelers have carried out at least the first step of natural state modeling, which consists of running the model for a long time in a simulation of the development of the geothermal field over geological time. The temperature distribution and surface outflows of heat and fluid (water and steam) in the model are compared with measured field data and the permeability structure of the model is adjusted to achieve a satisfactory match. The magnitude and location of the deep hot upflow may also need to be adjusted. The calibration of the natural state may require many iterations before a good match to the field data is achieved.

For EGS simulations, the geothermal fields for which models have been set up recently vary widely in terms of their state of development. Some have been operating for many years and some have a very short or no production history. A second history matching stage of calibration has been carried out for most systems that have some production history.

The process of model calibration both for natural state matching and past history matching is difficult and time consuming. It is sometimes difficult to decide which part of the model structure should be adjusted to improve the match to a particular field measurement. Some use of computerised model calibration has been made in improving a few geothermal models (White, 1995; Finsterle et al., 1997; O’Sullivan et al., 1998; White et al., 1998). In this case the computer is used to systematically adjust a few parameters until the differences between model results and field data are at a minimum. It is demanding in terms of

computer time and requires some manual intervention to select the particular parameters to be adjusted. These techniques replace the manual model adjustment by trial-and-error with an automated process that obtains optimal model parameters by computer. In addition to streamlining the model calibration process, inverse techniques provide quantitative model acceptance criteria, potentially leading to more reliable models with less subjective bias. The increased computational demands of inverse modeling have prompted the development of parallel processing techniques, not only for high-end massively parallel platforms, but also for economical clusters of workstations or PCs (Finsterle & Pruess, 1999). Geothermal reservoir models have usually been constrained by natural state modeling and well test analyses, and have been calibrated against reservoir engineering type data (flow rates and enthalpies of wells, reservoir pressures and temperatures, tracer concentrations). A relatively new trend is the utilization of geophysical and geochemical observations for model calibration, such as resistivity and microgravity changes, self-potential, microseismics, and tracer data (Osato et al., 1998; Rose et al., 1999; Simiyu, 1999).

A brief review of Italian case studies referred to experimentally investigated geothermal fields

In this paragraph few examples of numerical simulations of Italian geothermal reservoirs are introduced (Franco & Vaccaro, 2014). They are referred to very well known geothermal fields for which a lot of experimental data are also available.

Larderello geothermal field, 2010 model

Larderello field (Italy) is one of the most anciently known and studied geothermal areas of the world. This field has been widely drilled and developed, with an almost 100-year-old history in geothermal energy utilization for power purposes. Average fluid production in the Larderello field, after the most recent explorations and improvements is now about 3700 t/h. The exploration extended in the early 1950s to the near Travale field (10–15 km SE of Larderello), which has now increased its fluid production to an average value of 1000 t/h. For this reason, when talking about large scale model of this geothermal system, usually one can talk about the Larderello-Travale geothermal field.

A numerical model about the field has been recently realized and improved, increasing the dimensions of the geological domain considered (Romagnoli et al., 2010; Barelli et al., 2010; Arias et al., 2010). The model domain extent is 4,900 km² (70 km each side), with a total thickness of 7.5 km. The grid is made of 10,000 cells and 16 vertical layers. The geological scheme refers to five main rock formations: clayey–shaley caprock (0–500 m), fractured carbonate reservoir (500–1,000 m), metamorphic reservoir (1,000–5,000 m) and granitic intrusion as heat source of the system.

Sixteen rock materials are considered and an impermeability condition along the boundaries is assigned. Fixed state (time invariant) conditions of temperature are considered at the top (15 °C, atmospheric pressure) and at the bottom of the producing layer (350–400 °C). Natural manifestations and cold inflow from the shallow aquifers are the only interactions with the external environment. The simulation of natural state has been carried out (millions of years as temporal scale) and a simulation of the exploitation history of the field has also been modeled. The historical data of 700 wells have been represented with 20 “virtual” wells. The conclusions are that only few changes in the conditions of the natural system have been caused by industrial development of the area (Romagnoli et al., 2010).

Larderello geothermal field, 2008 model

A different model of this field has been proposed by Della Vedova et al. (2008). This model deals only with the natural state of the geothermal system, without considering the industrial exploitation. A very large temporal scale is considered (8–12 millions of years). The extent of the considered domain is 42 x 26 km², with a total thickness of 10 km. The total depth of the model is very high, to include the K-horizons and the data from fluid inclusions. K-horizons are considered to be the main reservoir bottom, corresponding to the

400 °C isotherm; collocated between 3,000 m in the Larderello zone and 104 m in the Travale zone. The mesh cell size is 1 x 1 x 0.3 km³. The upper surface boundary conditions are 20 °C and 0.1 MPa, impermeable and adiabatic conditions are assigned at the lateral boundaries. The bottom boundary is assumed to be impermeable and at a fixed temperature of 400–600 °C. A sensitivity analysis about thermal parameters is also considered. A lot of simulation have been run to match a composite target function, due to the uncertainty about several input data (geometry, rock data). The work considered is an example of deep field simulation, oriented to the comprehension of the deep field phenomena more than to a sustainable exploitation approach.

Mt. Amiata geothermal system

For the Tuscan geothermal system of Mt. Amiata a numerical model about the field has been recently realized (Barelli et al., 2010a).

The fields of Bagnore and Piancastagnaio have been explored and drilled (more than 100 wells) for about 50 years. In this field two main reservoirs are present: the first one is in the carbonatic formations, between 500 and 1,000 m deep, at average temperature of 150–220 °C; the second reservoir is in the Paleozoic metamorphic basement at depths of 2,500–4,000 m, at temperatures of 300–350 °C. The Mt. Amiata Volcanic Complex has a total area of 80 km². The peculiarity of the model is not only to analyze the exploitation of the reservoir but also to verify the possibilities of interaction between a phreatic aquifer (separated from the shallow aquifer by few hundred meters of impermeable formations) and the geothermal system. Moreover, another particular aspect is that the two main reservoirs are characterized by gaseous caps (gas, vapor), in structures named “traps”. This is a peculiarity of Mt. Amiata field, occurring in the definition of the pressure distribution and fluid circulation model. The surface extension of the model is more than 1,100 km², with a total thickness between -4 km and 1,738 km (a.s.l., Mt. Amiata top elevation). A time-constant heat flow (average 400 mW/m², with peaks of 600–700 mW/m²) is the bottom boundary condition. The model is globally closed, referring to inflow–outflow of water. The outputs match with the field data (Barelli et al., 2010a).

The Campi Flegrei magmatic system

Heat transfer in terms of conduction/convection is not easy to compute in active volcanic areas, where the thermal regime is strongly dependent upon the architecture of the magmatic plumbing system and its evolution through time. Accurate thermal models of magmatic intrusions require a detailed 3D definition of their geometries, which arises from thorough geological and geophysical studies.

This is the case for Campi Flegrei caldera (CFC), an active volcanic system located in a densely inhabited area (Napoli, Southern Italy), for which a large amount of geological, geophysical, petrological and geochemical data has been collected in the past decades. Such a large amount of data has been collected at CFC because the volcanic hazard is extremely high, also due to its explosive character. The CFC is in unrest since decades, with numerous uplift episodes, seismicity and strong degassing from a volatile rich source.

A 3D conductive/convective thermal model has been developed (Di Rienzo et al., 2016) with the aim of describing the thermal evolution and present state of the CFC magmatic system in the last 44 ka. The large availability of geophysical, geological and geochemical data integrated in 3D considerations have provided stringent constraints on boundary conditions, particularly depth, size and timing of the emplaced magmatic bodies, and the role played by the convective regime taking place within the hydrothermal system discontinuously permeating the caldera fill.

The Heat3D modeling results (Wohletz, 1999) show that both conduction since 44 ka and convection since 39 ka have played an important role in the thermal evolution of the CFC and have led to a better understanding of the evolution of the deep and shallow reservoirs involved in the last 44 ka volcanic activity. The estimation of the temperatures in 3D has also defined the time necessary to hydrothermal convection to be active. It has also allowed localizing, with a small uncertainty in x or y axis, the point coordinates, where the thermal gradient is calculated, in order to reproduce the measured thermal profiles. The thermal distribution resulting from the described evolution of the CFC magmatic system since

44 ka up to now, at the center of the CFc shows temperatures of 600–700 °C at 4–5 km of depth, in agreement with the estimated temperature for the brittle-ductile transition.

Modeling returns, in correspondence of the drillings at Mofete, San Vito and Licola, thermal profiles in agreement with the measured ones and the thermal gradient peaks at the caldera margins, in correspondence to the anomalies in measured surface gradients.

The Campi Flegrei hydrothermal system

A different approach to modeling the geothermal-hydrothermal system at CF has been implemented to understand the unrest episodes of the caldera. These set of models analyse in detail the physical behavior of the reservoir with the use of TOUGH2 code (Todesco, 2009). The study focusses on the effects of a deep fluid source on the evolution of the shallow hydrothermal system. Numerical simulations have been carried out to describe the fluid circulation as the system goes through an unrest phase, followed by a quiet period. During the unrest, specific properties of the fluid source (flow rate, fluid composition, source size, and unrest duration) are modified with respect to selected baseline values.

Two observable parameters, as gas composition and gravity changes, were chosen to represent the system evolution during and after the unrest period. The results describe the temporal evolution of these two observables and allow comparisons of the effects of different source properties.

The unrest period causes measurable changes in both of the observable parameters. These changes may last for several years, regardless of the unrest duration. Short-term changes reflect not only the characteristics of the unrest, but also the rock properties and initial conditions. With a different choice of rock permeability and initial conditions, the beginning of the unrest phase could pass unnoticed.

The long-term evolution is more strictly related to the characteristics of the unrest and to source properties, with greater unrest intensity leading to more extreme variations in the two observables. Peak values are reached only when the unrest is over, and the perturbation of the parameters lasts for decades, despite the steady behavior of the source during the quiet period.

Simulation results can lead to some interesting considerations in terms of volcano monitoring and hazard evaluation and emphasize the role of fluid flow rate in generating the signals that are eventually captured by the monitoring network. The important influence of permeability on the simulated observables confirms the relevance of rock properties in the control of the evolution of a volcanic system.

Continental and Basin Modelling for the Enhanced Geothermal Systems exploration

In recent years EGS conditions have been identified at drillable depths in many locations within Europe (Genter et al., 2003) (Fig. 6). These areas have been selected largely on the basis of observations of high near surface temperature gradients derived from surface heat flow values and magmatism (e.g. volcanic areas such as Iceland and Tuscany in central Italy) and or relatively high temperatures assessed in deep boreholes drilled mainly for hydrocarbon exploration and production (e.g. Soultz-sous-Forêt, Landau).

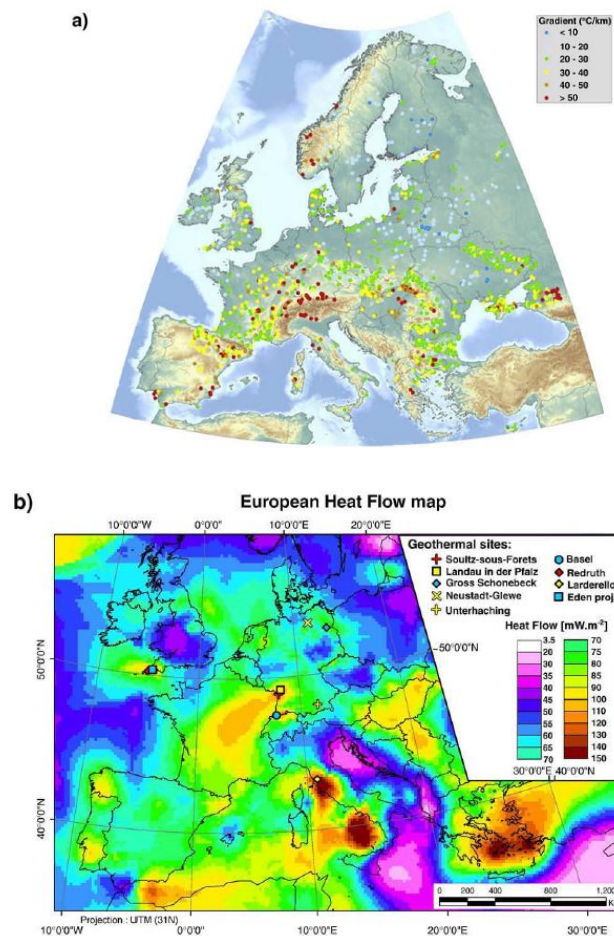


Fig. 6 Thermal signatures of Europe, described by measured temperature gradients and interpolated heat flow data. (a) Temperature gradient values (°C/km) in Europe extracted from the international heat flow database <http://www.heatflow.und.edu> and separated in 6 classes; (b) Corresponding surface heat flow extended with additional data (Haenel et al., 1988; Hurtig et al., 1992; Hurter and Haenel, 2002).

In addition, geological information (Fig. 7), world stress map information (Heidbach et al., 2008, Fig. 8) and natural seismicity (Fig. 9) can be used to identify active deforming basins and basement areas which are critically stressed. Microseismic monitoring shows that critically stressed pre-existing faults and fractures are preferential pathways for hydraulic stimulation, marked by a shear mode of fracturing (Häring et al., 2008). From exploration and production wells it appears that deep and widespread convective hydrothermal systems in the basement rock in favourable settings are capable of enhancing local heat flow. In the basement, natural fracture networks are conduits for fluid flow (Sanjuan et al., 2006).

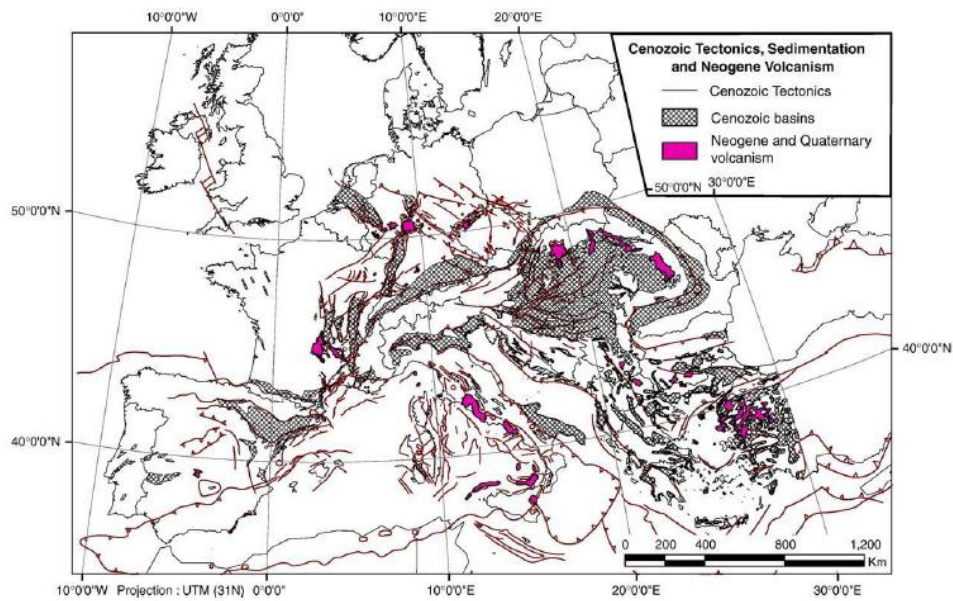


Fig. 7. Major tectonic fault zones, Cenozoic sedimentary basin configuration and distribution of Neogene and Quaternary volcanism in Europe (Cloetingh et al, 2010) .

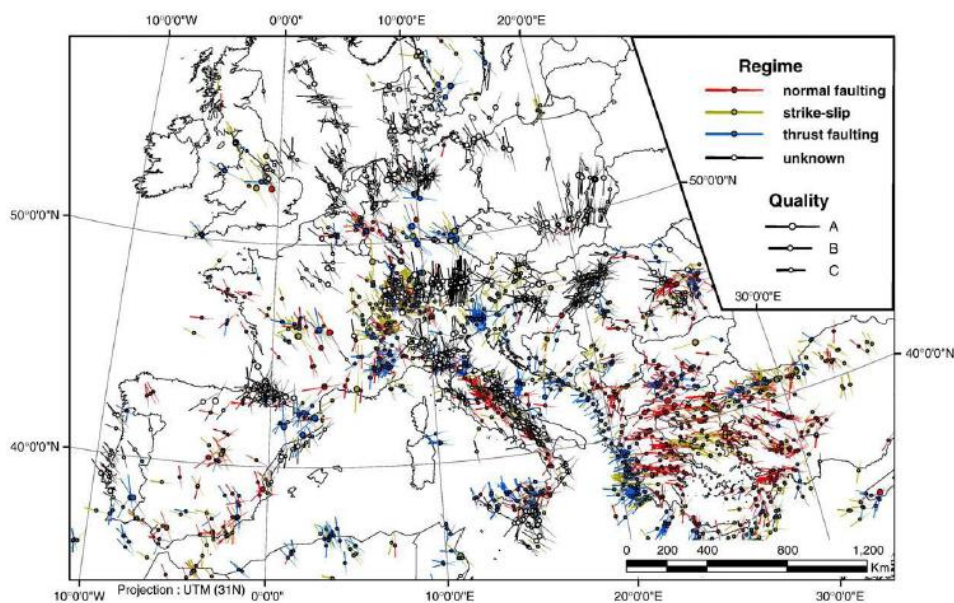


Fig. 8. Intraplate stress map for Europe, displaying the present-day orientation of the maximum horizontal stress (SHmax). Different colours stand for different stress regimes. Stress map data are extracted from the World Stress Map database (Heidbach et al., 2008)..

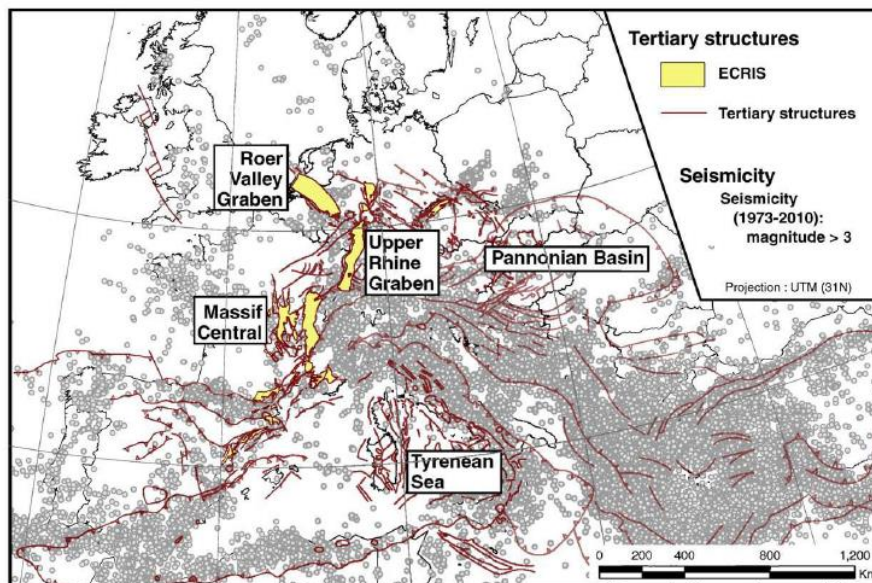


Fig. 9. Natural seismicity and main tectonic provinces in Europe (Cloetingh et al, 2010).

Continental Modelling

Assessment of exploration potential of continental intraplate regions for EGS is generally not taking into account lithosphere-scale tectonic models. At the same time, tectonics has been recognized to be of prime importance for the creation of favourable thermo-mechanical conditions (Genter et al., 2003). Instead, tectonic models can be used for the following purposes (Cloetingh et al, 2010):

- to understand the relationship between proven favourable conditions for EGS and underlying tectonic processes. Through this relationship new prospective EGS areas can be outlined in areas where near surface (well) data are missing. This integrated lithosphere scale approach sets the stage for more detailed follow up local analyses for targeted exploration purposes;
- to discriminate between regional tectonic heat flow and local hydrothermal and magmatic anomalies. This allows improving the robustness of vertical and horizontal extrapolation of temperatures, where no well control is available;
- to constrain crustal rheology and stress regimes. At large scale, tectonic models are capable to quantitatively assess active deformation zones as a function of intraplate stress field and layered lithosphere rheology. In more detail, tectonic models are capable to quantitatively predict the interplay of crustal stress and rheology (faults and fractured zones). These play an important role in fracture formation and opening of pre-existing fractures, induced (and triggered) seismicity and natural permeability of fractured rock mass.

The tectonic models that can be implemented include (Cloetingh et al, 2010):

Thermal models of the lithosphere. Key geodynamic factors control the thermal state and stress conditions in Europe's continental lithosphere. Introducing basic concepts on the compositional structure of the lithosphere and its relationship with thermal structure of the Earth up to ca. 100 km depth, the first order thermal constraints from surface heat flow and deep subsurface geophysical data sets can be jointly used to build and constrain thermal models of the lithosphere beyond well control. First order patterns can be well explained by both compositional controls and active tectonic processes. Modeled tectonic heat flows are limited to values of about 100 mW m^{-2} , but can occur in large areas which share the same geodynamic context. Higher values, observed locally are most likely the result of hydrothermal processes and magmatism.

Rheological models. The drivers for earth deformation are plate boundary forces, resulting in relatively uniform intraplate stress conditions. Rheological models for Europe are validated by testing if spatial

distributions of relatively low strength, predicted by the model, correspond with zones of active deformation, whereas relatively strong zones are shielded from deformation. The first order thermal and rheological model predictions fit in general very well with overall patterns of earthquake distribution, and localization of deformation and associated partitioning of relative rigid zones in Europe derived from geodetic measurements.

The combined interpretation of the thermal and rheological state of the lithosphere is in close agreement with independent other geophysical data such as the gravity field.

Validation of rheological models through analogue and numerical modelling of deformation processes over geological timescales demonstrates that first order rheological models fail to take into account lithosphere and crustal scale weak zones which are inherited from previous deformation. These weak zones/faults play an important role in distributing stress and strain in the upper crust representing the top 10 km in the Earth. Detailed geomechanical models linking crustal stresses and sub basin fault fabrics allow a validation of stress distributions in basins.

This type of modelling aids in predicting critically stressed faults and fractures. Active faults that most likely represent active hydrothermal zones enhance the probability of EGS favourable conditions, both in terms of hydraulic stimulation as well as natural fracture permeability).

The added value of tectonic modelling is highlighted for selected tectonic settings, marked by a specific deformation style. This relationship allows to approach in a rational fashion continent-scale exploration for geothermal resources and building hypotheses for thermal and mechanical characterization at depth.

Numerical kinematic thermal models allow quantifying the effect of these tectonic processes, demonstrating the key role of subcrustal mantle processes in heat flow elevation over broad areas.

This relationship allows to approach in a rational fashion continent-scale exploration for geothermal resources and to build hypotheses for both thermal and mechanical characterization at depth. The most favourable conditions for geothermal systems prevail in the active volcanic areas related to the deep lithosphere processes.

Unconventional high enthalpy geothermal systems could be developed in deeply buried fractured, karstified carbonate rocks in the Pannonian basin. Such rocks are found in 4–5 km depth overlain by Neogene sediments. The buried carbonate reservoirs comprise closed systems with water temperature of 200 °C, and overpressure higher than 30 MPa.

Basin Modelling

Temperature maps are of primary interest for the development of new geothermal projects (e. g., electricity production, heating). A geostatistical analysis of temperature in the French sedimentary basins was implemented (Bonté et al, 2010), that carried out a good estimation of the temperature in those areas that had a high density of temperature values.

A first step is a compilation of available deep-temperature data in sedimentary basins. A geostatistical treatment at country-scale is implemented with a 3D thermal model. The outputs are temperature maps, together with associated uncertainties.

Temperature maps are constructed using temperature data located in the French sedimentary basins. Most of the temperature data recorded in oil exploration boreholes needs to be corrected as thermal equilibrium is not achieved when the measurement is performed. An advanced analytical methodology [Goutorbe et al., 2007] was implemented, with a 3D kriging interpolation method constrained by a geostatistical data analysis in order to build a 3D thermal block.

The final representation is a series of iso-depth maps of the subsurface temperature, which can be used during the initial exploration phases of geothermal energy development programs. Temperature maps over geological structures, such as a geological interface for pre-targeted area of interest, can also be extracted from the 3D thermal block. As an example, in this paper we present iso-depth temperature maps in the French sedimentary basins, as well as iso-temperature maps and vertical cross-sections at the country scale (Fig. 10).

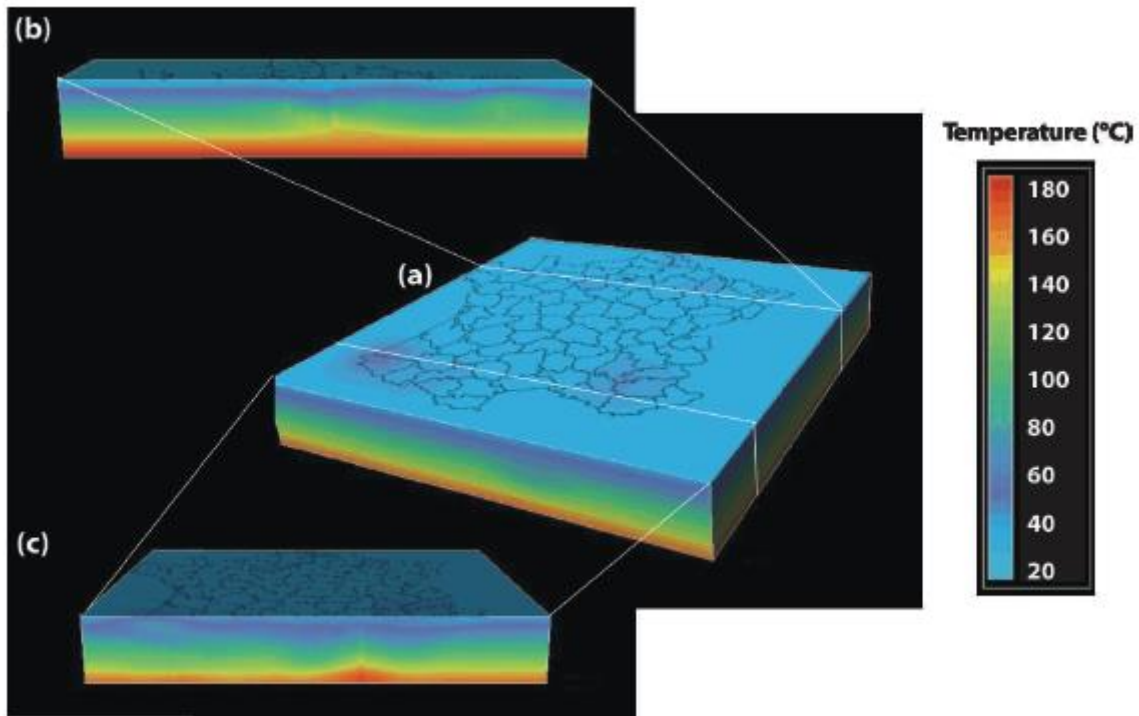


FIG. 10. Vertical slices in the 3D thermal block. The thickness of the block is 6000 m. (a) 3D thermal block showing the location of the slices. (b) Vertical slice from southern Aquitanian basin to Provence basin. (c) Vertical slice from western France to Alsace areas crossing the central part of the Paris basin (Bonté et al, 2010).

Analysis of temperature anomalies on a countrywidescale reveals anomalous zones within a restricted depth range, which is probably related to the maximum depth of any associated basins. However, it must be noted that fluid circulation within aquifers may also be invoked to explain specific features such as unexpected low temperature gradients within a given depth range.

In order to conduct the detailed exploration of geothermal energy in the Paris Basin, it is possible to take the available temperature values collected and used them to calibrate a model for the Paris Basin (Bonté et al, 2013). The model is a tectonic-heat flow modelling with a six-layer model for the sedimentary infill, plus three additional layers for the lithosphere.

The model describes the temperature through a purely conductive methodology, with the variation of temperature being the result only of differences in heat production and thermal conductivity.

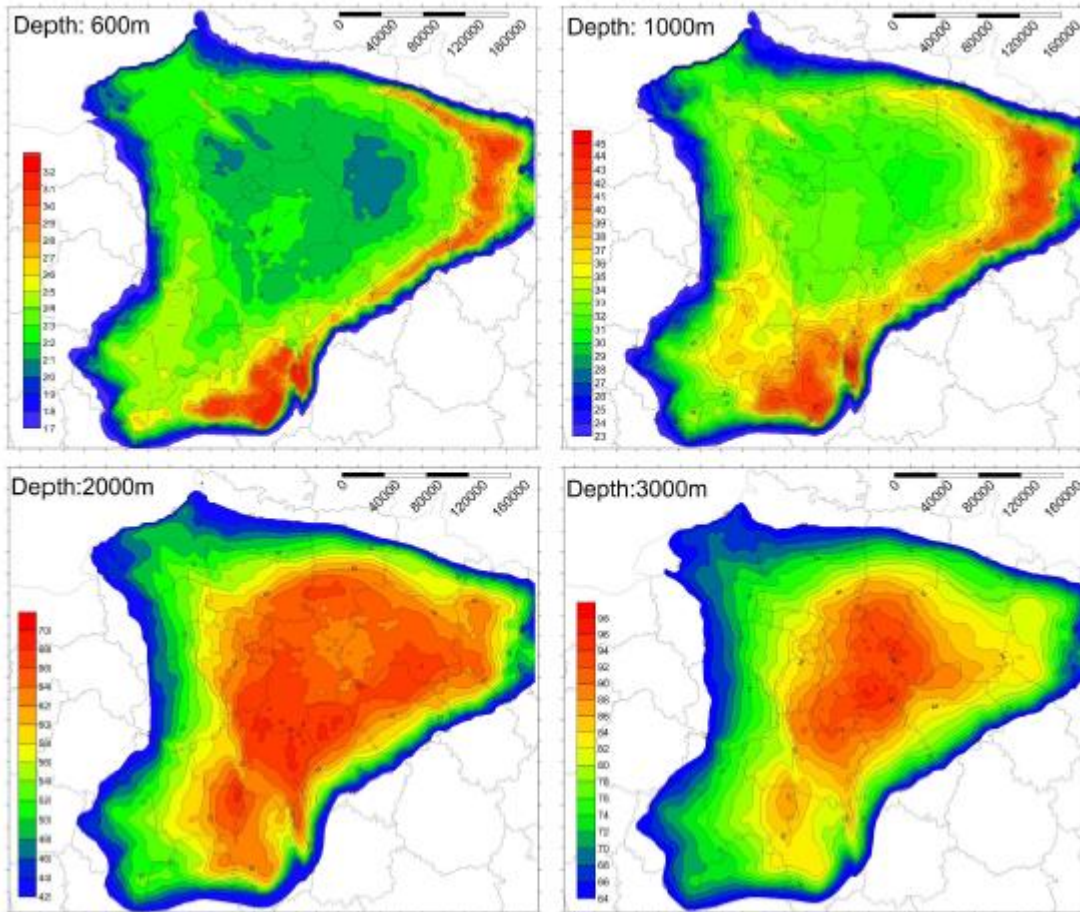


FIG. 11. Mapping representation of temperatures at several isodepths (600m, 1000m, 2000m, and 3000m), from the tectonic-heat flow modeling (Bonté et al, 2013).

Analysis of the temperature anomalies shows that in the sedimentary pile, the “Schistes Carton” (of Toarcian age) is the main impacting layer with a low thermal conductivity. Associated with the “bowl” shape of the sedimentary layers in the Paris Basin, the positive anomalies below this layer of low conductivity are localised on the borders of the basin at a shallow depth (i.e. 1000m) and “migrate” with depth toward the centre of the basin (Fig. 11). The basement also plays a role in the temperature variation in the sedimentary pile, with the heat flow at the base of the sediments indicating a high heat production that is probably related to radiogenic decay from an intrusive body or to a thick, Carboniferous, clay-filled halfgraben.

References

- Arias, A., Dini, I., Casini, M., Fiordelisi, A., Perticone, I., & Dell'Aiuto, P. (2010, April). Geoscientific feature update of the Larderello–Travale geothermal system (Italy) for a regional numerical modeling. In *Proceedings world geothermal congress* (p. 11).
- Barelli, A., Cei, M., Lovari, F., & Romagnoli, P. (2010). Numerical modeling for the Larderello–Travale geothermal system, Italy. In *Proceedings world geothermal congress*.
- Barelli, A., Ceccarelli, A., Dini, I., Fiordelisi, A., Giorgi, N., Lovari, F., & Romagnoli, P. (2010, April). A review of the Mt. Amiata geothermal system (Italy). In *Proceedings world geothermal congress* (pp. 1-4).
- Blanco-Martin, L., Reagan, M., Rutqvist, J., Valladao, C., Zheng, L.(ed.) (2015) Proceedings of the TOUGH Symposium 2015. Lawrence Berkeley National Laboratory.
- Bodvarsson, G., Pruess, K., & Lippmann, M. (1986). Modeling of geothermal systems. *Journal of petroleum technology*, 38(09), 1-007.
- Bonté, D., Guillou-Frottier, L., Garibaldi, C., Bourguine, B., Lopez, S., Bouchot, V., & Lucazeau, F. (2010). Subsurface temperature maps in French sedimentary basins: new data compilation and interpolation. *Bulletin de la Société Géologique de France*, 181(4), 377-390.
- Bonté, D., Van Wees, J. D., Guillou-Frottier, L., Bouchot, V., & Serrano, O. (2013, June). Deep temperatures in the Paris Basin using tectonic-heat flow modelling. In *European Geothermal Congress EGC 2013* (pp. 10-p).
- Butler, S. J., Sanyal, S. K., Henneberger, R. C., Klein, C. W., Puente, H. G., & de León, J. S. (2000). Numerical Modeling of the Cerro Prieto Geothermal Field, Mexico. *TRANSACTIONS-GEOTHERMAL RESOURCES COUNCIL*, 401-406.
- Charley, J., Cuenot, N., Dorbath, L., Dorbath, C., Haessler, H., & Frogneux, M. (2007). Large earthquakes during hydraulic stimulations at the geothermal site of Soultz-sous-Forêts. *International Journal of Rock Mechanics and Mining Sciences*, 44(8), 1091-1105.
- Cloetingh, S. A. P. L., Van Wees, J. D., Ziegler, P. A., Lenkey, L., Beekman, F., Tesauro, M., ... & Bonté, D. (2010). Lithosphere tectonics and thermo-mechanical properties: an integrated modelling approach for Enhanced Geothermal Systems exploration in Europe. *Earth-Science Reviews*, 102(3), 159-206.
- Della Vedova, B., Vecellio, C., Bellani, S., & Tinivella, U. (2008). Thermal modelling of the Larderello geothermal field (Tuscany, Italy). *International Journal of Earth Sciences*, 97(2), 317-332.
- DiPippo, R. (2012). *Geothermal power plants: principles, applications, case studies and environmental impact*. Butterworth-Heinemann.
- Di Renzo, V., Wohletz, K., Civetta, L., Moretti, R., Orsi, G., & Gasparini, P. (2016). The thermal regime of the Campi Flegrei magmatic system reconstructed through 3D numerical simulations. *Journal of Volcanology and Geothermal Research*, 328, 210-221.
- Finsterle, S., Pruess, K., Bullivant, D. P., & OSullivan, M. J. (1997). *Application of inverse modeling to geothermal reservoir simulation*(No. LBNL--39869; CONF-970114--1). Lawrence Berkeley National Lab., CA (United States).
- Finsterle, S., & Pruess, K. (1999). Automatic calibration of geothermal reservoir models through parallel computing on a workstation cluster. *Lawrence Berkeley National Laboratory*.

- Franco, A., & Villani, M. (2009). Optimal design of binary cycle power plants for water-dominated, medium-temperature geothermal fields. *Geothermics*, 38(4), 379-391.
- Franco, A. (2011). Power production from a moderate temperature geothermal resource with regenerative Organic Rankine Cycles. *Energy for Sustainable Development*, 15(4), 411-419.
- Franco, A., & Vaccaro, M. (2014). Numerical simulation of geothermal reservoirs for the sustainable design of energy plants: a review. *Renewable and Sustainable Energy Reviews*, 30, 987-1002.
- Genter, A., Guillou-Frottier, L., Feybesse, J. L., Nicol, N., Dezayes, C., & Schwartz, S. (2003). Typology of potential hot fractured rock resources in Europe. *Geothermics*, 32(4), 701-710.
- Gérard, A., Genter, A., Kohl, T., Lutz, P., Rose, P., & Rummel, F. (2006). The deep EGS (enhanced geothermal system) project at Soultz-sous-Forêts (Alsace, France).
- Haenel, R., Rybach, L., & Stegena, L. (1988). Fundamentals of geothermics. In *Handbook of terrestrial heat-flow density determination* (pp. 9-57). Springer Netherlands.
- Häring, M. O., Schanz, U., Ladner, F., & Dyer, B. C. (2008). Characterisation of the Basel 1 enhanced geothermal system. *Geothermics*, 37(5), 469-495.
- Heidbach, O., Tingay, M., Barth, A., Reinecker, J., Kurfeß, D., Müller, B., 2008. The World Stress Map database release 2008. doi:10.1594/GFZ.WSM.Rel2008.
- Hurter, S., Haenel, R., 2002. Atlas of Geothermal Resources in Europe. Commission of the European Communities, EC Publication Nr. 1781 1.
- Hurtig, E., Cermak, V., Haenel, R., & Zui, V. (1992). Geothermal Atlas of Europe, International Association for Seismology and Physics of the Earth's Interior, 156 pp. *Hermann Haack GmbH, Gotha*.
- Nakanishi, S., & Iwai, N. (2000, May). Reservoir simulation study of the Onikobe geothermal field, Japan. In *Proceedings of world geothermal congress*.
- O'Sullivan, M.J., 1985. Geothermal reservoir simulation. *Energy Research* 9, 313–332.
- O'Sullivan, M. J., Bullivant, D. P., Follows, S. E., & Mannington, W. I. (1998, May). Modelling of the Wairakei–Tauhara geothermal system. In *Proceedings of the TOUGH Workshop '98, Berkeley, California*(pp. 4-6).
- O'Sullivan, M. J., Pruess, K., & Lippmann, M. J. (2001). State of the art of geothermal reservoir simulation. *Geothermics*, 30(4), 395-429.
- Osato, K., Sato, T., White, S. P., Burnell, J., & Yokomoto, S. (1998, January). DEVELOPMENT OF AN INTEGRATED GEOTHERMAL RESERVOIR MODELLING SYSTEM (DATABASE & MAPPING SYSTEM FOR RESERVOIR MODELING/SIMULATION/MANAGEMENT, PRE-PROCESSOR SYSTEM AND POST-PROCESSOR SYSTEM). In *Proceedings of the 23rd Workshop on Geothermal Reservoir Engineering, Stanford University, Stanford, California* (pp. 26-28).
- Pritchett, J.W., 1995. STAR: A geothermal reservoir simulation system. In *Proceedings World Geothermal Congress '95, Florence, 18–31 May 1995*, pp. 2959–2963.
- Pruess, K. (1990). *TOUGH2: A general-purpose numerical simulator for multiphase fluid and heat flow* (p. 102). Berkeley, California: Lawrence Berkeley Lab..
- Pruess, K. (1990). Modeling of geothermal reservoirs: fundamental processes, computer simulation and field applications. *Geothermics*, 19(1), 3-15.

- Pruess, K., Oldenburg, C., & Moridis, G. (1998). Overview of TOUGH2, version 2.0. *LBNL–Lawrence Berkeley National Laboratory, Report: LBNL-41995, University of California, Lawrence Berkeley National Laboratory*, 307-314.
- Romagnoli, P., Arias, A., Barelli, A., Cei, M., & Casini, M. (2010). An updated numerical model of the Larderello–Travale geothermal system, Italy. *Geothermics*, 39(4), 292-313.
- Rose, P., Goranson, C., Salls, D., & Kilbourn, P. (1999, January). Tracer testing at Steamboat Hills, Nevada, using fluorescein and 1, 5-naphthalene disulfonate. In *Proc. The 24th Workshop on Geothermal Reservoir Engineering, Stanford University, Stanford, CA*.
- Sanjuan, B., Pinault, J. L., Rose, P., Gérard, A., Brach, M., Braibant, G., ... & Touzelet, S. (2006). Tracer testing of the geothermal heat exchanger at Soultz-sous-Forêts (France) between 2000 and 2005. *Geothermics*, 35(5), 622-653.
- Simiyu, S. M. (1999). Seismic application to geothermal evaluation and exploitation, Southern Lake Naivasha. 24th W/shop on Geoth. Res. Engineering.
- Stefansson, V. (2005, April). World geothermal assessment. In *Proceedings of the world geothermal congress* (pp. 24-29).
- Todesco, M. (2009). Signals from the Campi Flegrei hydrothermal system: Role of a “magmatic” source of fluids. *Journal of Geophysical Research: Solid Earth*, 114(B5).
- Ungemach, P., Papachristou, M., & Antics, M. (2007, May). Renewability versus sustainability. A reservoir management approach. In *European Geothermal Conference, Unterhaching, Germany*.
- Vinsome, P. K. W., & Shook, G. M. (1993). Multi-purpose simulation. *Journal of Petroleum Science and Engineering*, 9(1), 29-38.
- Vogt, C., Iwanowski-Strahser, K., Marquart, G., Arnold, J., Mottaghy, D., Pechinig, R., ... & Clauser, C. (2013). Modeling contribution to risk assessment of thermal production power for geothermal reservoirs. *Renewable energy*, 53, 230-241.
- White, D. E. (1973). Characteristics of geothermal resources. *EOS, Trans., Am. Geophys. Union*, 54(4).
- White, S. P. (1995). *Inverse Modelling of the Kawerau Geothermal Reservoir*, NZ (No. GEO-PROC-95-02). NZ Institute for Industrial Research and Development, Lower Hutt, NZ.
- White, S. P., Young, R. M., & Kissling, W. M. (1998, May). Using ITOUGH2 to improve geothermal reservoir models. In *Proceedings of the TOUGH Workshop '98, Berkeley, California* (pp. 4-6).
- Wohletz, K.H., 1999. HEAT3D: Magmatic Heat Flow Calculation. Los Alamos National Laboratory computer code LA-CC 99-27 (<http://geodynamics.lanl.gov/Wohletz/Heat.htm>). Los Alamos, New Mexico
- Yamaguchi, S., Akibayashi, S., Rokugawa, S., Fujinaga, Y., Tenma, N., & Sato, Y. (2000, May). The numerical modeling study of the Hijiori HDR test site. In *Proceedings of the World Geothermal Congress*. Auckland: International Geothermal Association.

Chapter 4 – Presentation of the main characteristics of HEAT3D numerical code

The KWare HEAT3D geophysical heat flow simulator

A large heat source is one of features that is essential to making a geothermal resource commercially viable. In most of numerical simulations that usually include the reservoir but not the crystalline basement, the mesh boundary conditions taken at the bottom usually are constant, i.e. the heat flux incoming on the base of the reservoir is assumed constant and equal to the heat flux outcoming from the surface (e.g. Todesco & Giordano, 2010). If in the simulation we include the crystalline basement and the magma chamber, a numerical model for quantitative heat transfer from the heat source in geologic materials must be used.

The quantitative study of heat transfer in geologic materials has evolved significantly (Lovering, 1935; Carslaw & Jaeger, 1947; Turcotte & Schubert, 1982; Furlong et al., 1991). Numerical computational techniques now make solution possible for heat transfer equations that express multiple dimensions with non-linear elements of rock heterogeneity, changing source character, and spatially and temporally varying convection (Kolstad & McGetchin, 1978; Zyvoloski, 1987), the latter of which introduces the detailed account for heat transfer in porous media.

The open KWare HEAT3D code (Wohletz, 1999) represents an evolving effort to quantify heat flow in and around magma bodies in order to better understand geothermal gradients in volcanic areas. The code models the thermal state by finite difference solution of energy and momentum conservation equations (i.e., Navier-Stokes equations). These equations express heat transfer by conduction and convection with nonlinearities arising from variations of thermal conductivity within a heterogeneous material and heat sources/sinks. We assume the existence of a heat source at depth, transferring the heat to other layers by conduction/convection and evaluate its characteristics.

HEAT3D is a 32-bit application suitable for workstations operating Windows O.S.. The graphical interface is readily used to develop and tailor the simulation to represent most geological conditions of magma intrusion and geological structure.

HEAT3D employs an explicit finite differencing scheme. The time step used in calculations is dependent upon size of spatial discretization and is set to conservatively achieve the necessary Courant condition for stability. Truncation errors that might evolve when using very short time steps are minimized by utilizing 64-bit precision. Continuous thermal gradients are assigned along the boundaries and initial conditions use a designated regional thermal gradient.

All rock/magma properties are assigned by the user and they include: density, porosity, fluid saturation, heat capacity, initial temperature, spatially and thermally varying thermal conductivities, and location.

For all rocks including magma, latent heats of fusion/crystallization are solved where temperatures are in that range. In the magma bodies, convective heat transfer is determined by analysis of the Rayleigh number (Ra)⁷ for each body. Where the calculated Ra is sufficient for convection, convection heat flow is calculated as a function of temperature and composition reaching a maximum Nusselt number (Nu)⁸ values of 3 for silicic magmas and 10 for mafic magmas.

Where geothermal fluid convection is modeled within reservoir rocks, if it occurs in fractured rocks, then an effective permeability is assumed by the model. Because effective permeabilities of fractured rocks are difficult to be assessed, they are usually averaged to the permeability of an equivalent porous medium

⁷ The Rayleigh number (Ra) for a fluid is a dimensionless number associated with free convection. When the Rayleigh number is below a critical value for that fluid, heat transfer is primarily in the form of conduction; when it exceeds the critical value, heat transfer is primarily in the form of convection.

⁸ In heat transfer at a boundary (surface) within a fluid, the Nusselt number (Nu) is the ratio of convective to conductive heat transfer across (normal to) the boundary. In this context, convection includes both advection and diffusion.

(with only interconnected porosity). As mentioned earlier, the code has been applied to several geologic areas to test its suitability.

Analytical Approach

While conduction dominates heat transfer in solid phases, convection is of great importance for fluid phases in porous media that are relatively permeable. A general mathematical expression for such heat transfer is given by the conservation of energy (Wohletz et al., 1999):

$$\rho_b C_b \frac{\partial T}{\partial t} = \nabla (K_b \nabla T) - \nabla (\rho_f C_f \mathbf{u}) + A \quad \text{Eq. 1}$$

where ρ and C are density and specific heat, respectively, T is temperature, K is rock thermal conductivity, \mathbf{u} is the convective velocity, and A represents heat loss or gain through radioactive decay, chemical reactions, and latent heat of crystallization and fusion.

Subscripts b and f refer to properties in bulk (rock + fluid) and the fluid, respectively. Eq. 1 shows that the temporal heat storage (left-hand side) equals to the conductive and the convective fluxes (first and second terms to the left-hand side respectively), taken together with a term for representing heat source/sinks.

Ignoring the convective flux and heat source/sink terms in Eq. 1., we expand the conductive flux term in cartesian coordinates for three-dimensions:

$$\frac{\partial T}{\partial t} = \frac{\partial \kappa_x}{\partial x} \frac{\partial T}{\partial x} + \frac{\partial \kappa_y}{\partial y} \frac{\partial T}{\partial y} + \frac{\partial \kappa_z}{\partial z} \frac{\partial T}{\partial z} + \kappa_x \frac{\partial^2 T}{\partial x^2} + \kappa_y \frac{\partial^2 T}{\partial y^2} + \kappa_z \frac{\partial^2 T}{\partial z^2} \quad \text{Eq. 2}$$

where k is the thermal diffusivity. Non-linearity results from heat diffusion not only reflecting local thermal gradients but also spatial variation of diffusivity with rock heterogeneity, temperature, and magma emplacement history.

Thermal conductivity varies with temperature and has been modeled as (Chapman & Furlong 1991):

$$K(T, z) = K_0 \left(\frac{1 + cz}{1 + bT} \right) \quad \text{Eq. 3}$$

For this equation thermal conductivity $K(T,z)$ is a function of crustal depth (z) and temperature (T) where K_0 is conductivity at 0 °C, c is the crustal depth constant equal to $1.5 \times 10^{-3}/\text{km}$, and b is the thermal constant equal to $1.5 \times 10^{-3}/^\circ\text{C}$ for the upper crust and $1.0 \times 10^{-3}/^\circ\text{C}$ for the lower crust.

This function adequately describes variations in most common rock thermal conductivities with temperature and fits those data for most magmas with exception of rhyolite (McBirney & Murase, 1984).

In derivation of the convective flux term of Eq. 1. one must consider conservation of mass for a steady state as (Parmentier, 1979):

$$\nabla (\rho_f \mathbf{u}) = 0 \quad \text{Eq. 4}$$

where ρ_f is convecting fluid density, and conservation of momentum, commonly expressed by Darcy's law expressed as (Norton & Cathles, 1979; Cathles, 1983):

$$\mathbf{u} = -\frac{k\rho}{\mu}(\nabla p - \rho_f \mathbf{g})$$

Eq. 5

where \mathbf{u} is the convective velocity, k is permeability, μ is the dynamic viscosity, p is pressure, and \mathbf{g} is gravitational acceleration. The term in parentheses in Eq. 5 is the net fluid pressure gradient, and because the lithostatic pressure gradient is greater than the hydrostatic gradient by a factor of about 3, fluids at lithostatic pressure will tend to ascend and transport heat upwards. Pressure is given by and integrated form of Darcy's law:

$$p = \int_0^z \left(\rho g - \frac{\mu}{k\rho} u_z \right) dz$$

Eq. 6

which shows that fluid pressure depends on fluid density and vertical flux. Finally the fluid equation of state is primarily a function of its coefficient of isobaric thermal expansion α :

$$\rho = \rho_0(1 - \alpha\Delta T)$$

Eq. 7

where ρ_0 is the reference density of the fluid and ΔT is the temperature difference driving the flow. Because the vertical pressure gradient in a convecting fluid system is nearly hydrostatic ($\nabla p = \rho_0 g$) convection is driven by the difference between the hydrostatic pressure gradient and that due to decrease fluid density at higher temperatures, the net pressure gradient is $\rho_0 \alpha \Delta T g$ and the vertical convective flux (Cathles, 1983) is then:

$$u_z = \frac{k\rho}{\mu} \rho_0 \alpha \Delta T g$$

Eq. 8

Convection also plays a role in cooling of magma chambers (Valentine, 1992) and can be evaluated by the thermal Rayleigh number (Ra). Where Ra is between 10^3 and 10^5 , magma chamber convection is likely and its overall influence on heat flow can be quantified by Nusselt number (Nu).

The major elements of heat sources for Eq. 1 are addition of new magma to the system and the latent heat of crystallization, while heat sinks are magma chamber volume decreases by eruption and latent heat of fusion of host rocks around magma chambers and fusion of cooled old magma by injection of new magma. To calculate this effect, HEAT3D considers crystallization and melting to occur over a range of temperatures between 650 °C and 1,000 °C, which is appropriate for a wide range of magma compositions. For simplicity, HEAT3D applies the assumption that melt fraction varies linearly with temperature over the above crystallization range and that an average latent heat for all phases is ~350 kJ/kg.

The most important aspect of numerical solution of Eq. 1. is the determination of appropriate boundary conditions that represent geologic structure and locations of various host rock bodies, magma chambers, and zones of fluid convection.

Method for Numerical Solution of Conductive Heat Flow

Recalling Eq. 2, an explicit forward time-centered space (FTCS) scheme is the simplest numerical approach, is a first-order approximation, and is inherently stable (Crank, 1956, Wohletz, 1999).

The finite difference solution requires discretization of derivatives following general rules (e.g., Differentiated Stirling approximation); for example for fictitious quantity A:

$$dA/dx = \Delta A/\Delta x = [A(j+1) - A(j-1)] / 2\Delta x . \quad \text{Eq. 9}$$

and

$$\begin{aligned} dA^2/dx^2 &= \Delta (\Delta A/\Delta x) / \Delta x = \{ [A(j+1) - A(j)] / 2x \} - [A(j) - A(j-1)] / 2x \} / x \\ &= [A(j+1) - 2 A(j) + A(j-1)] / \Delta x^2 . \end{aligned}$$

Eq. 10

Using the following notation:

$$\begin{array}{ll} T^n = \text{forward time temperature} & T^o = \text{backward time temperature} \\ \kappa_x = \kappa_x(i, j) & \kappa_{x1} = \kappa_x(i, j-1) & \kappa_{x2} = \kappa_x(i, j+1) \\ T = T(i, j) & T_{x1} = T_x(i, j-1) & T_{x2} = T_x(i, j+1) \\ \\ \kappa_y = \kappa_y(i, j) & \kappa_{y1} = \kappa_y(i-1, j) & \kappa_{y2} = \kappa_y(i+1, j) \\ T_{y1} = T_y(i-1, j) & T_{y2} = T_y(i+1, j) \end{array}$$

Eq. 11

Using cell-averaged values for coefficients of derivatives:

$$\begin{aligned} A(j-1) &= [A(j-1) + A(j)]/2 & A(j+1) &= [A(j+1) + A(j)]/2 \\ A(j) &= [A(j-1) + A(j+1)]/2 = [A(j-1) + 2A(j) + A(j+1)]/4 \end{aligned} \quad \text{Eq. 12}$$

$$\begin{aligned} (T^n - T) / [\Delta t] &= [(\kappa_{x2} - \kappa_{x1}) / (2\Delta x)] [(T_{x2} - T_{x1}) / (2\Delta x)] \\ &+ [(\kappa_{y2} - \kappa_{y1}) / (2\Delta y)] [(T_{y2} - T_{y1}) / (2\Delta y)] \\ &+ [(\kappa_{z2} - \kappa_{z1}) / (2\Delta z)] [(T_{z2} - T_{z1}) / (2\Delta z)] \\ &+ [T_{x1}(\kappa_{x1} + \kappa_x)/2 - 2T_x(\kappa_{x1} + 2\kappa_x + \kappa_{x2})/4 + T_{x2}(\kappa_x + \kappa_{x2})/2] / (\Delta x^2) \\ &+ [T_{y1}(\kappa_{y1} + \kappa_y)/2 - 2T_y(\kappa_{y1} + 2\kappa_y + \kappa_{y2})/4 + T_{y2}(\kappa_y + \kappa_{y2})/2] / (\Delta x^2) \\ &+ [T_{z1}(\kappa_{z1} + \kappa_z)/2 - 2T_z(\kappa_{z1} + 2\kappa_z + \kappa_{z2})/4 + T_{z2}(\kappa_z + \kappa_{z2})/2] / (\Delta x^2) \end{aligned}$$

Eq. 13

For $\Delta x = \Delta y = \Delta z$

$$\begin{aligned} T^n - T &= [\Delta t / (\Delta x^2)] [(\kappa_{x2}T_{x2} - \kappa_{x2}T_{x1} - \kappa_{x1}T_{x2} + \kappa_{x1}T_{x1}) / 4] \\ &+ [\Delta t / (\Delta x^2)] [(\kappa_{y2}T_{y2} - \kappa_{y2}T_{y1} - \kappa_{y1}T_{y2} + \kappa_{y1}T_{y1}) / 4] \\ &+ [\Delta t / (\Delta x^2)] [(\kappa_{z2}T_{z2} - \kappa_{z2}T_{z1} - \kappa_{z1}T_{z2} + \kappa_{z1}T_{z1}) / 4] \\ &+ [\Delta t / (\Delta x^2)] [(\kappa_{x1}T_{x1} + \kappa_xT_{x1})/2 - 2(\kappa_{x1}T_x + 2\kappa_xT_x + \kappa_{x2}T_x)/4 + (\kappa_xT_{x2} + \kappa_{x2}T_{x2})/2] \\ &+ [\Delta t / (\Delta x^2)] [(\kappa_{y1}T_{y1} + \kappa_yT_{y1})/2 - 2(\kappa_{y1}T_y + 2\kappa_yT_y + \kappa_{y2}T_y)/4 + (\kappa_yT_{y2} + \kappa_{y2}T_{y2})/2] \\ &+ [\Delta t / (\Delta x^2)] [(\kappa_{z1}T_{z1} + \kappa_zT_{z1})/2 - 2(\kappa_{z1}T_z + 2\kappa_zT_z + \kappa_{z2}T_z)/4 + (\kappa_zT_{z2} + \kappa_{z2}T_{z2})/2] \end{aligned}$$

Eq. 14

$$T^n = T + [\Delta t / (\Delta x^2)] \{ [D_{x1}T_{x1} - 2D_xT_x + D_{x2}T_{x2}] + [D_{y1}T_{y1} - 2D_yT_y + D_{y2}T_{y2}] + [D_{z1}T_{z1} - 2D_zT_z + D_{z2}T_{z2}] \}$$

Eq. 15

where:

$$\begin{aligned} D_{x1} &= (3\kappa_{x1} + 2\kappa_x - \kappa_{x2}) / 4; & D_{x2} &= (3\kappa_{x2} + 2\kappa_x - \kappa_{x1}) / 4 & D_x &= (\kappa_{x1} + 2\kappa_x + \kappa_{x2}) / 4; \\ D_{y1} &= (3\kappa_{y1} + 2\kappa_y - \kappa_{y2}) / 4; & D_{y2} &= (3\kappa_{y2} + 2\kappa_y - \kappa_{y1}) / 4 & D_y &= (\kappa_{y1} + 2\kappa_y + \kappa_{y2}) / 4; \\ D_{z1} &= (3\kappa_{z1} + 2\kappa_z - \kappa_{z2}) / 4; & D_{z2} &= (3\kappa_{z2} + 2\kappa_z - \kappa_{z1}) / 4 & D_z &= (\kappa_{z1} + 2\kappa_z + \kappa_{z2}) / 4; \end{aligned}$$

Eq. 16

Although stability of the numerical solution of Eq. 14 is guaranteed by the Courant-Friedrich-Lewy (CFL) stability condition ($\Delta t < 0.5 \Delta x^2 / D_{max}$) (Courant et alii, 1928), it is important to note with the above formulation that some values of D can be negative, which reflect a dominating effect of the diffusivity gradient and can cause numerical instability. This problem is corrected by using more conservative values of D:

$$\begin{aligned} D_{x1} &= (\kappa_{x1} + \kappa_x) / 2; & D_{x2} &= (\kappa_{x2} + \kappa_x) / 2 & D_x &= (\kappa_{x1} + 2\kappa_x + \kappa_{x2}) / 4; \\ D_{y1} &= (\kappa_{y1} + \kappa_y) / 2; & D_{y2} &= (\kappa_{y2} + \kappa_y) / 2 & D_y &= (\kappa_{y1} + 2\kappa_y + \kappa_{y2}) / 4; \\ D_{z1} &= (\kappa_{z1} + \kappa_z) / 2; & D_{z2} &= (\kappa_{z2} + \kappa_z) / 2 & D_z &= (\kappa_{z1} + 2\kappa_z + \kappa_{z2}) / 4; \end{aligned}$$

Eq. 17

Method for Solution of Convective Heat Flow

The differential equation is shown below (Wohletz, 1999):

$$\frac{\partial T}{\partial t} = -\mathbf{u} \cdot \nabla T$$

Eq. 18

By observing limiting boundary conditions, solutions to Eq. 18 can approximate the effects of convection in a fashion that numerically mimics effective diffusivity.

$$T^n = T + [\Delta t / \Delta 2x] [\mathbf{u}_x (T_{x1} - T_{x2}) + \mathbf{u}_y (T_{y1} - T_{y2}) + \mathbf{u}_z (T_{z1} - T_{z2})]$$

Eq. 19

Method for Solution of Heat Sources/Sinks

By assuming an explicit temperature range over which crystallization/melting occurs, a constant latent heat of fusion/crystallization, and a linear relationship between crystal content and temperature, an iterative solution is possible (Wohletz, 1999). For HEAT3D calculations this simplification is represented by:

$$\frac{\partial T}{\partial t} = - \frac{Q_l \delta T}{(c_p + 1) \Delta T_{sl}} = \frac{Q_l}{(c_p + 1) \Delta T_{sl}} (T - T^n)$$

Eq. 20

for which heat is expressed in kJ, Q_l is the latent heat, c_p is heat capacity, δT is an incremental change in temperature by conduction and convection, and ΔT_{sl} is the temperature difference between the liquidus and solidus.

Using HEAT3D

Options for the simulations

Different options can be checked during the simulations:

- **Magma Convection**
checking off this item makes the cooling of magma bodies only conductive. Magma convection is only calculated when the magma has a thermal Rayleigh number greater than ~ 2000 ; the maximum effective Nusselt number is 3 (silicic), 6 (intermediate), and 10 (basaltic) and decreases with temperature to a value of 0 when the magma's solidus temperature is approached
- **Latent Heat Magma**
checking this item includes heat production or loss. The amount of magma latent heat released is 0% when the magma is fully molten and 100% when fully solidified.
- **Latent Heat Rocks**
checking this item includes heat production or loss by molten rock crystallization or melting.
- **Intrusion Advection**
For Magmas when the Intrusion Advection option is checked, heat in cells where magma is added (intruded) is advected to nearby cells in a fashion that approximates mass conservation. This option may be important for a simulation that involves several or more periods of magma addition to the mesh during the course of calculation; for example, the step-wise growth of a magma intrusion. The effect of heat carried by displaced rock during intrusion cannot not be precisely calculated by HEAT3D because it requires knowledge of the constitutive properties of the rock (deformation mode under heat and pressure) and the state of stress in rocks represented in the mesh. However, heat conservation is maintained within a few percent for the approximation used. HEAT3D uses the following assumption for rock deformation during intrusion: that the advection has both horizontal and vertical components and the ratio of horizontal to vertical advection is the reciprocal of the intrusion aspect ratio (width/height). In this fashion the following criteria are met: (1) for dike-like intrusions with aspect ratios < 0.2 , an extensional environment is assumed in which deformation is primarily horizontal (heated rock is moved to either side of the intrusion such that the advection ratio is high); (2) for plug or pluton intrusions that have aspect ratios near unity, advection ratios will be such that horizontal and vertical deformation are both important; and (2) for sill-, lopolith-, or lacolith-like intrusions of very high aspect ratio, deformation is primarily vertical, such that heated rock is displaced upwards.
- **P-T Dependencies**
Rock conductivities (k) are generally tabulated for earth surface temperature and pressure. The effects of pressure and temperature on rock are calculated by the method of Chapman and Furlong (1990): $k(t,z) = k_0((1+cZ)/(1+bT))$; k increases with pressure but generally decreases with temperature:
 $k_0 = k$ at 0 deg C
 b (upper crust) = $1.5e-3/\text{deg}$
 b (lower crust) = $1.0e-4/\text{deg}$
 $c = 1.5e-3/\text{km}$, use $c = 0$ for negligible pressure effects
 $Z = \text{depth (km)}$; $T = \text{temp (deg C)}$

For magmas, temperature dependencies are from McBirney (1979): basalt k falls with T , andesite rises slightly, and rhyolite rises sharply; basalt $b = 0.00037/\text{deg}$, andesite (intermediate) $b = -0.00009/\text{deg}$, rhyolite (silicic) $b = -0.00054/\text{deg}$

Building up a mesh

The Mesh Design window allows the user to select a rock number or magma and then specify its position in the mesh, thermal conductivities (k), heat capacity (C_p), rock bulk density or for the case of magmas, silicic, intermediate, or mafic, and an option for convective fluid behavior that includes specification of the rock porosity.

The initial rock assignment determines the mesh domain size (width, height, depth). Subsequent additions must be within these limits. For this reason, a mesh design with more than one rock type requires overlaying the additional rock bodies on the domain set for the first rock body.

It is important to note that when the mesh is first designed (before any heat flow cycles have been calculated), the numerical code will map temperatures to rock cells based on their depth and pre-selected thermal gradient. For magmas, it will assign the currently specified magma temperature. The "Cons Temp" check box can be checked for specific problems for which the magma temperature is desired to remain at a constant temperature during the calculation (for example, when a magma body is being replenished at the same rate magma is removed by some unspecified process).

For Magmas when the Intrusion Advection option is checked, heat in cells where magma is added (intruded) is advected to nearby cells in a fashion that approximates mass conservation. HEAT3D uses the following assumption for rock deformation during intrusion: that the advection has both horizontal and vertical components and the ratio of horizontal to vertical advection is the reciprocal of the intrusion aspect ratio (width/height). In this fashion the following criteria are met: (1) for dike-like intrusions with aspect ratios < 0.2 , an extensional environment is assumed in which deformation is primarily horizontal (heated rock is moved to either side of the intrusion such that the advection ratio is high); (2) for plug or pluton intrusions that have aspect ratios near unity, advection ratios will be such that horizontal and vertical deformation are both important; and (3) for sill-, lopolith-, or lacolith-like intrusions of very high aspect ratio, deformation is primarily vertical, such that heated rock is displaced upwards.

References

- Carslaw, H.S., Jaeger, J.C., (1947). *Conduction of Heat in Solids*. Oxford university press.
- Cathles, L. M. (1983). An analysis of the hydrothermal system responsible for massive sulfide deposition in the Hokuroku Basin of Japan. *The Kuroko and related volcanogenic massive sulfide deposits*.
- CHAPMAN, D. S. (1992). Thermal state of the continental lower crust. *Continental lower crust*, 179-199.
- Chapman, D.S., Furlong, K.P., (1991). *Thermal state of the continental crust*. In: Continental Lower Crust, Elsevier, Amsterdam.
- Courant, R., Friedrichs, K., & Lewy, H. (1928). Über die partiellen Differenzgleichungen der mathematischen Physik. *Mathematische annalen*, 100(1), 32-74.
- Crank, J. (1956). *The mathematics of diffusion*. Oxford university press.
- Furlong, K.P., Hanson, R.B., Bowers, J.R., (1991). Modelling thermal regimes. In: Kerrick, D. Ed., Contact Metamorphism. *Rev. Mineral.*, 26, 437–506.
- Kolstad, C. D., & McGetchin, T. R. (1978). Thermal evolution models for the Valles caldera with reference to a hot-dry-rock geothermal experiment. *Journal of Volcanology and Geothermal Research*, 3(1-2), 197-218.
- Lovering, T. S. (1935). Theory of heat conduction applied to geological problems. *Geological Society of America Bulletin*, 46(1), 69-94.
- McBirney, A. R., & Murase, T. (1984). Rheological properties of magmas. *Annual Review of Earth and Planetary Sciences*, 12(1), 337-357.
- Norton, D., & Cathles, L. M. (1979). Thermal aspects of ore deposition. *Geochemistry of hydrothermal ore deposits*, 2, 611-631.
- Parmentier, E. M. (1979). Two phase natural convection adjacent to a vertical heated surface in a permeable medium. *International Journal of Heat and Mass Transfer*, 22(6), 849-855.
- Todesco, M., & Giordano, G. (2010). Modelling of CO₂ circulation in the Colli Albani area. SPECIAL PUBLICATION-GEOLOGICAL SOCIETY OF LONDON, 311-330.
- Turcotte D. L., & Schubert, G. (1982). *Geodynamics: Applications of continuum physics to geological problems*. Wiley.
- Valentine, G. A. (1992). Magma chamber dynamics. *Encyclopedia of Earth System Sciences*, 3, 1-17.
- Wohletz, K.H., 1999. HEAT3D: Magmatic Heat Flow Calculation. Los Alamos National Laboratory computer code LA-CC 99-27 (<http://geodynamics.lanl.gov/Wohletz/Heat.htm>). Los Alamos, New Mexico
- Wohletz, K., Civetta, L., & Orsi, G. (1999). Thermal evolution of the Phlegraean magmatic system. *Journal of Volcanology and Geothermal Research*, 91(2), 381-414.
- Zyvoloski, G. (1987). The effect of structural resurgence on the thermal evolution of the Creede caldera. *Geol. Soc. Am. Abstracts with Programs*, 19, no. 5.

Chapter 5 – Building of the conceptual model for the Roman Geothermal Province used in this work

Geological setting

The Roman Geothermal Province is associated with the main Quaternary caldera complexes in the Latium region and has been defined as such in Giordano et al. (2014). It is delimited to the N and to the NW by the Tuscan structures, to the NE by the Umbro-Marche-Sabine structures and in the S by the reliefs of the carbonate platforms of the Latium-Abruzzi successions.

The current tectonic setting results from the overprinting of the post-orogenic extensional tectonics (Plio-Pleistocene) on the compressional effects related to the development of the Apennine chain mainly throughout the Miocene. The relationships between extensional and compressional structures have been subsequently masked by the Plio-Quaternary volcanism related to the evolution of the Tyrrhenian margin (Mattei et al., 2010 and references therein).

There is little information about the Latium pre-Alpine history and its pre-Triassic metamorphic substratum, which discontinuously crops out only to the north in the Monti Romani and in the Zannone island to the S. The post-Hercynian sedimentary cycle begins with the Verrucano facies linked to the continental pre-rifting phases and to the evaporitic facies (Anidriti di Burano) of a predominantly dolomitic nature evolving towards limestone (Calcare Massiccio) till the lower Lias.

Starting from the middle Lias throughout the Cenozoic, a basin-platform system developed on the older Tethyan passive margin as a consequence of a rifting stage. The resulting paleogeography included a vast system of dismembered domains that partially subsided, giving rise to pelagic basins of varying depths, and partially persisted as topographic highs, hosting an intense carbonatic sedimentation, to compensate for a constant subsidence with the deposition of thousands of meters of dolomites and limestones). At this stage the main paleogeographic units of Central Italy are identified. These include (from the innermost to the outermost zone) the basin corresponding to the Tuscan units the Umbro-Sabine and Umbro-Marche basins, and the Latium-Abruzzi carbonate platform (Parotto & Praturlon, 1975; Praturlon, 1993). During the Apennine orogenic process, three main compressive events have been identified, that profoundly altered the original geometric relationships between the pre-existing paleogeographic units. These events mark the progression of the compression deformation towards the eastern quadrants and are summarized as follows:

1- The Oligo-Aquitainian event responsible for the overlapping of internal units (allochthonous flysch or Ligurian units) with the most external Tuscan and Umbro-Sabine units, that extensively occurs in Tuscany and partially in the Latium coastal area (Tolfa Mts, Sabatini Substrate, Sabina, Lepini Mts).

In particular, the unit of the allochthonous Flysch was encountered in the Sabatino-Vulsina region in many exploratory drillings for geothermal research carried out by ENEL (e.g. Latera, Marta, Vico, Bagnarello¹; see Funciello & Parotto, 1978; Di Filippo, 1993; Cimino¹, Vetralla, Allumiere, Cesano; see Barberi et al., 1994; Buonasorte et al., 1995).

2- The Tortonian-Messinian event responsible for the deformation of the Tuscan and Umbro-Sabine successions. From a structural point of view, a series of NS trending thrusts cutting the Tuscan series from the W onto the Umbro-Marche units to the E are identified. This interpretation is based on outcrop data, drilling and geophysical data (Buonasorte et al., 1987 and 1991; Barberi et al., 1994).

3- Lower Pliocene event. The southern part of the Umbro-Sabine structural units, already deformed during the previous Tortonian-Messinian event, are tectonically superimposed/overthrust towards E on the Latium-Abruzzi platform. This resulted in the activation of the Olevano-Antrdoco tectonic lineament involving the Laga Flysch in the northern part along the Sibillini Mts front.

Eventually, the extensional phase associated with the Tyrrhenian basin formation and evolution has produced, in the studied Latium margin, a setting characterized by NW-SE trending systems of aligned morpho-structural highs and lows bounded by regional faults. The extensional deformation migrated from

W to E, as testified by the first coastal syn-rift deposits of Messinian times as well as eastward extensional tectonics that was activated during the Pliocene.

During Pliocene and Quaternary times, the structurally depressed sectors acted as post-orogenic depositional basins filled with huge thicknesses of marine, lacustrine and alluvial sediments that presently mask the lateral contact between morpho-structural highs and lows (Funicello & Parotto, 1978). From the beginning of the Pliocene, a widespread magmatic activity developed along the Tyrrhenian margin of the Tuscan-Latium area along a NW-SE volcanic belt, with the initial emplacement of numerous intrusive bodies and the development of limited volcanic activity (Conticelli et al., 2010). During the lower Pleistocene, the alignment of the volcanic centers of Radicofani, Torre Alfina and the Cimino Mts developed. The significant change in the stress field linked to the opening of the southern Tyrrhenian basin resulted in significant positive vertical movements that accentuated in the middle and upper Pleistocene, linked to the arching of the Apennine Chain. The architecture of the Neogenic sediments reflects the tectonic movements of this phase. The volcanism of the Roman Magmatic Province (PMR) is characterized by mafic K-alkaline compositions and has developed in the intermediate sector placed in between the uplifting Apennine Chain and the subsiding Tyrrhenian Basin (Fig. 1). From about 600,000 years ago, extensive bodies made of ignimbrites are identified, characterizing the early stages of activity of the Vulsini, Vico, Sabatini and Colli Albani volcanic districts, with a significant peak of magmatic volumes emitted around 3-400,000 years ago (Conticelli et al., 2010 and references therein). After this period there is a decrease in both volcanic activity and extensional processes, possibly linked to the evolution of this sector from a rift phase to a post-rift stage. In this framework, the current heat flow anomaly would represent the residue of the thermal anomaly associated with neogenic distension (Mattei et al., 2010 and references therein).

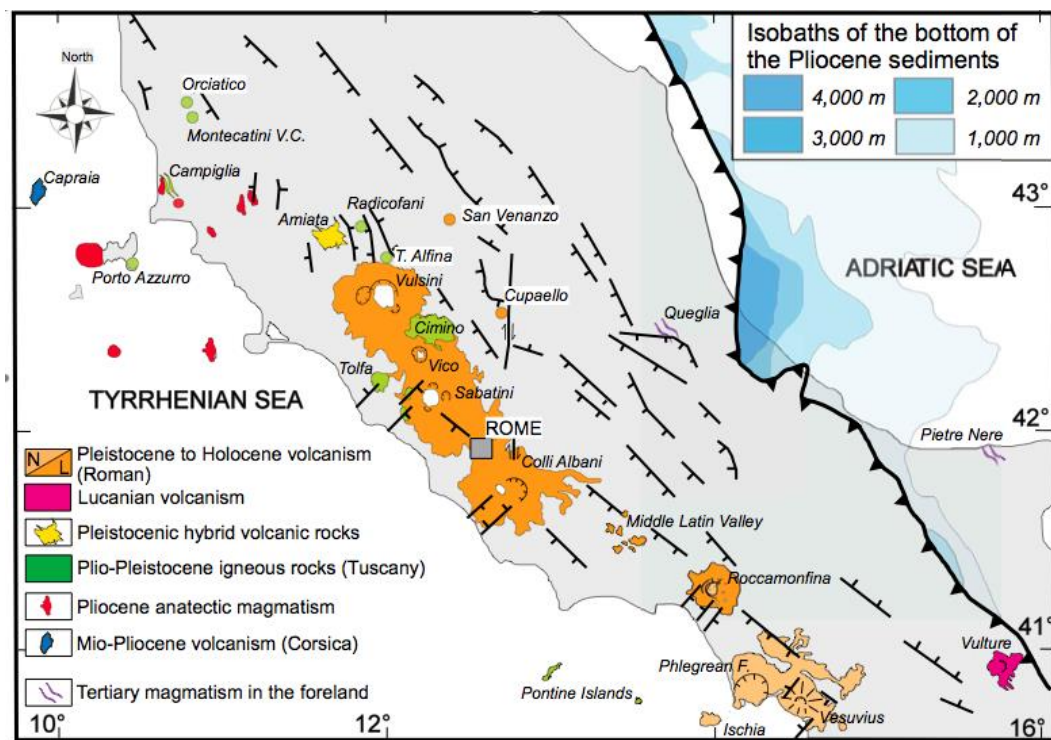


Fig.1 - Distribution of Plio-Pleistocene ultrapotassic igneous rocks and associated shoshonites and calc-alkaline rocks from Eastern Tyrrhenian Sea and Italian Peninsula (Tuscan, Roman and Lucanian Magmatic Provinces) (Conticelli et al., 2010).

Potential of the geothermal resource in Latium

In order to define the potential of a geothermal resource, several factors (here listed in order of relevance) must be considered.

Heat source

Geometry, depth and temperature of the heat source are the primary factors for the availability of geothermal resource. In this regard data are very scarce. Apart from the direct evidence of intrusions in the areas of Vulsini and Sabatini Mts, drilled by various exploration wells and whose relation to the main intrusion is not directly known (dykes, apophyses or batholiths roof?), there are essentially indirect indications only.

Thermal characteristics of the westernmost Tolfa-Cerite area (perhaps also of the south coast of Rome) and of Pontine islands are related to the Tuscan type of Pliocene volcanism and are connected with the emplacement of granitoid bodies with gross spheroidal geometry. It is not possible to define the volumes of intruded bodies from the small volumes of available/outcropping associated volcanites. The present day elevation of both the crystalline basement (Monti Romani and Zannone island) and of the Pliocene substratum (Barberi et al, 1994), suggest the presence of relatively shallow intrusions. In conclusion, these would have at least 2 Ma (a little younger at 1.3 Ma for the Cimini district; Conticelli et al., 2013) and cooling temperatures starting from T magma 750-850 ° C. The present day thermal characteristics of the volcanic belt are related to the volcanism of the Roman Magmatic Province, which is much more recent (upper Pleistocene, 0.6-0.02 Ma), with K-alkaline or ultrapotassic composition and cooling temperatures starting from T magma > 1000 ° C. The lower magma viscosity suggests geometries for chambers / batholiths characterized by a low aspect ratios with consequent lower lifting in surface. Surface intrusions are between 1 and 2 km in drillings (SH2, Latera), while most of the intrusive bodies should have depth > 3 km in northern Latium (Vulsini-Vico-Sabatini) and > 6 km in the Colli Albani area (Chiarabba et al., 2010 and references therein). Vulsini and Sabatini are large double caldera systems (2 caldera for each volcanic complex) with large lateral extension of the associated plumbing system. Colli Albani are also a large calderic complex. These three volcanic systems have erupted volume of ignimbrites individually in the order of 50-100 km³(Giordano et al., 2010), , while Vico has had maximum eruptions around 10-30 km³(Conticelli et al., 2013). The usual assumption for magma chambers is that they represent 10 times the volume of the related ignimbrites (Smith, 1979).

Generally peak values observable in both temperature and heat flow maps should reflect the geometry and location projected at depth of magmatic heat sources, plus or minus the effect of advection in convective layers.

Among the possible heat sources able to generate industrially exploitable geothermal systems, the thermal anomaly associated with magma chambers (magma intrusion) is the most interesting for providing the highest enthalpies. that. The heat source (magma chamber) is more favorable exploitable as it is younger, shallow, of large volume, and has remained for long time in the upper crust (Smith and Shaw, 1975). Because the magma that stagnates in a chamber slowly cools down, crystallizes and generates more advanced differentiated magmas (less basic), recent large volumes erupted of these evolved magma represent a first indication for the presence of a strong thermal anomaly. The caldera structures generated by the collapse of the rock to the roof of a shallow magmatic chamber, emptied by one or more voluminous eruptions, are usually associated with anomalous thermal zones. This volcanological-magmatic approach is one of the simplest and most effective techniques of geothermal exploration in volcanic areas at least in the search for the most promising sites (Barberi et al., 1994).

Many of the northern Latium complexes show a two phases volcanological-structural evolution (Acocella & Funicello, 2002). In a first phase, an extensional state accomplished by NW-SE normal faults (Apennine direction) produced decompression with magma rise and thermal anomalies generation in the upper crust. Subsequently, NE-SW transverse structures have controlled the emplacement of magma chambers at superficial levels in crusts, which fueled the eruptions of volcanic complexes in Central Italy and have generated relevant thermal anomalies (Fig. 2).

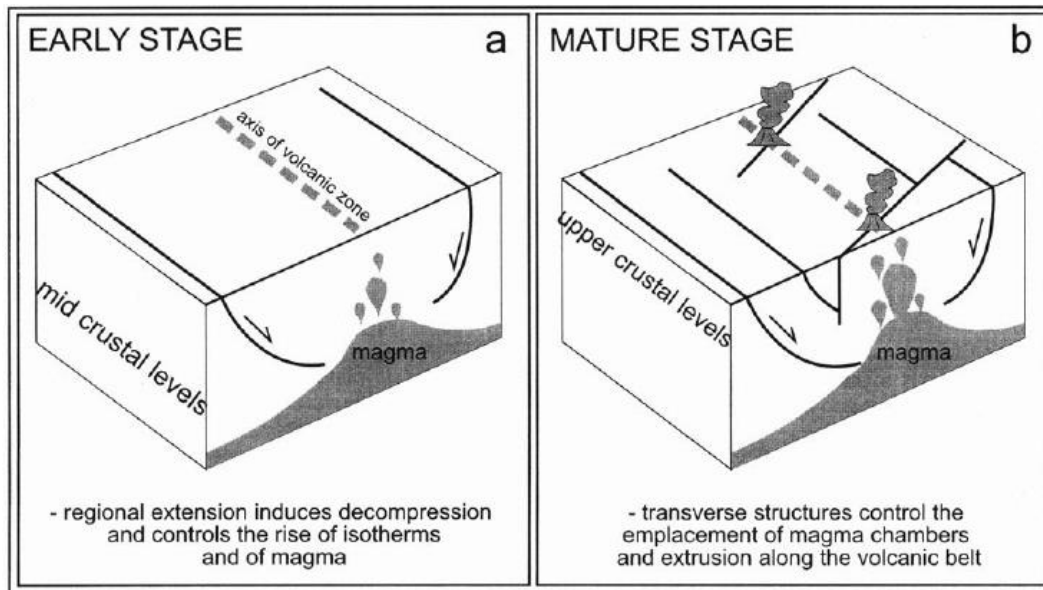


Fig. 2. Schematic model showing how different structures control, at different depths, the rise and position of magmas along the Tyrrhenian margin of Central Italy (Acocella & Funiciello, 2002).

Fig. 3 shows the frequency histograms of the K₂O content and the magnesium number (Mgv) for the volcanic products of northern Latium separated according to the age of eruption. Differentiated magmas generated by a long residence in a superficial magmatic chamber have low Mgv values and high K₂O levels. Also higher alkaline and silica values (Fig. 4) indicate evolved magma.

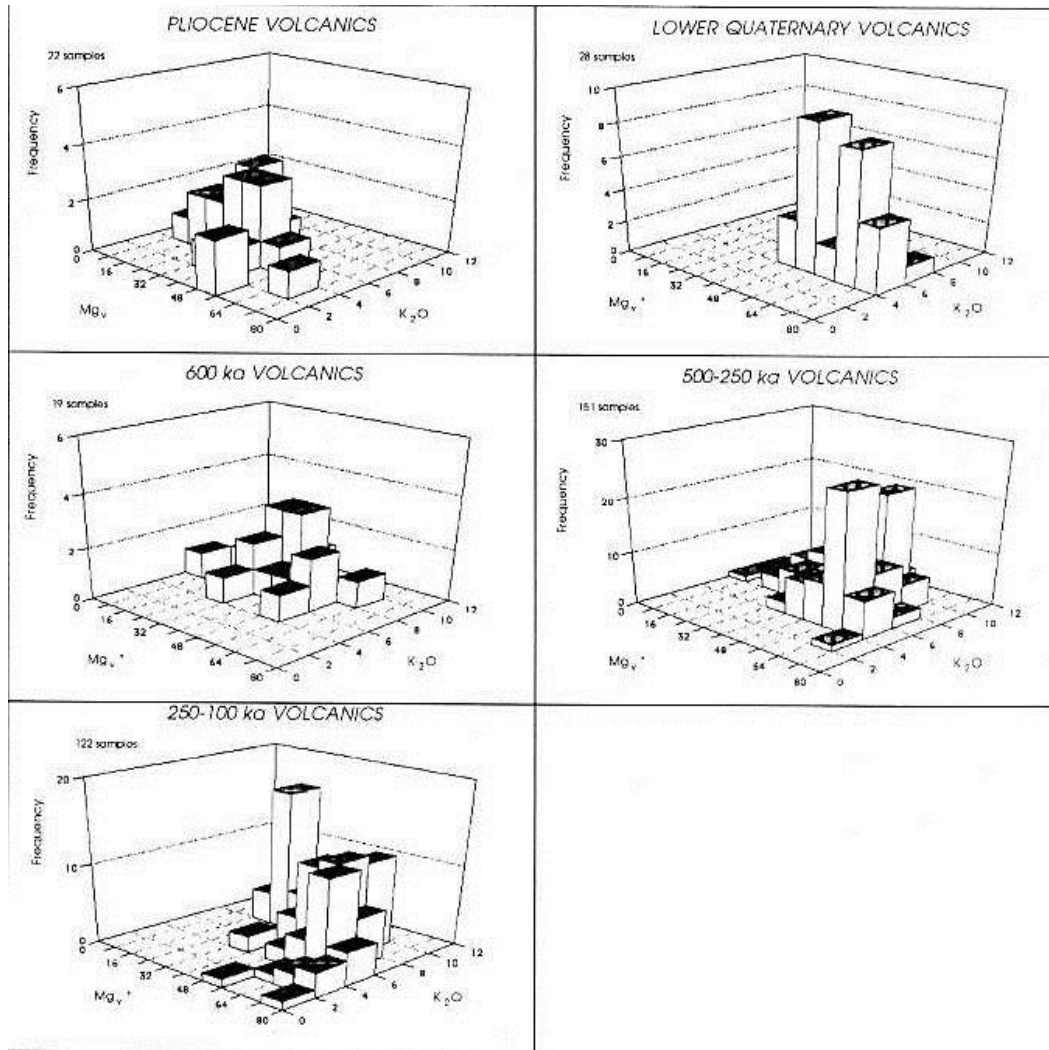


Fig. 3. Frequency histograms of content variations in K₂O and in the magnesium number (Mg_v) for the Plio-Quaternary volcanic rocks of northern Latium (Barberi et al, 1994).

Figs. 3 and 4 suggest that the period between 500 and 250 ka is the one in which the main magma chambers of northern Latium have been active and that have generated the present day surface thermal anomalies of the region.

The most recent phase of volcanic activity, between 250 and 100 ka, has generated mainly small volume eruptions and generally unevolved magmas not necessarily associated with important geothermal heat sources (Barberi et al., 1994).

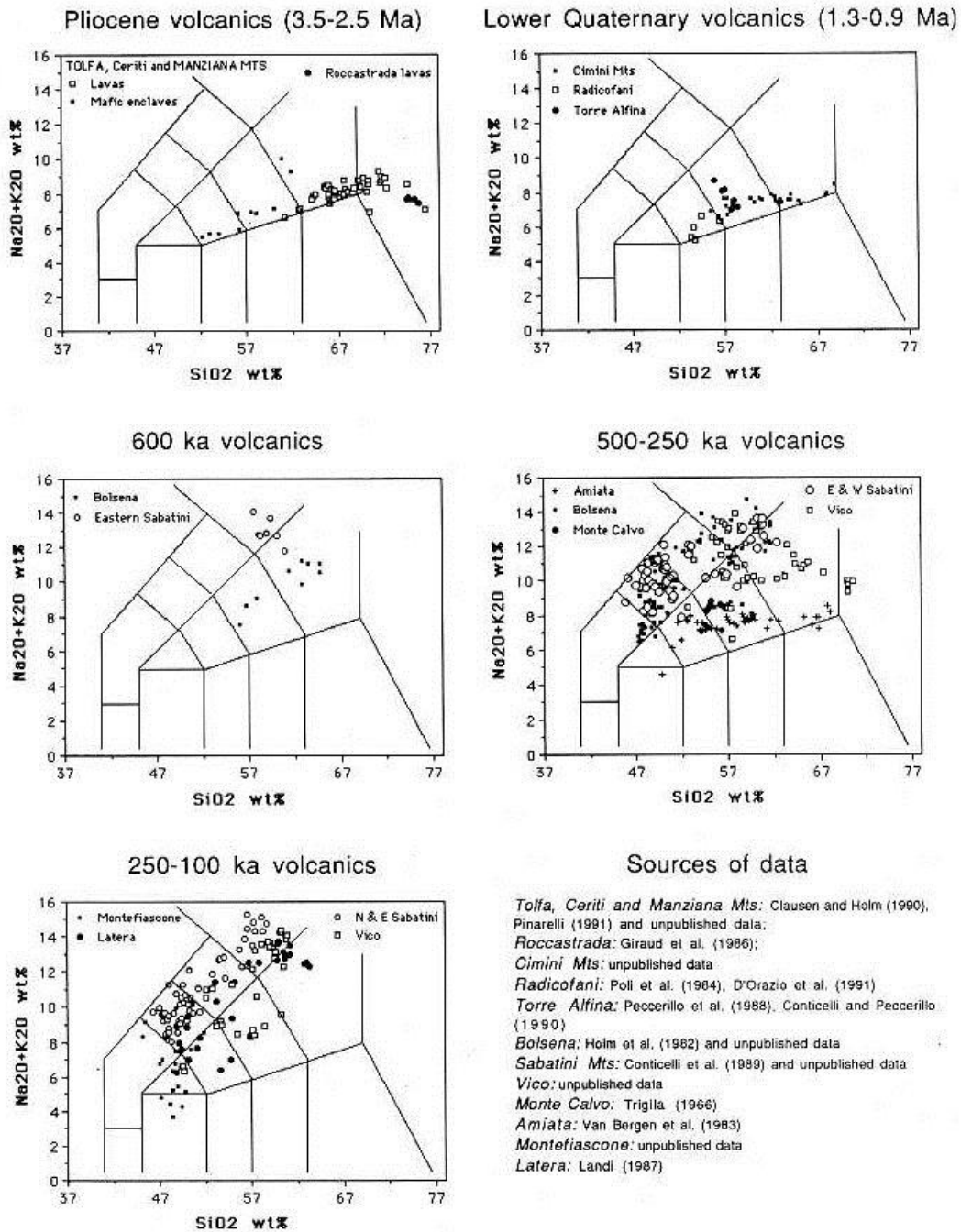


Fig. 4. Total alkali / silica graphs for Northern Latium volcanites, by age (Barberi et al., 1994)

Stratigraphy, structure and permeability

In an isotropic medium, heat propagates like a spherical wave from the source of perturbation. Variations in this sphericity may be due to the anisotropy of the medium, or else to different thermal conductivities of the affect the bodies. In addition, the presence of water and the variations in lateral permeability affect the heat propagation by conduction or by thermal convection. Following the stratigraphic data from the large dataset made available by the Italian Ministry for Economic Development (<http://unmig.mise.gov.it/>) a large deal of wells stratigraphies and related thermal/technical data, as well as reconstructions of the subsurface geometry of the geological structures, allow to define the general stratigraphic layout of the studied area that can be schematized from top to bottom as follows:

- 1 - volcanic products and Pleistocene sediments with average permeability, and thickness ranging from 0 to 500 m (VULC);
- 2 - neoautochthonous clay-sandy complex, generally of Pliocene times, with relative low permeability, and thickness ranging from 0 to 1000 m. This complex acts as a caprock (CAP1) ;
- 3 – calcareous-marly-clayey complex, member of the flysch succession of Cretaceous-Eocene times (CAP2 - Liguridi s.l., Flysch della Tolfa); siliciclastic and sandstone-clay flysch succession of Oligo-Miocene times (CAP2mac; Macigno). This complex represents the caprock (CAP2) of deep aquifers for its relatively low permeability. It is heterogeneous with thickness ranging from a few hundred to 2000 m.
- 4 Umbro-Marche and Tuscan successions of Jurassic-Eocene times, characterized by stratified limestones in condensed / lacunose successions, and frequent (interstratification/interformation) clayey levels, moderately-to-intensely fractured. The resulting permeability is locally variable depending both fracture intensity and on the clayey levels the thickness range between 400 -1000 m. These series represents the potential reservoir (RES1);
- 5 – The oldest considered succession consist of dolomites and “Anidriti di Burano Fm.” (Upper Triassic; 2,000 m thick), and of “Calcare massiccio Fm.” (Lower Jurassic p.p.; 500 m thick). This succession is generally massive and characterized by intensely fractured zones that result in a relatively high permeability. Thicknesses can be > 1,000-2,000 m. This series is the potential reservoir (RES2).

Based on this general scheme and on the analysis of stratigraphy and thermals found in the deep wells, some end-member types can be distinguished (Fig. 5).

- 1 - structural highs (transition from CAP2-RES1 at low depths -500 / -700 m from surface level, Vico1, Bagnarello). In these cases temperatures at the passage are low (<100 ° C) and remain low in RES, as the gradient is related to the convection in these shallow portions.
- 2 - structural lows (transition from CAP2-RES1 at high depths -1400 / > 2000 m from surface level, Cimino1, Sabatini8, Roma2). In these cases temperatures at the passage are high (> 100 ° C).

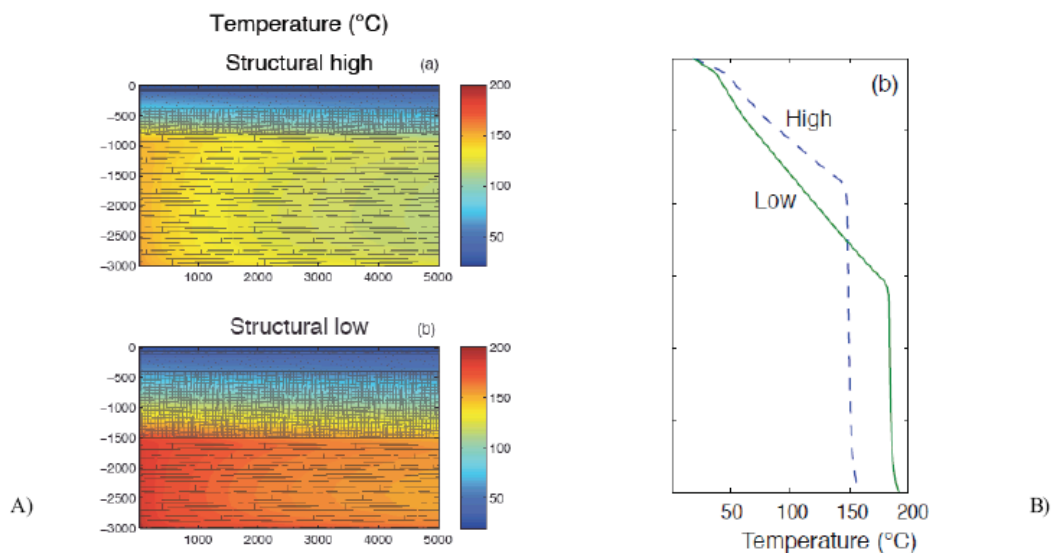


Fig. 5 - A) simulation of temperature distribution in structural high and low with initial heat flow at the base of 100 mW / m²; B) average gradients for structural high and low (Todesco & Giordano, 2010).

These two situations can be related to some causes and can determine some useful effects for understanding geothermal potential (Figure 5):

- a) in structural highs, a reduced CAP thickness and a RES with opened fractures (capable of effectively transferring at low depths the geothermal fluid) determine the effective heat dissipation over time. In these areas, it is possible to have widespread travertine plates, active or ancient, and manifestation of hyperthermal waters on the surface (e.g. Monte Razzano area near Viterbo);

b) in structural lows, a great thickness of CAP and a RES suffering high lithostatic load (that keeps closed the existing fractures) promote conditions of relatively low heat dissipation. In these areas, there are possible gases and cold manifestations as well as concentrated areas of hypo and mesothermal waters, which are more susceptible to impulsive phenomena (strong variations in flow rates and temperature in relation to earthquakes).

Obviously, RES thickness and permeability will determine the degree of convection and the associated thermal gradient.

Recharging and vertical permeability

Wells that are spatially close, with similar stratigraphy and very different thermal conditions, such as Roma1 and Roma2 (Fig. 6), are of great interest (Conforto, 1962). Such situations may result from either a strong heterogeneity of the heat source or an additional anisotropy factor.

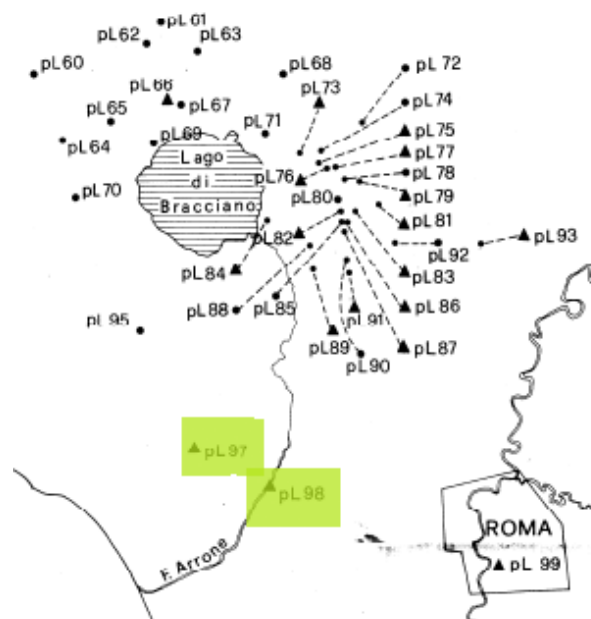


Fig. 6 Wells Roma1 (pL 98) and Roma2 (pL 97)

Such differences could be related to the horizontal fabric, e.g. belonging to different tectonic fragment, with similar stratigraphies but with independent circulation links.

Alternatively, preferential heat dissipation pathways may be linked to vertical open fracture corridors, which determine the presence of "chimneys" capable of concentrating fluid upstream. In fact, the nature and the mechanical behavior of the CAP are highly variable and still poorly investigated (Corrado et al., 2014; Maffucci et al., 2015). CAP1 (Neogenic clay) is lithologically more homogeneous than CAP2 (allochthonous and sin-orogenic flysch) and their thermal gradient could be very different according to their fracture density (Todesco & Giordano 2010).

Seismicity can play a fundamental role. Earthquake swarms (e.g. at Colli Albani) can locally enhance secondary permeability and produce lateral recharges from nearby karst aquifers that in this way are responsible for the collapse of the geothermal flow (Fig. 7). Like several times mentioned in the ENEL reconstructions (Enel & Cnr, 1988). The existence of seismically-induced secondary permeability would also justify the extreme lateral variability of the known geothermal fields, the presence of "closed pockets" evolving in brine, in the absence of recharging, and productive reservoirs with limited range.

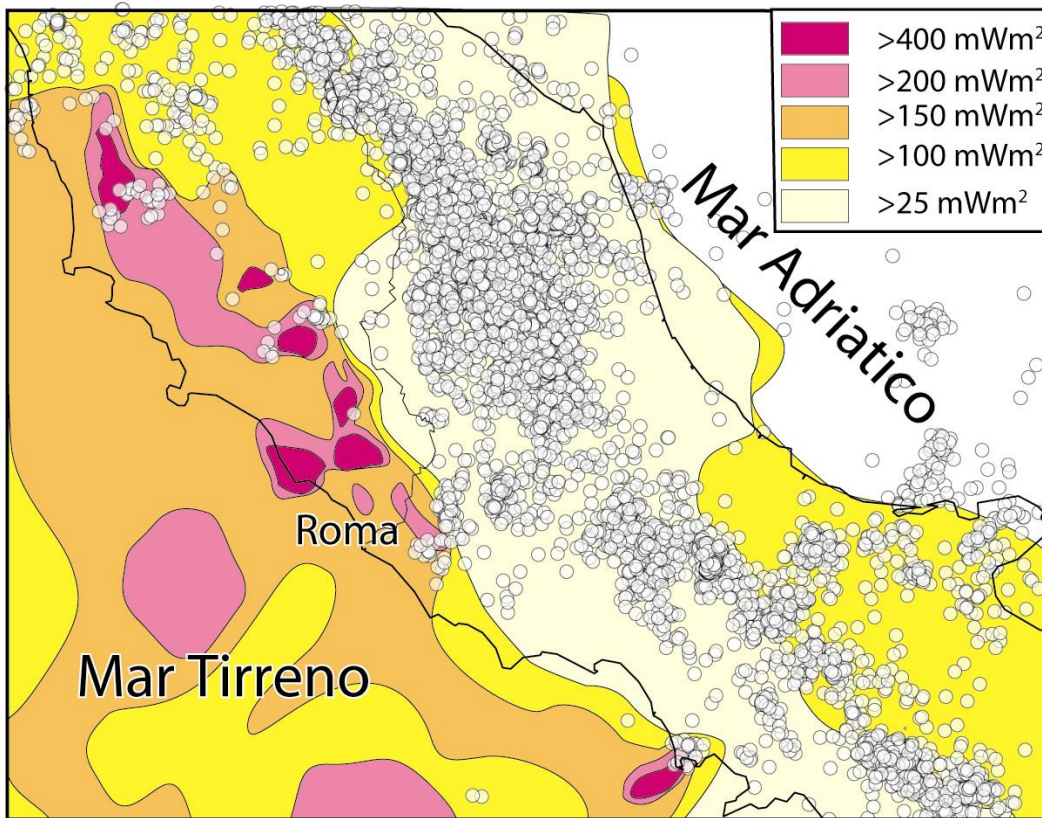


Fig. 7 - Earthquakes distribution in central Italy and heat flow (Mattei et al., 2008).

Heat Flow in the area (Fig 8) (Marini, L., et al., 1993) confirms the analysis of Geological Setting and of the Potential of the geothermal resource

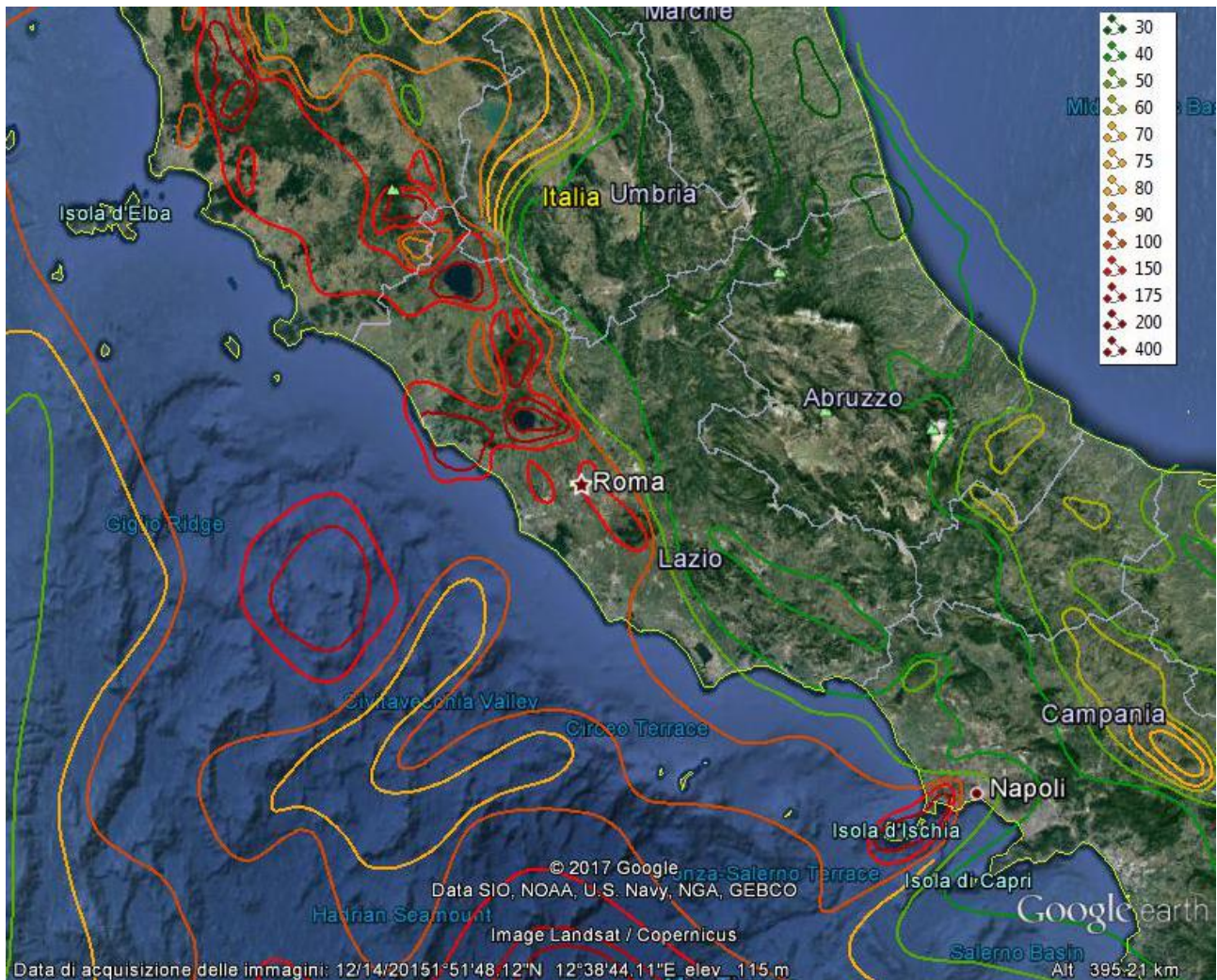


Fig. 8 Heat flow (in the legend in mW/m^2) (Marini, L., et al., 1993)

The conceptual model

Based on the analysis implemented before, it is possible to build up a generalized conceptual model for geothermal resources in Latium.

In Colli Albani, 2D cross-section and interpretation of gravimetry (Di Filippo & Toro, 1995; Giordano et al. 2014) indicate that the gravimetric high in the Ciampino area can be partly due to a shallow horst but needs to involve a rise of the crystalline basement likely along a deep thrust and an intrusion which represents the top of the Colli Albani magma chamber.

In particular, by studying the xenoliths from the maar of the Colli Albani and their thermo-metamorphism, it was identified the presence of a largely Sabina Meso-Cenozoic carbonatic sequence (RES1a and RES1b in fig 6 c) and a significant thermo-metamorphism associated with pure-limestone and dolostone protoliths (De Benedetti et al., 2010, and references therein; Danese & Mattei, 2010, and references therein). This suggests an extensive presence of magmatic intrusions at the base of the thick Triassic-Liassic sequences (RES2 in fig. 6 c). Furthermore the presence of quartzite clasts suggests the involvement of the Paleozoic basement (Verrucano Fm).

Based on density contrast with respect to the crystalline basement, it is possible to model the residual gravity anomaly in terms of 4 layers with differential density contrast with respect to the crystalline basement (Di Filippo & Toro, 1995). From the bottom to the surface we can model: 1. the crystalline basement; 2. the Meso-Cenozoic Sabina carbonate succession with a differential density of $-100 \text{ kg}/\text{m}^3$; 3.

The allocthonous clayey-marly flysch with a differential density of -250 kg/m^3 ; 4. The Quaternary volcanic deposits and Pliocene clayey-sandy marine deposits with a differential density of -600 kg/m^3 (fig. 9 a; fig. 9 b).

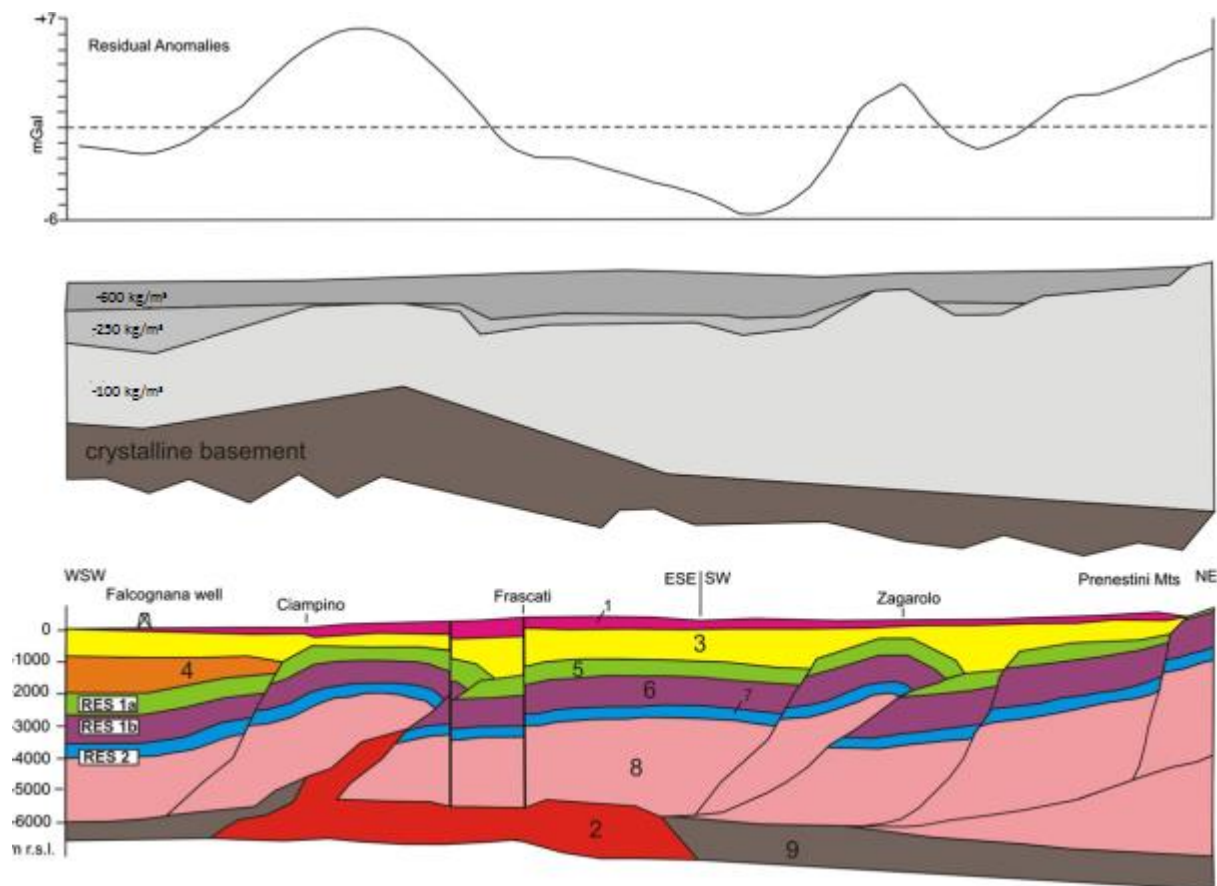


Fig. 9 a) Residual gravity anomalies (Di Filippo & Toro, 1995); b) Inversion of gravity data (Di Filippo & Toro, 1995), based on density contrast with respect to the crystalline basement; c) Geological cross-section through the Colli Albani volcano geothermal system. 1 = Quaternary volcanics; 2 = Colli Albani magma reservoir; 3 = Pliocene marine deposits; 4 = Allocthonous clayey-marly flysch; 5,6 = Jurassic-Miocene Sabina succession; 7 = Liassic "Calcare massiccio Fm."; 8 = Triassic "Anidriti di Burano Fm."; 9 = Paleozoic basement. Geothermal reservoir intervals RES1a, RES1b and RES2 are defined in the text. (Giordano et al. 2014).

The crystalline basement is unknown in the Roman region, but it crops out to the north in the Monti Romani area (northern Latium) and in a limited outcrop at the Zannone island to the south. Based on these outcrops the Paleozoic basement should be made largely of Quartzite (Verrucano Fm) and Schists (Hercynian basement) with average density values of $2,750 \text{ kg/m}^3$ (Eppelbaum et al., 2014). As a consequence, by using the abovementioned differential values (Di Filippo & Toro, 1995), the carbonates should have density of $2,650 \text{ kg/m}^3$, the allocthonous flysch of $2,500 \text{ kg/m}^3$, the Pliocene-Quaternary cover of $2,150 \text{ kg/m}^3$. These values are in substantial agreement with those selected in other papers (Todesco & Giordano, 2010, and references therein; Cloetingh et al., 2010, and references therein).

Petrological studies indicate that the reservoir relative to the caldera-forming phase (600-350 ka) had a cumulative eruptive volume of 300 km^3 (Giordano and the CARG team, 2010) related to the crystal fractionation of about 60-70% of mafic magmas (Boari et al., 2009). This corresponds to a minimum intrusive volume left inside the magma chamber of $450-700 \text{ km}^3$. This is a minimum intrusive volume because it disregards the usually larger volume of intrusions that did not feed the extraction of eruptible magma. In fact, the caldera forming ignimbrites represent about 10% of the relative intrusive body (Smith, 1979). We therefore consider the Colli Albani magma chamber to be reliably approximated by a cumulative volume of $1,000-3,000 \text{ km}^3$. The absence of evidence of significant assimilation of limestones in the

ignimbrites indicates that the magma chamber was probably located largely inside the Paleozoic basement with only the top in contact with the Mesozoic carbonates (Boari et al, 2009) (Fig. 10)

Based on the above studies we model the magma chamber as a cylinder with radius equal to the structural radius of the caldera (Giordano et al., 2010), with top located near the contact between the Paleozoic basement and the Mesozoic carbonates, at 6-6.5 km. The thickness of the intrusive body, to accommodate the intrusive volume of 1,000-3,000 km³ estimated as above, extends well below 10 km in depth.

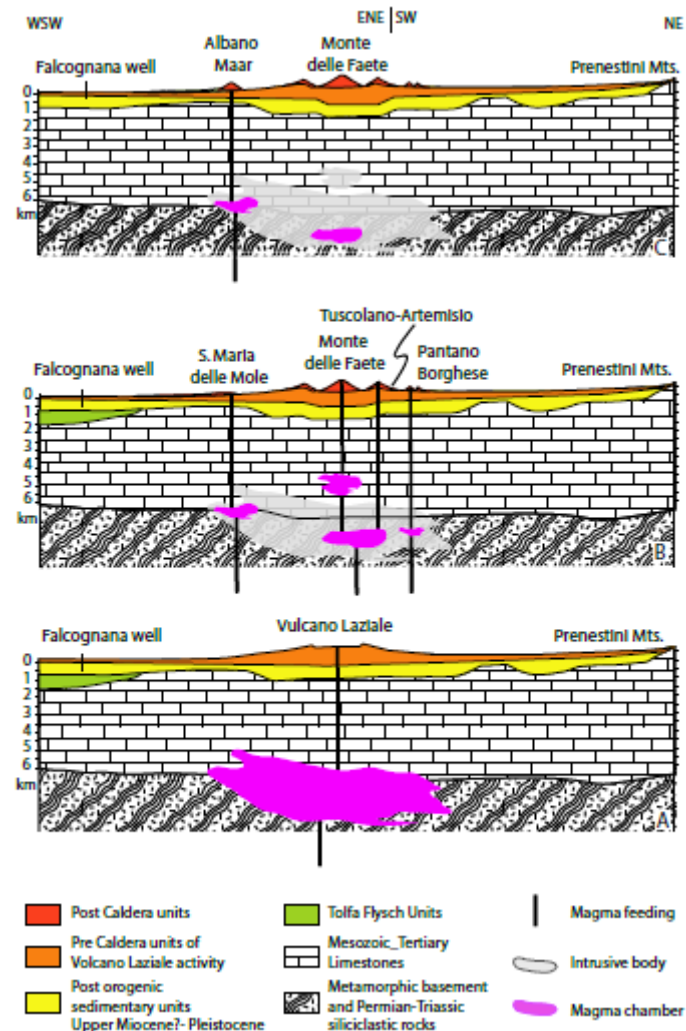


Fig. 10 The evolution of the Colli Albani plumbing system. Here the magma chamber and plumbing systems have been reconstructed with petrological, isotopic, and geochemical data and geological and geophysical interpretations of the geological and structural setting of the Colli Albani pre volcanic units. Xenoliths from the Colli Albani volcanic rocks together with information from deep wells drilled in the area, allow reconstruction of the stratigraphy of the substratum of the volcano, whereas the thickness of the main geological units derives from gravimetric and seismic data. Legend: A) Vulcano Laziale Period (600-350 ka); B) Tuscolano-Artemisio and Faete Period (350-250 ka); C) Via dei Laghi phreatomagmatic Period (200-0 ka) (Boari et al, 2009, and references therein)

At the Sabatini Mts, crustal modeling is based on the inversion of gravimetric data constrained by thicknesses of main lithological units derived from deep bore-holes (Di Filippo et al, 1993). The structural setting is at the first order made of 1-2 km of cap rocks.

Summarizing the available knowledge on geology, we notice that at the first order the overall stratigraphic, structural and magmatic settings are very similar. These similarities allow to simplify the geological conceptual model to produce a computational conceptual model that can represent at a first order the

geothermal systems of both Sabatini and Colli Albani extending towards Roma, from NW and from SE respectively.

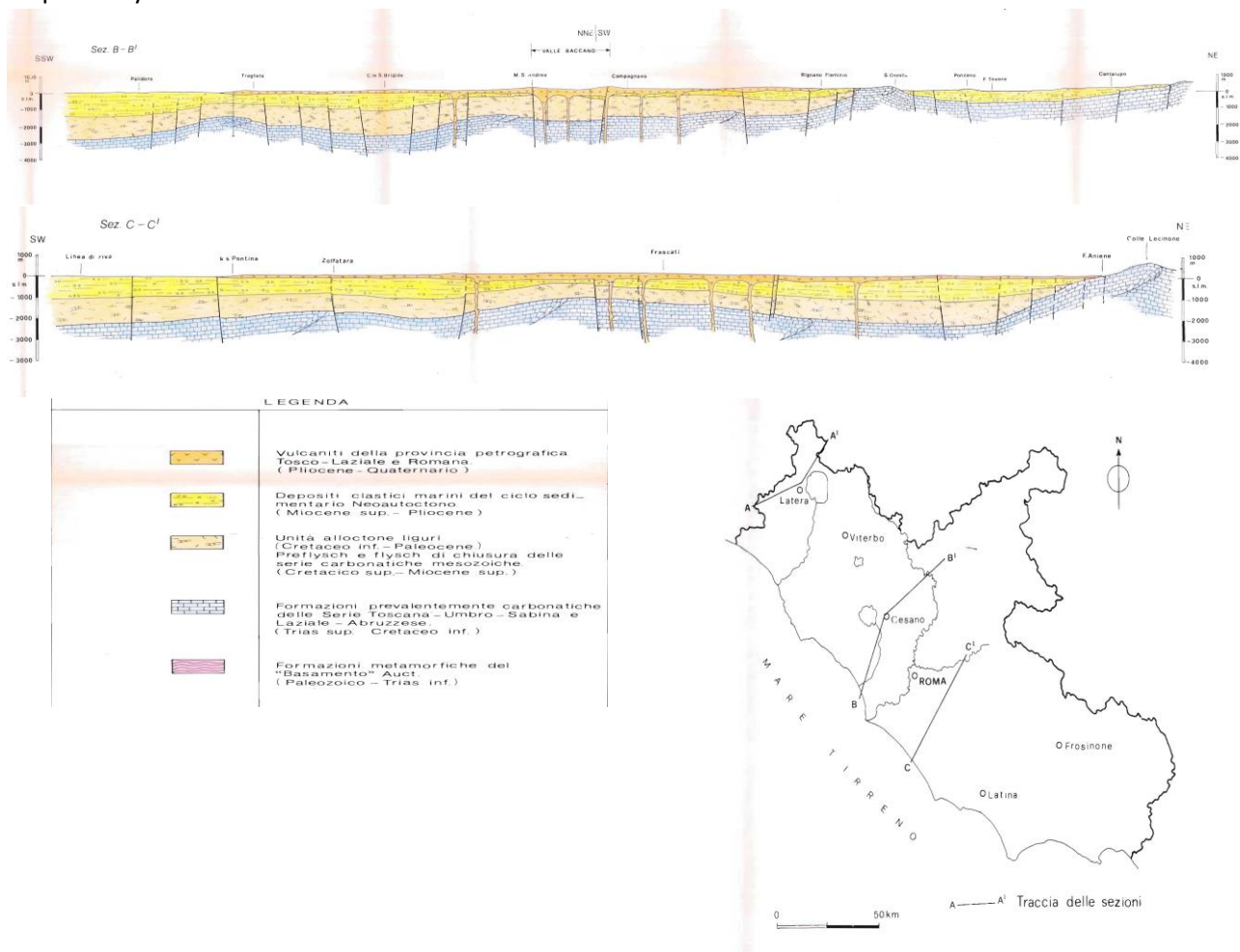


Fig. 11 Geological cross sections in central part of Latium with stratigraphic successions (Enel & Cnr, 1988).

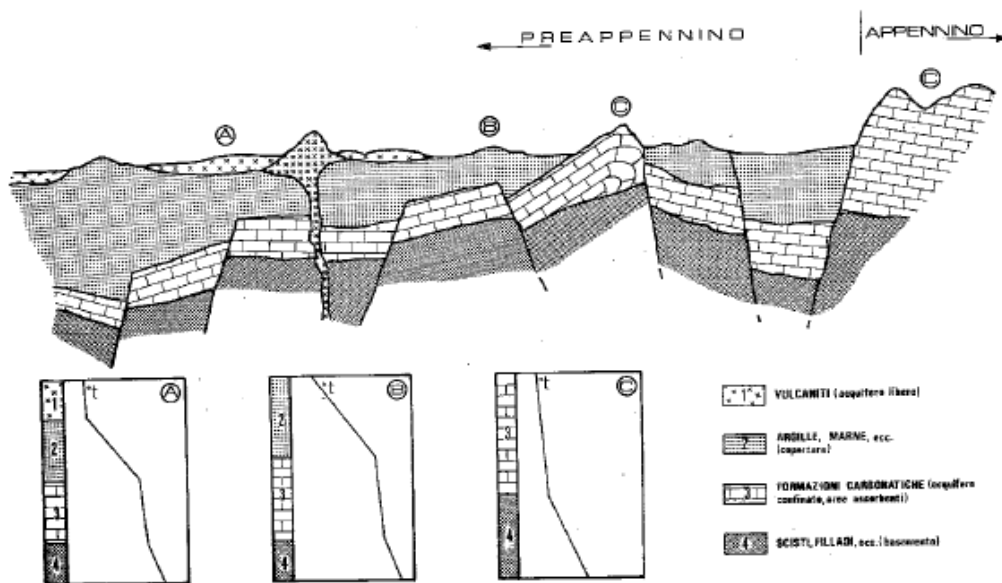


Fig. 12 Hydrogeological model for the toscano-latium Preapennines belt. A, B, C - Geothermal profiles with successions: A leaky aquifer - cap rock - confined aquifer - basement; B cap rock - confined aquifer- basement; C absorption surface - basement (Calamai et al., 1976)

Based on available data we consider a simplified geometry and stratigraphy of the geological conceptual model made of horizontal layers that represent:(Fig. 11 & Fig. 12):

- cap rock, between 0 km and 1.5 km
- reservoir, between 1.5 km and 6 km
- basement, below 6 km to the bottom of the computational mesh at 10 km
- magma chamber, with horizontal dimension of 10 km representative of the average diameters of the calderas.

The horizontal layering is of course an oversimplification of the complex tectonic structure which is known to produce highs and lows of the interface between cap rock and reservoir. However, we have decided to keep an average depth at 1.5 km as the present work focusses on the first order effect of the heat source on the regional geothermal gradient so that local complications are not of interest. Similar considerations apply to the flat morphology of the base of the reservoir, which also is an oversimplification. However the large uncertainties associated with this surface cannot justify the attribution of a morphological/tectonic relief. A regional west to east deepening of this surface is proposed by gravity data (e.g. Barberi et al, 1984), but this is orthogonal to the trend of the volcanic chain, which is the direction of interest for our purposes.

References

- Acocella, V., & Funiciello, R. (2002). Transverse structures and volcanic activity along the Tyrrhenian margin of central Italy. *Bollettino della Società geologica italiana*, 121(1), 739-747.
- Barberi, F., Buonasorte, G., Cioni, R., Fiordelisi, A., Foresi, L., Iaccarino, S., ... & Villa, I. M. (1994). Plio-Pleistocene geological evolution of the geothermal area of Tuscany and Latium. *Mem. Descr. Carta Geol. Ital*, 49, 77-134.
- Boari, E., Avanzinelli, R., Melluso, L., Giordano, G., Mattei, M., De Benedetti, A. A., ... & Conticelli, S. (2009). Isotope geochemistry (Sr–Nd–Pb) and petrogenesis of leucite-bearing volcanic rocks from “Colli Albani” volcano, Roman Magmatic Province, Central Italy: inferences on volcano evolution and magma genesis. *Bulletin of Volcanology*, 71(9), 977-1005.
- Buonasorte, G., Fiordelisi, A., Pandeli, E., Rossi, U., & Sollevanti, F. (1987). Stratigraphic correlations and structural setting of the pre-neoautochthonous sedimentary sequences of Northern Latium. *Periodico di Mineralogia*, 56, 111-122.
- Buonasorte, G., Carboni, M. G., & CoNTI, M. A. (1991). Il substrato Plio-Pleistocenico delle vulcaniti sabatine; considerazioni stratigrafiche e paleoambientali. *Bollettino della Società Geologica Italiana*, 110(1), 35-40.
- Buonasorte, G., Cameli, G. M., Fiordelisi, A., Parotto, M., & Perticone, I. (1995, May). Results of geothermal exploration in Central Italy (Latium-Campania). In *Proceedings of the World Geothermal Congress, Florence, Italy* (pp. 18-31).
- Calamai, A., Cataldi, R., Locardi, E., & Praturlon, A. (1976, October). Distribuzione delle anomalie geotermiche nella fascia pre-Appenninica tosco-laziale (Italia). In *Proc. Int. Symposium on Geothermal Energy in Latin-America, Guatemala City* (pp. 189-229).
- Chiarabba, C., Giordano, G., Mattei, M., & Funiciello, R. (2010). The 3D structure of the Colli Albani volcano. SPECIAL PUBLICATION-GEOLOGICAL SOCIETY OF LONDON, 29-41.
- Cloetingh, S. A. P. L., Van Wees, J. D., Ziegler, P. A., Lenkey, L., Beekman, F., Tesauro, M., ... & Bonté, D. (2010). Lithosphere tectonics and thermo-mechanical properties: an integrated modelling approach for Enhanced Geothermal Systems exploration in Europe. *Earth-Science Reviews*, 102(3), 159-206.
- Conforto, B. (1962). A Pliocene formation W of Roma. *Quaternaria*, 5, 119-130.
- Conticelli, S., Laurenzi, M. A., Giordano, G., Mattei, M., Avanzinelli, R., Melluso, L., ... & Perini, G. (2010). Leucite-bearing (kamafugitic/leucititic) and-free (lamproitic) ultrapotassic rocks and associated shoshonites from Italy: constraints on petrogenesis and geodynamics. *Journal of the Virtual Explorer*, 36(20).
- Conticelli, S., Avanzinelli, R., Poli, G., Braschi, E., & Giordano, G. (2013). Shift from lamproite-like to leucititic rocks: Sr–Nd–Pb isotope data from the Monte Cimino volcanic complex vs. the Vico stratovolcano, Central Italy. *Chemical Geology*, 353, 246-266.
- Corrado, S., Aldega, L., Celano, A. S., De Benedetti, A. A., & Giordano, G. (2014). Cap rock efficiency and fluid circulation of natural hydrothermal systems by means of XRD on clay minerals (Sutri, Northern Latium, Italy). *Geothermics*, 50, 180-188.
- Danese, E., & Mattei, M. (2010). The sedimentary substrate of the Colli Albani volcano. The Geological Society of London.

- De Benedetti, A. A., Caprilli, E., Rossetti, F., & Giordano, G. (2010). Metamorphic, metasomatic and intrusive xenoliths of the Colli Albani volcano and their significance for the reconstruction of the volcano plumbing system. *The Colli Albani Volcano, Special Publication of IAVCEI*, 3, 153-176.
- Di Filippo, M. (Ed.). (1993). *Sabatini volcanic complex: Progetto finalizzato geodinamica*. Consiglio nazionale delle ricerche.
- Di Filippo, M., & Toro, B. (1995). Gravity features. *The Volcano of the Alban Hills. Tipografia SGS, Roma*, 213-219.
- Enel & Cnr, (1988). Inventari o delle Risorse Geotermiche Nazionali—Indagine D'insieme Sul Territorio Nazionale. *Ministero dell'Industria, del Commercio e dell'Artigianato (currently Ministero dello Sviluppo Economico)*, 75.
- Eppelbaum, L., Kutasov, I., & Pilchin, A. (2014). Thermal properties of rocks and density of fluids. In *Applied geothermics* (pp. 99-149). Springer Berlin Heidelberg.
- Funciello, R., & Parotto, M. (1978). Il substrato sedimentario nell'area dei Colli Albani: considerazioni geodinamiche e paleogeografiche sul margine tirrenico dell'Appennino centrale. *Geologica Romana*, 17, 233-287.
- Giordano, G. & THE CARG TEAM (2010). Stratigraphy, volcano tectonics and evolution of the Colli Albani volcanic field. *The Colli Albani Volcano, Special Publication of IAVCEI*, 3., 43– 98
- Giordano, G., De Benedetti, A. A., Bonamico, A., Ramazzotti, P., & Mattei, M. (2014). Incorporating surface indicators of reservoir permeability into reservoir volume calculations: Application to the Colli Albani caldera and the Central Italy Geothermal Province. *Earth-Science Reviews*, 128, 75-92.
- Maffucci, R., Corrado, S., Aldega, L., Bigi, S., Chiodi, A., Di Paolo, L., ... & Invernizzi, C. (2016). Cap rock efficiency of geothermal systems in fold-and-thrust belts: Evidence from paleo-thermal and structural analyses in Rosario de La Frontera geothermal area (NW Argentina). *Journal of Volcanology and Geothermal Research*, 328, 84-95.
- Marini, L., Franceschini, F., Ghigliotti, M., Guidi, M., & Merla, A. (1993). Valutazione del potenziale geotermico nazionale. *ENEA-Geotermica Italiana Report for the Ministero dell'Industria, del Commercio e dell'Artigianato*.
- Mattei, M., Funciello, R., & Parotto, M. (2008). Roma e contesto geodinamico recente dell'Italia Centrale. *MEMORIE DESCRITTIVE DELLA CARTA GEOLOGICA D'ITALIA*, 70, 13-24.
- Mattei, M., Conticelli, S., & Giordano, G. (2010). The Tyrrhenian margin geological setting: from the Apennine orogeny to the K-rich volcanism. *The Colli Albani volcano. Special Publications of IAVCEI*, 3, 7-27.
- Parotto, M., & Praturlon, A. (1975). Geological summary of the Central Apennines. *Quaderni della Ricerca Scientifica*, 90, 257-300.
- Praturlon, A. (1993). Inquadramento geologico. *Guide geologiche regionali: Lazio. BE-MA editrice*, 18-38.
- Smith, R. L. (1979). Ash-flow magmatism. *Geological Society of America Special Papers*, 180, 5-28.
- Smith, R. L., & Shaw, H. R. (1975). Igneous-related geothermal systems. *US Geol. Surv. Circ*, 726, 58-83.
- Todesco, M., & Giordano, G. (2010). Modelling of CO₂ circulation in the Colli Albani area. *SPECIAL PUBLICATION-GEOLOGICAL SOCIETY OF LONDON*, 311-330.

Chapter 6 – Description of how the conceptual model is implemented in HEAT3D: mesh, rocks physical parameters, thermal gradients and time steps

THE BASE CONFIGURATION

COMPUTATIONAL MODEL, SELECTION OF THE CELL-SIZE, SELECTION OF THE HORIZONTAL AND VERTICAL EXTENT

The computational domain that we construct is based on the simplified conceptual model described in the previous chapter and is designed to minimise the effects of local stratigraphic and structural dishomogeneities.

The cell-grid is cells of 0.5 km x 0.5 km, small enough to represent the main features of the geothermal reservoir but large enough to average local effects.

For a similar magmatic geothermal system at Campi Flegrei a cell grid of 1 km x 1 km has been used, well suited to account for first order geometry and optimize computational resources (Di Rienzo et al., 2016).

Moreover, a smaller cell-size would require larger computational resources that would be necessary to run the model, while the uncertainties in the geological knowledge would not support such refined scale of work.

The X-Z domain is 60 km long and 10 km deep (120 x 20 cells) (see Fig. 1).

The horizontal distance between the central axis and the edge of the domain is 30 km: this is the distance between the centre of Bracciano caldera lake and the centre of Rome and between the centre of Colli Albani caldera and the centre of Rome. In this way it is possible to compare the model output with the set of measured data to calibrate the model parameters.

Based on the above, the computational domain can be summarised as it follows

- cap rock: this layer includes and averages the contribution of all rock types above the regional geothermal reservoir; the rocks that most contribute to the impervious role of this layer are the post-orogenic Pliocene-Pleistocene marine clays and the allocthonous clayey flysch; the shallower and thinner rock types include volcanic products and continental sediments, although these are not necessarily impermeable; the chosen lithology that averages the behavior of the cap rock is claystone.
- reservoir: the reservoir is simplified in one single lithology without internal tectonic structures. The lithology chosen is limestone, which is the most represented in the Meso-Cenozoic carbonatic successions that form the regional geothermal reservoir in the Roman Geothermal Province. This is of course a major simplification as the reference geological model do show the presence of such structures both compressional (thrusts) and extensional (normal faults). We also know that in many systems the interplay between the internal stratigraphy and the structure produces local compartmentalization that can be very important (e.g. Vignaroli et al., 2013). However, we are approaching here a first order modeling that could benefit of internal complications only if those have been ascertained, while there are no works available that have detailed well enough the internal structure if not purely in a qualitative way.
- basement: the lithology of this layer ranges as characteristics, according to available geological knowledge, from low grade slates to granites.
- magma chamber: the lateral extent of the magma chamber is constrained (conservatively) by the extent of the calderas; the vertical extent is constrained by the estimation of the volume of the intrusive complex based on the volume of erupted products and the calculation of their degree of differentiation/assimilation; the magma type, depth, internal temperature and thermal characteristics of the magma chamber are constrained by the petrology of erupted products.

The cap rock occupies the first layer from 0 km to -1.5 km; the geothermal reservoir occupies the second layer from -1.5 km to -6 km and the crystalline basement is located in the bottom layer from -6 km to -10 km. The magma chamber has its roof -6.5 km along the z axis and the length is 10 km from km 25 to km 35 along the x-axis.

In our case the minimum distance required by our computational mesh is 500 m that represents the distance from the top of the magma chamber and the base of the carbonatic reservoir. The domain is symmetrical with respect to the central vertical axis. In this way the boundary conditions are the same in vertical and horizontal plane respect to this axis.

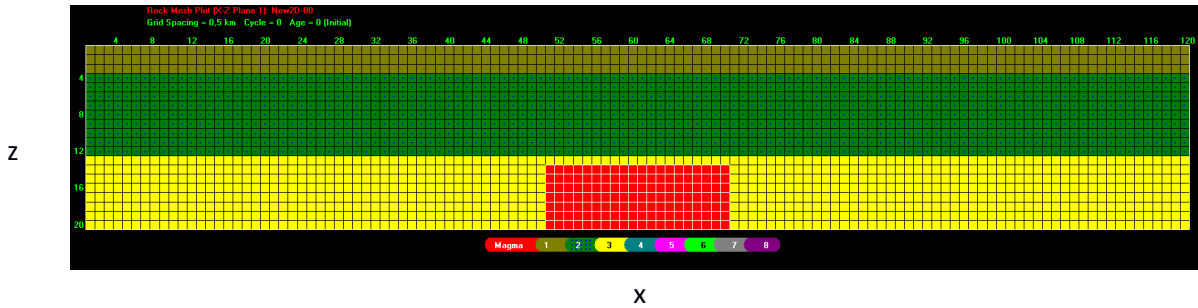


Fig. 1 Heat3D X-Z base mesh

INITIAL ROCK TEMPERATURES

In Heat3D, initial rock temperatures are assigned based upon the surface temperature their depth and physical parameters and the specified thermal gradient.

SURFACE TEMPERATURE

The surface temperature is set at 20 °C.

VALUES OF PHYSICAL PARAMETERS IN BASE SIMULATIONS

Following the data available in literature that define the “Physical Parameters for different Rocks” (ANNEX 1)) the base simulation is implemented with the following physical parameters (Table 1):

Cap Rock: density ρ 2,200 kg/m³, specific heat c_p 1,100 J/kg*K, thermal conductivity k 1.5 W/m*K (thermal diffusivity $6.20 \cdot 10^{-7}$ m²/s).

Geothermal reservoir: density ρ 2,650 kg/m³, specific heat c_p 900 J/kg*K, thermal conductivity k 2.7 W/m*K (thermal diffusivity $1.13 \cdot 10^{-6}$ m²/s) – porosity 0.05 (Bono, 1981).

Crystalline basement: density ρ 2,750 kg/ m³, specific heat c_p 1,100 J/kg*K, thermal conductivity k 2.5 W/m*K (thermal diffusivity $8.26 \cdot 10^{-7}$ m²/s).

Magma: mafic (specific heat c_p 1,200 J/kg*K, thermal conductivity k 1.7 W/m*K, density ρ 2,750 kg/m³, thermal diffusivity $5.15 \cdot 10^{-7}$ m²/s); temperature 900 °C.

	k	c_p	ρ	T	Porosity	Thermal diffusivity
Cap Rock	1.5	1,100	2,200	/	/	$6.20 \cdot 10^{-7}$
Geothermal Reservoir	2.7	900	2,650	/	0.05	$1.13 \cdot 10^{-6}$
Crystalline basement	2.5	1,100	2,750	/	/	$8.26 \cdot 10^{-7}$
Magma	1.7	1,200	2,750	900	/	$5.15 \cdot 10^{-7}$

Table 1 Summary of basic physical parameters

Permeabilities (P) are assumed to be a function of porosity, f, such that:

$$P \approx 10^{-20} * \exp(71*f) \quad \text{Eq. 1}$$

With porosity set at its maximum ($f = 0.40$), P is $\sim 2.5 \cdot 10^4$ d, typical of non-cemented gravels; at $f = 0.15$ to 0.20, P ranges from 0.4 to 16 md, typical of many sediments; and at $f = 0.05$, P is near a μ d, which is typical of cemented sediments and welded tuffs.

The chosen porosity value (Bono, P., 1981 and references therein) is a conservative proposal, a mean value that take in account that we are simulating the thermal evolution in a sub regional area.

HEAT3D calculates convective behavior by adding a convective term to the solved heat flow equation. The magnitude of the convective term is limited by an effective Nusselt number. For saturated rocks, HEAT assumes a high maximum effective Nusselt number (~100) in the region where convection is assigned and it decreases with falling porosity (permeability) in rocks and rising fluid temperature.

THERMAL GRADIENT

The DGS-UNMIG (General Directorate- For Safety Of Mining And Energy Activities - National Mining Office For Hydrocarbons And Georesources) of the Italian Ministry of Economic Development has made available a database for Italian Municipalities. In the database it is possible to find relevant information regarding geothermal resources.

For each municipality the databes makes available: name, province Region and ISTAT (Italian Institute of Statistics) code; temperature (in °C) mean, minimum and maximum at 1 km, 2km and 3 km deep; the mean, minimum and maximum heat flow (in mW/m²); the mean, minimum and maximum depth of the regional carbonatic reservoir top (in m).

Considering a soil temperature of 20 °C, it is possible to build up an estimation of the thermal gradient:

$$\text{Mean thermal gradient} = d(T_{3000_mean} - 20^{\circ}\text{C}) / 3 \text{ K/km}$$

It is possible to implement the analysis for Italy (Fig. 2).

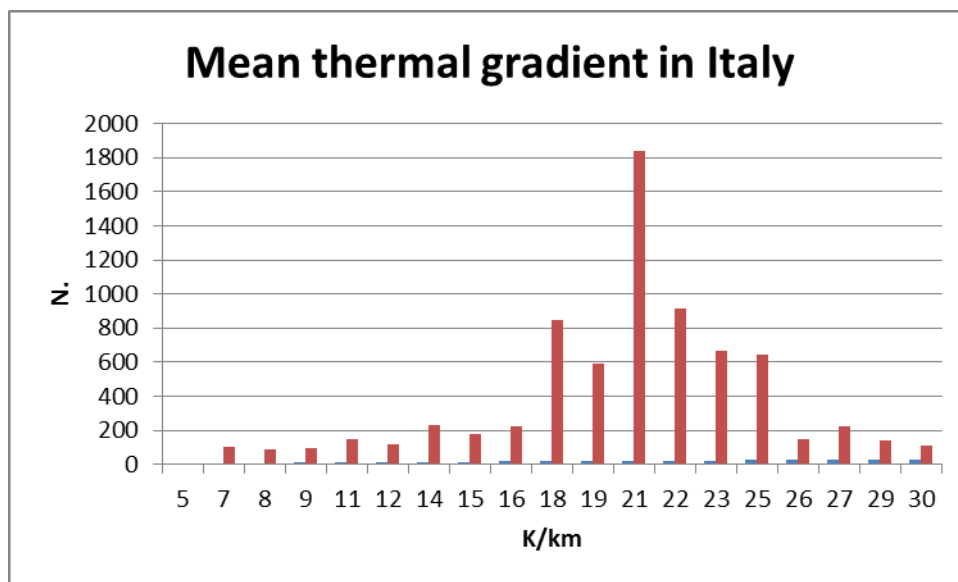


Fig. 2 Thermal gradient distribution in Italy

Based on available data the average temperature gradient in Italy is 20.8 K/km (95% of data are included below 30 K/km). This value can be considered the regional thermal gradient for Italy. This value is not exact as it is normalized to the number of municipalities and not to their actual areas, but at first approach we take it as representative.

It is possible to implement the same analysis for the Municipalities in Lazio Region and in Province of Rome (Fig. 3 and Fig. 4).

In Lazio Region the temperature gradient is 22.8 K/km (95% of data are included below 71 K/km). Also in this case this value is not exact as it is normalized to the number of municipalities and not to their actual areas, but again at first approach we take it as representative. It is notable the different shape of distribution between Italy and Lazio Region.

In the Province of Rome we have 26.6 K/km for average temperature gradient (95% of data are included till 60 K/km). This distribution is qualitatively similar to that of Lazio Region, but with a bimodal distribution more pronounced.

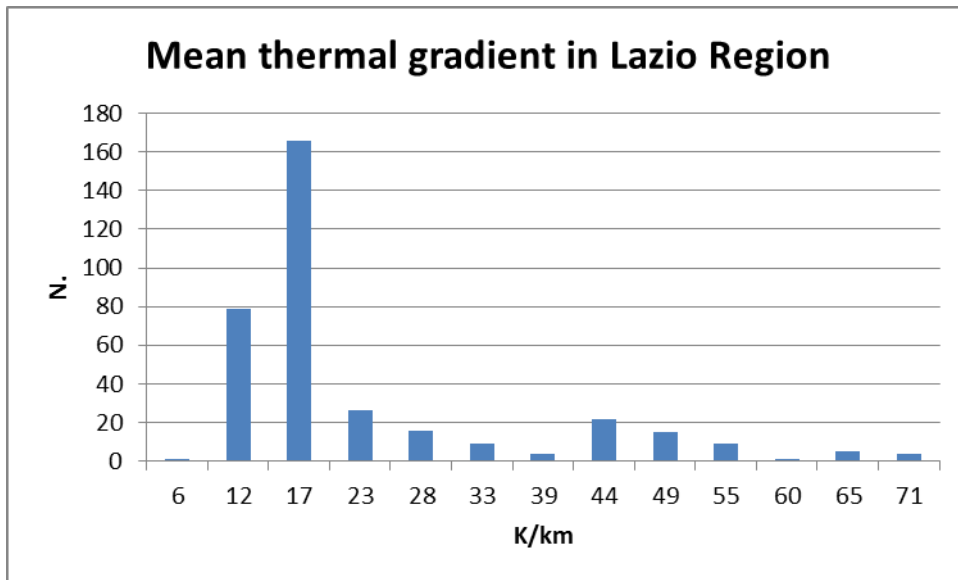


Fig. 3 Thermal gradient distribution in Lazio Region

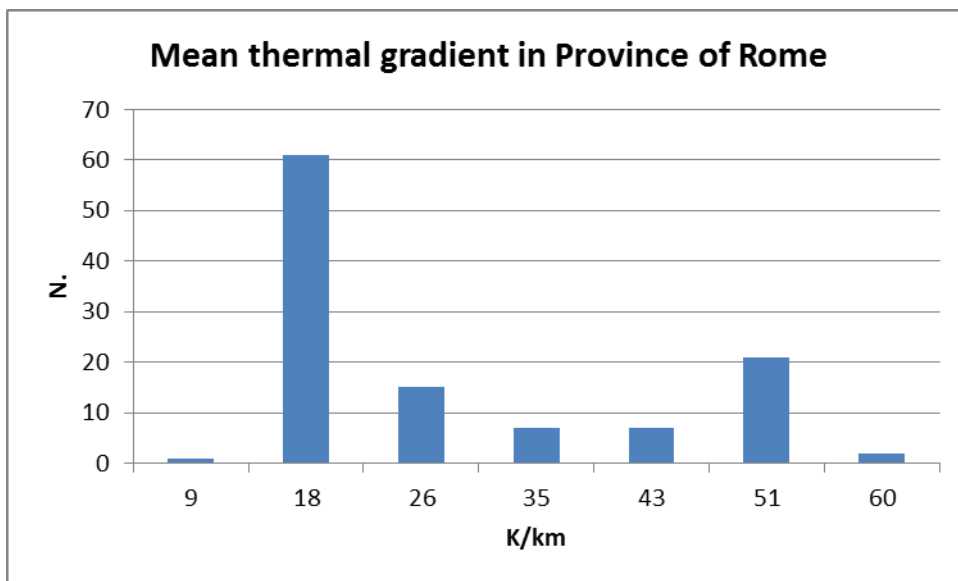


Fig. 4 Temperature gradient distribution in Province of Rome

For the City of Rome, 45.9 K/km is the average temperature gradient using the UNMIG database.

Analysing the Monti Sabatini caldera area (NW of Rome), we can evaluate the thermal gradient considering the four Municipalities that are located around the area of volcanic caldera (a small part of the area belongs to Municipality of Rome, but data of Rome are not included in this analysis) (Tab.2 and in Fig.5).

Municipality	Temperature gradient K/km
Anguillara Sabazia	85,3
Bracciano	78,0
Campagnano Di Roma	75,1
Trevignano Romano	93,4

Tab. 2 Municipalities and Temperature gradient around the Bracciano lake

The average temperature gradient is 83.0 K/km.

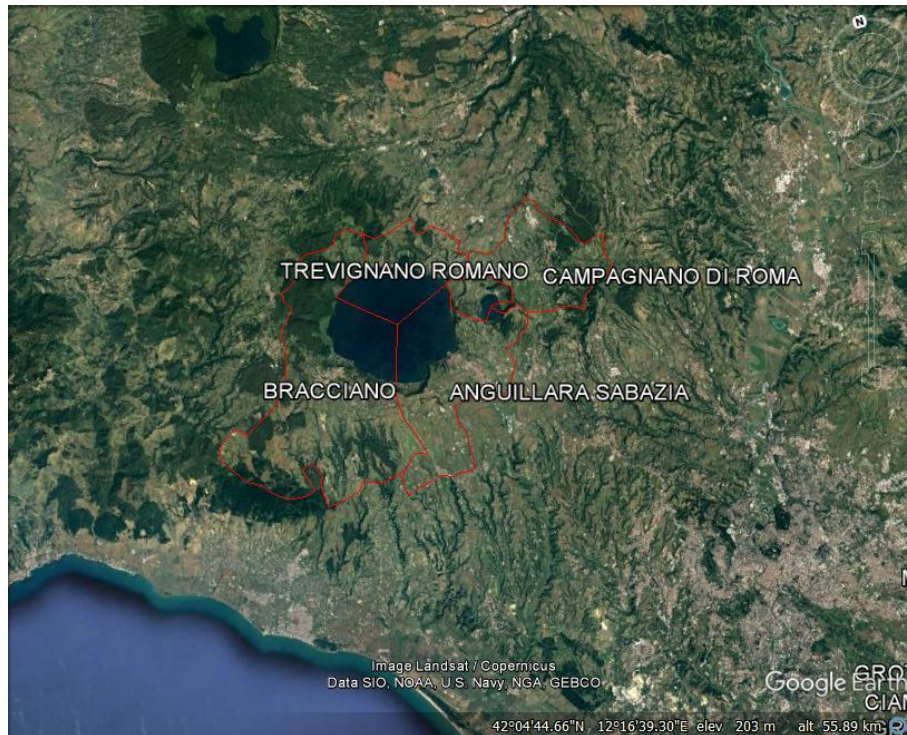


Fig. 5 The municipalities around the Bracciano lake area

The same effort can be implemented for Colli Albani area (SE of Rome)

We consider the Municipalities that are located around the area of the caldera (a small part of the area belongs to Municipality of Rome, but data of Rome are not included in this analysis) (Tab.3 and in Fig.6).

Municipality	$d(T3000_mean-20^{\circ}C)/3$
Albano Laziale	43,1
Ariccia	43,3
Castel Gandolfo	43,1
Ciampino	43
Frascati	44,9
Genzano di Roma	44,2
Grottaferrata	44,1
Labico	22,7
Lariano	33,1

Municipality	$d(T3000_mean-20^{\circ}C)/3$
Marino	43
Montecompatri	42
Monte Porzio Catone	45,8
Nemi	44,1
Rocca di Papa	44,6
Rocca Priora	43,6
San Cesareo	34,1
Velletri	43,2

Tab. 3 Municipalities and Temperature gradient in Colli Albani area

The average temperature gradient is 41.3 K/km.

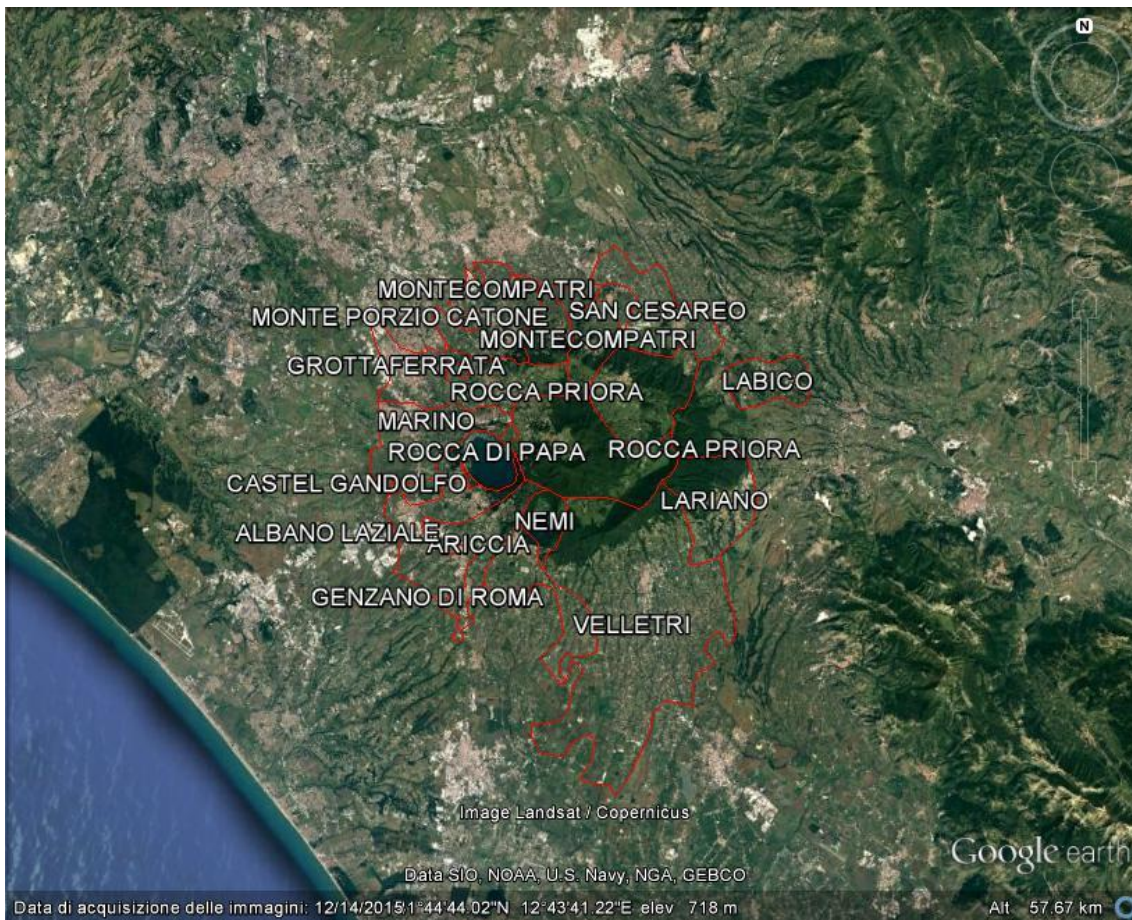


Fig. 6 The municipalities in Colli Albani area

For the simulations, we will include 3 regional geothermal gradient in the domain: 0 K/km, 20 K/km and 40 K/km.

- 0 K/km is the unperturbed situation. With this option it is possible study the effects of different simulations without external effects.
- 20 K/km is the average temperature gradient in Italy, Lazio Region and the Province of Rome, and is taken as the realistic boundary condition.
- 40 K/km is a stronger temperature gradient, more like the thermal gradient for the City of Rome, Colli Albani area and is intended to represent the pre-heating of the crust related to the history of magmatism that modified the local gradient before the starting point taken in the simulations

SIMULATIONS IMPLEMENTED

For heat transmission in the geothermal reservoir, **four sets of different simulations** are implemented:

- heat transmitted by conduction by a magma chamber instantaneously inserted in the computational domain;
- heat transmitted by convection in geothermal reservoir (porosity 0,05) by a magma chamber instantaneously inserted in the computational domain.
- heat transmitted by conduction in geothermal reservoir, with magma kept at constant temperature to represent an actively recharged magma chamber;
- heat transmitted by convection in geothermal reservoir, with magma kept at constant temperature to represent an actively recharged magma chamber.

TIME STEP

The **time step** of calculations is set at 50 ky and the time window is taken at 350 ky. This time window allows to encompass the time-lag from the peak of magmatism in the Roman Region and today, allowing to sample conditions at any shorter times, should the local volcanology suggest shorter time lags from last magma recharge.

This setting allows to study the interval from time 0 till 350 ky (8 steps) for magma not fed that dissipates heat during the simulation;

For the simulations that study magma kept at constant temperature to represent an actively recharged magma chamber the time lag is taken from time 0 till 500 ky (11 steps) with magma temperature unvaried, while the following time-steps from time 550 till 850 ky (7 steps) represent magma losing temperature.

OPTIONS FOR THE SIMULATIONS

For the base simulation, with the initial temperature chosen at 900 °C, the mafic magma is solid. This is to represent the average conditions of magma reservoirs that are largely crystalline and only periodically host small percentages of eruptible magma (up to maximum 30%)(e.g. Cashman and Giordano, 2014). In such conditions Magma Convection and Latent Heat Magma give no extra thermal contribution, like Latent Heat Rocks and therefore are not considered (Wohletz, 1999).

INTRUSION/ADVECTION

In our simulations we disregard the Intrusion/Advection option that would account for recharge within an active magma chamber, which could be very important in areas of active volcanism such as Campi Flegrei (Wohletz et al., 1999; Di Rienzo et al., 2016). This choice reflects the essentially quiescent state of the Latium calderas, for which there is no current evidence of recharge of the crustal reservoirs (Chiarabba et al., 2010). We accordingly designed the simulations to show the heat transfer from the magma reservoir to the country rocks starting from the end of the recharge history. Therefore the initial magmatic temperature of the magma reservoir is only declining over time. The time-lag of simulations (350 kyr with steps of 50 kyr) allows to sample the associated thermal values at any time since last recharge, which takes into account the complexity of the volcanic history and does not imply that this time lag represents the expected interval time representing present-day conditions. For example, at Colli Albani, the large magma reservoir associated with the caldera forming eruptions reduced its recharge considerably after 350 ka; however volcanism with lesser intensity and average eruption rates extended up to 25 ka. Data analysis therefore may allow to evaluate possible influence of post-caldera recharge by considering time-dependent thermal data in comparison with the present state.

P-T DEPENDENCIES

Rock conductivities (k) are generally tabulated for earth surface temperature and pressure. The effects of pressure and temperature on rock are calculated by the method of Chapman and Furlong (1990):

$$k(t,z) = k_0((1+cZ)/(1+bT)) \quad \text{Eq. 2}$$

where

$k_0 = k$ at 0 °C

b (upper crust) = 1.5e-3/deg

b (lower crust) = 1.0e-4/deg

$c = 1.5e-3/\text{km}$ ($c = 0$ for negligible pressure effects)

$Z = \text{depth (km)}$; $T = \text{temp (°C)}$

k increases with pressure but generally decreases with temperature.

For magmas, temperature dependencies are from McBirney (1979): basalt k falls with T, andesite rises slightly, and rhyolite rises sharply; basalt b = 0.00037/deg, andesite (intermediate) b = -0.00009/deg, rhyolite (silicic) b = -0.00054/deg

To evaluate the effect of pressure and temperature on rock (P-T dependencies), simulation with this option switched off and on have been implemented.

Defining $V\%(X,Y,Z,T)$ the percentage variation like:

$$V\%(X,Y,Z,T_{350ka})=100*(NC(X,Y,Z,T_{350ka})-C(X,Y,Z,T_{350ka}))/NC(X,Y,Z,T_{350ka}) \quad \text{Eq. 3}$$

where

NC(X,Y,Z,T) is the value of temperature (in K) when the option is No Checked

C(X,Y,Z,T) is the value of temperature (K) when the option is Checked

In the Geothermal Reservoir the $V\%_{MAX}(X,Y,Z, T_{350ka})$ is 8.1% and $V\%_{MIN}(X,Y,Z, T_{350ka})$ is -9.4% with heat transmitted by conduction and thermal gradient 40 K/km.

We disregard this option because the maximum variation is less than 10%. Moreover, using this option implies to lose the control on rocks physical parameters. These values are strictly connected with the conceptual model that we adopted in our hypotheses.

HEAT CONSERVATION

Heat Conservation: Heat3D allows to monitor the percentage of heat lost or gained within the mesh. Generally, this value stays within a range of +/- a few percent, and gives a measure of calculational accuracy and precision. The calculated value takes into consideration the heat source and sink caused by magma crystallization/fusion latency but not that of high temperature rocks. Some heat is lost to the margins of the mesh, which are held at a constant temperature consistent with the specified thermal gradient and mesh top temperature. **Because convection simulation is an approximation, the mesh should show some heat gained in the mesh (up to 10%) while convection is active. If this value rises and persists much beyond +/-10% then one should suspect mesh design attributes that cannot be adequately calculated.** If the mesh is edited during a calculation, then the value is reset to 0%.

In the simulations, we have assumed the maximum acceptable value at +/- 20%. If this value is reached, and in the next time steps it remains on this value or, worse, it is overcome, the simulation is stopped and it is considered only before the reach of this chosen value.

ANNEX 1 PHYSICAL PARAMETERS FOR DIFFERENT ROCKS

	Density kg/m ³	Thermal Conductivity W m ⁻¹ K ⁻¹	Specific Heat J/kg * K	Thermal Diffusivity m ² /s	Porosity
Sedimentary					
Argillite	2300 2555	1,67 2,09	860	9,94 9,76	
Carbonate	2800	1,1	900		0,1
Clay	2080 2490 – 2540 2520	1,43 0,8 – 1,5	1100	3,21 7,3	
	1750	1,5	1000		0,35
Clay slate	2620 – 2830 2680				
Clay marl	2430 – 2640 2540				
Clayey limestone	2650 2644			9,05	
Clayey sandstone	2500			14,3	
Clayey siltstone	2566			10,8	
Claystone	2360 – 2830 2600				
Dolomite	2750 – 2830 2753 2530 – 2720 2630		920	9,95	
	2700 – 2850	3,2-5			
Line marl	2430 – 2620 2530				
Limestone	1600 – 2700	2 – 3,4			
	2600 2700 2714 2410 – 2670 2550 2580 – 2660 2620	2,37 3,44	890 840	9,6 10,92	
Limestone, parallel	2600				
Limestone, perpend.	2690				
Marl	1970 2590 – 2670 2630	1,78	1550	4,04 7,53	
Marly clay	2460 – 2490 2470				
Pisolithic Tuffs	1500	0,8	900		0,35
Quartz-sandstone	2645				
Quartz-sandstone, parallel	2640				
Quartz-sandstone, perpend.	2650				
Quartzite schist	2710			18	
Sand	2300	2	1000		0,25
		1,79 1,1 – 2,1	960 800 957		
Sandy shale	2057			3,21	
Sandstone	1900 – 2500	1,5 – 4,2			
	2350 – 2970 2650	2,5	920		
Sandstone, fine-grained	2550			7,19	
Sandstone, fine-grained	2400			10,5	
Sandstone, oil saturated	2200			11,57	
Sandstone, oil-bearing	2090 2198			12,54 11,57	
Sandstone, water saturated	2300			12,8	
Schistose clay	2420 – 2570 2490				
Shale	2100 – 2700	1,2 – 3			
	1100 -2100	1,1 – 2,1			
Siltstone	2550	1,58	870	10,8 10,28	
Siltstone, oil-bearing	2300			12,9	
Slate, parallel	2700				
Slate, perpend.	2760				
Volcanics	2000	0,8	900		0,45

Turcotte, D. L., & Schubert, G. (2014). Geodynamics. Cambridge University Press.

Eppelbaum, L., Kutasov, I., & Pilchin, A. (2014). Applied geothermics. Springer Berlin Heidelberg.

Todesco, M., Giordano, G. (2010). Modeling of CO₂ circulation in the Colli Albani area. Geological Society of London.

Cloetingh, S. A. P. L., Van Wees, J. D., Ziegler, P. A., Lenkey, L., Beekman, F., Tesauro, M., ... & Bonté, D. (2010). Lithosphere tectonics and thermo-mechanical properties: an integrated modelling approach for Enhanced Geothermal Systems exploration in Europe. *Earth-Science Reviews*, 102 (3), 159-206.

	Density kg/m ³	Thermal Conductivity W m ⁻¹ K ⁻¹	Specific Heat J/kg * K	Thermal Diffusivity m ² /s	Porosity
Metamorphic					
Amphibole	2800 – 3150	2, 1 – 3,8			
		2,39 – 3,33	1130	6,84	
Gneiss	2600 – 2850	2, 1 – 4,2			
		2,41 2,7 – 3,1	1020	7,98	
Gneiss-granite		2,04	1110	7,24	
Marble	2670 – 2750	2, 5 – 3			
Quartzite		5 – 5,03			
	2650	2,5	1050		
Schist		2,55	1100	9,6	
Slate	2730				
Slate, parallel	2700				
Slate, perpend.	2760				
	Density kg/m ³	Thermal Conductivity W m ⁻¹ K ⁻¹	Specific Heat J/kg * K	Thermal Diffusivity m ² /s	Porosity
Igneous					
Andesite		1,87 – 2,26			
Anorthosite	2640-2920	1,7 – 2,1			
Augite			800		
Basalt	2950	1,3 – 2,9			
		2,11 – 1,69	1230 – 840	5,34	
Diabase	2900	2 – 4			
		2,5 – 2,2	870	9,93	
Diorite	2800	2,8 – 3,6			
		2,1 – 2,5	1000	6,38	
	2900	2,8	1050		
Gabbro	2950	1,9 – 4,0			
		2,47 – 2,57	980	9,7	
Gabbro-norite		2,22			
Granite	2650	2,4 – 3,8			
		2,68 – 3,07	950 – 790	9,13	
Granodiorite	2700	2,0 – 3,5			
		2,79 – 2,63	1020	5,15	
Harzburgite		2,69			
Hypersthene			800		
Hornblende			840		
Olivine gabbro	3300	3,5	1050		
		2,65			
Pyroxenite	3250	4,1 – 5			
Porphyrite		1,74	910	9,54	
	Density kg/m ³	Thermal Conductivity W m ⁻¹ K ⁻¹	Specific Heat J/kg * K	Thermal Diffusivity m ² /s	Porosity
Mantle					
Dunite	3000 – 3700	3,7 – 4,6			
		2,77			
Peridotite	3250	3 – 4,5			
	Density kg/m ³	Thermal Conductivity W m ⁻¹ K ⁻¹	Specific Heat J/kg * K	Thermal Diffusivity m ² /s	Porosity
Miscellaneous					
Anhydrite	2650 – 2910 2800	5,43			
Halite	2160				
Ice	917	2,2			
		2,1			

Turcotte, D. L., & Schubert, G. (2014). Geodynamics. Cambridge University Press.

Eppelbaum, L., Kutasov, I., & Pilchin, A. (2014). Applied geothermics. Springer Berlin Heidelberg.

Todesco, M., Giordano, G. (2010). Modeling of CO₂ circulation in the Colli Albani area. Geological Society of London.

Cloetingh, S. A. P. L., Van Wees, J. D., Ziegler, P. A., Lenkey, L., Beekman, F., Tesauro, M., ... & Bonté, D. (2010). Lithosphere tectonics and thermo-mechanical properties: an integrated modelling approach for Enhanced Geothermal Systems exploration in Europe. *Earth-Science Reviews*, 102 (3), 159-206.

REFERENCES

- Bono, P. (1981). Valutazione preliminare del potenziale geotermico della regione laziale. *Geol Rom*, 2.
- Cashman, K. V., & Giordano, G. (2014). Calderas and magma reservoirs. *Journal of Volcanology and Geothermal Research*, 288, 28-45.
- Chiarabba, C., Giordano, G., Mattei, M., & Funicello, R. (2010). The 3D structure of the Colli Albani volcano. SPECIAL PUBLICATION-GEOLOGICAL SOCIETY OF LONDON, 29-41.
- Cloetingh, S. A. P. L., Van Wees, J. D., Ziegler, P. A., Lenkey, L., Beekman, F., Tesauro, M., ... & Bonté, D. (2010). Lithosphere tectonics and thermo-mechanical properties: an integrated modelling approach for Enhanced Geothermal Systems exploration in Europe. *Earth-Science Reviews*, 102(3), 159-206.
- Di Renzo, V., Wohletz, K., Civetta, L., Moretti, R., Orsi, G., & Gasparini, P. (2016). The thermal regime of the Campi Flegrei magmatic system reconstructed through 3D numerical simulations. *Journal of Volcanology and Geothermal Research*, 328, 210-221.
- Eppelbaum, L., Kutasov, I., & Pilchin, A. (2014). Applied geothermics. Springer Berlin Heidelberg.
- Todesco, M., Giordano, G. (2010). Modeling of CO₂ circulation in the Colli Albani area. Geological Society of London.
- Turcotte, D. L., & Schubert, G. (2014). Geodynamics. Cambridge University Press.
- Vignaroli, G., Pinton, A., De Benedetti, A. A., Giordano, G., Rossetti, F., Soligo, M., & Berardi, G. (2013). Structural compartmentalisation of a geothermal system, the Torre Alfina field (central Italy). *Tectonophysics*, 608, 482-498.
- Wohletz, K., Civetta, L., & Orsi, G. (1999). Thermal evolution of the Phlegraean magmatic system. *Journal of Volcanology and Geothermal Research*, 91(2), 381-414.
- Wohletz, K.H., 1999. HEAT3D: Magmatic Heat Flow Calculation. Los Alamos National Laboratory computer code LA-CC 99-27 (<http://geodynamics.lanl.gov/Wohletz/Heat.htm>). Los Alamos, New Mexico

Chapter 7 – Presentation of the parametric study of the main variables (density, specific heat, thermal conductivity) in the basement, and in the magma source (temperature, depth of the top and geometry)

In this chapter, we present a parametric study implemented to verify the influence on the results of numerical modeling of the uncertainties related to the lack of reliable data on the physical characteristics of the basement and on temperature and geometry of the magma chamber.

The results compare the percentage change by which each of the uncertain parameter is varied respect to the arbitrary central value, with the relative percentage change of the temperature at the base of the geothermal reservoir (-6 km) at the end of the run-time (350 ky). It is therefore evaluated how much the uncertainties affect the results of numerical simulations.

The conceptual model presented in Ch. 5 and rendered as mesh file in Ch. 6 well reflects the up-to-date geological knowledge of the study area. However, the degrees of uncertainty related to the geometry and nature of its fundamental constituents (i.e. the cap rock, the geothermal reservoir, the basement, the magma chamber, the regional geothermal gradient at $t=0$) varies in the computational domain. For example, the nature and thickness of the cap rock and of the geothermal reservoirs are reasonably well constrained by direct and indirect data, so that we can select their relative physical characteristics with high degree of confidence from available literature (e.g. Cloetingh et al., 2010; Eppelbaum et al., 2014; Turcotte & Schubert, 2014; Bono, 1981; Calamai et al., 1976; Cataldi et al., 1995; Todesco & Giordano, 2010).

Much larger uncertainties are related to the nature of the basement, which relies only on the limited outcrops present at the margin of the Roman region, some 100 km from the City of Rome.

Similarly, significant uncertainties also relate to the depth and 3D geometry of the magma chambers (although the caldera margins are taken as good constraints of the lateral extent) and of their average temperature, which may vary from supraliquidus to that of the eutectic or lower, depending on the volumetric amount and distribution of eruptible magma present within the crystal mush and the thermal state of the latter (e.g. Cashman and Giordano, 2014).

In order to explore to what extent such uncertainties may affect the thermal input at the base of the geothermal reservoir, this chapter presents the results of a parametric study where the thermal and physical properties of the basement rocks are varied to encompass the largest range of likely rock types forming the basement of the Roman Geothermal Province (e.g. granites to slates); in the second part the geometry of the magma chamber is varied, shifting its top between 6 and 8 km in depth, that is from being directly in contact with the geothermal reservoir and 2 km below; furthermore the uncertainty about the geometry of the chamber is approached by varying both the lateral and vertical extent. Finally, a variation of average temperature is investigated, between 900°C and 1100°C.

For each of the changing parameter, the simulations are replicated for 3 temperature gradients in the domain: 0 K/km, 20 K/km and 40 K/km, like described previously.

Furthermore, for each parameter changed, the geothermal reservoir is simulated as:

- purely conductive;
- conductive-convective (porosity 0.05).

The data are analysed in terms of variation of temperature related to changing input parameters at the base of geothermal reservoir, in order to test how much the previously described uncertainties would affect the thermal input.

The percentage of temperature change in each run due to the variation of the selected parameter, respect to arbitrary conditions taken as reference (we take as reference the central value of each parameter respect to the maximum variance we use in the runs), is evaluated in each cell (x,y) at final time-step at 350 ky as:

$$\text{VAL\%}(x,z,t_{350ky}) = (T(x,z,t_{350ky}) - T_p(x,z,t_{350ky})) / T(x,z,t_{350ky})$$

where $\text{VAL\%}(x,z,t_{350ky})$ is the percentage of variation of temperature, $T(x,z,t_{350ky})$ is the temperature obtained in the cell x,y with the use of the parameter at its central value, and $T_p(x,z,t_{350ky})$ is the temperature obtained with the selected parameter changed.

Of course, at the base of the geothermal reservoir, **if the temperature obtained with the changed parameter is greater than that obtained with the central value, the percentage change appears as negative.**

The total number of simulations performed for this parametric study is 102.

Parametric variation in crystalline basement

In the crystalline basement, three different parametric variations are implemented for thermal conductivity k , specific heat c_p and density ρ (see Table 1). For each set of runs dedicated to evaluate the weight of the variation of one parameter, the others are kept fixed at the central value. Each configuration is then run twice for a purely conductive and for conductive-convective conditions in the geothermal reservoir. The variance of each parameter expresses at the extremes the possibility that the basement is made by rock types from slates to granites by encompassing and extending beyond values known for such rock types in literature (see Chapter 6, Annex 1).

	k	c_p	ρ	Runs
	W/m*K	J/kg*K	kg/m ³	
1 thermal conductivity	1.0 – 2.5 – 4.0	1,100	2,750	18
percentage change of the extremes of selected parameter respect to central value	60.0%	/	/	
2 specific heat	2.5	800 – 1,100 – 1,400	2,750	18
percentage change of the extremes of selected parameter respect to central value	/	27.3%	/	
3 density	2.5	1,100	2,000 – 2,750 – 3,500	18
percentage change of the extremes of selected parameter respect to central value	/	/	27.3%	

Table 1 Summary of parametric variations of physical parameters in the crystalline basement

Parametric variation in temperature and geometry for the magma chamber

For the magma chamber we have implemented one parametric variation for temperature and three parametric variations for the geometry (Table 2).

	T	Top Level	Length	Runs
	°C	km	km	
1 Magma temperature	900 – 1,100	- 6.5	10.0	12
percentage change respect the base value (900°C)	22.2%	/	/	
2 Top of magma chamber	900	- 6.0 - -6.5 - -8.0	10.0	18
percentage change of the extremes of selected parameter respect to central value	/	8.3% - 23.1%	/	
3 Lateral extent of magma chamber	900	-6.5	6.0 – 10.0 – 14.0	18
percentage change of the extremes of selected parameter respect to central value	/	/	40.0%	

Table 2 Summary of parametric variations for temperature and geometry in magma chamber

The meshes implemented for the geometry variations are shown in Annex 1 (Fig. A.1 e A.2)

Outputs analysis for the parametric variations in the crystalline basement

Variation of thermal conductivity k

Basement thermal conductivity k is varied among $1 \text{ W/m}^*\text{K}$, $2.5 \text{ W/m}^*\text{K}$ (central value) and $4 \text{ W/m}^*\text{K}$. This range of values encompasses a percentage change respect to central value ($2.5 \text{ W/m}^*\text{K}$) of $\pm 60\%$.

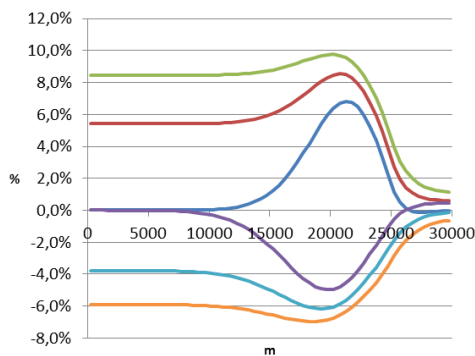
18 runs have been performed for this set of simulations (i.e. one for each max, central and mean values at the 3 geothermal gradient conditions of 0, 20, 40 K/km for pure conduction and conduction-convection in the geothermal reservoir; Table 1).

Table 3 summarizes the maximum and minimum percentage change of temperature found across all simulations respect to central value, among all cells at -6 km in the domain, i.e. along the base of the geothermal reservoir.

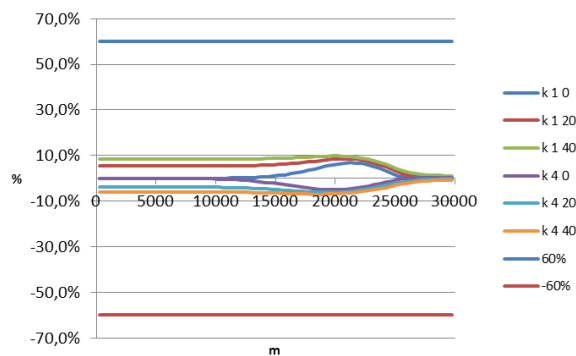
	$k=1 \text{ W/m}^*\text{K} - 0 \text{ K/km}$	$k=1 \text{ W/m}^*\text{K} - 20 \text{ K/km}$	$k=1 \text{ W/m}^*\text{K} - 40 \text{ K/km}$	$k=4 \text{ W/m}^*\text{K} - 0 \text{ K/km}$	$k=4 \text{ W/m}^*\text{K} - 20 \text{ K/km}$	$k=4 \text{ W/m}^*\text{K} - 40 \text{ K/km}$
Conduction						
min	-0,13%	0,63%	1,16%	-4,98%	-6,17%	-6,96%
max	6,83%	8,54%	9,76%	0,45%	-0,15%	-0,66%
Convection						
min	0,00%	1,67%	2,33%	-2,98%	-4,92%	-6,43%
max	3,82%	6,10%	8,05%	-0,01%	-1,09%	-1,65%

Tab. 3 Maximum and minimum values of temperature variation, for the variation of thermal conductivity, expressed as percentage respect to values obtained in runs that used the central value of k

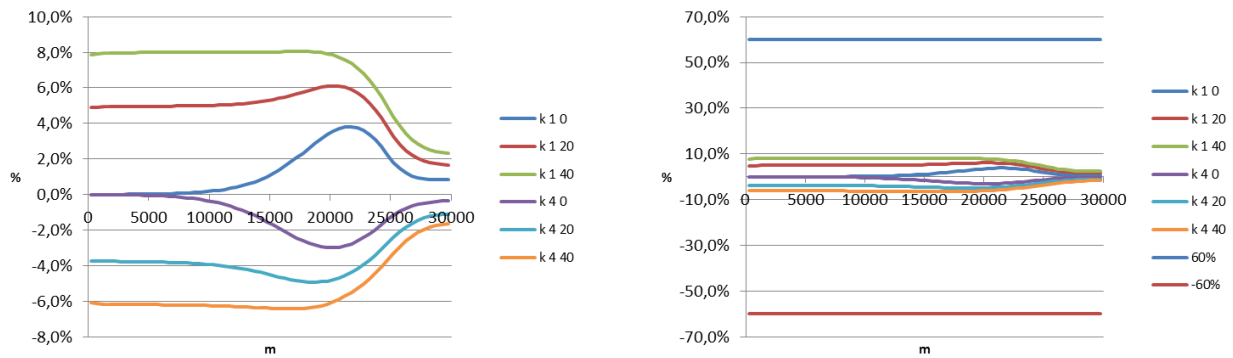
The data graphs in Fig. 1 show the full T variation expressed as percentage change respect to central value at the base of the geothermal reservoir, i.e. along the cells at -6 km . The x axis indicates distance in m and starts from the edge of the domain ($x=0 \text{ m}$) and ends at the cell in correspondence of the centre of the Magma Chamber ($x=30,000 \text{ m}$). This graph allows to verify where the maximum variations occur.



a)



a')



b) **b')**
 Fig. 1 Percentage change of temperature vs x axes at – 6 km, i.e. at the base of the geothermal reservoir, as a function of variation of basement thermal conductivity. a) case study with heat transmission by pure conduction in the geothermal reservoir; b) case study with heat transmission by conduction-convection in the geothermal reservoir; a') and b') same as previous graphs but the percentage change scale is enlarged to compare data with the blue and red bars at +60% that indicate the max and min percentage change of input thermal conductivity values.

Interestingly, the maxima of percentage change do not occur above the magma chamber (i.e. between 30,000m and 25,000m) but away from it. We interpret this for the relative proximity of the top of magma chamber to the base of geothermal reservoir (500m). The percentage changes are felt between 25,000m and 10,000m, with maxima between 18,000m and 22,000m.

The summary of data shows that the percentage change of temperature increases at increasing regional geothermal gradient and that the fork between values in purely conductive vs conductive-convective geothermal reservoir decreases at increasing geothermal gradient. These data indicate that the net effect of the geothermal gradient is not merely additive. In fact the geothermal gradient controls the modality by which the heat is transferred from the magma source to the country rocks and acts by modifying what could be called “thermal potential” in analogy with other potentials such as the hydraulic or the electric. In this sense, the increase in geothermal gradient reduces the “thermal potential”, i.e. the temperature difference between the hot source and the colder country rock that drives the heat exchange. Our data indicate that the thermal conductivity is more important in modulating the heat transfer when the “thermal potential” is low, respect to conditions where the heat transfer is dominated by high “thermal potential”.

Another interesting observation is that the convection in the geothermal reservoir affects the results measured at – 6 km, that is below it.

More importantly, when compared with the percentage change of the input parameter k (+/- 60% reported as colored bars in Fig. 1a' and b'), the percentage changes in the thermal field are limited among all explored configurations to a maximum of +10% and a minimum of -7% (remember that the sign is inverted), suggesting that the uncertainty about the real value of k in the basement will not introduce errors above 10%.

Variation of specific heat c_p

Basement specific heat c_p is varied among 800 J/kg*K, 1,100 J/kg*K (central value) and 1,400 J/kg*K. This range of values encompasses a percentage change respect to central value (1,100 J/kg*K) of $\pm 27.3\%$.

18 runs have been performed for this set of simulations (see Table 1).

As for the previous case, Table 4 summarizes the maximum and minimum percentage change of temperature found across all simulations respect to central value, among all cells at – 6 km in the domain, i.e. along the base of the geothermal reservoir in different configurations (purely conductive and conductive-convective).

	800 J/kg*K - 0 K/km	800 J/kg*K - 20 K/km	800 J/kg*K - 40 K/km	1,400 J/kg*K - 0 K/km	1,400 J/kg*K - 20 K/km	1,400 J/kg*K - 40 K/km
Conduction						
min	-3,24%	-4,05%	-4,59%	-0,10%	0,13%	0,32%
max	0,21%	-0,16%	-0,48%	2,18%	2,72%	3,08%
Convection						
min	-1,94%	-3,19%	-4,20%	0,00%	0,49%	0,72%
max	0,00%	-0,72%	-1,08%	1,24%	2,01%	2,66%

Tab. 4 Maximum and minimum values of temperature variation, for the variation of specific heat, expressed as percentage respect to values obtained in runs that used the central value of specific heat c_p

The data graphs in Fig. 2 show the T variation at the base of the geothermal reservoir, i.e. along the cells at – 6 km (X axis shows the distance in m like in previous Fig. 1).

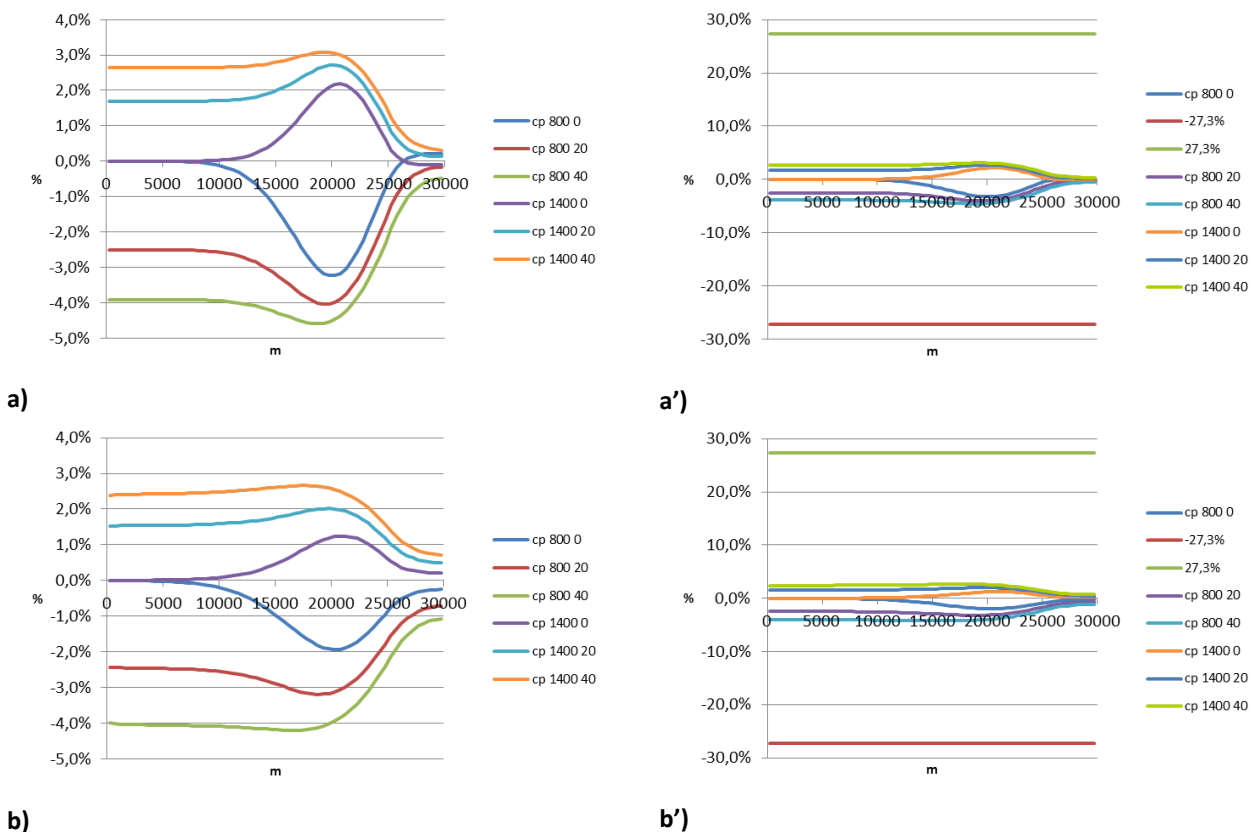


Fig. 2 Percentage change of temperature vs distance (m) as a function of variation of basement specific heat. a) case study with heat transmission by conduction in geothermal reservoir; b) case study with heat transmission by conduction-convective in geothermal reservoir; (a' and b') same as previous graphs but the percentage change scale is enlarged to compare data with the blue and red bars at +/- 27.3% that indicate the max and min percentage change of input specific heat values.

The interpretation of data for the effect of changing C_p is very similar to what has been discussed for variation in k . Data show that, when compared with the percentage change of the input parameter C_p (+/- 27.3% reported as colored bars in Fig. 2a' and b'), the percentage changes in the thermal field are limited

among all explored configurations to a maximum of +3% and a minimum of -4% (remember that the sign is inverted), suggesting that the uncertainty about the real value of C_p in the basement will not introduce errors above 5%.

Variation of density

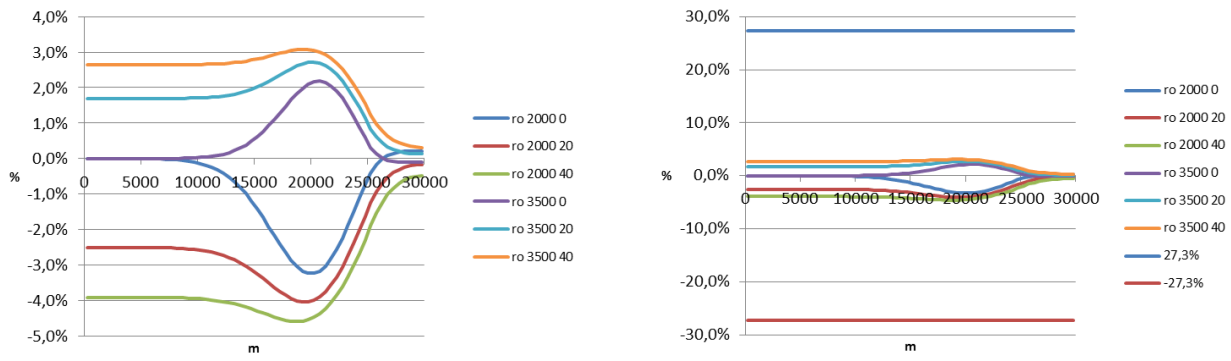
Basement density ρ is varied among 2,000 kg/m³, 2,750 kg/m³ (central value) and 3,500 kg/m³. This range of values encompasses a percentage variation respect to central value (2,750 kg/m³) of $\pm 27.3\%$ and goes well beyond the likely rock types for the Roman basement and therefore certainly encompasses all uncertainties.

As for the previous cases, Table 5 summarizes the maximum and minimum percentage change of temperature found across all simulations respect to central value, among all cells at – 6 km in the domain, i.e. along the base of the geothermal reservoir in different configurations (purely conductive and conductive-convective).

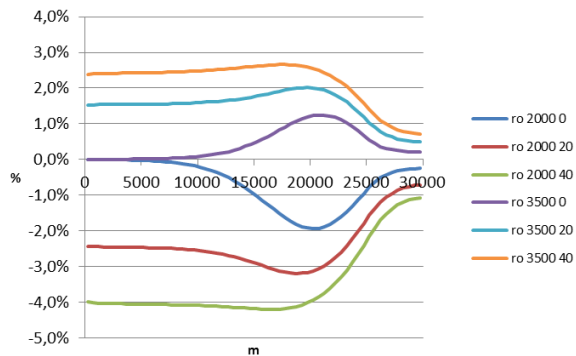
		ρ 1 W/m ² K - 0 K/km	ρ 2,000 kg/m ³ - 20 K/km	ρ 2,000 kg/m ³ - 40 K/km	ρ 3,500 kg/m ³ - 0 K/km	ρ 3,500 kg/m ³ - 20 K/km	ρ 3,500 kg/m ³ - 40 K/km
Conduction	min	-3,24%	-4,05%	-4,59%	-0,10%	0,13%	0,32%
	max	0,21%	-0,16%	-0,48%	2,18%	2,72%	3,08%
Convection	min	-1,94%	-3,19%	-4,20%	0,00%	0,49%	0,72%
	max	0,00%	-0,72%	-1,08%	1,24%	2,01%	2,66%

Tab. 5 Maximum and minimum values of temperature variation, for the variation of density, expressed as percentage respect to values obtained in runs that used the central value of density ρ

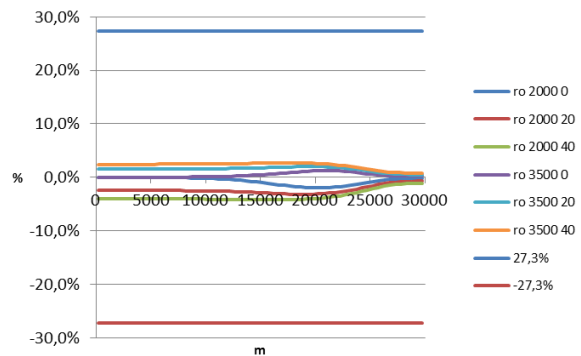
The data graphs in Fig. 3 show the T variation at the base of the geothermal reservoir, i.e. along the cells at – 6 km (X axis shows the distance in m like in previous Figs).



a)



a')



b)

b')

Fig. 3 Percentage change of temperature vs distance (m) as a function of variation of basement density ρ . a) case study with heat transmission by conduction in geothermal reservoir; b) case study with heat transmission by conduction-convection in geothermal reservoir; (a' and b') same as previous graphs but the percentage change scale is enlarged to compare data with the blue and red bars at at $\pm 27.3\%$ that indicate the max and min percentage change of input density values.

The interpretation of data for the effect of changing density is very similar to what has been discussed for variations in k and C_p . Data show that, when compared with the percentage change of the input parameter ρ ($\pm 27.3\%$ reported as colored bars in Fig. 3a' and b'), the percentage changes in the thermal field are limited among all explored configurations to a maximum of $+3\%$ and a minimum of -5% (remember that the sign is inverted), suggesting that the uncertainty about the real value of C_p in the basement will not introduce errors above 5% .

Outputs analysis for parametric variation in temperature and geometry for the magma chamber

Variation of the magma chamber temperature T

Magma temperature T is varied between $900\text{ }^\circ\text{C}$ and $1,100\text{ }^\circ\text{C}$. This range represents a reasonable approximation of conditions between liquidus and solidus temperatures of a mafic-alkaline intrusive complex (alkali-syenite in composition).

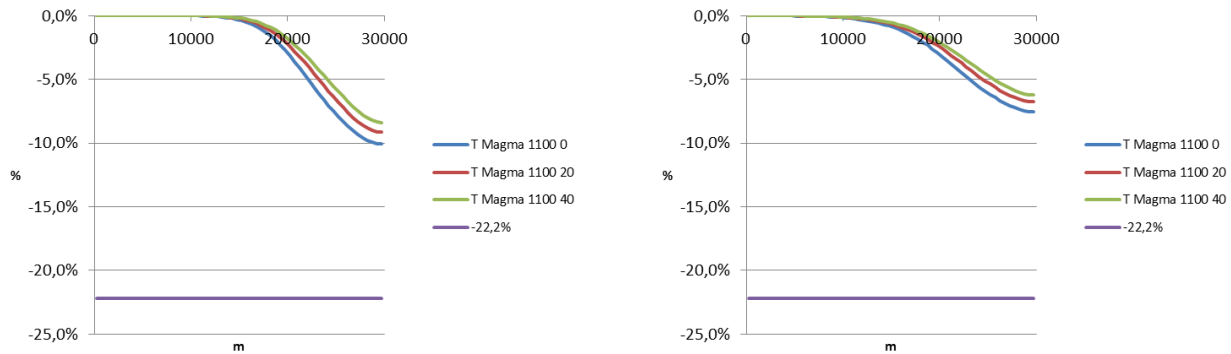
The percentage change respect to $900\text{ }^\circ\text{C}$ is $+22.2\%$.

At the base of reservoir (-6 km), the maximum and minimum values of temperature variation expressed as percentage respect to the runs at 900°C, are shown in Table 6.

		1,100 °C - 0 K/km	1,100 °C - 20 K/km	1,100 °C - 40 K/km
Conduction				
	min	-10,1%	-9,2%	-8,4%
	max	0,0%	0,0%	0,0%
Convection				
	min	-7,5%	-6,8%	-6,2%
	max	0,0%	0,0%	0,0%

Tab. 6 Maximum and minimum values of temperature variation at – 6 km, for the variation of temperature T expressed as percentage respect to runs at magma initial T=900°C

The data graphs in Fig. 4 show the T variation at the base of the geothermal reservoir, i.e. along the cells at – 6 km (X axis shows the distance in m like in previous Figs. 1, 2).



a) **b)**
 Fig. 4 Percentage change of temperature vs distance (m) as a function of variation of Magma Temperature. a) case study with heat transmission by conduction in the geothermal reservoir; b) case study heat transmission by conduction-convection in the geothermal reservoir.

By contrast with previous cases, the variation in T of the magma chamber clearly has a strong effect in the basement above it. The effect fades laterally at 15000m for the purely conductive case and at 10000m for the conductive-convective case indicating the importance of lateral advection in geothermal reservoirs also on the basal input of heat. The percentage change in T at -6km reaches 10% for the selected range of magma T. Given that in this set of simulations we have used only 2 values considered as reasonable end-members, the resulting variations can be considered as the full range of variability.

In summary, the net effect of the uncertainty in T of the magma source can introduce an error in the evaluation of the T at the base of the geothermal reservoir within a 10% range.

Variation of magma chamber top level

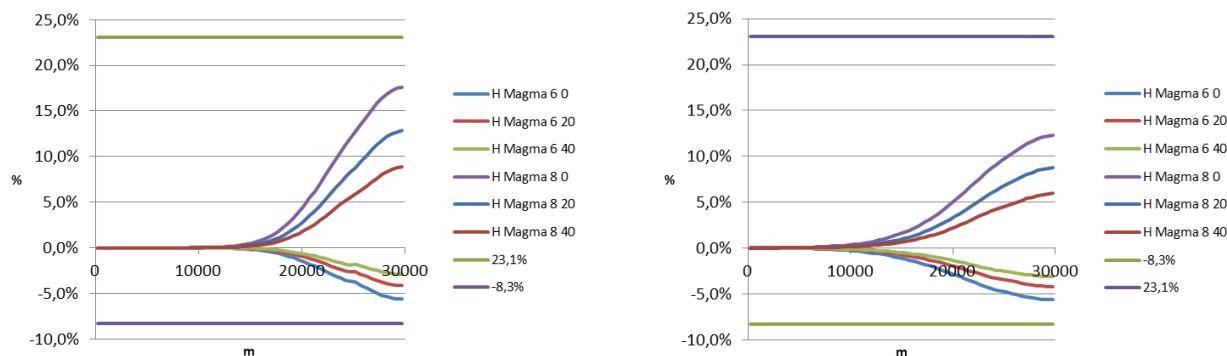
The Magma Chamber Top Level is varied among -6,000 m, -6,500 m (reference value) and -8,000 m. This range of values represent the uncertainties related to present knowledge of magma chamber depth and encompasses a percentage variation respect to reference value (6,500 m) of 8.3% and -25%.

The maximum and minimum values of temperature variation at the base of reservoir (-6km), expressed as percentage change respect to runs that used the reference value for the top of magma chamber are shown in Table 7.

		-6,000 m - 0 K/km	-6,000 m - 20 K/km	-6,000 m - 40 K/km	-8,000 m - 0 K/km	-8,000 m - 20 K/km	-8,000 m - 40 K/km
Conduction	min	-5,6%	-4,2%	-3,0%	0,0%	0,0%	0,0%
	max	0,0%	0,0%	0,0%	17,6%	12,8%	8,8%
Convection	min	-5,63%	-4,20%	-3,12%	0,01%	0,01%	0,00%
	max	-0,01%	-0,01%	-0,01%	12,27%	8,77%	5,96%

Tab. 7 Maximum and minimum values of temperature variation at – 6 km, for the variation of temperature T expressed as percentage respect to runs at Magma Chamber Top -6.5 km

The data graphs in Fig. 5 show the T variation at the base of the geothermal reservoir, i.e. along the cells at – 6 km (X axis shows the distance in m like in previous Figs).



a)

b)

Fig. 5 Percentage change of temperature vs distance (m) as a function of variation of Top of Magma Chamber. a) case study with heat transmission by conduction in the geothermal reservoir; b) case study heat transmission by conduction-convection in the geothermal reservoir.

The changes in depth of the top of the magma chamber introduce changes in temperature up to 18%, although these values occur in the simulations at 0 K/km, and decrease to <12% for simulations with 20 and 40 K/km geothermal gradients. For realistic natural conditions, i.e. with an existing geothermal gradient, the net effect of uncertainties related to present knowledge of the depth of the magma source affects the T at the base of the geothermal reservoir by maximum +/-12%. Obviously much greater effect may be expected in case the magma chamber is installed inside the geothermal reservoir, i.e. at shallower levels, and this case will be discussed in Ch. 9. Laterally the effect fades out at 15000m (for the conductive case, that means at 10 km away from magma chamber edge and 15 from center of magma chamber) and 10000m (for the convective-conductive case, that means at 5 km away from magma chamber edge and 15 from center of magma chamber).

Variation of magma chamber length

The Magma Chamber Length is varied among 6,000 m, 10,000 m (central value) and 14,000 m, in order to encompass possible uncertainties related to mismatches between caldera diameter and effective magma chamber length.

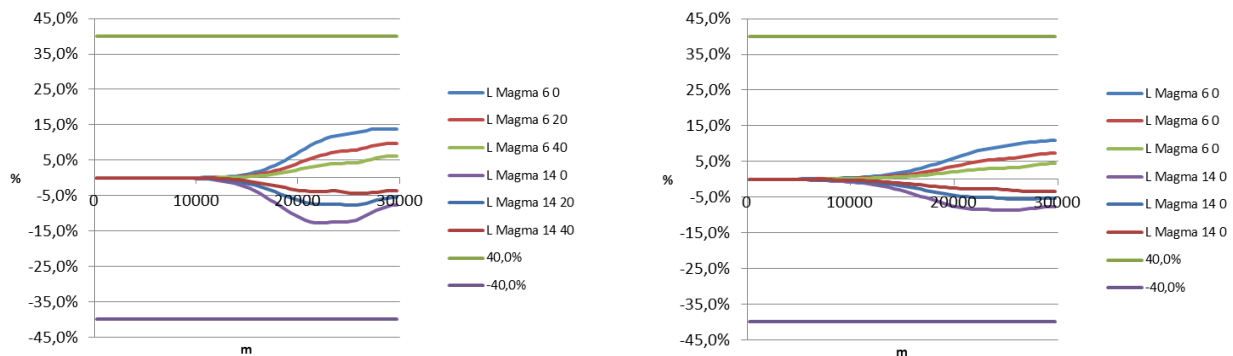
This range of values encompasses a percentage variation respect to central value (10,000 m) of $\pm 40.0\%$.

The maximum and minimum values of temperature variation at the base of reservoir (-6km), expressed as percentage change respect to runs that used the central value of 10 km for the length of magma chamber are shown in Table 8.

		6,000 m - 0 K/km	6,000 m - 20 K/km	6,000 m - 40 K/km	14,000 m - 0 K/km	14,000 m - 20 K/km	14,000 m - 40 K/km
Conduction	min	0,0%	0,0%	0,0%	-12,7%	-7,7%	-4,4%
	max	13,9%	9,7%	6,2%	0,0%	0,0%	0,0%
Convection	min	0,0%	0,0%	0,0%	-8,7%	-5,6%	-3,4%
	max	10,9%	7,3%	4,5%	0,0%	0,0%	0,0%

Tab 8. Maximum and minimum values of temperature variation at – 6 km, for the variation of temperature T expressed as percentage respect to runs with Magma Chamber Length of 10 km

The data graphs in Fig. 5 show the T variation at the base of the geothermal reservoir, i.e. along the cells at – 6 km (X axis shows the distance in m like in previous Figs)



a)

b)

Fig. 6. Percentage change of temperature vs distance (m) as a function if Magma Chamber Length. a) case study with heat transmission by conduction in the geothermal reservoir; b) case study heat transmission by conduction-convection in the geothermal reservoir.

The changes in length of the magma chamber introduce changes in temperature up to 13%, although these values occur in the simulations at 0 K/km, and decrease to <10% for simulations with 20 and 40 K/km geothermal gradients. For realistic natural conditions, i.e. with an existing geothermal gradient, we then evaluate the net effect of uncertainties related to the lateral extent of the magma source to affect the T at the base of the geothermal reservoir by maximum $\pm 10\%$.

Summary

The parametric variation of physical parameters in the basement shows that the relative temperature percentage variation at the base of reservoir is smaller of about of one order of magnitude respect the percentage variation of parameters k , C_p and ρ . Such variations of physical parameters encompass the possible rock types that can be present in the Roman basement, and their uncertainties should not introduce an error larger than $\pm 10\%$ in the temperature field at the base of the geothermal reservoir, taken here at -6km .

In order to account for uncertainties of temperature and geometry of the magma chamber we have also varied magma T between 900 and $1,100^\circ\text{C}$ and both the depth of the top of the magma chamber and its lateral extent. In all possible cases the variation of each parameter introduces variations in T at the base of the geothermal reservoir at -6km that are within 10% from central values.

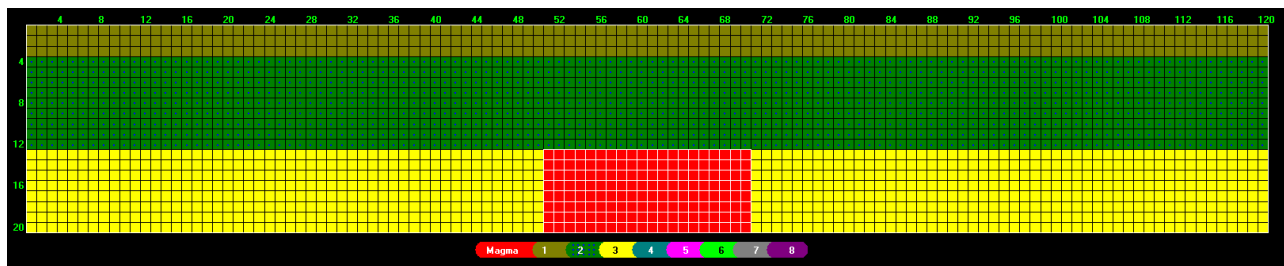
In summary, we consider acceptable to work with the central values of k , C_p and ρ , for the basement, assuming that results can be affected by an error of $\pm 10\%$.

The magma T of 900°C is taken as a better conservative option respect to the 1100°C that is the eruptive temperature for mafic magmas, because the average temperature of the reservoir, though recharged by such magmas, must integrate the presence of differentiated magmas and of crystallized domains.

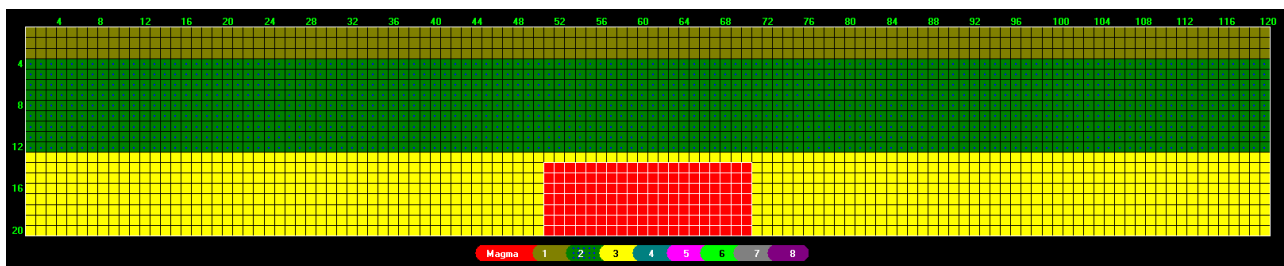
Uncertainties in the selection of T_{magma} also may affect the results with an error of $\pm 10\%$.

Finally we take the -6.5 km depth for the top of the magma chamber and a lateral extent of 10km which are both consistent with available geological data, as variations in depth and length of magma chamber also result in errors of $\pm 10\%$.

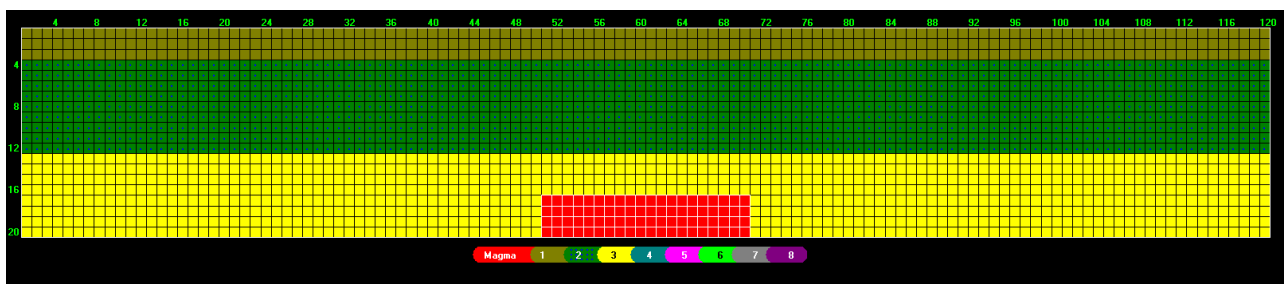
ANNEX 1 Meshes implemented for the variation in geometry of the magma chamber



a)

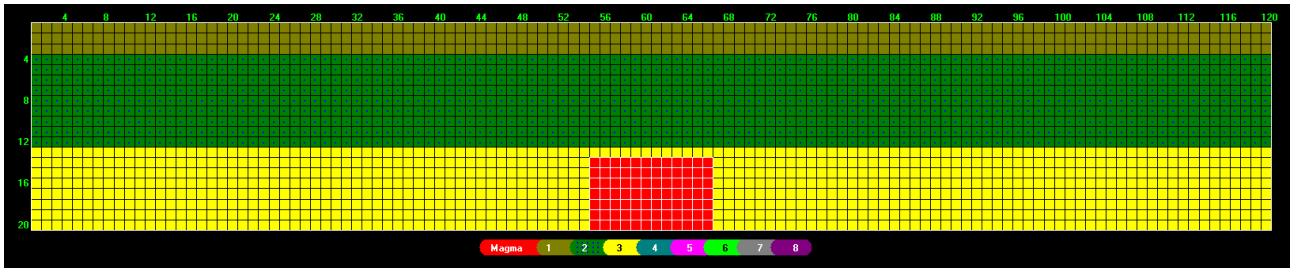


b)

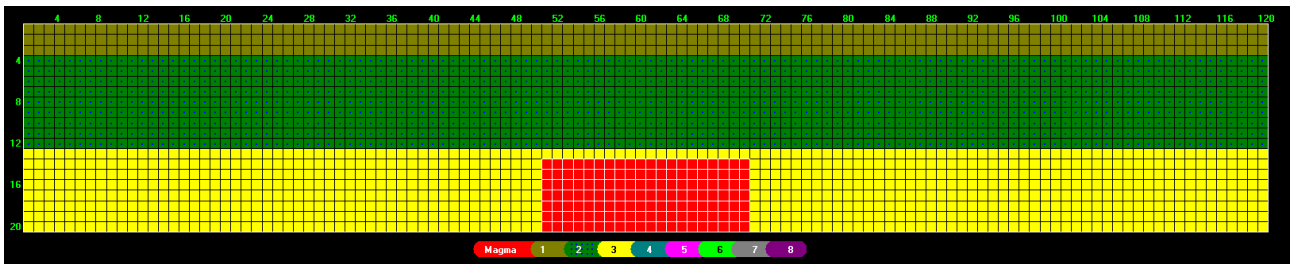


c)

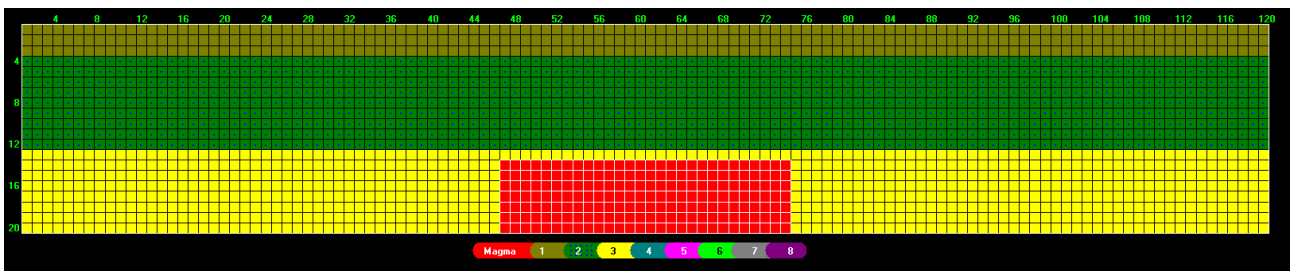
Fig. A1.1 Mesh implemented for the variation of the top of magma chamber: a) -6,000 m; b) -6,500 m; c) -8,000 m



a)



b)



c)

Fig. A1.2 Mesh implemented for the variation of the width of magma chamber: a) 6,000 m; b) 10,000 m; c) 14,000 m

References

- Bono, P. (1981). Valutazione preliminare del potenziale geotermico della regione laziale. *Geol Rom*, 2.
- Calamai, A., Cataldi, R., Locardi, E., & Praturlon, A. (1976, October). Distribuzione delle anomalie geotermiche nella fascia pre-Appenninica tosco-laziale (Italia). In *Proc. Int. Symposium on Geothermal Energy in Latin-America, Guatemala City* (pp. 189-229).
- Cashman, K. V., & Giordano, G. (2014). Calderas and magma reservoirs. *Journal of Volcanology and Geothermal Research*, 288, 28-45.
- Cataldi, R., Mongelli, F., Squarci, P., Taffi, L., Zito, G., & Calore, C. (1995). Geothermal ranking of Italian territory. *Geothermics*, 24(1), 115-129.
- Cloetingh, S. A. P. L., Van Wees, J. D., Ziegler, P. A., Lenkey, L., Beekman, F., Tesauro, M., ... & Bonté, D. (2010). Lithosphere tectonics and thermo-mechanical properties: an integrated modelling approach for Enhanced Geothermal Systems exploration in Europe. *Earth-Science Reviews*, 102(3), 159-206.
- Eppelbaum, L., Kutasov, I., & Pilchin, A. (2014). Thermal properties of rocks and density of fluids. In *Applied geothermics* (pp. 99-149). Springer Berlin Heidelberg.
- Todesco, M., & Giordano, G. (2010). Modelling of CO₂ circulation in the Colli Albani area. *SPECIAL PUBLICATION-GEOLOGICAL SOCIETY OF LONDON*, 311-330.
- Turcotte D. L., & Schubert, G. (1982). *Geodynamics: Applications of continuum physics to geological problems*. Wiley.

**Chapter 8 - Presentation and analysis of the main outputs
obtained with the model configuration selected after the
parametric study**

- In this chapter we use the selected configuration described in Ch. 5 to test the behavior of the numerical model by varying the regional geothermal gradient (0-20-40 K/km) and the conductive vs convective heat transmission inside the geothermal reservoir.

Output Analysis

Conductive Temperature field in the Computational Domain

Using the selected configuration (Tab. 1) and the selected mesh (Fig. 1), the temperature field in the domain is analyzed, at different time steps (50 ka, 150 ka, 250 ka and 350 ka), with thermal gradient = 0 K/km and in conductive heat transmission in the geothermal reservoir.

The temperature field for 50 ka, 150 ka, 250 ka and 350 ka output is shown in Figs 2 and 3.

	k	c _p	ρ	T	Porosity	Thermal diffusivity
Cap Rock	1.5	1,100	2,200	/	/	6.20 10 ⁻⁷
Geothermal Reservoir	2.7	900	2,650	/	0.05	1.13 10 ⁻⁶
Crystalline basement	2.5	1,100	2,750	/	/	8.26 10 ⁻⁷
Magma	1.7	1,200	2,750	900	/	5.15 10 ⁻⁷

Table 1 Summary of basic physical parameters used for the numerical simulations

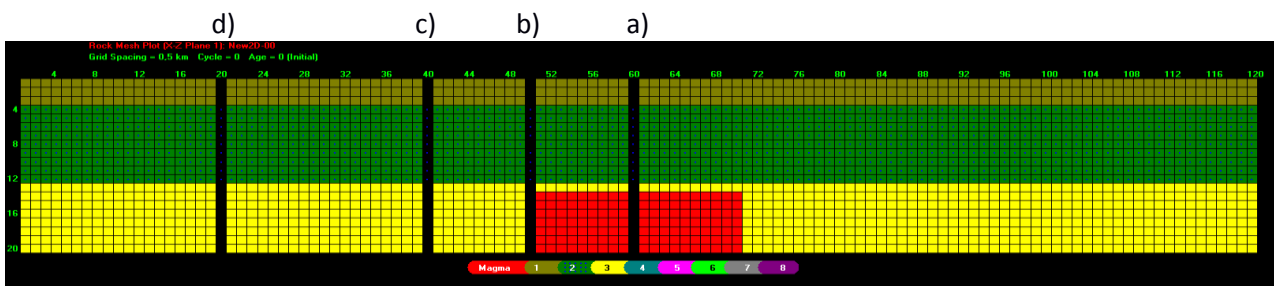
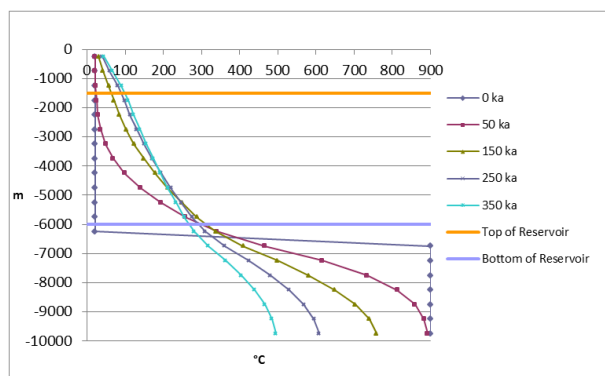
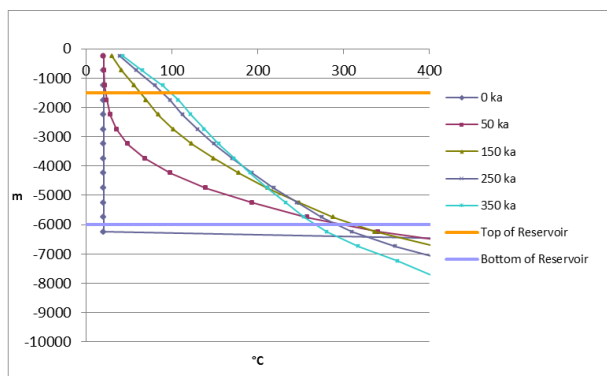


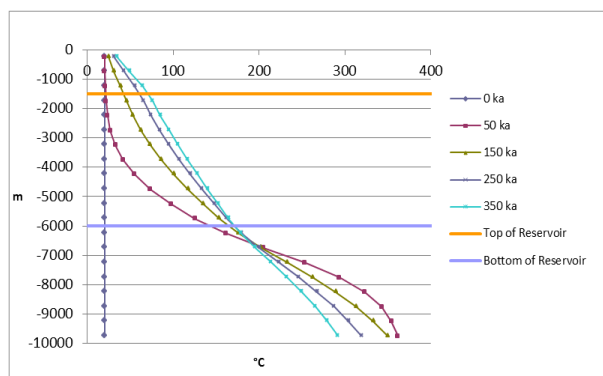
Fig. 1 Heat3D X-Z selected mesh 60 km x 10 km. The points are considered in the next figures: a) centre of Magma Chamber (MC) (column 60); b) 5 km far from centre of MC (column 50); c) 10 km far from centre of MC (column 40); d) 20 km far from centre of MC (column 20).



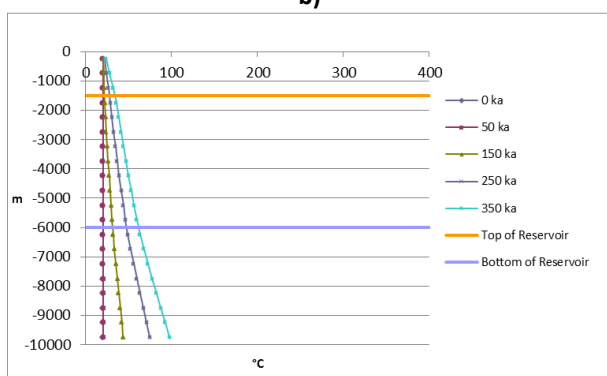
a)



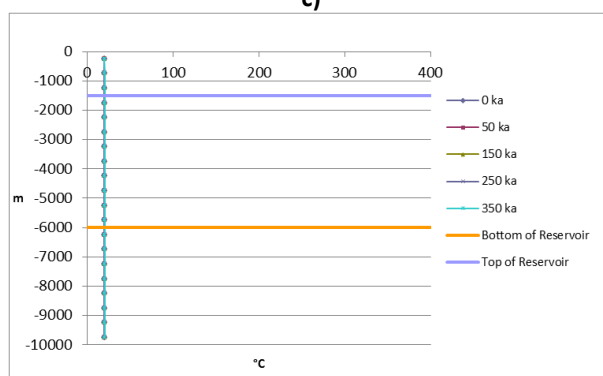
b)



c)



d)



e)

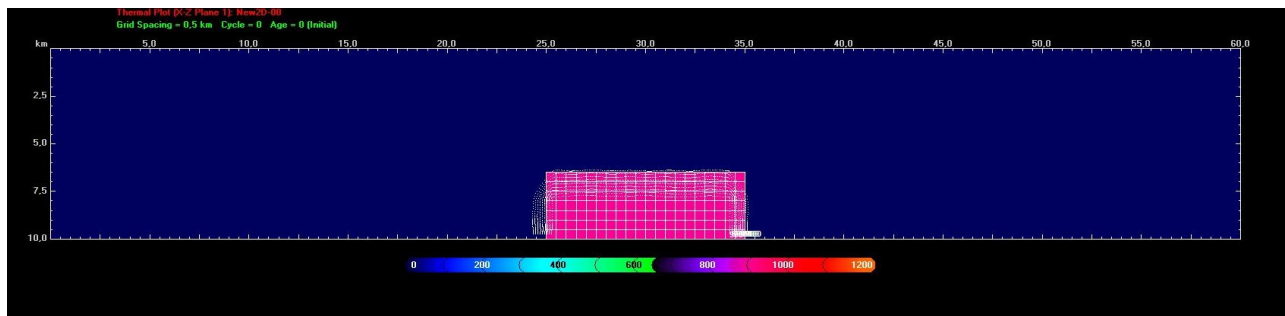
Fig. 2 Temperature field in the domain - t (°C) vs z (m) for different time steps (at 50 ka, 150 ka, 250 ka and 350 ka). Thermal gradient 0 K/km. Conductive heat transmission in the geothermal reservoir.

a) in the centre of magmatic chamber full temperature field; b) in the centre of magmatic chamber with temperature field cut-off at 400 °C; c) 5 km far from the centre of MC; d) 10 km far from the centre of MC; e) 20 km far from the centre of MC.

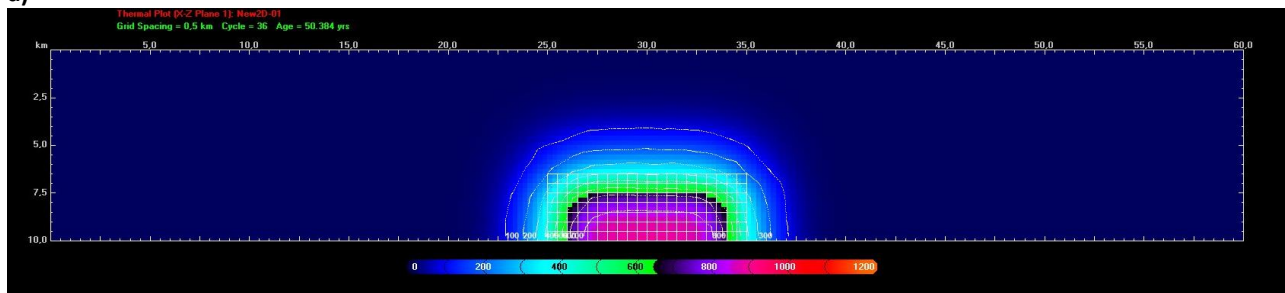
The diagrams of Fig. 2 show some very important features:

- 1) the thermal anomaly attenuates laterally to negligible already at 10 km from magma reservoir centre (Fig. 4d), that is just 5 km from its margin, where the total gradient built after 350 ka is only 10 K/km. At 20 km from MC centre there there is no sign of thermal anomaly (Fig. 4e);
- 2) The proximal thermal profiles at 0 and 5 km (Fig. 4a-c) show a substantial modification respect to initial conditions, where the magma chambers cools to less than half of its initial temperature transferring heat upward where the thermal gradient rises quickly within the first 150 ka and then progressively tends to stabilize so that the temperature differences between 250 ka and 350 ka are minimal; this pattern suggests that the chosen initial conditions thermally inflate the reservoir on time scales of 250 ka, and then the gain over time, though still occurring, is negligible. This result is important as it stresses the relevance, in geothermal modeling, of reliable geochronological datasets that allow to constrain the life-span of magma chambers.

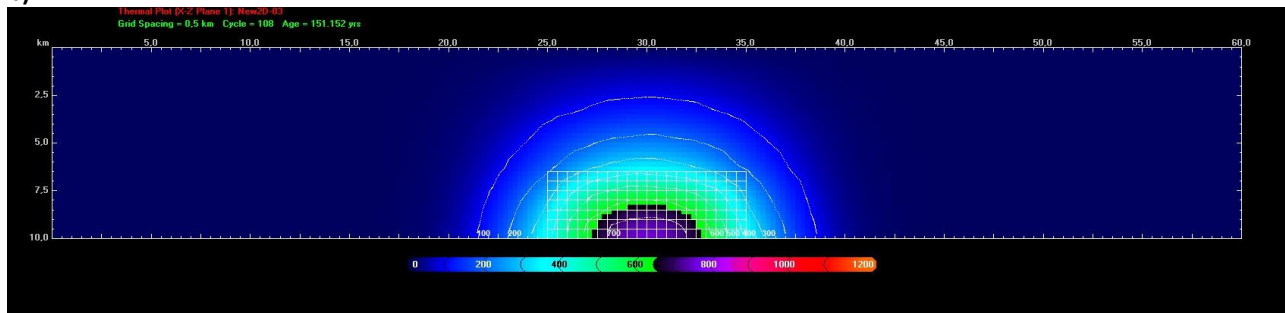
3) the shape of thermal gradients in the geothermal reservoir is complex above MC whereas is linear laterally away (10 km)



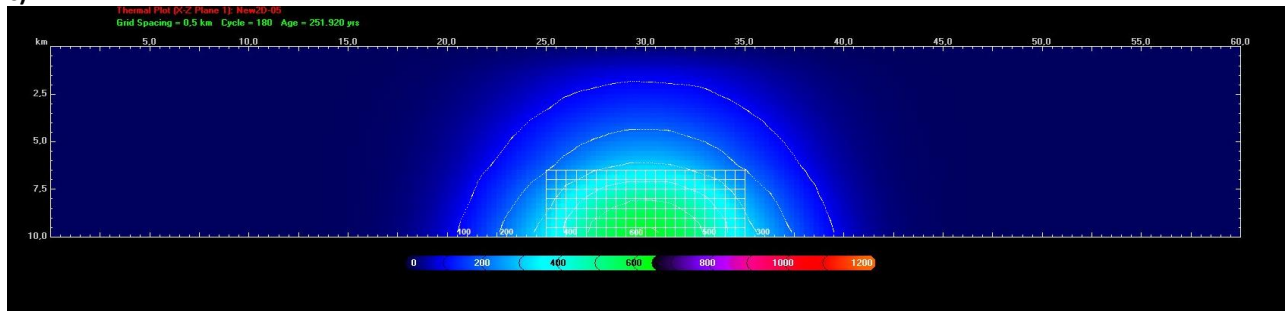
a)



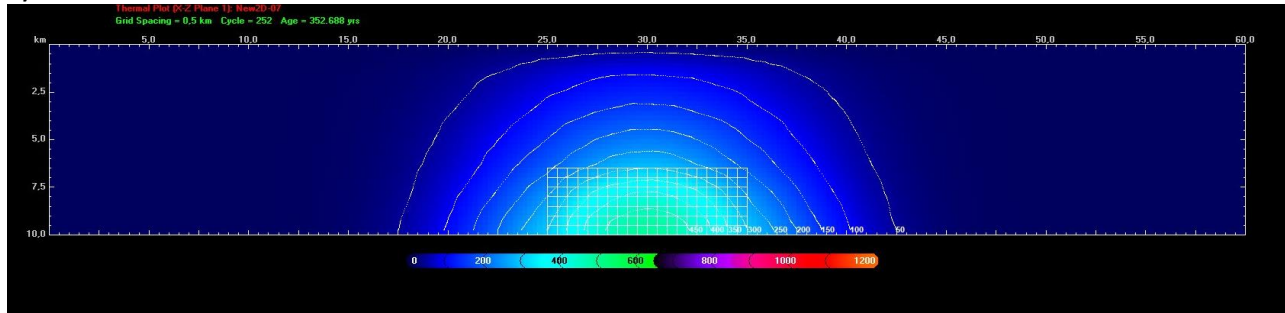
b)



c)



d)



e)

Fig. 3 Temperature field evolution in the domain. Thermal gradient 0 K/km. Conductive heat transmission in geothermal reservoir. a) 0 ka; b) 50 ka; c) 150 ka; d) 250 ka and e) 350 ka)

The same kind of data shown in Fig. 2 are shown in Fig. 4, for simulations within a geothermal gradient of 20 K/km, in conductive heat transmission within the geothermal reservoir.

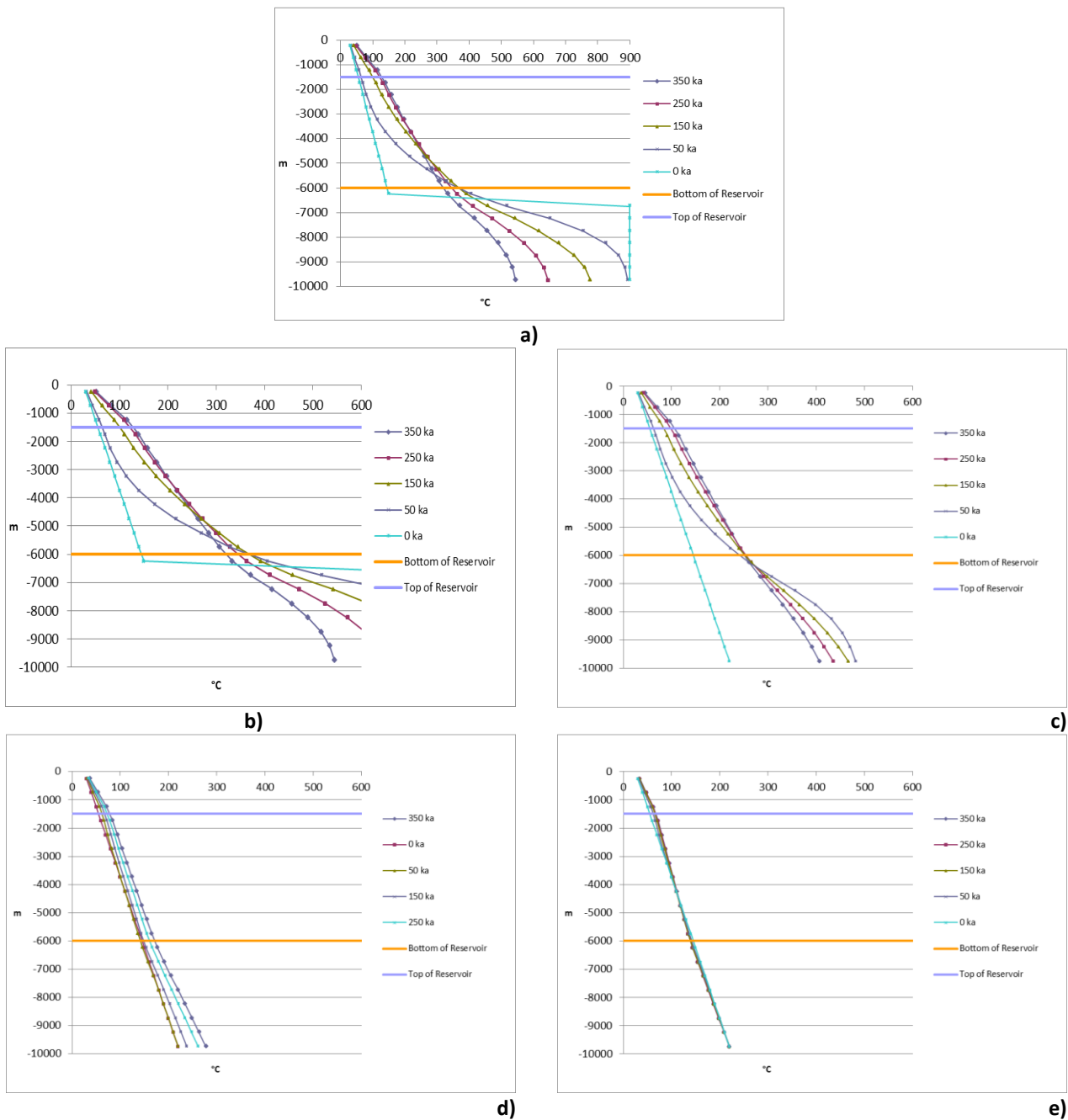


Fig. 4 Temperature field in the domain for different time steps (at 50 ka, 150 ka, 250 ka and 350 ka). Thermal gradient 20 K/km. Conductive heat transmission in geothermal reservoir.

a) in the centre of magmatic chamber full temperature field; b) in the centre of magmatic chamber with temperature cut-off at 600 °C; c) 5 km far from the centre of MC; d) 10 km far from the centre of MC; e) 20 km far from the centre of MC .

The time-temperature pattern shown by these simulations is the same as previous, and identifies (a) an horizontal length scale of 10 km from MC centre wherein the thermal anomaly attenuates to negligible and (b) a time-scale of 150 ka for attaining almost stable thermal conditions that then persist to the end of simulation at 350ka

Under the same conditions, in Fig. 5 the temperature field at 50 ka, 150 ka, 250 ka and 350 ka respectively is shown.

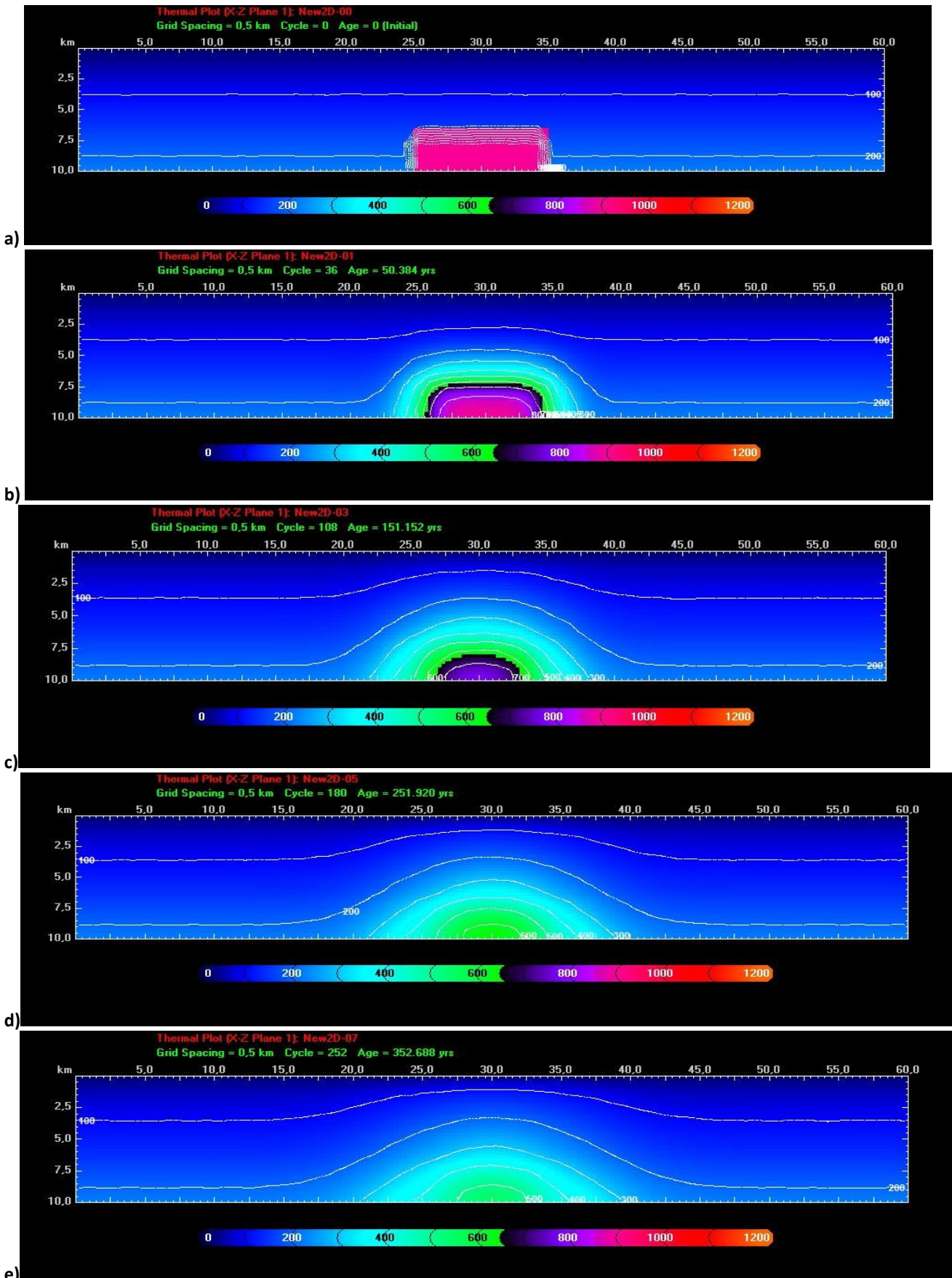


Fig. 5 Temperature field in the domain. Thermal gradient 20 K/km. Conductive heat transmission in geothermal reservoir. a) 0 ka; b) 50 ka; c) 150 ka; d) 250 ka and e) 350 ka

Fig. 6 and Fig. 7 show the evolution over time of temperature during the cooling of MC with regional geothermal gradient of 40 K/km, in conductive heat transmission within the geothermal reservoir.

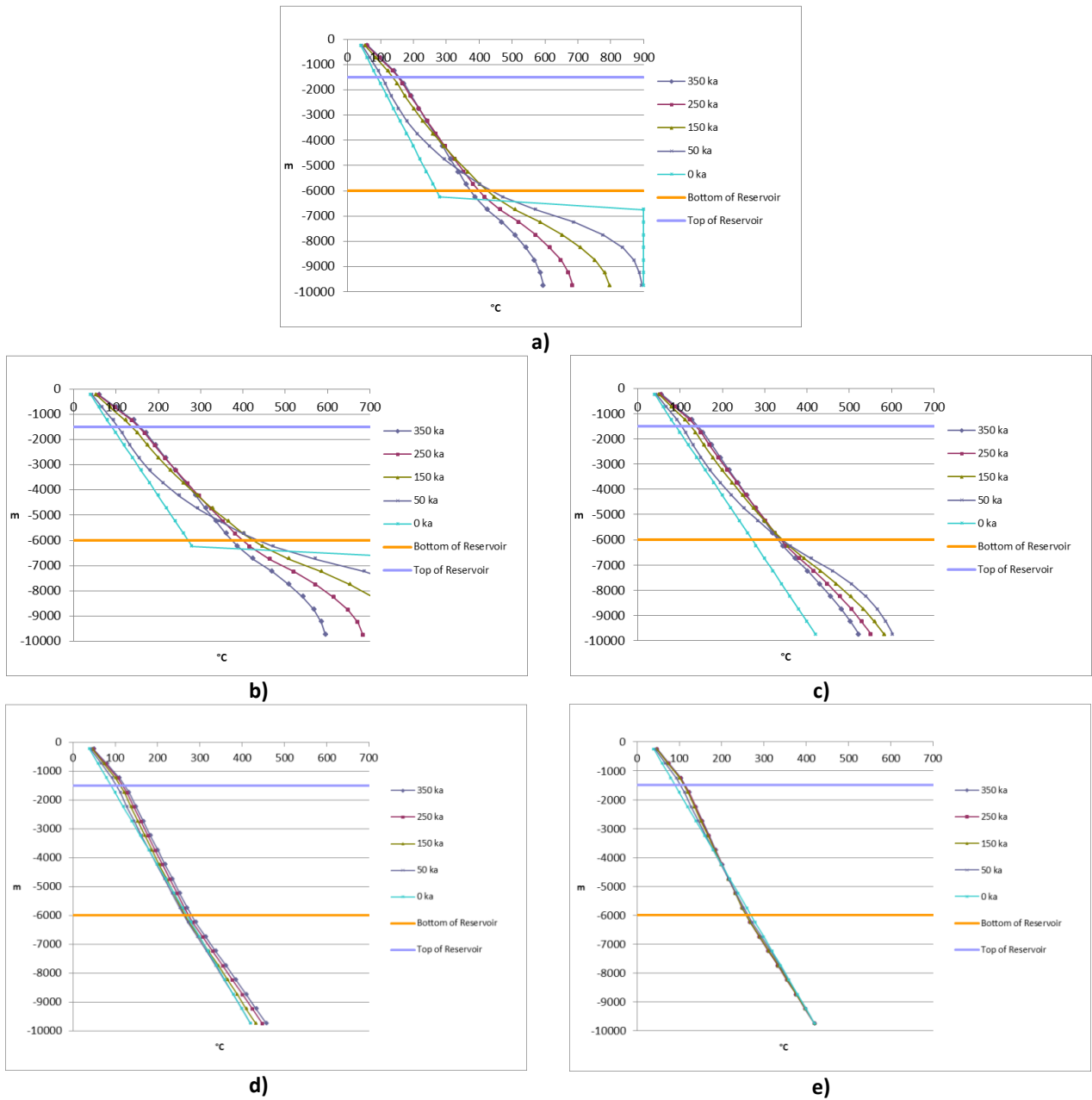
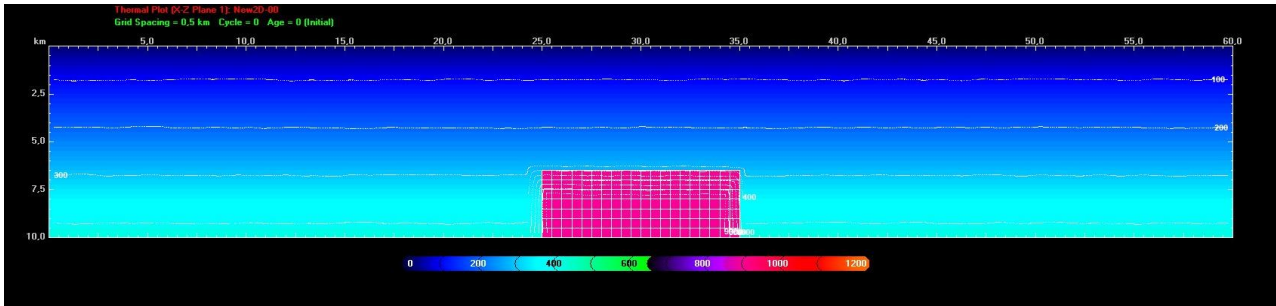
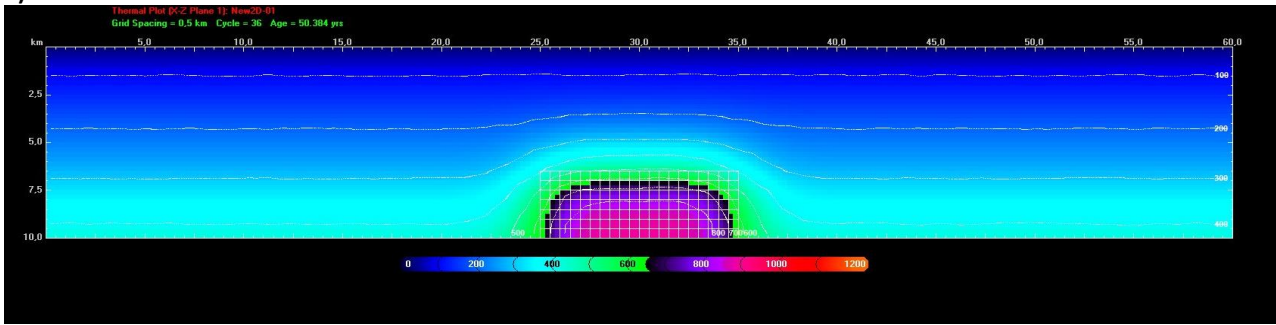


Fig. 6 Temperature field in the domain for different time steps (initial configuration, 50 ka, 150 ka, 250 ka and 350 ka). Thermal gradient 40 K/km. Conductive heat transmission in geothermal reservoir.

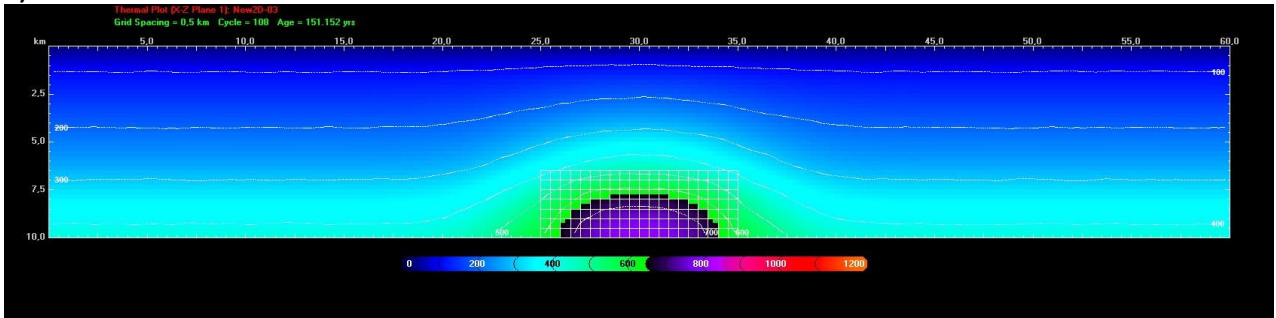
a) in the centre of magmatic chamber full temperature field; b) in the centre of magmatic chamber with temperature cut-off 700 °C; c) 5 km far from the centre of MC; d) 10 km far from the centre of MC; e) 20 km far from the centre of MC.



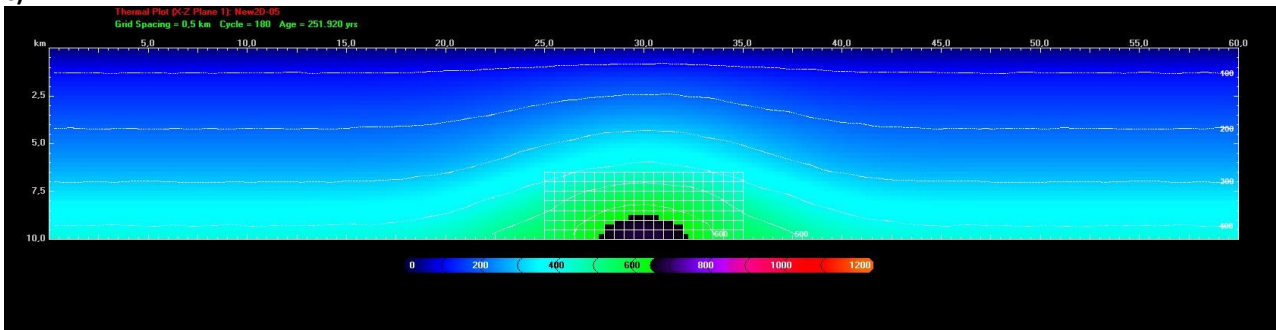
a)



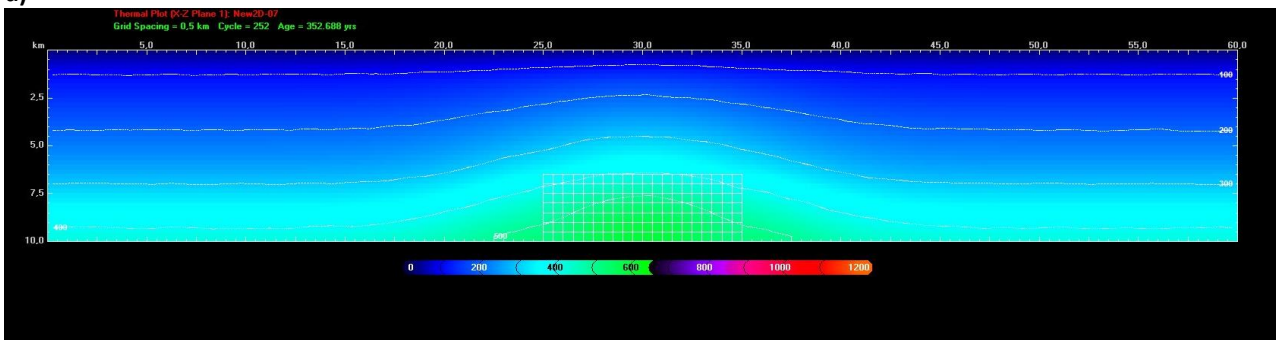
b)



c)



d)



e)

Fig. 7 Temperature field in the domain. Thermal gradient 40 K/km. Conductive heat transmission in geothermal reservoir. a) 0 ka; b) 50 ka; c) 150 ka; d) 250 ka and e) 350 ka

This simulation shows similar patterns to the previous although the external “forcing” provided by the regional geothermal gradient appears to anticipate the attainment of stable gradient conditions at less than 150 ka

From the comparison of data obtained by the set of simulations in 0, 20 and 40 K/km regional geothermal gradients, some information can be deduced for the conductive regime:

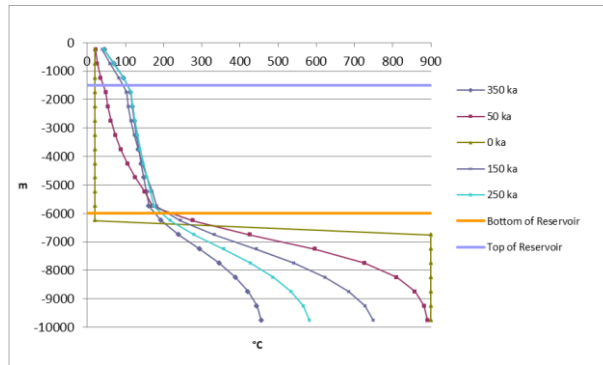
1. In correspondence of the centre of the Magma Chamber (MC) and laterally to 5 km away (i.e. at the margin of MC), the variation of temperature in the geothermal reservoir rises quickly up to 150 ka and then stabilizes till 350 ka with an exponential trend as a function of time.
2. 10 km far from the centre of MC, in function of time, thermal effect of MC produces a linear increasing of temperature that continues to increment over time. The linearity depends on the physical parameters in the basement, reservoir and cap rock.
3. 20 km far from the centre of MC, there is a negligible effect in temperature for the thermal contribution of MC compared with the external field contribution (thermal gradient in the domain).
4. Thermal gradient in the domain acts like a relevant external force for the temperature dynamic.

The same analysis implemented for conductive heat transmission in geothermal reservoir can be implemented for convective heat transmission in geothermal reservoir.

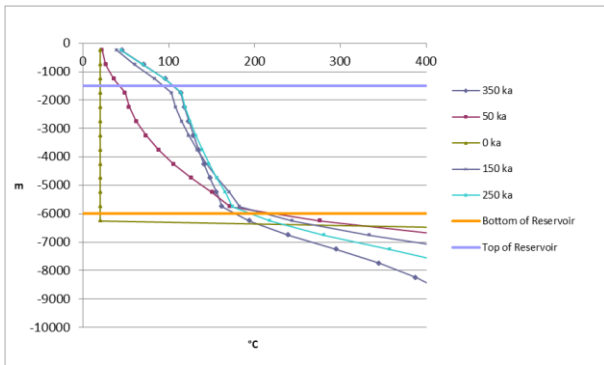
Conductive-Convective Temperature field in the Mesh Domain

Under convective heat transmission in the geothermal reservoir, the temperature field in the domain, with different time steps (at 50 ka, 150 ka, 250 ka and 350 ka) and regional geothermal gradient = 0 K/km is analyzed in Fig. 8.

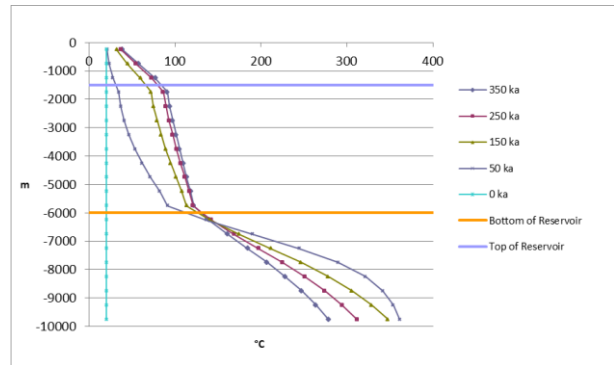
The temperature field for 50 ka, 150 ka, 250 ka and 350 ka output is shown in Fig. 9.



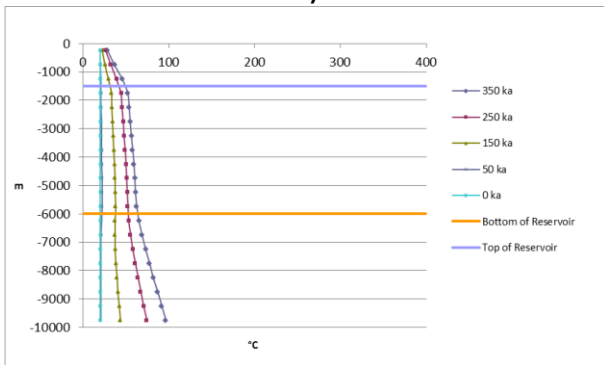
a)



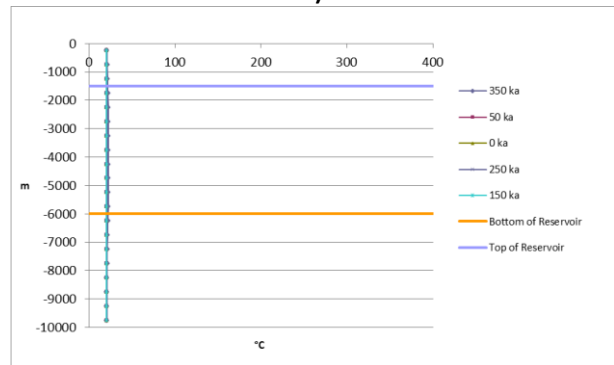
b)



c)



d)

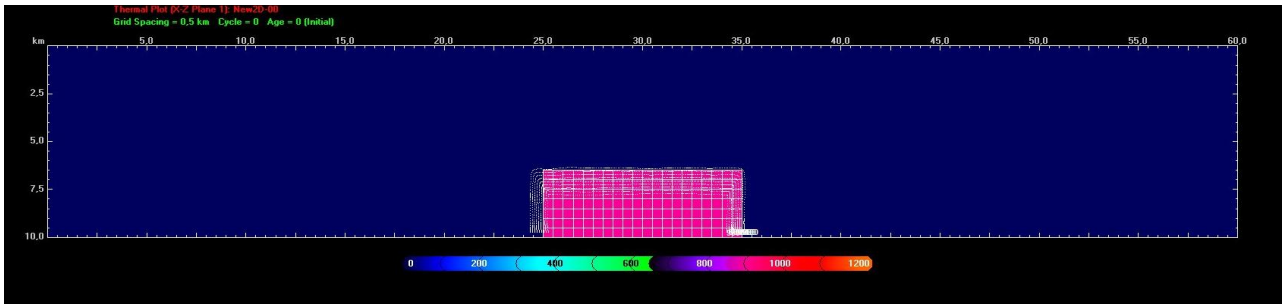


e)

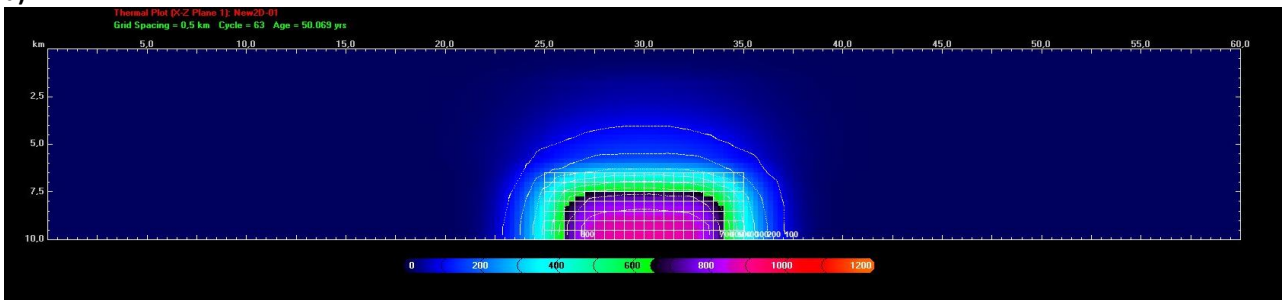
Fig. 8 Temperature field in the domain - t ($^{\circ}\text{C}$) vs z (m) - for different time steps (at 50 ka, 150 ka, 250 ka and 350 ka). Thermal gradient 0 K/km. Convective heat transmission in geothermal reservoir.

a) in the centre of magma chamber full temperature field; b) in the centre of magma chamber with temperature field till 400 $^{\circ}\text{C}$; c) 5 km far from the centre of MC with temperature field cut-off at 400 $^{\circ}\text{C}$; d) 10 km far from the centre of MC; e) 20 km far from the centre of MC.

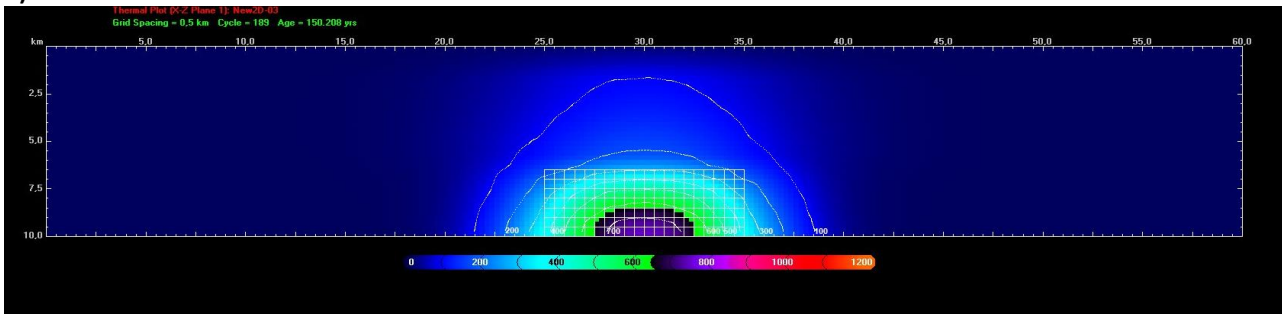
The temperature field for 50 ka, 150 ka, 250 ka and 350 ka output is shown in Fig. 9.



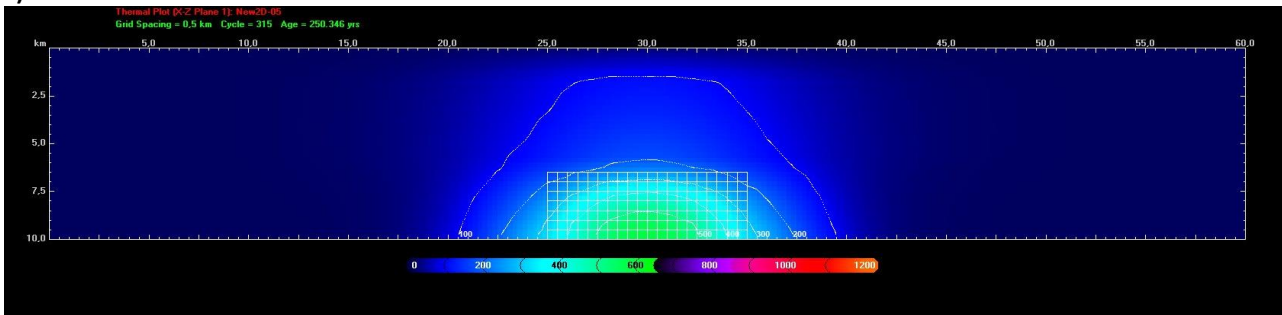
a)



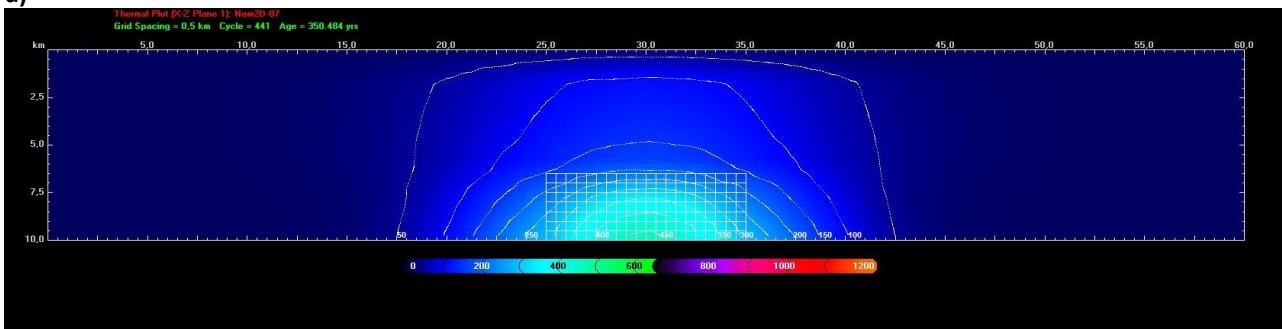
b)



c)



d)

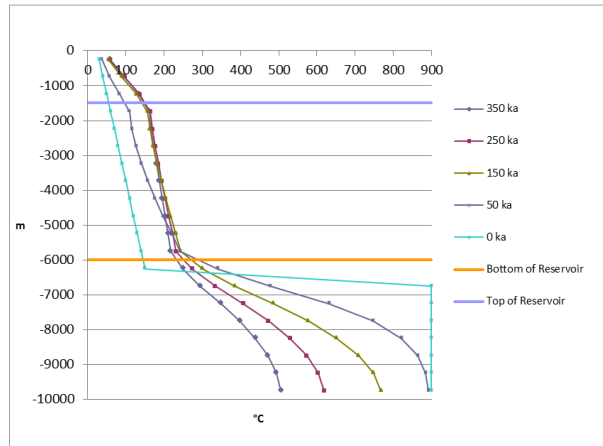


e)

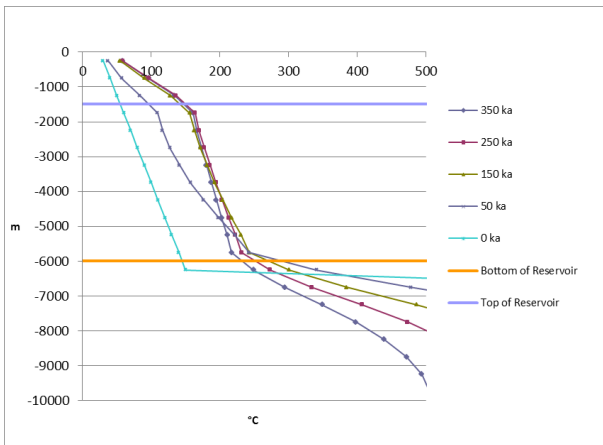
Fig. 9 Temperature field in the domain. Thermal gradient 0 K/km. Convective heat transmission in geothermal reservoir. a) 0 ka; b) 50 ka; c) 150 ka; d) 250 ka and e) 350 ka

The same data with thermal gradient of 20 K/km, in convective heat transmission in geothermal reservoir, is in Fig. 10. The temperature field for 50 ka, 150 ka, 250 ka and 350 ka is shown in Fig. 11.

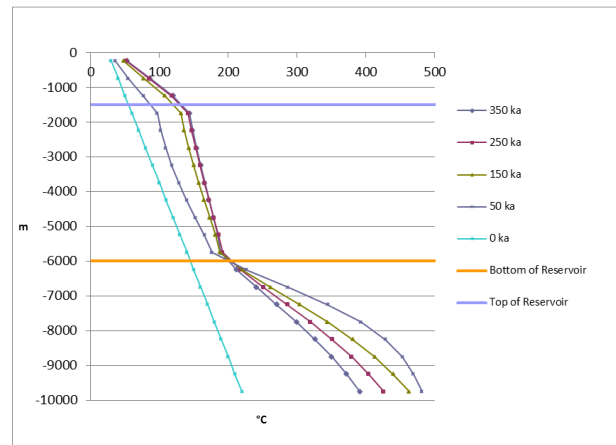
Finally, the case with thermal gradient of 40 K/km, in convective heat transmission in geothermal reservoir, is in Fig. 12. The temperature field for 50 ka, 150 ka, 250 ka and 350 ka is shown in Fig. 13.



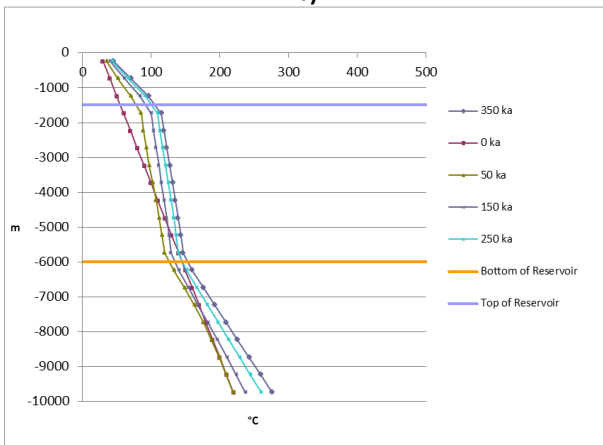
a)



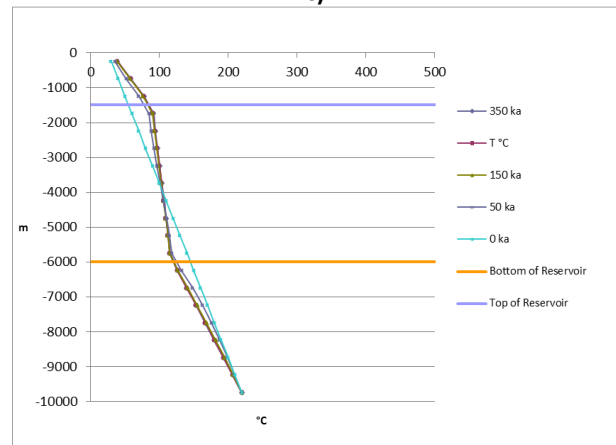
b)



c)



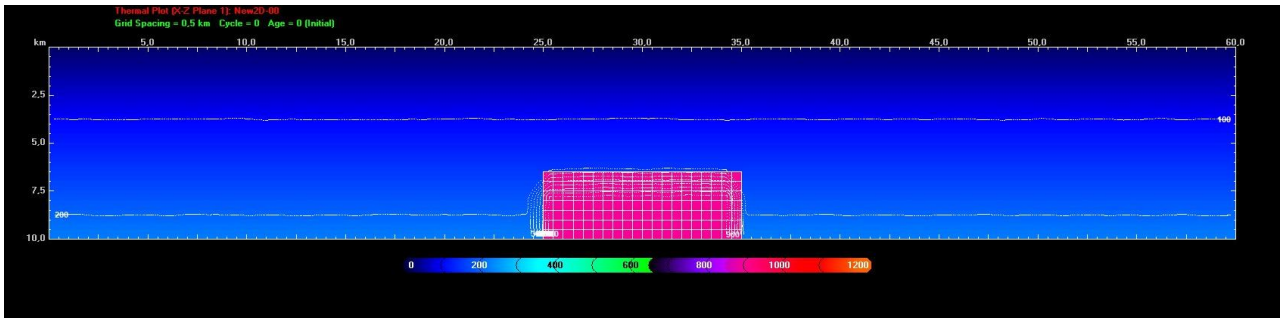
d)



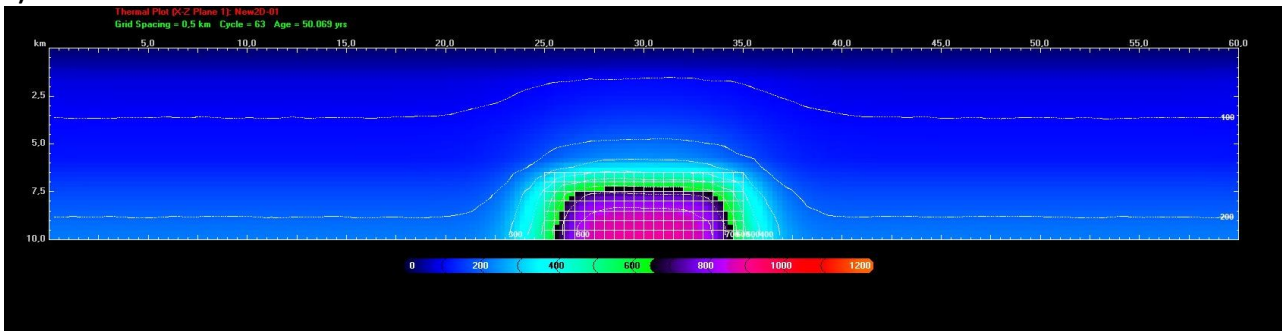
e)

Fig. 10 Temperature field in the domain for different time steps (initial configuration, 50 ka, 150 ka, 250 ka and 350 ka). Thermal gradient 20 K/km. Convective heat transmission in geothermal reservoir.

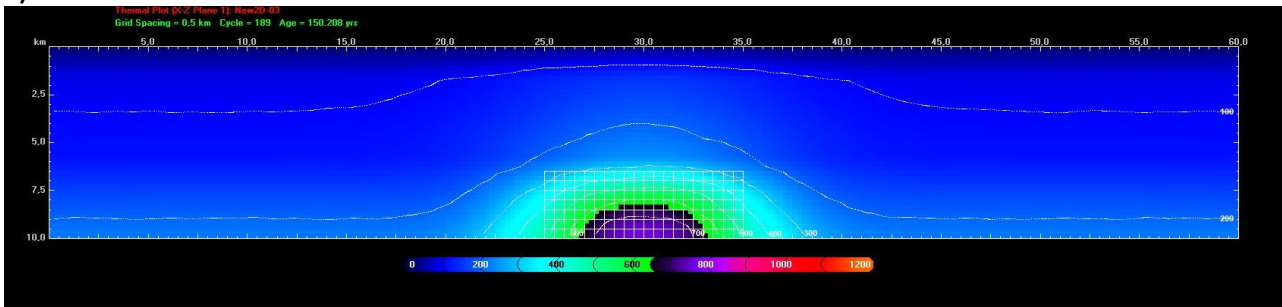
a) in the centre of magma chamber full temperature field; b) in the centre of magma chamber with temperature field cut-off at 500 °C; c) 5 km far from the centre of MC; d) 10 km far from the centre of MC; e) 20 km far from the centre of MC.



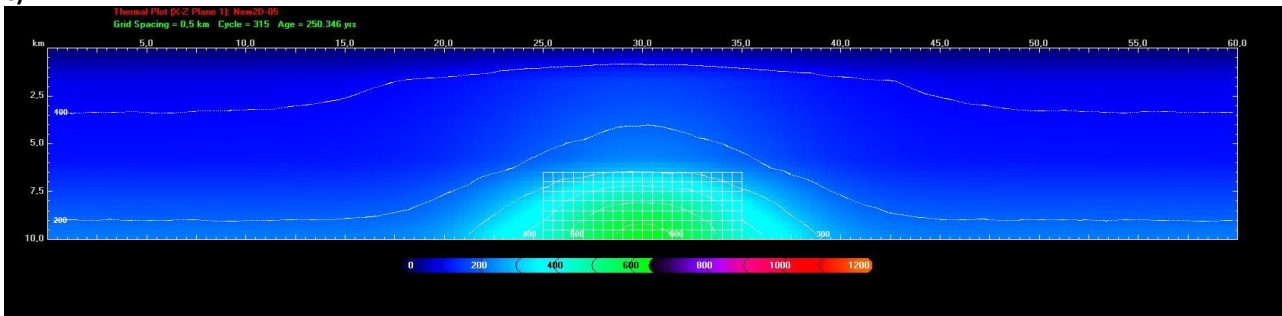
a)



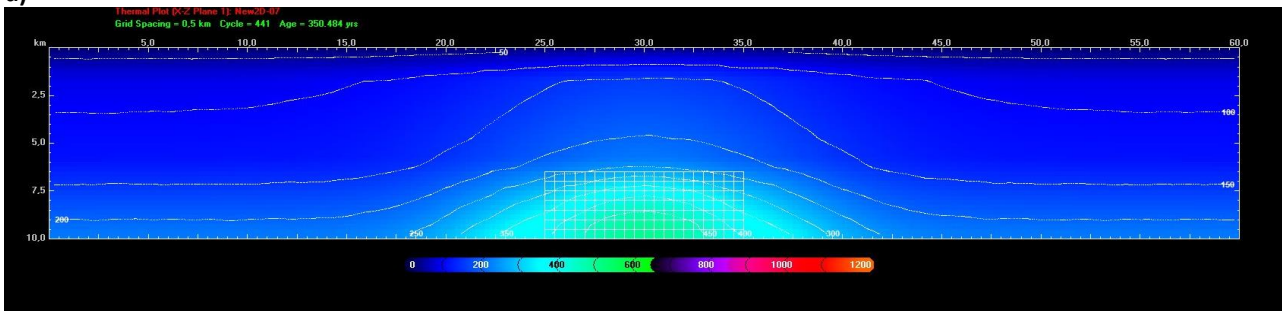
b)



c)



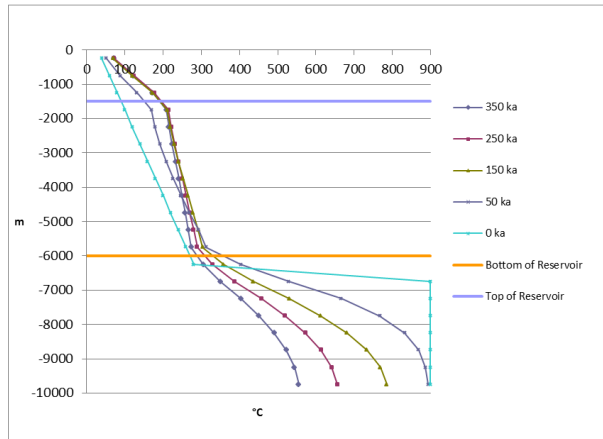
d)



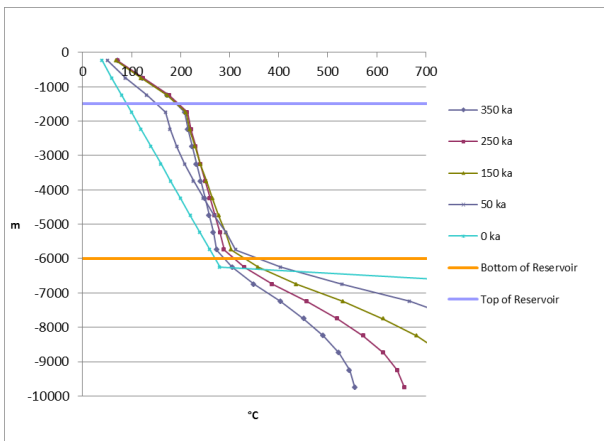
e)

Fig. 11 Temperature field in the domain. Thermal gradient 20 K/km. Convective heat transmission in geothermal reservoir. a) 0 ka; b) 50 ka; c) 150 ka; d) 250 ka and e) 350 ka)

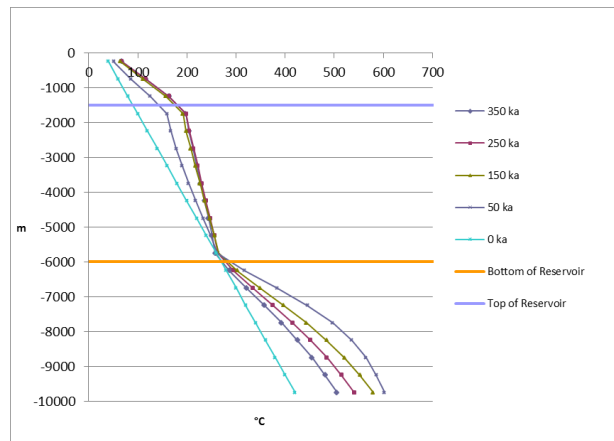
Finally, the same data, proposed so far, is presented for the thermal gradient 40 K/km in Fig. 12 and 13.



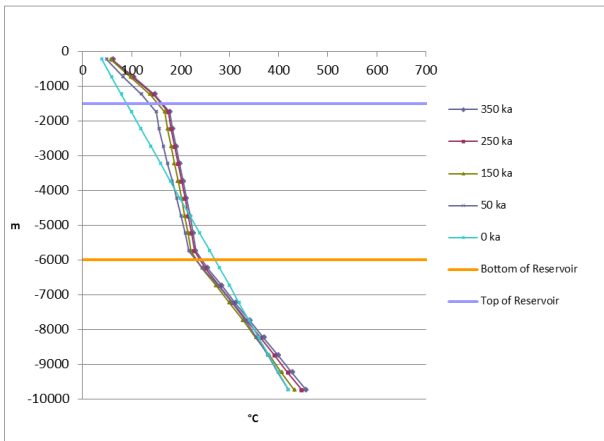
a)



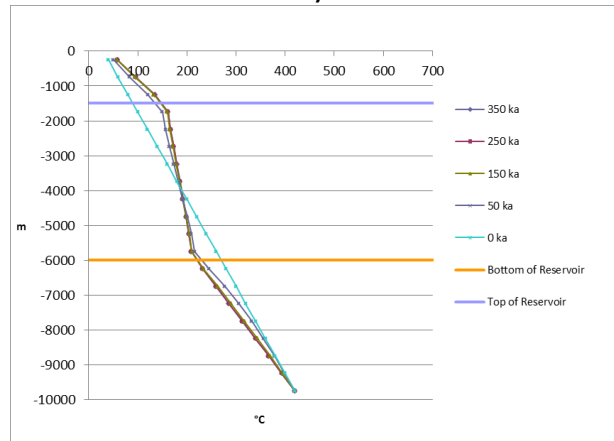
b)



c)



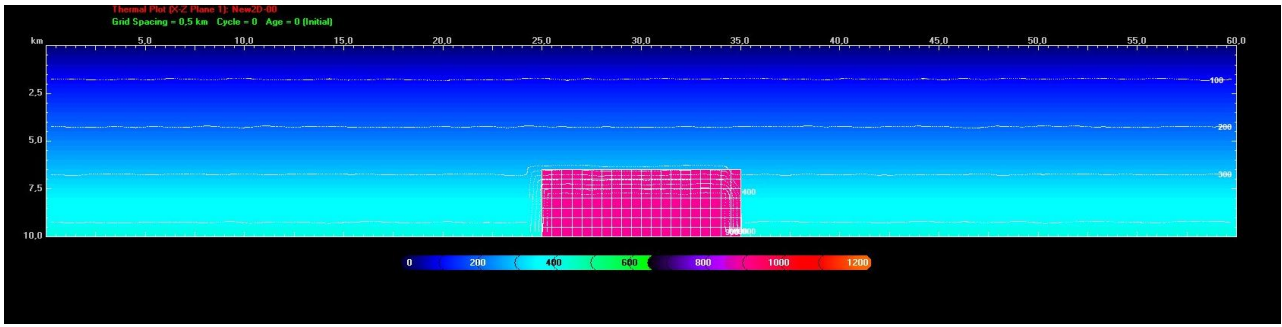
d)



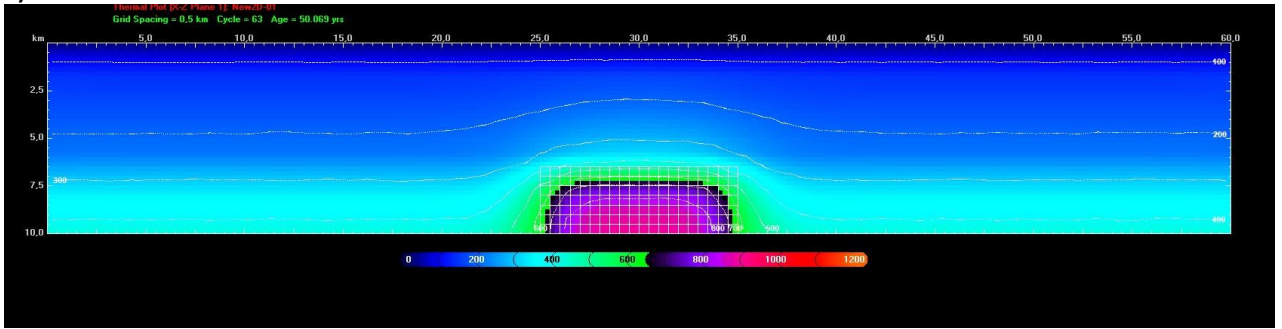
e)

Fig. 12 Temperature field in the domain for different time steps (initial configuration, 50 ka, 150 ka, 250 ka and 350 ka). Thermal gradient 40 K/km. Convective heat transmission in geothermal reservoir.

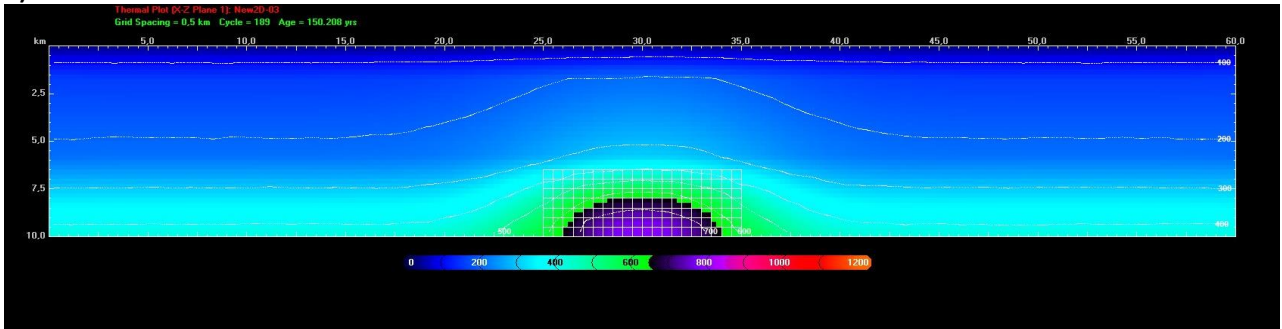
a) in the centre of magmatic chamber full temperature field; b) in the centre of magmatic chamber with temperature cut-off at 700 °C; c) 5 km far from the centre of MC; d) 10 km far from the centre of MC; e) 20 km far from the centre of MC.



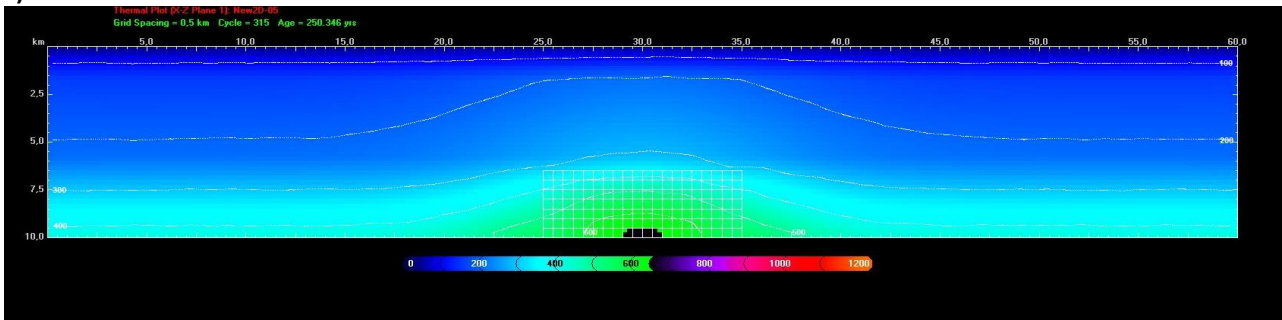
a)



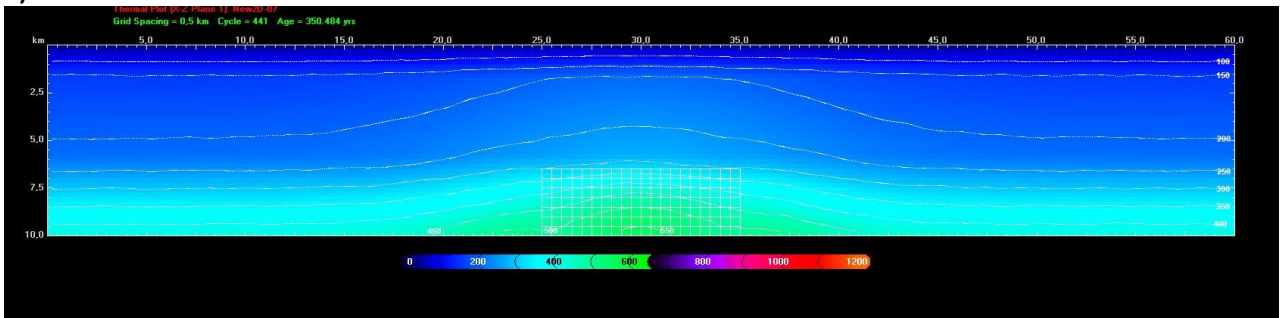
b)



c)



d)



e)

Fig. 13 Temperature field in the domain. Thermal gradient 40 K/km. Convective heat transmission in geothermal reservoir. a) 0 ka; b) 50 ka; c) 150 ka; d) 250 ka and e) 350 ka

The main obvious difference between this set of simulations and the previous is the more effective convective thermal plume that rises the temperatures within the geothermal reservoir; on the other side, there are also significant similarities such as:

1. Most of the thermal variation in the geothermal reservoir occurs within 150 ka from the beginning of simulations, leading to almost steady conditions until the end of simulations at 350 ka;
2. At 10 km far from the centre of MC the thermal variations are limited. Convection in the geothermal reservoir affects the slope gradient and interestingly the larger increase in T at the top of the geothermal reservoir corresponds to a decrease at its base;
3. 20 km far from the centre of MC, there is no effect on temperature for the thermal contribution of MC.

Chapter 9 - Calibration of the model respect to existing thermal data

In this Chapter, starting from the results of previous chapters, the calibration of the model is implemented. For the Monti Sabatini and Colli Albani areas, the calibration is implemented using the UNMIG database introduced before as reference dataset.

HISTORY OF MAGMA CHAMBER BUILDS UP THE THERMAL GRADIENT?

From the elements collected for the Conceptual Model, we know that in the Roman Geothermal Province volcanic activity started about 600 kyr ago and the climax of caldera-forming events, with ignimbritic eruptions of volumes between 10 km³ and 100 km³, occurred around 350 kyr ago. Such climax was then followed by volcanic activity till Upper Pleistocene time and in the case of Colli Albani area close to Holocene, but characterized by events of much lower intensity and magnitude (e.g. Mattei et al., 2010).

Obviously, the occurrence of caldera forming eruptions at one date implies that a large volume magma chamber had time previously to be installed at upper crustal levels, by prolonged episodes of magmatic injection and crystallization, crust assimilation until the modification of a volume of country rock into a magma chamber. We have no constraints on the duration and processes of such magmatic build-up phase that precedes volcanism in general and more so caldera forming eruptions. From a geothermal point of view the question is how much this process influenced the local geothermal gradient, and if so, whether we can take into account and how such pre-volcanism modified gradient to account for this “unwitnessed” but essential process of magmatic build-up.

To answer to this question, we set up simulations where the initial regional geothermal gradient in the domain is 20 K/km, which is an average value for the Latium Region far from the geothermal areas (see Ch. 6), the heat diffusion in the geothermal reservoir is taken as conductive. With this configuration we then compare conditions where the Magma Chamber is instantaneously inserted in the domain and let cool spontaneously for 350 kyr, with conditions where the magma chamber is first kept at the constant temperature of 900 °C for 500 kyr and then cools down spontaneously for 350 kyr.

As previously stated, the longevity of the pre-caldera stage is an assumption without a strong geological evidence. The idea is only to verify possible effects of the longevity of the Magma Chamber with a constant temperature on the local geothermal gradient.

Another problem is that under the conditions defined before for magma kept at constant temperature, the model parameter that controls the percentage of heat lost or gained within the mesh fastly reaches values out of the limits of confidence, which implies that the model is not stable and results cannot be taken as numerically valid. In the simulations, we have assumed the maximum acceptable value as +/- 20%. In this simulation that we have just described, after 500 ky the parameter has the value of 47,8%. So the result of the simulation is only qualitative. Nevertheless the simulation outputs are interesting.

In all simulations we use the selected geometrical configuration described in Chapter 7.

The first simulation is run with magma chamber instantaneously inserted in the domain and let cooling for 350 ky. The temperature gradient in K/km is taken at:

$$\begin{aligned} -1,000 \text{ m} &= (T_{1000} - T_{0=20 \text{ °C}}); \\ -2,000 \text{ m} &= (T_{2000} - T_{0=20 \text{ °C}}) / 2; \\ -3,000 \text{ m} &= (T_{3000} - T_{0=20 \text{ °C}}) / 3; \end{aligned}$$

The geothermal gradients in the geothermal reservoir, calculated from surface at 20 °C at -1000m, -2000m and -3000m are reported in Table 1, at various distances from magma chamber center indicated in Fig. 1.

	Centre of MC	5 km far from MC	10 km far from MC	20 km far from MC	30 km far from MC
-1,000 m	63	51	34	28	28
-2,000 m	60	48	32	26	26
-3,000 m	53	42	28	23	23

Tab 1 Thermal Gradient (K/km) at the end of simulation (350 ky) for different distance from the centre of Magma Chamber (MC). The gradient is calculated always from from surface at 20°C and then respect to temperature at -1000m, -2000m and -3000m

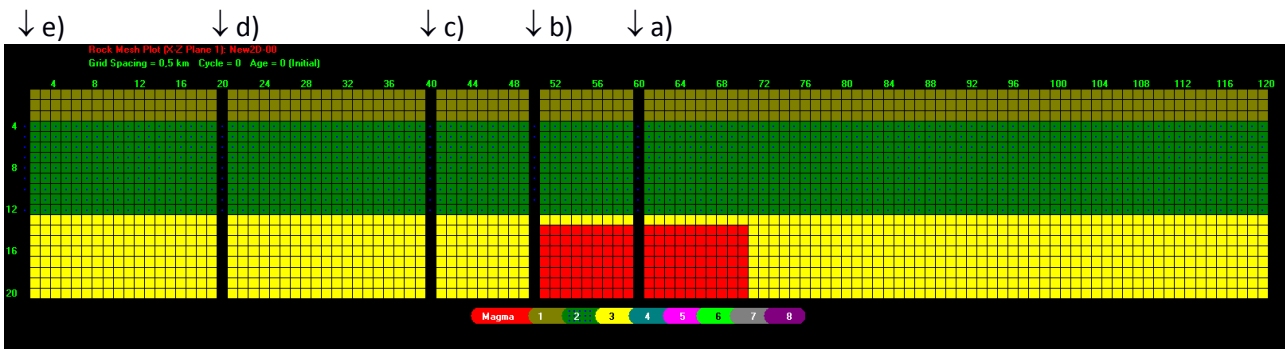


Fig. 1 Computational domain for the selected geometrical configuration described in Ch. 7 and used as fixed in this set of simulations, with the vertical points where outputs are shown. a) Centre of Magma Chamber (MC); b) 5 km far from MC; c) 10 km far from MC; d) 10 km far from MC; e) 30 km far from MC.

At the end of the second simulation, i.e. after 500 kyr with magma chamber kept at constant T + 350 kyr with magma chamber cooling, the geothermal gradients in the geothermal reservoir, calculated from surface at 20°C at -1000m, -2000m and -3000m and at various distances from magma chamber center are reported in Table 2.

	Centre of MC	5 km far from MC	10 km far from MC	20 km far from MC	30 km far from MC
-1,000 m	130	110	71	31	29
-2,000 m	120	101	66	29	27
-3,000 m	102	86	56	25	23

Tab. 1 Monti Sabatini. Thermal Gradient (K/km) at the end of simulation (500 ky + 350 ky) for different distance from the centre of Magma Chamber (MC) – see fig 1

The results of both simulations show that the lateral extent of the thermal anomaly propagates up to 10 km far, that is 5 km away from edge of magma chamber, where the local geothermal gradient is still substantially greater than the undisturbed. By contrast at 20 km far from the center of magma chamber the modification of the geothermal gradient is negligible.

Interestingly the geothermal gradient in the Monti Sabatini area around the Bracciano caldera , i.e. at the edge of the presumed lateral extension of the magma chamber, is 83.0 K/km (see data in previous Ch.6) which coincidentally is very similar to that obtained in the simulation. Of course, this does not imply any particular similarity between the conditions imposed to the run and reality

Comparing Table 1 and Table 2 we can affirm:

- Effects of heat diffusion under very different starting conditions affect the domain as far as 10 km from the centre of magma chamber, but fades out laterally to become almost negligible at 20 km. This length scale is rather similar to that reconstructed by the Heat Flow map of Italy (Cataldi et al., 1995) and suggest that, though locally modified by advection, most of the magma related geothermal anomalies in central Italy are controlled by conductive heat diffusion
- The process of building and establishment of the magma chamber affects the thermal gradient in a relevant way;
- Also, when the model relaxes in the select configuration, an increment of thermal gradient is detected.

MODEL CALIBRATION

We define the root-mean-square deviation (RMSD) of predicted values \hat{y}_i for observations y_i as the square root of the sums of the squares of the deviations:

$$\text{RMSD} = \left(\sum_{i=1}^n \frac{(\hat{y}_i - y_i)^2}{n} \right)^{1/2} \quad \text{Eq. 1}$$

The coefficient of variation of the RMSD, $\text{CV}(\text{RMSD})$, is the ratio of the RMSD with the mean value of y :

$$\text{CV}(\text{RMSD}) = \frac{\text{RMSD}}{\bar{y}} \quad \text{Eq. 2}$$

The mean absolute error (MAE) is a measure of difference between predicted values \hat{y}_i and observations y_i :

$$\text{MAE} = \sum_{i=1}^n \frac{|\hat{y}_i - y_i|}{n} \quad \text{Eq. 3}$$

The relative error is the ratio of the MAE with the mean value of y :

$$\text{RelErr} = \frac{\text{MAE}}{\bar{y}} \quad \text{Eq. 4}$$

MODEL CALIBRATION IN COLLI ALBANI AREA

The DGS-UNMIG (Directorate-General For Safety Of Mining And Energy Activities National Mining Office For Hydrocarbons And Georesources) of Italian Ministry of Economic Development has prepared a database for Italian Municipalities. In the database it is possible to find relevant information regarding geothermal resources. For each municipality is available: name, province Region and ISTAT (Italian Institute of Statistics) code; temperature (in °C) mean, minimum and maximum at 1 km, 2km and 3 km deep; the mean, minimum and maximum heat flow (in mW/m²); the mean, minimum and maximum deep of the carbonatic reservoir top (in m).

For the Colli Albani area, we consider the Municipalities in Tab. 3. The area covered by these Municipalities is about 440 km².

Municipality	d(T3000_mean-20°C)/3
Albano Laziale	43,1
Ariccia	43,3
Castel Gandolfo	43,1

Municipality	d(T3000_mean-20°C)/3
Marino	43
Montecompatri	42
Monte Porzio Catone	45,8

Ciampino	43
Frascati	44,9
Genzano di Roma	44,2
Grottaferrata	44,1
Labico	22,7
Lariano	33,1

Nemi	44,1
Rocca di Papa	44,6
Rocca Priora	43,6
San Cesareo	34,1
Velletri	43,2

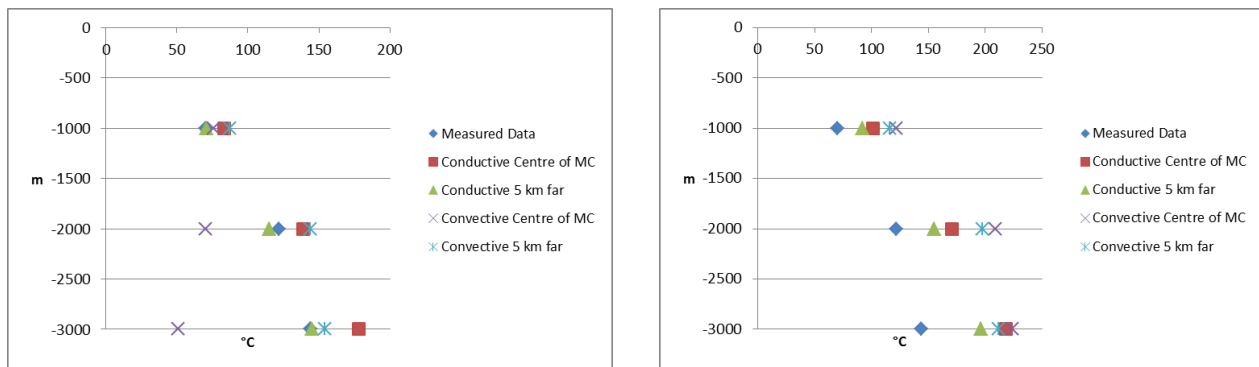
Tab. 3 Municipalities and Temperature gradient in Colli Albani area

In Tab 4. we have the mean value for the fields T1000_mean; T2000_mean and T3000_mean, i.e. mean temperature at -1 km, -2 km and -3 km deep, and the temperature gradient, i.e. $(T_{1000} - T_{0=20\text{°C}})$; $(T_{2000} - T_{0=20\text{°C}})/2$, $(T_{3000} - T_{0=20\text{°C}})/3$.

z (m)	-1000	-2000	-3000
T (°C)	70	122	144
dT/dz (K/km)	50	51	41

Tab. 4 T and dT/dz values at -1,000, -2,000 and -3,000 in Colli Albani area

Among all the data collected in our simulation, we consider four simulation: those with thermal gradient equal to 20 K/km and 40 K/km and the heat transmitted by conduction and by convection-conduction in the reservoir. Moreover we consider two vertical points: the centre of Magma Chamber and 5 km far from the centre of Magma Chamber (Fig. 2), that is the edge of it.



a) b) Fig. 2. Measured data and numerical model outputs; in the centre of MC and 5 km far from the centre of MC; convection and conduction heat transmission in reservoir. a) thermal gradient 20 K/km; b) thermal gradient 40 K/km.

We have implemented a statistical analysis among the numerical modeling profiles and the DGS-UNMIG data, including RMSD(T) in K, CV(T) in %, MAE(T) in K, RelErr(T) in %, RMSD(dT/dz) in K/km, CV(dT/dz) in %, MAE(dT/dz) in K/km, and RelErr(dT/dz) in % (Tab. 5).

Thermal Gradient 20 K/km - Conductive Heat Transmission in Reservoir - Centre of MC							
RMSD(T) K	CV(T) %	MAE(T) K	RelErr(T) %	RMSD(dT/dz) K/km	CV(dT/dz) %	MAE(dT/dz) K/km	RelErr(dT/dz) %
23,2	6,0	21,3	5,5	11,3	23,9	11,2	23,7
Thermal Gradient 20 K/km - Convective Heat Transmission in Reservoir - Centre of MC							
RMSD(T) K	CV(T) %	MAE(T) K	RelErr(T) %	RMSD(dT/dz) K/km	CV(dT/dz) %	MAE(dT/dz) K/km	RelErr(dT/dz) %
31,8	8,3	31,3	8,1	19,4	40,9	18,2	38,4
Thermal Gradient 20 K/km - Conductive Heat Transmission in Reservoir - 5 km far from Centre of MC							
RMSD(T) K	CV(T) %	MAE(T) K	RelErr(T) %	RMSD(dT/dz) K/km	CV(dT/dz) %	MAE(dT/dz) K/km	RelErr(dT/dz) %
4,1	1,1	3,0	0,8	1,9	3,9	1,6	3,3
Thermal Gradient 20 K/km - Convective Heat Transmission in Reservoir - 5 km far from Centre of MC							
RMSD(T) K	CV(T) %	MAE(T) K	RelErr(T) %	RMSD(dT/dz) K/km	CV(dT/dz) %	MAE(dT/dz) K/km	RelErr(dT/dz) %
17,1	4,4	16,3	4,2	11,9	25,0	10,6	22,2
Thermal Gradient 40 K/km - Conductive Heat Transmission in Reservoir - Centre of MC							
RMSD(T) K	CV(T) %	MAE(T) K	RelErr(T) %	RMSD(dT/dz) K/km	CV(dT/dz) %	MAE(dT/dz) K/km	RelErr(dT/dz) %
54,3	14,1	51,3	13,3	27,0	57,0	26,9	56,7
Thermal Gradient 40 K/km - Convective Heat Transmission in Reservoir - Centre of MC							
RMSD(T) K	CV(T) %	MAE(T) K	RelErr(T) %	RMSD(dT/dz) K/km	CV(dT/dz) %	MAE(dT/dz) K/km	RelErr(dT/dz) %
74,5	19,4	73,0	19,0	41,9	88,3	40,6	85,5
Thermal Gradient 40 K/km - Conductive Heat Transmission in Reservoir - 5 km far from Centre of MC							
RMSD(T) K	CV(T) %	MAE(T) K	RelErr(T) %	RMSD(dT/dz) K/km	CV(dT/dz) %	MAE(dT/dz) K/km	RelErr(dT/dz) %
37,8	9,8	35,7	9,3	18,7	39,5	18,6	39,1
Thermal Gradient 40 K/km - Convective Heat Transmission in Reservoir - 5 km far from Centre of MC							
RMSD(T) K	CV(T) %	MAE(T) K	RelErr(T) %	RMSD(dT/dz) K/km	CV(dT/dz) %	MAE(dT/dz) K/km	RelErr(dT/dz) %
64,6	16,8	63,3	16,4	36,9	77,7	35,6	74,9

Tab. 5. RMSD(T), CV(T), MAE(T), RelErr(T), RMSD(dT/dz), CV(dT/dz), MAE(dT/dz), and RelErr(dT/dz) for simulations with thermal gradient equal to 20 K/km and 40 K/km, convection and conduction heat transmission in reservoir, in the centre of Magma Chamber and 5 km far from the centre of Magma Chamber.

The best fit is with the thermal Gradient equal to 20 K/km, with Conductive Heat Transmission in Reservoir and at 5 km far from Centre of Magma Chamber (Tab. 6). The considered area is equivalent to the area of a 12 km radius circumference. The point at 5 km from the center of the magmatic chamber can be seen as middle point for this radius.

Thermal Gradient 20 K/km - Conductive Heat Transmission in Reservoir - 5 km far from Centre of MC							
RMSD(T) K	CV(T) %	MAE(T) K	RelErr(T) %	RMSD(dT/dz) K/km	CV(dT/dz) %	MAE(dT/dz) K/km	RelErr(dT/dz) %
4,1	1,1	3,0	0,8	1,9	3,9	1,6	3,3

Tab. 6. Best fit between measured data and numerical simulation outputs: thermal Gradient 20 K/km, Conductive Heat Transmission in Reservoir at 5 km far from Centre of Magma Chamber

MODEL CALIBRATION IN MONTI SABATINI AREA

The same procedure implemented for Colli Albani is implemented for Monti Sabatini Area. We consider the Municipalities in Tab. 7. The area covered by these Municipalities is about 300 km².

Municipality	$d(T_{3000_mean}-20^{\circ}C)/3$
Anguillara Sabazia	85,3
Bracciano	78,0
Campagnano Di Roma	75,1
Trevignano Romano	93,4

Tab. 7 Municipalities and Temperature gradient around the Bracciano lake

Considering the Municipalities in Tab. 7, in Tab 8. we have the mean value for the fields T1000_mean; T2000_mean and T3000_mean, i.e. mean temperature at -1 km, -2 km and -3 km deep, and the temperature gradient, i.e. $(T_{1000} - T_{0=20^{\circ}C})$; $(T_{2000} - T_{0=20^{\circ}C})/2$, $(T_{3000} - T_{0=20^{\circ}C})/3$.

z(m)	-1000	-2000	-3000
T (°C)	121	221	269
dT/dz (k/km)	101	101	83

Tab. 8 T and dT/dz values at -1,000, -2,000 and -3,000 in Monti Sabatini area

To calibrate the numerical model in this area, the first step is to follow the same procedure implemented before (Fig. 3). Statistical analysis data, implemented for the centre on Magma Chamber, is in Tab. 9. Statistical analysis data, implemented for 5 km far from the centre on Magma Chamber, is in Tab. 10.

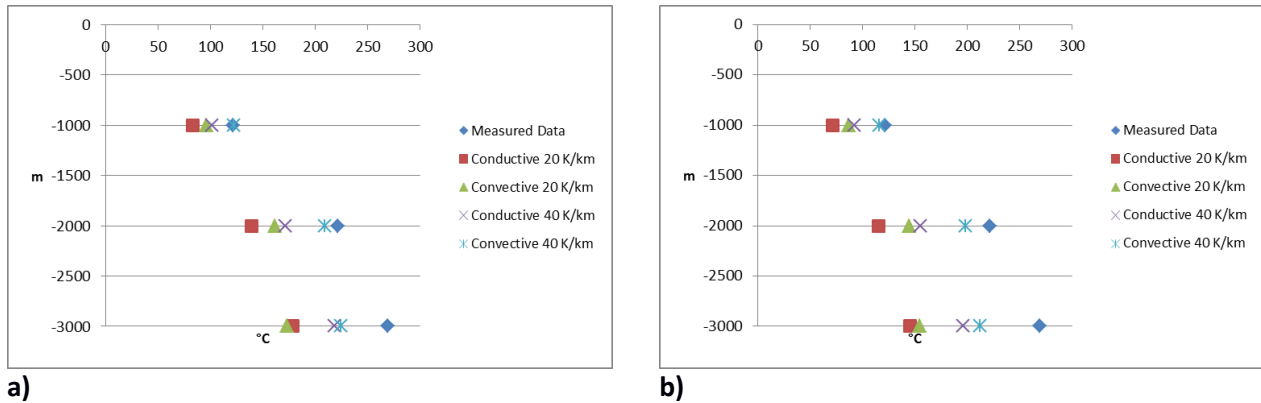


Fig 3. Measured data and numerical model outputs; convection and conduction heat transmission in reservoir; thermal gradient 20 K/km and 40 K/km. a) in the centre of MC; b) 5 km far from the centre of MC

Thermal Gradient 20 K/km - Conductive Heat Transmission in Reservoir - Centre of MC							
RMSD(T) K	CV(T) %	MAE(T) K	RelErr(T) %	RMSD(dT/dz) K/km	CV(dT/dz) %	MAE(dT/dz) K/km	RelErr(dT/dz) %
74,0	15,5	70,3	14,8	36,4	38,4	36,2	38,1
Thermal Gradient 20 K/km - Convective Heat Transmission in Reservoir - Centre of MC							
RMSD(T) K	CV(T) %	MAE(T) K	RelErr(T) %	RMSD(dT/dz) K/km	CV(dT/dz) %	MAE(dT/dz) K/km	RelErr(dT/dz) %
66,9	14,0	60,3	12,7	29,3	30,9	29,2	30,8
Thermal Gradient 40 K/km - Conductive Heat Transmission in Reservoir - Centre of MC							
RMSD(T) K	CV(T) %	MAE(T) K	RelErr(T) %	RMSD(dT/dz) K/km	CV(dT/dz) %	MAE(dT/dz) K/km	RelErr(dT/dz) %
42,8	9,0	40,3	8,5	20,7	21,9	20,5	21,6
Thermal Gradient 40 K/km - Convective Heat Transmission in Reservoir - Centre of MC							
RMSD(T) K	CV(T) %	MAE(T) K	RelErr(T) %	RMSD(dT/dz) K/km	CV(dT/dz) %	MAE(dT/dz) K/km	RelErr(dT/dz) %
26,9	5,6	19,3	4,1	9,5	10,0	7,5	7,9

Tab. 9. RMSD(T), CV(T), MAE(T), RelErr(T), RMSD(dT/dz)m, CV(dT/dz), MAE(dT/dz), and RelErr(dT/dz) for simulations with thermal gradient equal to 20 K/km and 40 K/km, convection and conduction heat transmission in reservoir, in the centre of Magma Chamber.

Thermal Gradient 20 K/km - Conductive Heat Transmission in Reservoir - 5 km far from the Centre of MC							
RMSD(T)	RMSD(dT/dz)	CV(T)	CV(dT/dz)	MAE(T)	MAE(dT/dz)	RelErr(T)	RelErr(dT/dz)
98,509	20,660	93,333	19,574	48,08759369	50,70748016	47,83333333	50,43936731
Thermal Gradient 20 K/km - Convective Heat Transmission in Reservoir - 5 km far from the Centre of MC							
RMSD(T)	RMSD(dT/dz)	CV(T)	CV(dT/dz)	MAE(T)	MAE(dT/dz)	RelErr(T)	RelErr(dT/dz)
82,280	17,256	75,333	15,799	36,888	38,898	36,833	38,8400703
Thermal Gradient 40 K/km - Conductive Heat Transmission in Reservoir - 5 km far from the Centre of MC							
RMSD(T)	RMSD(dT/dz)	CV(T)	CV(dT/dz)	MAE(T)	MAE(dT/dz)	RelErr(T)	RelErr(dT/dz)
59,234	12,423	56,000	11,745	29,093	30,678	28,833	30,404
Thermal Gradient 40 K/km - Convective Heat Transmission in Reservoir - 5 km far from the Centre of MC							
RMSD(T)	RMSD(dT/dz)	CV(T)	CV(dT/dz)	MAE(T)	MAE(dT/dz)	RelErr(T)	RelErr(dT/dz)
35,604	7,467	28,333	5,942	13,143	13,860	11,833	12,478

Tab. 10. RMSD(T), CV(T), MAE(T), RelErr(T), RMSD(dT/dz)m, CV(dT/dz), MAE(dT/dz), and RelErr(dT/dz) for simulations with thermal gradient equal to 20 K/km and 40 K/km, convection and conduction heat transmission in reservoir, 5 km far from the centre of MC.

The best simulation is that with Thermal Gradient 40 K/km - Convective Heat Transmission in Reservoir – in the centre of MC. This difference from Colli Albani suggest two possibilities. One is a substantially different pre-heating history relative to a prolonged build-up of the magmatic system that may have changed the

local geothermal gradient. However there are no substantial differences in the volcanic histories of Colli Albani versus Sabatini that may suggest that. An alternative is that the top of the magma chamber is shallower as a series of papers have suggested based on geophysical data as well as direct drilling of intrusive bodies set within the geothermal reservoir at depths of around 3 km (Molina & Sonaglia, 1969; De Rita et al., 1983; De Rita et al., 1996, Capelli et al., 2005) (See Fig. 4).

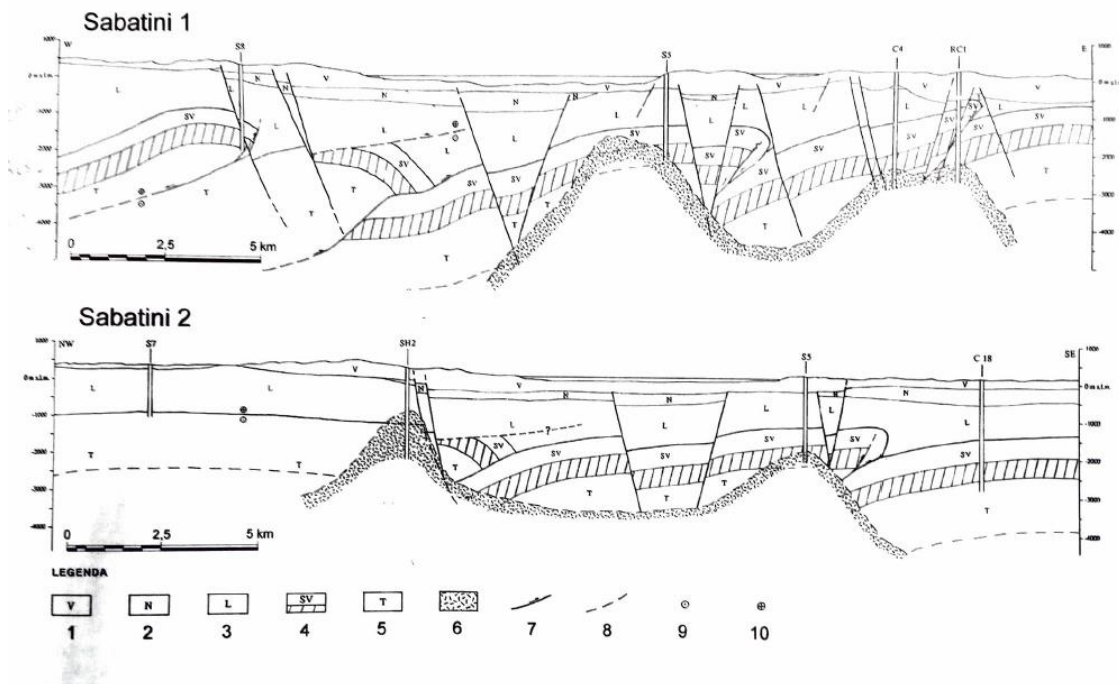


Fig 4. Geological cross-sections in Monti Sabatini area. In Legenda, 6 indicates thermometamorphosis complex plus dikes systems. (Capelli et al., 2005)

We therefore devised a new set of simulations shifting upward the Magma Chamber Top Level to -6 km, -5 km, -4 km and -3 km.

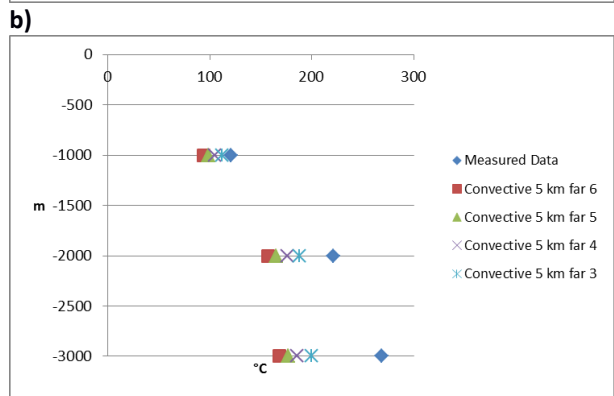
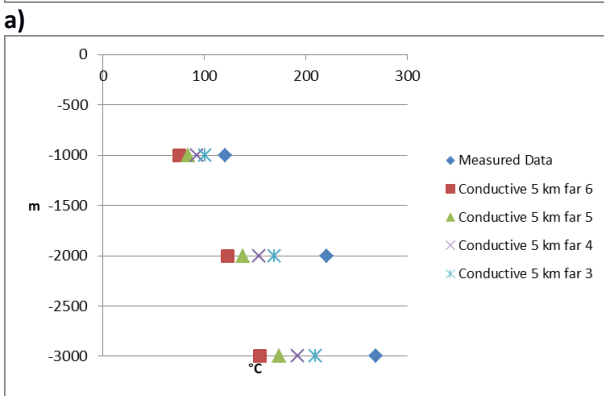
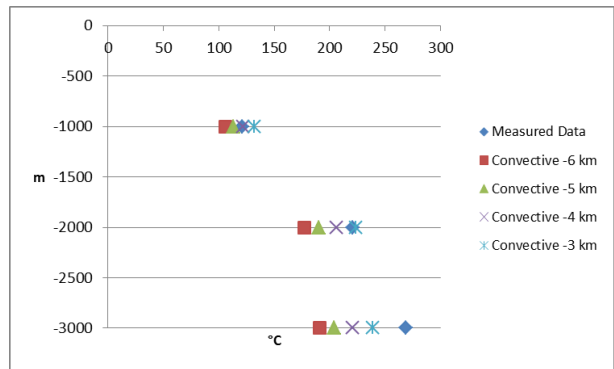
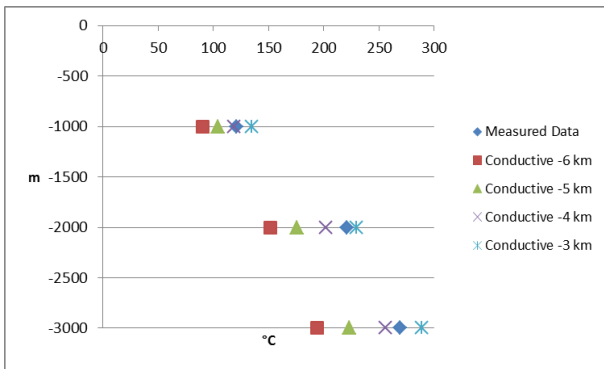


Fig 5. Measured data and numerical model outputs; thermal gradient 20 K/km. a) conduction heat transmission in reservoir in the centre of MC; b) convection heat transmission in reservoir in the centre of MC; c) conduction heat transmission in reservoir 5 km far from the centre of MC; d) convection heat transmission in reservoir 5 km far from the centre of MC

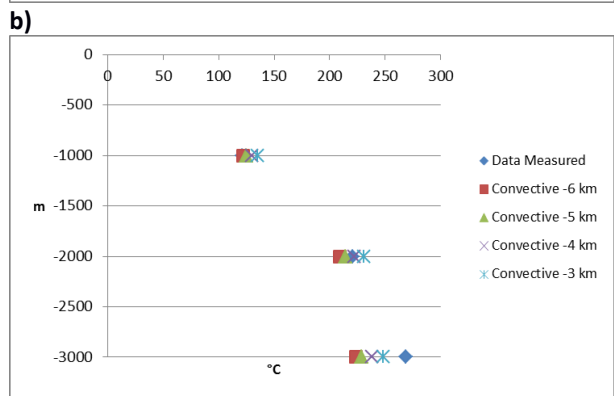
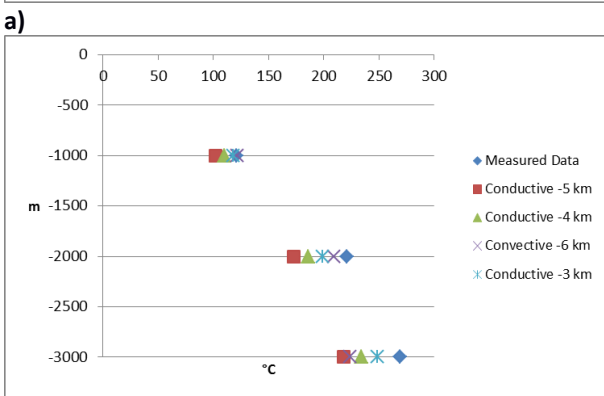
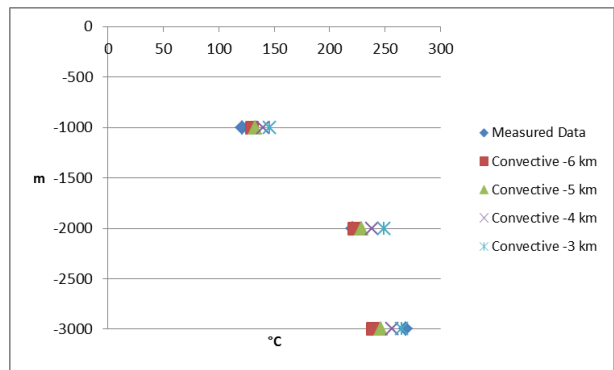
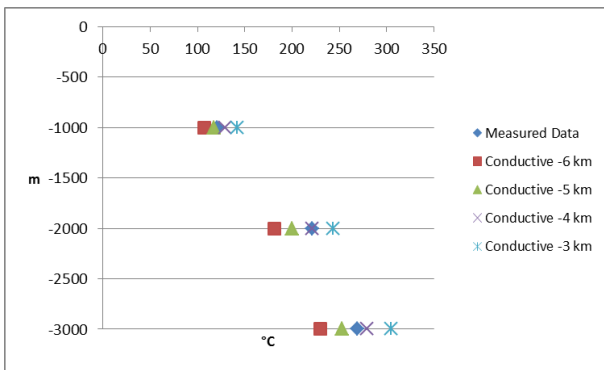


Fig 6. Measured data and numerical model outputs; thermal gradient 40 K/km. a) conduction heat transmission in reservoir in the centre of MC; b) convection heat transmission in reservoir in the centre of MC; c) conduction heat transmission in reservoir 5 km far from the centre of MC; d) convection heat transmission in reservoir 5 km far from the centre of MC

transmission in reservoir 5 km far from the centre of MC; d) convection heat transmission in reservoir 5 km far from the centre of MC

Thermal Gradient 20 K/km - Conductive Heat Transmission in Reservoir - Centre of MC - MCTL -6 km							
RMDS(T) K	CV(T) %	MAE(T) K	RelErr(T) %	RMDS(dT/dz) K/km	CV(dT/dz) %	MAE(dT/dz) K/km	RelErr(dT/dz) %
61,5	12,9	58,3	12,2	30,4	32,1	30,2	31,8
Thermal Gradient 20 K/km - Convective Heat Transmission in Reservoir - Centre of MC - MCTL -6 km							
RMDS(T) K	CV(T) %	MAE(T) K	RelErr(T) %	RMDS(dT/dz) K/km	CV(dT/dz) %	MAE(dT/dz) K/km	RelErr(dT/dz) %
52,4	11,0	45,7	9,6	21,5	22,7	21,0	22,1
Thermal Gradient 20 K/km - Conductive Heat Transmission in Reservoir - Centre of MC - MCTL -5 km							
RMDS(T) K	CV(T) %	MAE(T) K	RelErr(T) %	RMDS(dT/dz) K/km	CV(dT/dz) %	MAE(dT/dz) K/km	RelErr(dT/dz) %
38,4	8,1	36,0	7,6	18,5	19,5	18,3	19,3
Thermal Gradient 20 K/km - Convective Heat Transmission in Reservoir - Centre of MC - MCTL -5 km							
RMDS(T) K	CV(T) %	MAE(T) K	RelErr(T) %	RMDS(dT/dz) K/km	CV(dT/dz) %	MAE(dT/dz) K/km	RelErr(dT/dz) %
41,8	8,8	34,7	7,3	16,1	16,9	15,1	15,9
Thermal Gradient 20 K/km - Conductive Heat Transmission in Reservoir - Centre of MC - MCTL -4 km							
RMDS(T) K	CV(T) %	MAE(T) K	RelErr(T) %	RMDS(dT/dz) K/km	CV(dT/dz) %	MAE(dT/dz) K/km	RelErr(dT/dz) %
13,3	2,8	11,3	2,4	6,1	6,5	5,3	5,6
Thermal Gradient 20 K/km - Convective Heat Transmission in Reservoir - Centre of MC - MCTL -4 km							
RMDS(T) K	CV(T) %	MAE(T) K	RelErr(T) %	RMDS(dT/dz) K/km	CV(dT/dz) %	MAE(dT/dz) K/km	RelErr(dT/dz) %
29,0	6,1	21,3	4,5	10,2	10,8	8,2	8,6
Thermal Gradient 20 K/km - Conductive Heat Transmission in Reservoir - Centre of MC - MCTL -3 km							
RMDS(T) K	CV(T) %	MAE(T) K	RelErr(T) %	RMDS(dT/dz) K/km	CV(dT/dz) %	MAE(dT/dz) K/km	RelErr(dT/dz) %
15,0	3,2	14,3	3,0	9,3	9,8	8,4	8,8
Thermal Gradient 20 K/km - Convective Heat Transmission in Reservoir - Centre of MC - MCTL -3 km							
RMDS(T) K	CV(T) %	MAE(T) K	RelErr(T) %	RMDS(dT/dz) K/km	CV(dT/dz) %	MAE(dT/dz) K/km	RelErr(dT/dz) %
18,5	3,9	14,7	3,1	8,6	9,1	7,5	7,9

Tab. 11. RMDS(T), CV(T), MAE(T), RelErr(T), RMDS(dT/dz)m, CV(dT/dz), MAE(dT/dz), and RelErr(dT/dz) for simulations with thermal gradient equal to 20 K/km, convection and conduction heat transmission in reservoir, in the centre of Magma Chamber and with MCTL equal to -6 km, -5 km, -4 km and -3 km.

Tab. 11 includes the outputs with thermal gradient = 20 K/km, convection and conduction heat transmission in reservoir, in the centre of Magma Chamber, Magma Chamber Top Level (MCTL) at -6 km, -5 km, -4 km and -3 km.

Thermal Gradient 40 K/km - Conductive Heat Transmission in Reservoir - Centre of MC - MCTL -6 km							
RMDS(T) K	CV(T) %	MAE(T) K	RelErr(T) %	RMDS(dT/dz) K/km	CV(dT/dz) %	MAE(dT/dz) K/km	RelErr(dT/dz) %
33,3	7,0	31,0	6,5	16,0	16,8	15,7	16,5
Thermal Gradient 40 K/km - Convective Heat Transmission in Reservoir - Centre of MC - MCTL -6 km							
RMDS(T) K	CV(T) %	MAE(T) K	RelErr(T) %	RMDS(dT/dz) K/km	CV(dT/dz) %	MAE(dT/dz) K/km	RelErr(dT/dz) %
18,1	3,8	13,3	2,8	7,8	8,2	6,5	6,9
Thermal Gradient 40 K/km - Conductive Heat Transmission in Reservoir - Centre of MC - MCTL -5 km							
RMDS(T) K	CV(T) %	MAE(T) K	RelErr(T) %	RMDS(dT/dz) K/km	CV(dT/dz) %	MAE(dT/dz) K/km	RelErr(dT/dz) %
15,4	3,2	13,7	2,9	7,2	7,6	6,6	7,0
Thermal Gradient 40 K/km - Convective Heat Transmission in Reservoir - Centre of MC - MCTL -5 km							
RMDS(T) K	CV(T) %	MAE(T) K	RelErr(T) %	RMDS(dT/dz) K/km	CV(dT/dz) %	MAE(dT/dz) K/km	RelErr(dT/dz) %
15,7	3,3	14,3	3,0	8,5	9,0	7,9	8,3
Thermal Gradient 40 K/km - Conductive Heat Transmission in Reservoir - Centre of MC - MCTL -4 km							
RMDS(T) K	CV(T) %	MAE(T) K	RelErr(T) %	RMDS(dT/dz) K/km	CV(dT/dz) %	MAE(dT/dz) K/km	RelErr(dT/dz) %
7,4	1,6	6,0	1,3	5,0	5,3	3,8	4,0
Thermal Gradient 40 K/km - Convective Heat Transmission in Reservoir - Centre of MC - MCTL -4 km							
RMDS(T) K	CV(T) %	MAE(T) K	RelErr(T) %	RMDS(dT/dz) K/km	CV(dT/dz) %	MAE(dT/dz) K/km	RelErr(dT/dz) %
16,5	3,5	16,3	3,4	12,3	12,9	10,6	11,2
Thermal Gradient 40 K/km - Conductive Heat Transmission in Reservoir - Centre of MC - MCTL -3 km							
RMDS(T) K	CV(T) %	MAE(T) K	RelErr(T) %	RMDS(dT/dz) K/km	CV(dT/dz) %	MAE(dT/dz) K/km	RelErr(dT/dz) %
27,2	5,7	26,3	5,5	15,3	16,2	14,7	15,5
Thermal Gradient 40 K/km - Convective Heat Transmission in Reservoir - Centre of MC - MCTL -3 km							
RMDS(T) K	CV(T) %	MAE(T) K	RelErr(T) %	RMDS(dT/dz) K/km	CV(dT/dz) %	MAE(dT/dz) K/km	RelErr(dT/dz) %
21,8	4,6	19,0	4,0	16,6	17,5	13,4	14,2

Tab. 12. RMDS(T), CV(T), MAE(T), RelErr(T), RMDS(dT/dz)m, CV(dT/dz), MAE(dT/dz), and RelErr(dT/dz) for simulations with thermal gradient equal to 40 K/km, convection and conduction heat transmission in reservoir, in the centre of Magma Chamber and with MCTL equal to -6 km, -5 km, -4 km and -3 km.

Tab. 12 includes the outputs with thermal gradient = 40 K/km, convection and conduction heat transmission in reservoir, in the centre of Magma Chamber, Magma Chamber Top Level (MCTL) at -6 km, -5 km, -4 km and -3 km.

Tab. 13 includes the outputs with thermal gradient = 20 K/km, convection and conduction heat transmission in reservoir, 5 km far from the centre of Magma Chamber, Magma Chamber Top Level (MCTL) at -6 km, -5 km, -4 km and -3 km.

Finally, Tab. 14 includes the outputs with thermal gradient = 40 K/km, convection and conduction heat transmission in reservoir, 5 km far from the centre of Magma Chamber, Magma Chamber Top Level (MCTL) at -6 km, -5 km, -4 km and -3 km.

Thermal Gradient 20 K/km - Conductive Heat Transmission in Reservoir - 5 km far from the Centre of MC - MCTL -6 km							
RMSD(T) K	CV(T) %	MAE(T) K	RelErr(T) %	RMSD(dT/dz) K/km	CV(dT/dz) %	MAE(dT/dz) K/km	RelErr(dT/dz) %
90,8	19,0	86,0	18,0	44,6	47,0	44,3	46,7
Thermal Gradient 20 K/km - Convective Heat Transmission in Reservoir - 5 km far from the Centre of MC - MCTL -6 km							
RMSD(T) K	CV(T) %	MAE(T) K	RelErr(T) %	RMSD(dT/dz) K/km	CV(dT/dz) %	MAE(dT/dz) K/km	RelErr(dT/dz) %
70,8	14,8	64,0	13,4	31,0	32,7	30,9	32,6
Thermal Gradient 20 K/km - Conductive Heat Transmission in Reservoir - 5 km far from the Centre of MC - MCTL -5 km							
RMSD(T) K	CV(T) %	MAE(T) K	RelErr(T) %	RMSD(dT/dz) K/km	CV(dT/dz) %	MAE(dT/dz) K/km	RelErr(dT/dz) %
75,9	15,9	71,7	15,0	36,9	39,0	36,7	38,7
Thermal Gradient 20 K/km - Convective Heat Transmission in Reservoir - 5 km far from the Centre of MC - MCTL -5 km							
RMSD(T) K	CV(T) %	MAE(T) K	RelErr(T) %	RMSD(dT/dz) K/km	CV(dT/dz) %	MAE(dT/dz) K/km	RelErr(dT/dz) %
63,5	13,3	56,7	11,9	27,1	28,6	26,9	28,4
Thermal Gradient 20 K/km - Conductive Heat Transmission in Reservoir - 5 km far from the Centre of MC - MCTL -4 km							
RMSD(T) K	CV(T) %	MAE(T) K	RelErr(T) %	RMSD(dT/dz) K/km	CV(dT/dz) %	MAE(dT/dz) K/km	RelErr(dT/dz) %
61,1	12,8	57,3	12,0	29,2	30,8	29,1	30,6
Thermal Gradient 20 K/km - Convective Heat Transmission in Reservoir - 5 km far from the Centre of MC - MCTL -4 km							
RMSD(T) K	CV(T) %	MAE(T) K	RelErr(T) %	RMSD(dT/dz) K/km	CV(dT/dz) %	MAE(dT/dz) K/km	RelErr(dT/dz) %
55,3	11,6	48,0	10,1	22,6	23,8	22,1	23,3
Thermal Gradient 20 K/km - Conductive Heat Transmission in Reservoir - 5 km far from the Centre of MC - MCTL -3 km							
RMSD(T) K	CV(T) %	MAE(T) K	RelErr(T) %	RMSD(dT/dz) K/km	CV(dT/dz) %	MAE(dT/dz) K/km	RelErr(dT/dz) %
46,9	9,8	43,7	9,2	22,1	23,3	21,9	23,1
Thermal Gradient 20 K/km - Convective Heat Transmission in Reservoir - 5 km far from the Centre of MC - MCTL -3 km							
RMSD(T) K	CV(T) %	MAE(T) K	RelErr(T) %	RMSD(dT/dz) K/km	CV(dT/dz) %	MAE(dT/dz) K/km	RelErr(dT/dz) %
44,5	9,3	37,0	7,8	17,1	18,1	16,2	17,0

Tab. 13. RMSD(T), CV(T), MAE(T), RelErr(T), RMSD(dT/dz)m, CV(dT/dz), MAE(dT/dz), and RelErr(dT/dz) for simulations with thermal gradient equal to 20 K/km, convection and conduction heat transmission in reservoir, 5 km far from the centre of Magma Chamber and with MCTL equal to -6 km, -5 km, -4 km and -3 km.

Thermal Gradient 40 K/km - Conductive Heat Transmission in Reservoir - 5 km far from the Centre of MC - MCTL -6 km							
RMSD(T) K	CV(T) %	MAE(T) K	RelErr(T) %	RMSD(dT/dz) K/km	CV(dT/dz) %	MAE(dT/dz) K/km	RelErr(dT/dz) %
53,1	11,1	50,0	10,5	25,8	27,2	25,6	26,9
Thermal Gradient 40 K/km - Convective Heat Transmission in Reservoir - 5 km far from the Centre of MC - MCTL -6 km							
RMSD(T) K	CV(T) %	MAE(T) K	RelErr(T) %	RMSD(dT/dz) K/km	CV(dT/dz) %	MAE(dT/dz) K/km	RelErr(dT/dz) %
26,9	5,6	19,3	4,1	9,3	9,9	7,3	7,7
Thermal Gradient 40 K/km - Conductive Heat Transmission in Reservoir - 5 km far from the Centre of MC - MCTL -5 km							
RMSD(T) K	CV(T) %	MAE(T) K	RelErr(T) %	RMSD(dT/dz) K/km	CV(dT/dz) %	MAE(dT/dz) K/km	RelErr(dT/dz) %
41,9	8,8	39,3	8,2	20,2	21,3	20,0	21,1
Thermal Gradient 40 K/km - Convective Heat Transmission in Reservoir - 5 km far from the Centre of MC - MCTL -5 km							
RMSD(T) K	CV(T) %	MAE(T) K	RelErr(T) %	RMSD(dT/dz) K/km	CV(dT/dz) %	MAE(dT/dz) K/km	RelErr(dT/dz) %
23,6	4,9	17,0	3,6	8,3	8,7	6,9	7,3
Thermal Gradient 40 K/km - Conductive Heat Transmission in Reservoir - 5 km far from the Centre of MC - MCTL -4 km							
RMSD(T) K	CV(T) %	MAE(T) K	RelErr(T) %	RMSD(dT/dz) K/km	CV(dT/dz) %	MAE(dT/dz) K/km	RelErr(dT/dz) %
29,3	6,1	27,0	5,7	13,7	14,5	13,4	14,1
Thermal Gradient 40 K/km - Convective Heat Transmission in Reservoir - 5 km far from the Centre of MC - MCTL -4 km							
RMSD(T) K	CV(T) %	MAE(T) K	RelErr(T) %	RMSD(dT/dz) K/km	CV(dT/dz) %	MAE(dT/dz) K/km	RelErr(dT/dz) %
18,6	3,9	13,7	2,9	7,9	8,3	6,6	7,0
Thermal Gradient 40 K/km - Conductive Heat Transmission in Reservoir - 5 km far from the Centre of MC - MCTL -3 km							
RMSD(T) K	CV(T) %	MAE(T) K	RelErr(T) %	RMSD(dT/dz) K/km	CV(dT/dz) %	MAE(dT/dz) K/km	RelErr(dT/dz) %
17,3	3,6	15,0	3,1	7,6	8,0	6,9	7,3
Thermal Gradient 40 K/km - Convective Heat Transmission in Reservoir - 5 km far from the Centre of MC - MCTL -3 km							
RMSD(T) K	CV(T) %	MAE(T) K	RelErr(T) %	RMSD(dT/dz) K/km	CV(dT/dz) %	MAE(dT/dz) K/km	RelErr(dT/dz) %
15,7	3,3	15,0	3,1	9,5	10,0	8,7	9,1

Tab. 14. RMSD(T), CV(T), MAE(T), RelErr(T), RMSD(dT/dz)m, CV(dT/dz), MAE(dT/dz), and RelErr(dT/dz) for simulations with thermal gradient equal to 40 K/km, convection and conduction heat transmission in reservoir, 5 km far from the centre of Magma Chamber and with MCTL equal to -6 km, -5 km, -4 km and -3 km.

Comparing the results of Tab. 11, Tab. 12, Tab. 13 and Tab. 14, the best results is that with thermal Gradient of 40 K/km, Heat Transmitted by conduction in reservoir, MCTL at -4 km in the centre of Magma Chamber (Fig. 6). The area considered is equivalent to the area of a radius of 10 km radius. However, the Bracciano caldera, at the center of the simulation domain, is the place where the heat transmission should be concentrated.

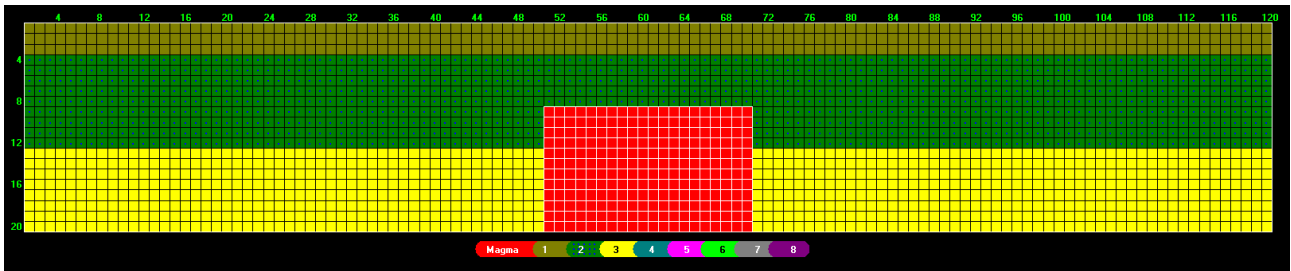


Fig. 7 Best fitting mesh for Monti Sabatini

Finally, the values of best fitting outputs for the two areas are comparable (Tab. 15).

	RMSD(T) K	CV(T) %	MAE(T) K	RelErr(T) %	RMSD(dT/dz) K/km	CV(dT/dz) %	MAE(dT/dz) K/km	RelErr(dT/dz) %
Monti Sabatini	7,4	1,6	6,0	1,3	5,0	5,3	3,8	4,0
Colli Albani	4,1	1,1	3,0	0,8	1,9	3,9	1,6	3,3

Tab. 15 Statistical of best fitting outputs for Monti Sabatini and Colli Albani

COMPARING NUMERICAL MODEL OUTPUT WITH WELLS DATA IN MONTI SABATINI AREA

To verify the quality of numerical model to fit the reference data set, output data is compared with the wells temperature data in Monti Sabatini area only. In fact, wells are not available in Colli Albani area.

We have selected 15 wells: 7 of them have the temperature profile data with stabilized temperature (Kutasov & Eppelbaum, 2015) and 7 of them have the temperature profile data with extrapolated temperature using Barelli Palamà method (Barelli & Palamà, 1981). One well of them (CESANO14) has the

first data set of temperature (from 400 m to 1,000 m) with stabilized temperature and the second data set of temperature (from 1,636 m to 2,574 m) with extrapolated temperature with the Barelli Palamà method.

Data sets exclude temperature data obtained with the static profile (Di Pippo, 2016).

10 wells are unproductive, 5 have geothermal fluid: no one is exploited.

We separately analyse wells with stabilized temperature and wells with extrapolated temperature.

The statistical analysis is implemented as follows.

A depth of the numeric model (-500 m, -1000 m,) is fixed and the relative temperature of the profile is considered. Among the well profile levels to which the temperature is measured, the level nearest to the numerical model level is selected and the its temperature is considered.

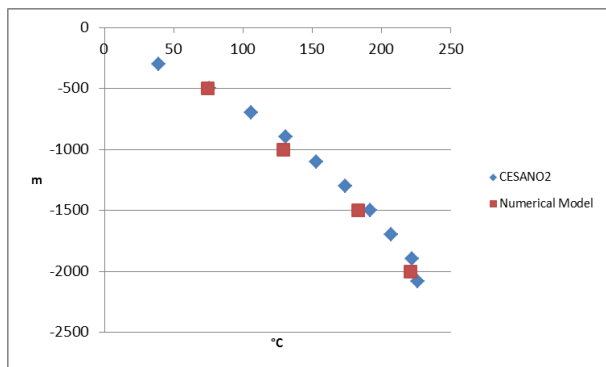
The maximum distance allowed is ± 250 m. If there are no level in well profile that meet the criterion, the depth level is not considered.

No interpolation among the well temperature data is performed.

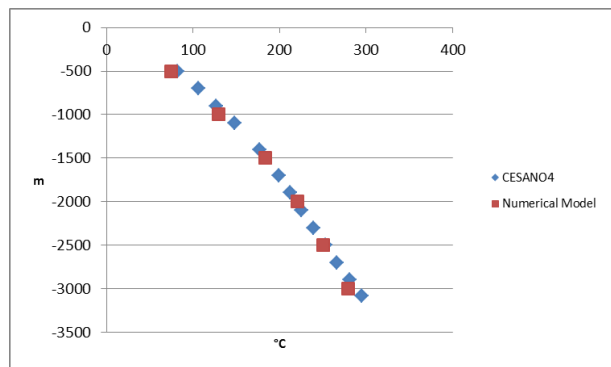
WELLS WITH STABILIZED TEMPERATURE DATA

The 7 wells with stabilized temperature are: Cesano2; Cesano4; Cesano5; Cesano7; Cesano8; Cesano14; Cesano18.

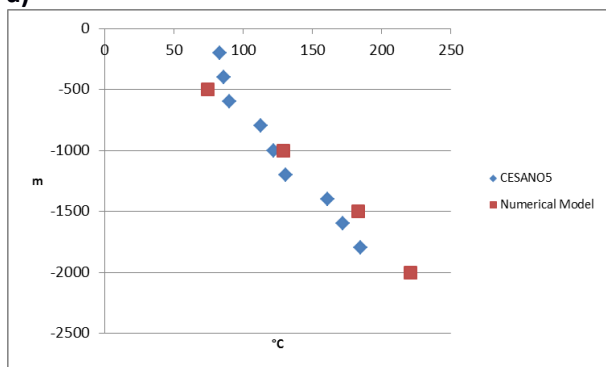
In Fig. 8 wells temperature profiles are compared with the selected numerical model temperature profile.



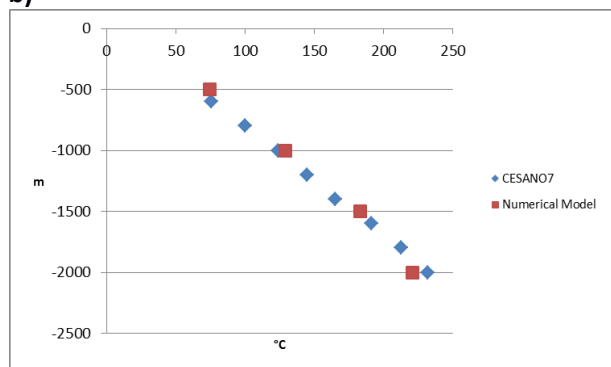
a)



b)



c)



d)

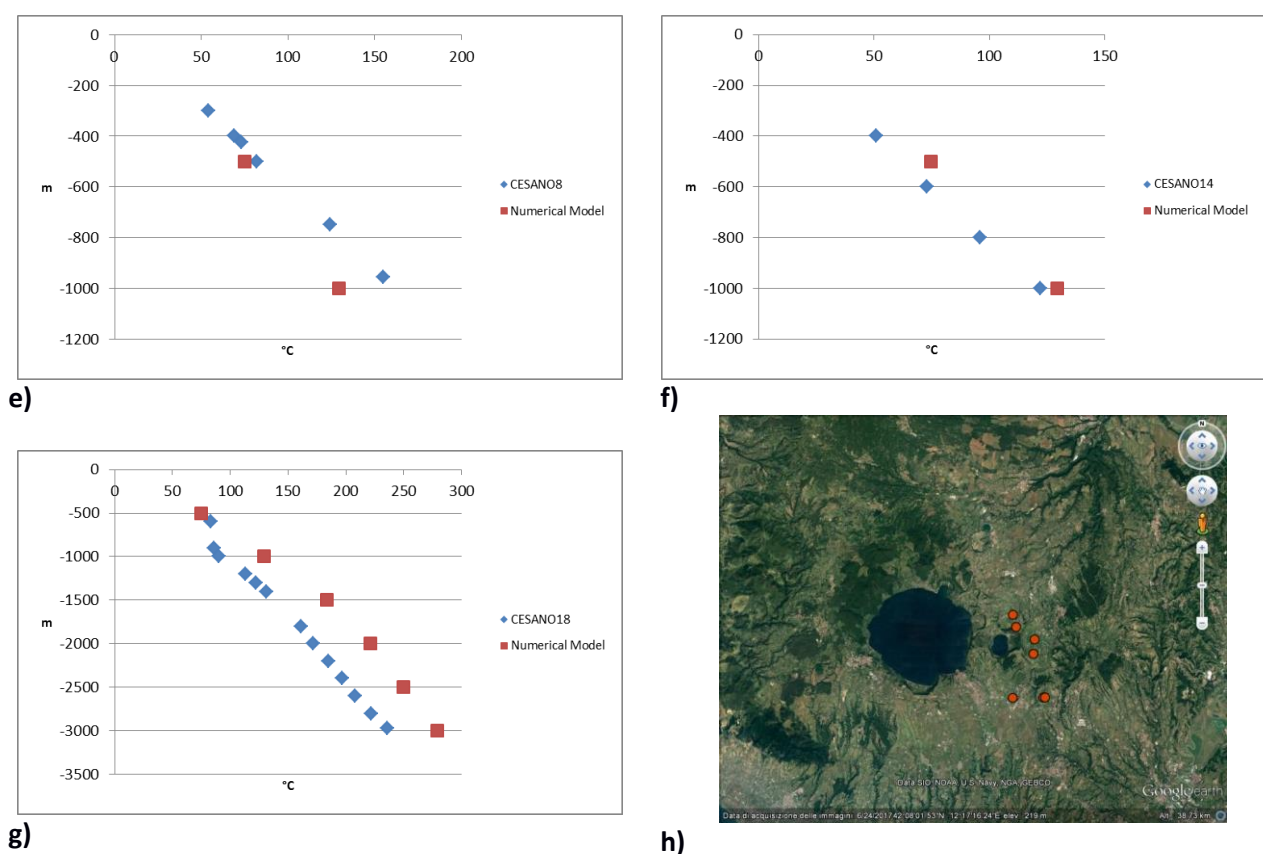


Fig. 8 Data wells profiles compared with selected numerical model data. a) Cesano2; b) Cesano4; c) Cesano5; d) Cesano7; e) Cesano8; f) Cesano14; g) Cesano18; h) wells localization

	Status	RMSD(T) K	CV(T) %	MAE(T) K	RelErr(T) %
Cesano2	unproductive	8,1	1,9	6,9	1,6
Cesano4	unproductive	8,6	1,8	7,2	1,6
Cesano5	geothermal fluid	21,2	5,1	18,2	4,4
Cesano7	geothermal fluid	6,7	1,6	5,7	1,3
Cesano8	geothermal fluid	18,8	4,8	16,4	4,2
Cesano14	unproductive	10,4	2,9	10,1	2,8
Cesano18	unproductive	42,4	10,0	39,8	9,3
		RMSD(T) K	CV(T) %	MAE(T) K	RelErr(T) %
	Thermal Gradient 40 K/km; Heat Transmitted by conduction in reservoir; MCTL at -4 km; in the centre of Magma Chamber	7,4	1,6	6,0	1,3

Tab. 13 Statistical analysis for Monti Sabatini wells temperature profile with stabilized temperature data. Yellow rows indicate the wells with only 2 or 3 points usable for the analysis

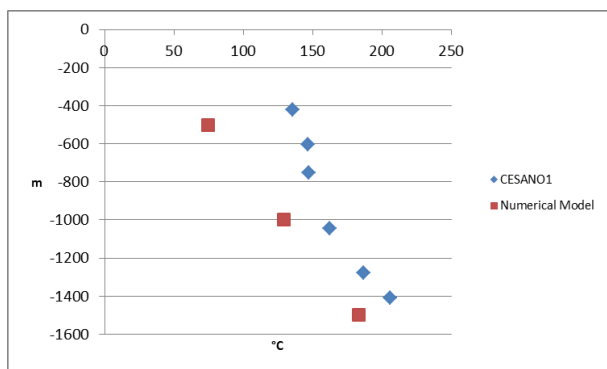
In Tab. 16 a statistical analysis is implemented between each well temperature profile and the selected numerical model temperature profile. Statistical data of the best numerical model selected before is included and indicate that the best fit is provided by a magma chamber with a top at -4 km within a geothermal gradient of 40K/km and conductive conditions. The latter condition is quite important as, though we refer the carbonates at the regional geothermal reservoir, their thermal behavior appear dominated by conduction rather than convection at regional scale, probably justifying the large number of unproductive wells that were drilled in the past.

Among the wells considered with more than 3 points usable for the analysis, three of them agree with the statistics of the numerical model. For two wells, statistical parameters fit less well to the numeric model. In the first 1000 m, their profiles are strongly convective and this explains the difference, that is graphically evident in Fig. 8 c) and g).

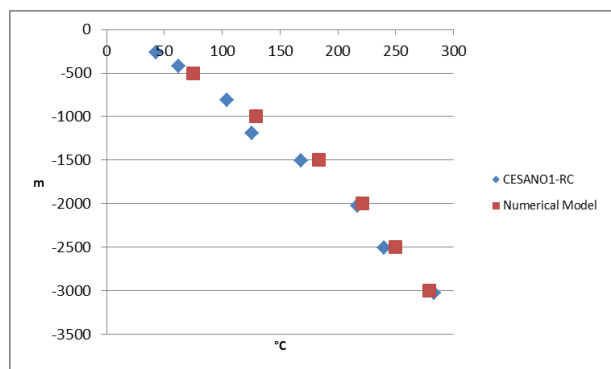
WELLS WITH WITH EXTRAPOLATED TEMPERATURE DATA

The 7 wells with extrapolated temperature data are: Cesano1; Cesano1-RC; Cesano3; Cesano6; Cesano13; Cesano14; Sabatini2; Sabatini5; SH-2.

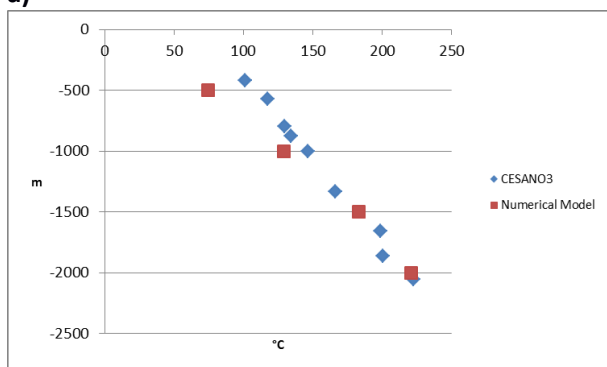
In Fig. 9 wells profile are compared with the selected numerical model profile.



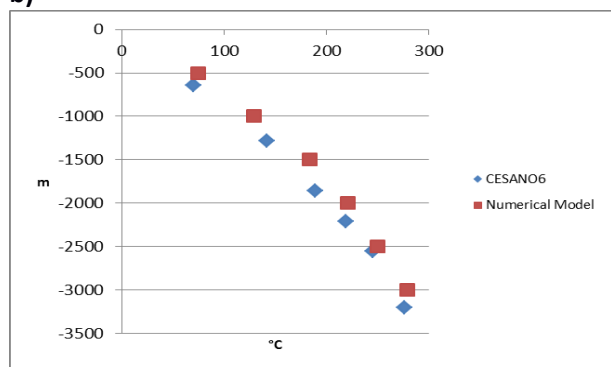
a)



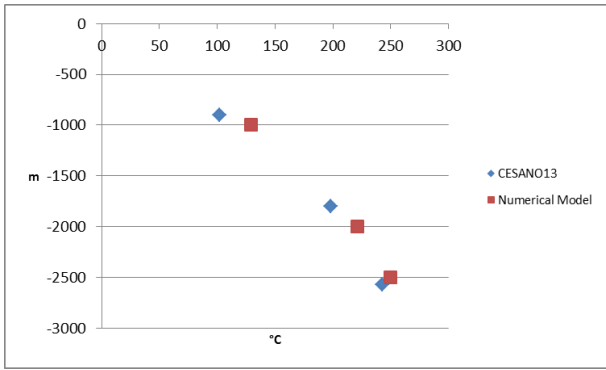
b)



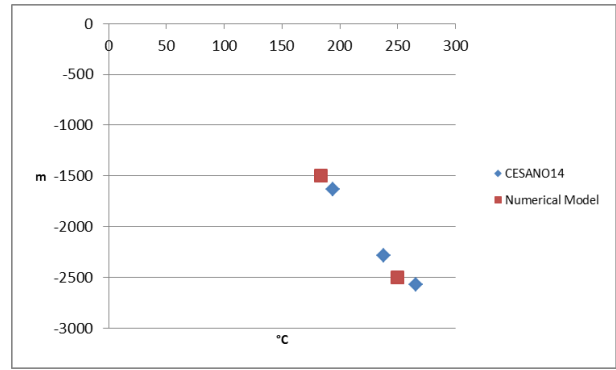
c)



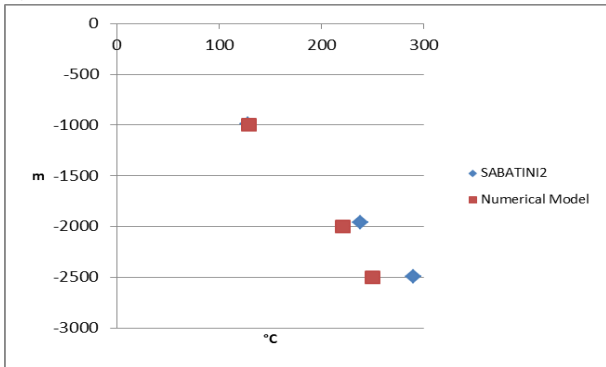
d)



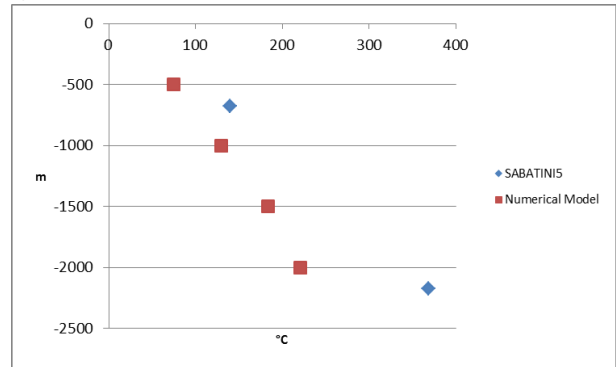
e)



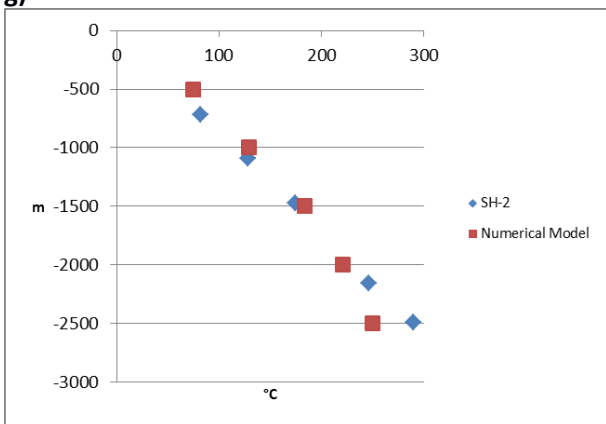
f)



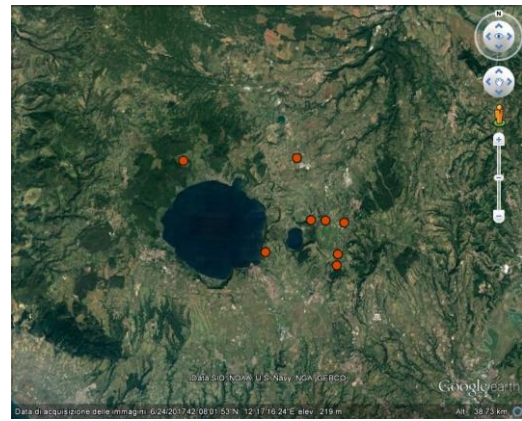
g)



h)



i)



j)

Fig. 9 Data wells profiles with extrapolated temperature data compared with selected numerical model data. a) Cesano1; b) Cesano1-RC; c) Cesano3; d) Cesano6; e) Cesano13; f) Cesano14; g) Sabatini2; h) Sabatini5; g) SH-2; j) wells localization

	Status	RMSD(T)	CV(T)	MAE(T)	RelErr(T)
Cesano1	geothermal fluid	42,1	9,5	38,8	8,8
Cesano1-RC	unproductive	14,0	3,1	12,0	2,6
Cesano3	unproductive	24,6	5,5	19,6	4,4
Cesano6	geothermal fluid	23,6	5,2	17,0	3,7
Cesano13	unproductive	21,0	4,6	19,1	4,2
Cesano14	unproductive	13,6	2,7	13,3	2,6
Sabatini2	unproductive	25,1	5,1	19,4	4,0
Sabatini5	unproductive	113,7	21,6	106,1	20,1
SH-2	unproductive	21,7	4,7	16,2	3,5
		RMSD(T) K	CV(T) %	MAE(T) K	RelErr(T) %
	Thermal Gradient 40 K/km; Heat Transmitted by conduction in reservoir; MCTL at -4 km; in the centre of Magma Chamber	7,4	1,6	6,0	1,3

Tab. 14 Statistical analysis for Monti Sabatini wells temperature profile with extrapolated temperature data. Yellow rows indicate the wells with only 2 or 3 points usable for the analysis

In Tab. 14 a statistical analysis is implemented between each well temperature profile and the selected numerical model temperature profile. Statistical data for best numerical model is included.

Among the wells considered with more than 3 points usable for the analysis, for all of them the statistical parameters fit less well to the numeric model. These differences can be attributed to the way the wells temperature profiles have been processed.

CONCLUSIONS

A numerical model, with magma kept at constant temperature of 900 °C for 500 ky to represent an actively recharged magma chamber and then able to relax for 350 ky, shows that the process is able to significantly increase the mean thermal gradient laterally as far as 10-15 km far from the centre of MC.

Then a model calibration was implemented considering separately the Colli Albani and Monti Sabatini areas.

A first relevant result is that the best fit for both the areas uses a conductive heat diffusion in geothermal reservoir.

In the Colli Albani area, the best model is that one with an initial thermal gradient of 20 K/km. The best fitting is obtained at a distance of 5 km from the centre of magma chamber.

Since the area covered by the considered municipalities (440 km²) can be approximated with the area of a circumference of 12 km radius, the 5 km point is intermediate between the center and the perimeter of the circumference.

In the Monti Sabatini area, the best model is that one with an initial thermal gradient of 40 K/km and the Magma Chamber Top Level at -4 km. The best fitting is obtained in the centre of magma chamber.

In Monti Sabatini area, the thermal gradient is exactly the double of the Colli Albani thermal gradient. This explains the initial thermal gradient of 40 K/km.

The Magma Chamber Top Level at -4 km is a numerical approximation of the suggestion from the literature of a magmatic mass with ellipsoidal body having the central point at approximately 7 to 10 km depth and the upper level very near to surface, and with lateral dimensions of the order of about 12-15 km. The mesh used in the numerical simulation (Fig. 7) is a quite good geometric description.

The best fitting obtained in the centre of magma chamber rather than 5 km far from the centre seems to suggest that the main thermal effect is concentrated up on the Magma Chamber.

Wells are not available in Colli Albani area. Thermal profiles in Monti Sabatini area wells that we have analysed are obtained with two different methodologies: stabilized temperature and extrapolated temperature (we have not included data inferred with static profile).

One third of them have geothermal fluids, but no one is exploited.

In our numerical simulations we have used a convective heat diffusion in geothermal reservoir with the porosity of 5%. If we consider the numerical simulation a good approximation of geothermal reality, we can explain the low number of wells with geothermal fluids. For 60% of stabilized temperature data wells, statistical analysis among thermal profiles and numerical model outputs yielded comparable results with statistical parameters obtained with numerical simulation compared to the average data of the UNIMIG database.

Statistical analysis is worse considering wells with stabilized temperature data. It is possible that this result is related to the methodology used to determine the wells thermal profile.

REFERENCES

- Barelli, A., & Palama, A. (1981). A new method for evaluating formation equilibrium temperature in holes during drilling. *Geothermics*, 10(2), 95-102.
- Capelli, G., Mazza, R., Gazzetti, C., & Merloni, G. (2005). *Strumenti e strategie per la tutela e l'uso compatibile della risorsa idrica nel Lazio. Gli acquiferi vulcanici*. Gangemi.
- Cataldi, R., Mongelli, F., Squarci, P., Taffi, L., Zito, G., & Calore, C. (1995). Geothermal ranking of Italian territory. *Geothermics*, 24(1), 115-129.
- De Rita, D., Funicello, R., Rossi, U., & Sposato, A. (1983). Structure and evolution of the Sacrofano-Baccano caldera, Sabatini volcanic complex, Rome. *Journal of Volcanology and Geothermal Research*, 17(1), 219-236.
- De Rita, D., Di Filippo, M., & Rosa, C. (1996). Structural evolution of the Bracciano volcano-tectonic depression, Sabatini Volcanic District, Italy. *Geological Society, London, Special Publications*, 110(1), 225-236.
- DiPippo, R. (Ed.). (2016). *Geothermal Power Generation: Developments and Innovation*. Woodhead Publishing.
- Kutasov, I. M., & Eppelbaum, L. V. (2015). *Pressure and Temperature Well Testing*. CRC Press.
- Mattei, M., Conticelli, S., & Giordano, G. (2010). The Tyrrhenian margin geological setting: from the Apennine orogeny to the K-rich volcanism. *The Colli Albani volcano. Special Publications of IAVCEI*, 3, 7-27.
- Molina, F., & Sonaglia, A. (1969). Rilevamento geomagnetico degli apparati vulcanici Vicano e Sabazio. *Annals of Geophysics*, 22(2), 147-162.

Chapter 10 – Forward modeling of the geothermal system across Roma Capital City

An HEAT3D model for the Province of Rome

From the outcomes of calibration process, it is possible to implement a first HEAT3d model for the Province of Rome.

In both calibration process we have used these physical parameters (Tab. 1)

	k	c_p	ρ	T	Porosity	Thermal diffusivity
Cap Rock	1.5	1,100	2,200	/	/	6.20 10 ⁻⁷
Geothermal Reservoir	2.7	900	2,650	/	0.05	1.13 10 ⁻⁶
Crystalline basement	2.5	1,100	2,750	/	/	8.26 10 ⁻⁷
Magma	1.7	1,200	2,750	900	/	5.15 10 ⁻⁷

Tab. 1 Summary of basic physical parameters 1n calibration process

In the computational domain:

- The cap rock occupies the first layer from 0 km to -1.5 km;
- The geothermal reservoir occupies the second layer from -1.5 km to -6 km;
- The crystalline basement is located in the bottom layer from -6 km to -10 km;
- The magma chamber has the length is 10 km;
- In Geothermal Reservoir heat is transmitted by conduction.

For Colli Albani area the parameters of simulation are:

- Thermal Gradient in the domain 20 K/km (the same in Province of Rome, see Chapter 6);
- Roof of magma chamber at -6.5 km along the z axis

For Monti Sabatini area the parameters of simulation are:

- Thermal Gradient in the domain 40 K/km;
- Roof of magma chamber at -4.0 km along the z axis

Magma Chambers have the same horizontal dimension of that selected during the calibration process (10 km).

Preparing the mesh for the simulation in Province of Rome, for Monti Sabatini area the question is how to link the two different Thermal Gradients in the domain.

We have used a decreasing thermal gradient. Considering the x axis we will have the follow thermal gradients:

- 40 K/km from the centre of Monti Sabatini Magma Chamber till 10 km away;
- 30 K/km from 10 km away from the centre of MC till 20 km away (buffer zone);
- 20 K/km in the remainder of the domain.

The mesh becomes (Fig. 1):

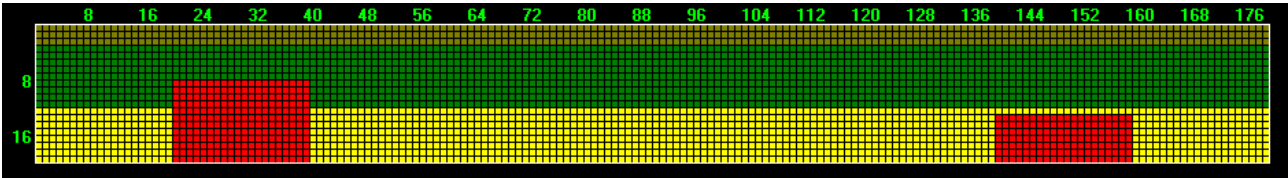


Fig. 1 The mesh for the Province of Rome model

The thermal field at the beginning of simulation is in Fig. 2.

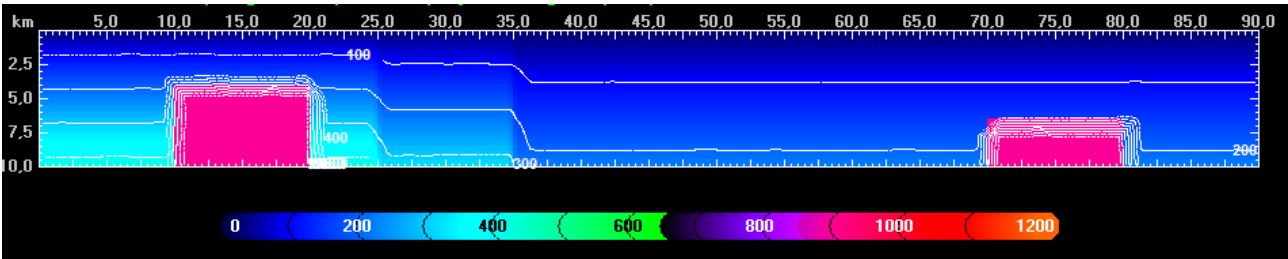


Fig. 2 Thermal field at $t = 0$ kyr

The domain is 90 km (x axis) x 10 km (z axis) and it is oriented North (west part of mesh) – South (east part of mesh). The West part of domain represents the Monti Sabatini area, the East part represents the Colli Albani area.

The distance between the edges of Magma Chambers is 50 km. This is a good approximation for the geographic distance between the two areas. In this way, Rome is exactly in the centre of the domain.

The centre of the City of Rome is included in a Ring Road (Fig. 3) with a diameter of 20 km.

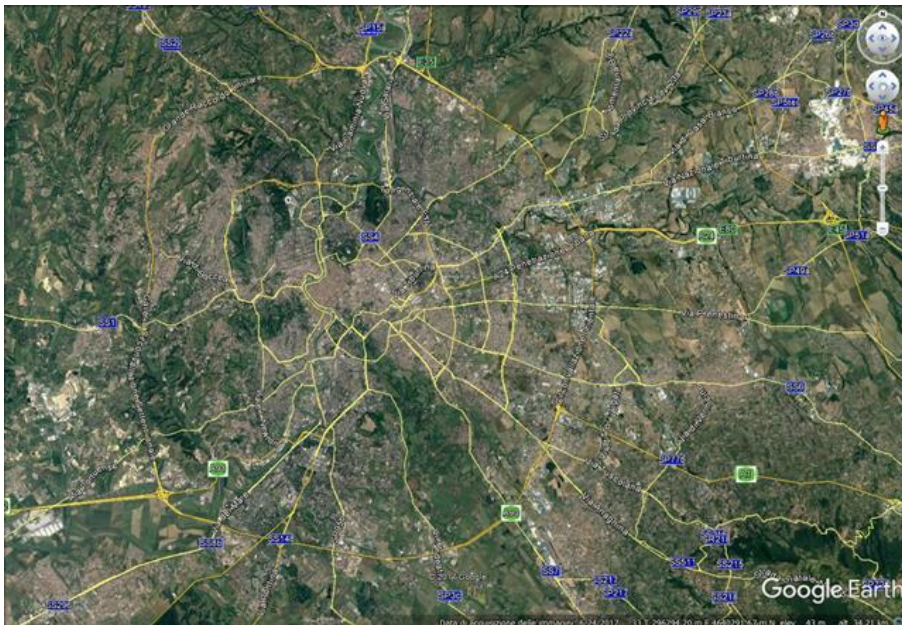
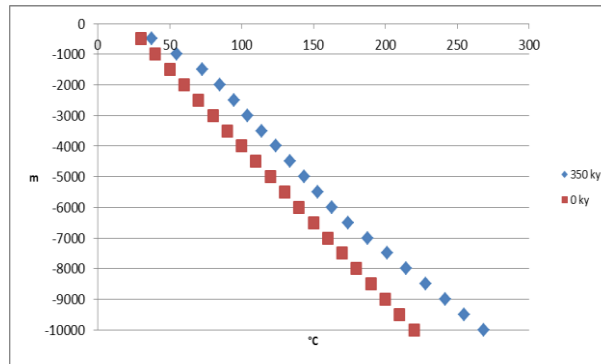


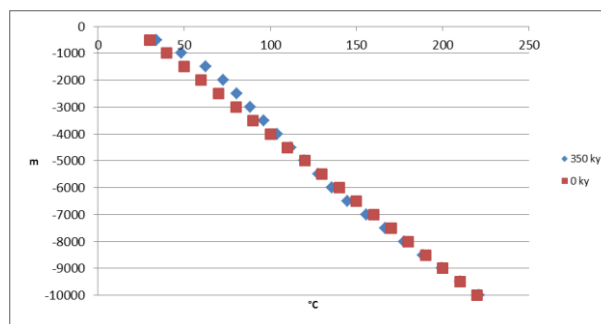
Fig. 3 The Ring Road around Rome

Outputs from the purely conductive model

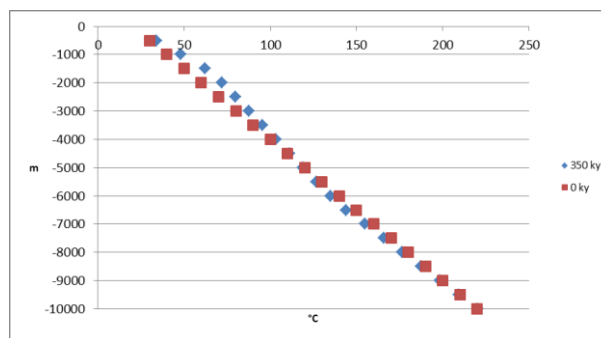
Fig. 4 includes the vertical profiles for the purely conductive model for the centre of the Domain (geographically Rome) and 10 km far from this point (towards West and East, the border of Ring Road). Each profile include initial and final steps of simulation, i.e. $t = 0$ kyr and $t = 350$ kyr.



a)



b)



c)

Fig. 4 Purely convective model. Temperature ($^{\circ}\text{C}$) vs Depth (m). Vertical profiles in: a) 10 km left from the centre of the mesh; b) centre of the mesh; c) 10 km right from the centre of the mesh.

Tab.2 shows temperature data ($^{\circ}\text{C}$) at -1000 m, -2000 m and -3000 m at $t = 350$ kyr in the three point and temperature at $t = 0$ kyr.

	10 km left	Centre	10 km right	$t = 0$ ky
-1000 m	55	48	48	40
-2000 m	85	73	72	60
-3000 m	104	88	88	80

Tab. 2 temperature data ($^{\circ}\text{C}$) at -1000 m, -2000 m and -3000 m at $t = 350$ kyr in the three point and temperature at $t = 0$ kyr

In Tab.3 temperature gradients (K/km) at -1000 m, -2000 m and -3000 m at t = 350 kyr in the three point and a t = 0 kyr are included, where

$$\begin{aligned} -1,000 \text{ m} &= (T_{1000} - T_{0=20 \text{ }^\circ\text{C}}); \\ -2,000 \text{ m} &= (T_{2000} - T_{0=20 \text{ }^\circ\text{C}}) / 2; \\ -3,000 \text{ m} &= (T_{3000} - T_{0=20 \text{ }^\circ\text{C}}) / 3; \end{aligned}$$

	10 km left	Centre	10 km right	t = 0 ky
-1000 m	35	28	28	20
-2000 m	33	26	26	20
-3000 m	28	23	23	20

Tab. 3 Thermal gradient (K/km) at -1000 m, -2000 m and -3000 m at t = 350 kyr in three point and a t = 0 kyr

Unfortunately we have not a benchmark for the temperature in Rome. In fact, Rome has a huge surface (after London, Rome is second City in Europe for extension), covering from Monti Sabatini area to Colli Albani area. UNMIG database doesn't offers information limited on the City of Rome inside the Road Ring. In Tab. 4 UNMIG data for Rome is presented.

	T1000_mean	T1000_min	T1000_max	T2000_mean	T2000_min	T2000_max	T3000_mean	T3000_min	T3000_max
T °C	66	38	135	120	51	262	158	76	309
dT/dz K/km	46	18	115	50	16	121	46	19	96

Tab. 4. UNMIG data for Rome.

In Tab. 5 absolute differences in temperature (K) between t = 350 kyr and t = 0 kyr are presented

	10 km left	Centre	10 km right
-1000 m	15	8	8
-2000 m	25	13	12
-3000 m	24	8	8

Tab 5 Absolute differences in temperature (K) between t = 350 kyr and t = 0 kyr

In Tab. 6 differences in temperature (%) between t = 350 kyr and t = 0 kyr are presented

	10 km left	Centre	10 km right
-1000 m	5	3	3
-2000 m	7	4	4
-3000 m	7	2	2

Tab 6 Differences in temperature (%) between t = 350 kyr and t = 0 kyr

The west profile (10 km left) is influenced by Monti Sabatini area. A temperature increase is detectable in – 2,000 m and -3,000 m, with a difference of about 25 °C, i.e. 7%.

In the Centre of Domain (the centre of City of Rome) and 10 km towards Colli Albani area, a temperature increase is detectable in – 2,000 m, with a difference of about 13 °C, i.e. 4%.

In the simulation, temperature gradients increases, passing from the initial 20 K/km to 28 k/km - 35 K/km in the first 1,000 m depth.

Outputs from the conductive-convective model

Fig. 5 provides an interpretative scheme of deep geothermal fluid circulation in the Central Italy Geothermal Province. The base map is the reconstruction of the top of the reservoir from ENEL (1987). The heat sources are associated with the Quaternary calderas, where permeable volcano-tectonic faults allow lateral advection of hot fluids along trajectories of maximum buoyancy, i.e. accommodating structural

high. Some paths from the Sabatini Mountains area and the Colli Albani area converge in Rome (Giordano et al., 2014). So we have decided to include a conductive-convective zone in the computational domain.

In geothermal reservoir, a convective area 20 km length under the City of Rome (exactly under the Ring Road) is included, simulating a possible conductive-convective zone. Porosity is 0.05, like stated in Tab. 1 (Bono, 1981).

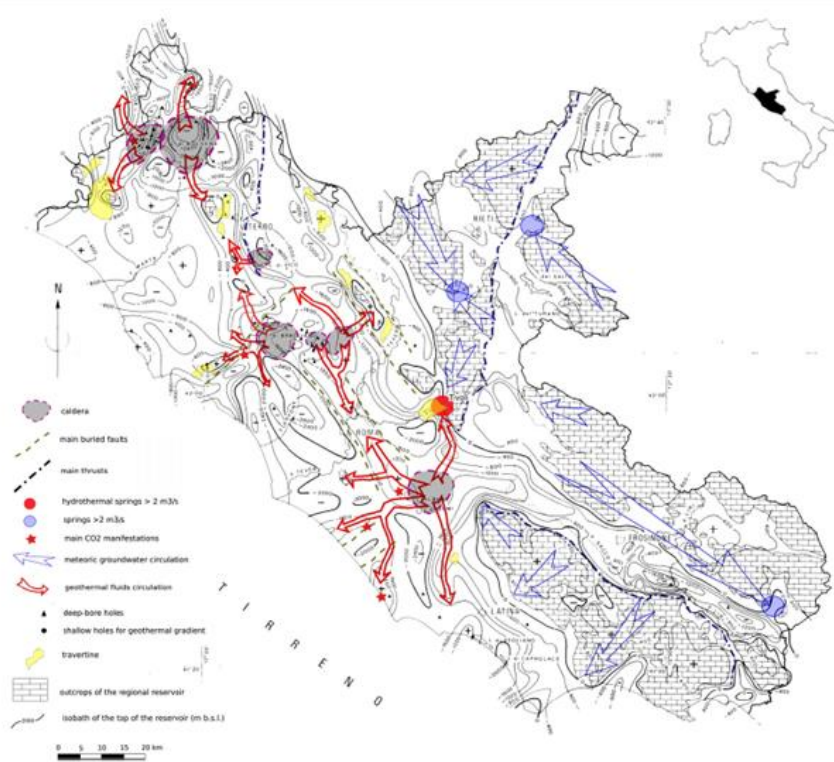


Fig. 5 Interpretative scheme of deep geothermal fluid circulation in the Central Italy Geothermal Province (Capelli et al., 2012; Giordano et al., 2014).

The computational domain becomes like in Fig. 6:

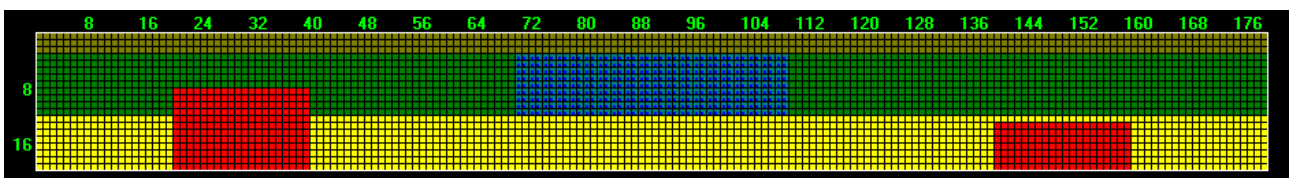
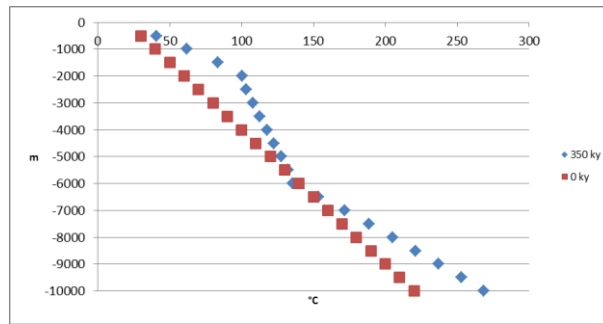


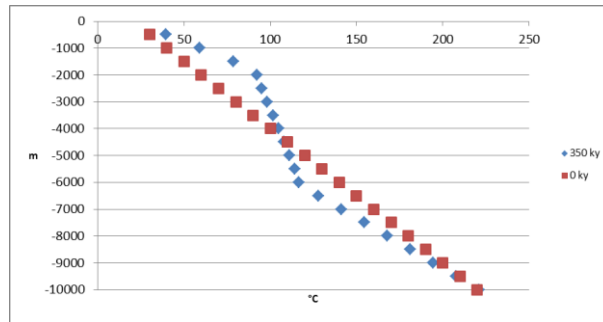
Fig. 6 Computational domain for the conductive-convective model

The thermal field at the beginning of simulation is unvaried, like Fig. 2.

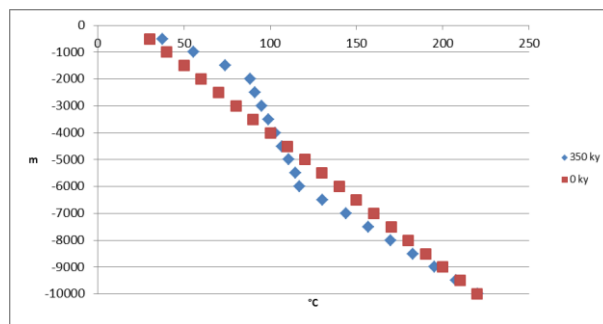
Fig. 7 includes the vertical profiles for the conductive-convective model for the centre of the Domain (geographically Rome) and 10 km far from this point (towards West and East). Profiles for $t = 0$ kyr and $t = 350$ kyr are included.



a)



b)



c)

Fig. 7 Conductive-convective model. Temperature (°C) vs Depth (m). Vertical profiles in: a) 10 km left from the centre of the mesh; b) centre of the mesh; c) 10 km right from the centre of the mesh.

These profiles are typically conductive-convective kind, and show a clear difference from the purely conductive profiles.

In Tab.7 temperature data (°C) at -1000 m, -2000 m and -3000 m in the three point and a t = 0 kyr are included.

	10 km left	Centre	10 km right	t = 0 ky
-1000 m	62	59	56	40
-2000 m	100	92	89	60
-3000 m	108	98	95	80

Tab. 7 temperature data (°C) at -1000 m, -2000 m and -3000 m in three point and a t = 0 kyr

In Tab.8 temperature gradients (K/km) at -1000 m, -2000 m and -3000 m in the three point and a t = 0 kyr are included, where

$$\begin{aligned}
 -1,000 \text{ m} &= (T_{1000} - T_{0=20^\circ\text{C}}); \\
 -2,000 \text{ m} &= (T_{2000} - T_{0=20^\circ\text{C}}) / 2; \\
 -3,000 \text{ m} &= (T_{3000} - T_{0=20^\circ\text{C}}) / 3;
 \end{aligned}$$

	10 km left	Centre	10 km right	t = 0 ky
-1000 m	42	39	36	20
-2000 m	40	36	34	20
-3000 m	29	26	25	20

Tab. 8 Thermal gradient (K/km) at -1000 m, -2000 m and -3000 m in three point and a t = 0 kyr

In Tab. 9 absolute differences in temperature (K) between t = 350 kyr and t = 0 kyr are presented

	10 km left	Centre	10 km right
-1000 m	22	19	16
-2000 m	40	32	29
-3000 m	28	18	15

Tab 9 Absolute differences in temperature (K) between t = 350 kyr and t = 0 kyr

In Tab. 10 differences in temperature (%) between t = 350 kyr and t = 0 kyr are presented

	10 km left	Centre	10 km right
-1000 m	7	6	5
-2000 m	12	10	9
-3000 m	8	5	4

Tab 10 Differences in temperature (%) between t = 350 kyr and t = 0 kyr

Again the west profile (10 km left) is influenced by Monti Sabatini area. A strong temperature increase is detectable in – 2,000 m, with a difference of 40 °C, i.e. 12%.

In the Centre of Domain (the centre of City of Rome) and 10 km towards Colli Albani area, a temperature increase is detectable in – 2,000 m, with a difference of about 30 °C, i.e. 10%.

Conclusion

Although this study is a first attempt to implement HEAT3D in Province of Rome, some results can be outlined.

From the calibration process, different magma chambers are implemented in the mesh. Moreover, different thermal gradients are included in the numerical model to meet the calibration outputs. A process to link the Monti Sabatini thermal gradient with the domain thermal gradient is implemented, including a buffer zone.

The final mesh includes the City of Rome and its surroundings, where geothermal information are really poor.

Two different configurations are implemented.

- The first is purely conductive, like in calibration process;
- The second is convective-conductive, under the City of Rome.

In the conductive numerical model, the west profile (10 km left from the centre of the domain) is influenced by Monti Sabatini area.

A temperature increase is detectable in – 2,000 m and -3,000 m, with a difference of about 25 °C, i.e. 7%.

In the Centre of Domain (the centre of City of Rome) and 10 km towards Colli Albani area, a temperature increase is detectable in – 2,000 m, with a difference of about 13 °C, i.e. 4%.

Consequently, temperature gradients increases, passing from the initial 20 K/km to 28 k/km - 35 K/km in the first 1,000 m depth.

This data is relevant for the low enthalpy geothermal energy production.

Even more interesting is the conductive - convective simulation.

Again the west profile (10 km left) is influenced by Monti Sabatini area. A strong temperature increase is detectable in – 2,000 m, with a difference of 40 °C, i.e. 12%.

Also in the Centre of Domain (the centre of City of Rome) and 10 km towards Colli Albani area, an interesting temperature increase is detectable in – 2,000 m, with a difference of about 30 °C, i.e. 10%.

Thermal gradient increases especially till -2,000 m, passing from the initial 20 K/km to 34 K/km - 42 K/km.

These results push towards a more intensive exploration and towards (when it is possible) the exploitation of medium - low enthalpy geothermal energy.

References

Bono, P. (1981). Valutazione preliminare del potenziale geotermico della regione laziale. *Geol Rom*, 2.

Capelli, G., Mastrorillo, L., Mazza, R., & Petitta, M. (2012). Carta delle Unità Idrogeologiche della Regione Lazio, scala 1: 250.000.

ENEL. (1987). *Inventario delle Risorse Geotermiche Nazionali*—Regione Lazio, Pisa. Internal report.

Giordano, G., De Benedetti, A. A., Bonamico, A., Ramazzotti, P., & Mattei, M. (2014). Incorporating surface indicators of reservoir permeability into reservoir volume calculations: Application to the Colli Albani caldera and the Central Italy Geothermal Province. *Earth-Science Reviews*, 128, 75-92.

Summary and conclusion

Climate change is the starting point for this work, in particular GHG emission mitigation through the reduction of fossil fuels consumption and their replacement with energy efficiency actions and the use of renewable energy sources (Cap. 1).

Geothermal energy is considered a strategic resource in many countries, even if its use appears to be often marginal in the national energy systems (Cap. 2).

Italy is among those countries that can easily access this resource, though the efforts over the years have been directed mainly towards high enthalpy geothermal sources.

However, exploitation of medium and low enthalpy geothermal resources can contribute to achieving in Italy the mitigation targets set by the European Union.

The use of numerical models is an important element both during the phases of exploration and exploitation of the geothermal resource. Numerical modelling can best address local geothermal research, even in the light of the new exploitation technologies that require particular attention to geothermal resource sustainability (Cap. 3).

A different approach, addressed to the characterization of larger areas (i.e. the order of $\sim 10^3\text{-}10^5$ km²) including the magmatic heat sources, can provide information especially in those areas where drillings are very scarce or even null and therefore where numerical local models don't have input data to solve their equations (Cap. 4).

This work is devoted to the latter target, using the open source code HEAT3D. This model allows to create meshes in 2D and 3D where the physical parameters of the rocks are user definable and magmatic heat sources can be modeled in the mesh.

However, whatever be the modeling strategy adopted, two steps are essential before to produce reliable results: to start from a robust conceptual model and to implement the calibration analysis.

The definition of the conceptual model for the area of interest, the Geothermal Roman Province, was realized starting from the geological history of the area and then deepening the elements that characterize the geothermal potential: the source of heat, the stratigraphy, the structure and the permeability (Cap. 5). The synthesis of these data has provided a robust conceptual model that has allowed to customize the general first order scheme of a geothermal system in terms of extension of the various successions (cap rock, thermal reservoir and basement) and of thermal and geometrical characteristics of magma chamber.

From this conceptual model, within the HEAT3D numeric code, we defined a reference model in which the mesh, the physical parameters and the geometry and the temperature of the magma chamber are defined. (Cap. 6)

However, although the physical parameters for cap rock and geothermal reservoir are well-known (their values are deductible from the literature grounded on a large wealth of direct and indirect data), uncertainties remain on the values of the physical parameters for the crystalline basement (k , C_p and ρ) and on the geometry and on the temperature for the magma chamber. The first part of the work was devoted to verify the influence of the uncertainties related to the lack of reliable data on the physical characteristics of the basement and on temperature and geometry of the magma chamber on the results of numerical modeling (Cap. 7).

In accordance with what defined in the conceptual model, the parameters have been varied within a range, whose values have been deduced from the literature, where the central value is that defined in the reference model. The results compare the percentage change respect to the central value, with the relative percentage change of the temperature at the base of the geothermal reservoir (-6 km) at the end of the

run-time (350 ky). It is therefore evaluated how much the uncertainties affect the results of numerical simulations.

In summary, we consider acceptable to work with the central values of k , C_p and ρ , for the basement, assuming that results can be affected by an error of $\pm 10\%$.

Uncertainties in the selection of T_{magma} also may affect the results with an error of $\pm 10\%$.

Variations in depth and length of magma chamber also result in errors of $\pm 10\%$.

Another interesting observation is that the convection in the geothermal reservoir affects the results measured at the top of the basement at ~ 6 km, implying complex feedbacks between conductive and convective layers.

After the analysis of the uncertainties in the basement, we used the selected configuration to test the behavior of the numerical model by varying the regional geothermal gradient (0-20-40 K/km) and the conductive vs convective-conductive heat transmission inside the geothermal reservoir (Cap. 8).

The main obvious difference between the two heat transmission modes inside the geothermal reservoir is the more effective convective thermal plume that rises the temperatures within the geothermal reservoir

From both the different heat transmissions, some information can be deduced:

1. In correspondence of the centre of the Magma Chamber (MC) and laterally to 5 km away (i.e. at the margin of MC), the variation of temperature in the geothermal reservoir rises quickly up to 150 kyr and then stabilizes till 350 kyr with an exponential trend as a function of time.
2. 10 km far from the centre of MC, in function of time, the thermal variations are limited. Under conduction in the geothermal reservoir, thermal effect of MC produces a linear increasing of temperature that continues to increment over time. Convection in the geothermal reservoir affects the slope gradient and interestingly the larger increase in T at the top of the geothermal reservoir corresponds to a decrease at its base;
3. 20 km far from the centre of MC, there is a negligible effect in temperature (more pronounced in the convective case) for the thermal contribution of MC compared with the external field contribution (thermal gradient in the domain). In fact, thermal gradient in the domain acts like a relevant external force for the temperature dynamic.

Data indicates that the geothermal gradient controls the modality by which the heat is transferred from the magma source to the country rocks and acts by modifying what could be called "thermal potential" in analogy with other potentials such as the hydraulic or the electric. In this sense, the increase in regional geothermal gradient reduces the "thermal potential", i.e. the temperature difference between the hot source and the colder country rock that drives the heat exchange. Our data qualitatively indicate that the thermal conductivity is more important in modulating the heat transfer when the "thermal potential" is low, respect to conditions where the heat transfer is dominated by high "thermal potential".

For the model calibration, two activities have been carried out, one for the Colli Albani area and the other for the Monti Sabatini area (Cap. 9).

Preliminarily, a simulation was implemented to understand the role played by an actively recharged magma chamber to modify the local geothermal gradient. To this aim, a simulation with thermal gradient of 20 K/km, conductive heat diffusion in reservoir and with magma kept at constant temperature of 900 °C for 500 ky to represent an actively recharged magma chamber was implemented. After this period the Magma Chamber temperature could decrease and system relaxed for 350 ky. Qualitative results show that an actively recharged magma chamber is a driving force for the geothermal gradient implementation.

To implement calibration, data for comparison are that included in the DGS-UNMIG (Directorate-General For Safety Of Mining And Energy Activities National Mining Office For Hydrocarbons And Georesources - Italian Ministry of Economic Development) database of Italian Municipalities. Among the many data, for each municipality, mean, minimum and maximum temperatures (in °C) are available to a depth of 1 km, 2 km and 3 km. Separately we have selected the municipalities belonging to each area and we have calculated the average temperature values at different depths.

Numerical modelling has been implemented with thermal gradient of 20 K/km and 40 K/km and conductive and conductive convective heat transmission in reservoir and compared with DGS-UNMIG data.

For Colli Albani area the best simulation is that with the conductive heat transmission in reservoir and with the thermal gradient of 20 K/km.

For Monti Sabatini area, to improve the simulation, the thermal gradient was selected to 40 K/km and the magma chamber top level was raised till -4 km depth. Papers support the hypothesis of a Magma Chamber Top Level inside geothermal reservoir (see Chapter 9.). In Monti Sabatini area, a geomagnetic survey for the vertical component of the earth's field has led to the conclusion of the existence of a magmatic mass with upper level very near to surface.

Statistical analysis implemented for both the simulations gives comparable outputs.

Finally, for Monti Sabatini area, a comparison was made between the numerical simulation and the wells present in the area (there are no wells in the Colli Albani area). The results obtained are good for wells with stabilized temperature profile, less good for wells with extrapolated temperature profile.

Finally, a numerical modeling for the City of Rome area was implemented, extending from the Sabatini to the Colli Albani area (Cap. 10).

From the calibration process, different conditions for the magma chambers of Sabatini and Colli Albani are implemented in the mesh. Moreover, different thermal gradients are included in the numerical model to meet the calibration outputs. A process to link the Monti Sabatini thermal gradient with the domain thermal gradient is implemented, using a buffer zone.

The final mesh includes the City of Rome and its surroundings, where geothermal information are really poor.

Two different configurations are implemented.

- The first is purely conductive, like in calibration process;
- The second is convective-conductive, under the City of Rome.

In the conductive numerical model, the west profile (10 km left from the centre of the domain) is influenced by Monti Sabatini area. A temperature increase is detectable in - 2,000 m and -3,000 m, with a difference of about 25 °C, i.e. 7%. In the Centre of Domain (the centre of City of Rome) and 10 km towards Colli Albani area, a temperature increase is detectable in - 2,000 m, with a difference of about 13 °C, i.e. 4%. Consequently, temperature gradients increases, passing from the initial 20 K/km to 28 k/km - 35 K/km in the first 1,000 m depth.

This data is relevant for the low enthalpy geothermal energy production.

More interesting is the conductive - convective simulation. Again the west profile (10 km left) is influenced by Monti Sabatini area. A strong temperature increase is detectable in - 2,000 m, with a difference of 40 °C, i.e. 12%. Also in the Centre of Domain (the centre of City of Rome) and 10 km towards Colli Albani area, an interesting temperature increase is detectable in - 2,000 m, with a difference of about 30 °C, i.e. 10%. Thermal gradient increases especially till -2,000 m, passing from the initial 20 K/km to 34 K/km - 42 K/km. These results push towards a more intensive exploration and towards (when it is possible) the exploitation of medium - low enthalpy geothermal energy.